

3  
2008

**LIBRARY**  
**Michigan State**  
**University**

This is to certify that the  
dissertation entitled

**ANALYTICAL APPLICATIONS  
OF FLUORESCENCE QUENCHING**

presented by

**MELISSA SUE MEANEY**

has been accepted towards fulfillment  
of the requirements for the

Ph.D. degree in Chemistry

Victoria McGuffee

Major Professor's Signature

12/21/2007

Date

*MSU is an affirmative-action, equal-opportunity employer*

**PLACE IN RETURN BOX** to remove this checkout from your record.  
**TO AVOID FINES** return on or before date due.  
**MAY BE RECALLED** with earlier due date if requested.

DATE DUE	DATE DUE	DATE DUE

**ANALYTICAL APPLICATIONS OF FLUORESCENCE QUENCHING**

**By**

**Melissa Sue Meaney**

**A DISSERTATION**

**Submitted to  
Michigan State University  
in partial fulfillment of the requirements  
for the degree of**

**DOCTOR OF PHILOSOPHY**

**Department of Chemistry**

**2008**



## **ABSTRACT**

### **ANALYTICAL APPLICATIONS OF FLUORESCENCE QUENCHING**

By

Melissa Sue Meaney

Fluorescence quenching has many forms, from trivial mechanisms involving primary and secondary absorption to more selective formation of ground- and excited-state complexes. Much work has been done to eliminate quenching interferences from traditional solution-phase fluorescence measurements, but little effort has focused on tuning the fluorophore chemistry for selective detection of quencher molecules. Pyrene has demonstrated a sensitive and selective quenching interaction with nitrated explosives, allowing a 40-fold improvement in signal-to-noise ratio compared with traditional UV absorbance. Our Stern-Volmer data indicate that phenol red, malachite green, and brilliant purpurin R are suitable, less toxic replacements for pyrene for the detection of nitrated materials. In comparison to pyrene, these fluorophores demonstrate comparable sensitivity and greater selectivity for model nitrated compounds than for potential interfering species. When compared to Rehm-Weller theory, the data suggest an electron-transfer mechanism is responsible for the quenching signal.

For utility in a field device, the fluorescence of malachite green is investigated in the solid state. Because the greatest solution-phase fluorescence is observed in dioxane, matrices with similar polarity to dioxane are considered. Fluorescence of malachite green is not observed when adsorbed onto filter paper,

but is observed in a poly(ethylene glycol) thin film. Poly(ethylene glycol) films containing malachite green are coated onto filter paper and silica particles and their fluorescence investigated for application as a wipe material and air sampling tube for explosives detection, respectively.

In addition to the application for nitrated explosives detection, an indirect fluorescence method has been developed for the detection of acids. The pH sensitivity of fluorescein demonstrates a novel method for selective identification of acids in complex samples. The relationship between the logarithm of acid concentration and fluorescence power of fluorescein is sigmoidal and dependent on the fluorescein concentration as well. The method is demonstrated for any acid with  $pK_a \leq 5.5$  such that proton transfer to fluorescein is possible. Most importantly, the approach provides a single calibration curve for acids of varying strength and number of proton-donating sites. This method has been applied to characterization of acids in fruit-derived beverages and food products such as juice, wine, and vinegar following liquid chromatography.

A forensic extension of this method has been made to the determination of  $\gamma$ -hydroxybutyric acid (GHB) in adulterated beverages, including beer, wine, rum, cola, and coffee. GHB is a common drug of abuse and is often found in alleged sexual assault cases. The limit of detection of this method is 3 mM GHB in various beverages, which corresponds to 90 mg GHB in an 8-oz beverage. This detection limit is an order of magnitude below the therapeutic dose of GHB, and 20 – 40 times below the typical recreational dose. The sensitivity of the method indicates that GHB may be detectable in beverage residues at a crime scene.

**To My Friends and Family, and To Andrew, with Love**

## **ACKNOWLEDGEMENTS**

This road through graduate school has been challenging, enjoyable, frustrating, and enlightening, and often all in the same day. As an undergraduate, I never imagined being on this path, but I am grateful to those who directed me to a future that involved higher education. I have been very blessed over the past five and a half years at Michigan State University in meeting many amazing friends and scientists and having numerous noteworthy experiences. The skills and knowledge base that I have gained during graduate school will no doubt guide me through the rest of my scientific career.

For the content of this dissertation, as well as the guidance only a true mentor can give, I must thank my thesis advisor, Dr. Victoria McGuffin. Without her continued support and encouragement, despite my own doubts and frustrations, I would not have completed the research contained within this dissertation. I am grateful for her genuine interest in the projects and areas of interest to me, and for working diligently to keep the focus of my many projects on high-quality, analytical forensic science. Vicki's practical expertise and vast knowledge of spectroscopy and separation science are directly reflected in the content and structure of this work. In addition to her scientific advising, I have also been blessed with an amazing woman role model who is incredibly successful and more than willing to share her knowledge and experience. Endless insight into the processes of peer-reviewed publication, grant preparation and submission, education, and ethics has prepared me for any career, and especially for a future in academia.

I would also like to thank the members of my thesis committee, Dr. Merlin Bruening, Dr. John McCracken, Dr. Jay Siegel, and Dr. Gary Blanchard. I greatly appreciate Merlin's feedback on my dissertation and the time spent truly thinking about the concepts I presented. I was also lucky to have spent several semesters as a teaching assistant under Merlin's guidance, and his trust in my instructional ability only deepened my interest in teaching. I was also fortunate to have the enjoyable experience of teaching for John in my final semester. Jay was also very influential in my graduate studies, by accepting me into the forensic science program and recommending that I pursue a Ph.D. in chemistry. I must also thank Gary for always supporting me and stepping in to join my committee in the final weeks. On a related note, I want to thank Lisa Dillingham, who was always a friend and confidant to me, and who made many difficult situations much more bearable.

I was fortunate enough to work with Heidi Bonta, an amazing undergraduate student, on this work. Heidi worked diligently for three semesters to design and properly characterize a field device for explosives detection. As a B.S. Chemistry major, she managed to fit undergraduate research into her already overloaded schedule. Heidi's creativity and hard work helped us overcome a number of hurdles during this research project, and her enthusiasm and dedication are what made this project so enjoyable. I am greatly appreciative of her hard work and positive attitude, and truly I am very happy to consider her a colleague and a friend.

Lastly, I must thank my friends and family who have supported me

through my time in graduate school. Thanks to Sam and Carl for teaching me so much about what it means to be a Ph.D. student. Thanks to John Goodpaster for numerous emails and phone calls that saved me days of work. Thanks to Amber for sharing in every aspect of being a McGuffin group member, and for becoming one of my best friends. To the other members of the group: Xiaoping, Rashad, Kahsay, Heidi, Lucas, John, and Melissa, for making the everyday tasks more enjoyable. Thanks to Elizabeth, the one person with whom I shared nearly every moment of graduate school and life – I couldn't have done it without you. Thanks to Audrey for being a great scientist, roommate, and friend, and to Anne and Jason for helping me to realize that there's more to life than work. Thanks to Alli, Lucas, Dan, and Lisa for being amazing friends, and knowing when it's about work and when it's not. Thanks to Erin, Sarah, Kristin, and Lisa for keeping me grounded. Thanks to my softball team for keeping me active and sharing lots of memories on and off the field. Thanks to Mom, Dad, Melinda, Jerrod, Matt, Stephanie, Gerri, Don, Geoff, Donna, and Kevin, as well as many other family members, for their willingness to accept my absence at many family events and for their support throughout my graduate career. A special thank you to my parents for believing in me and encouraging me to pursue my goals and dreams from as far back as I can remember. Thanks to my nieces and nephews who just love their Aunt Mel. Lastly, thanks to Andrew, for being by my side unconditionally through this process and for loving me so truly. We have been on an amazing journey through these past few years, and I can't wait for it to continue as I spend the rest of my life with you.

## TABLE OF CONTENTS

<b>LIST OF TABLES .....</b>	<b>xi</b>
<b>LIST OF FIGURES .....</b>	<b>xiii</b>
<b>CHAPTER 1. INTRODUCTION AND BACKGROUND .....</b>	<b>1</b>
1.1 Fluorescence and Fluorescence Quenching .....	1
1.2 Luminescence-Based Methods in Forensic Science .....	6
1.3 Explosives .....	7
1.4 Luminescence-Based Methods for Explosives Detection .....	14
1.4.1 Direct Detection Methods .....	15
1.4.1.1 High-Energy Techniques .....	15
1.4.1.2 Reaction-Based Methods .....	17
1.4.2 Indirect Detection Methods .....	22
1.4.2.1 Quenching of Solution-Phase Fluorophores .....	22
1.4.2.2 Quenching of Immobilized Fluorophores .....	24
1.4.2.3 Quenching by Solid-State Fluorophores .....	31
1.4.2.4 Indirect Laser-Induced Fluorescence .....	38
1.4.2.5 Fluorescence Immunoassay .....	40
1.4.2.6 Reactions Producing Fluorescent Species .....	46
1.5 Research Objectives .....	48
1.6 References .....	50
<b>CHAPTER 2. SOLUTION-PHASE INVESTIGATIONS OF COMMON FLUOROPHORES FOR THE DETECTION OF NITRATED EXPLOSIVES .....</b>	<b>62</b>
2.1 Introduction and Background .....	63
2.1.1 Analysis of Nitrated Explosives .....	63
2.1.2 Solution-Phase Fluorescence Quenching .....	63
2.2 Experimental Methods .....	67
2.2.1 Reagents .....	67
2.2.2 Determination of Quenching Constants .....	67
2.2.3 Determination of Fluorescence Lifetimes .....	70
2.2.4 Determination of Redox Potentials .....	71
2.2.5 Determination of Singlet Excitation Energies .....	72
2.3 Results and Discussion .....	72
2.3.1 Fluorophore Characterization .....	72
2.3.2 Quenching of Pyrene by Nitrated Explosives .....	73
2.3.3 Preliminary Investigation of Selected Fluorophores .....	78
2.3.4 Quenching of Purpurin by Nitrated Explosives .....	78
2.3.5 Quenching of Malachite Green by Nitrated Explosives .....	81
2.3.6 Quenching of Phenol Red by Nitrated Explosives .....	85
2.3.7 Proposed Quenching Mechanism .....	89
2.3.7.1 Fluorescence Lifetimes .....	90

2.3.7.2	Redox Potentials .....	94
2.3.7.3	Singlet Excitation Energies .....	94
2.3.7.4	Comparison to Rehm-Weller Theory .....	96
2.4	Conclusions .....	101
2.5	References .....	103

### **CHAPTER 3. INVESTIGATION OF POTENTIAL FIELD-READY DEVICES FOR THE DETECTION OF NITRATED EXPLOSIVES VIA FLUORESCENCE QUENCHING..... 104**

3.1	Experimental Methods .....	105
3.1.1	Reagents .....	105
3.1.2	Fluorescence Measurements .....	105
3.1.3	Preparation of Solid Substrates .....	106
3.2	Results and Discussion .....	108
3.2.1	Solution-Phase Fluorescence and Quenching .....	108
3.2.2	Solid-Phase Fluorescence .....	115
3.2.3	Poly(ethylene glycol)-Coated Substrates .....	123
3.3	Conclusions and Future Work .....	130
3.4	References .....	131

### **CHAPTER 4. pH-ENHANCED FLUORESCENCE DETECTION OF ACIDS.. 132**

4.1	Introduction and Background .....	132
4.2	Experimental Methods .....	138
4.2.1	Reagents .....	138
4.2.2	Chromatographic System .....	139
4.2.3	Spectroscopic System .....	141
4.3	Results and Discussion .....	142
4.3.1	Method Development and Optimization .....	142
4.3.1.1	Analysis of Test Acids .....	143
4.3.1.2	Chromatographic Optimization .....	148
4.3.1.3	Detector Optimization .....	151
4.3.2	Analysis of Real Samples .....	159
4.3.2.1	Analysis of Grape Juice .....	159
4.3.2.2	Analysis of Wines .....	159
4.3.2.3	Analysis of Vinegars .....	161
4.4	Conclusions .....	168
4.5	References .....	173

### **CHAPTER 5. pH-ENHANCED FLUORESCENCE DETECTION OF $\gamma$ -HYDROXYBUTYRIC ACID IN BEVERAGES ..... 176**

5.1	Introduction and Background .....	177
5.1.1	GHB .....	177
5.1.2	Illicit GHB and Forensic Implications .....	177



5.1.3	Determination of GHB .....	180
5.2	Experimental Methods.....	182
5.2.1	Sample Preparation.....	182
5.2.2	Experimental System.....	184
5.3	Results and Discussion .....	184
5.3.1	GHB Calibration Curve .....	184
5.3.2	Beverage Analysis.....	185
5.3.2.1	GHB in Alcoholic Beverages .....	188
5.3.2.2	GHB in Non-Alcoholic Beverages.....	188
5.3.2.2	Effect of Ethanol on GHB Retention .....	194
5.3.3	Interconversion of GHB to GBL .....	196
5.4	Conclusions .....	196
5.5	References .....	199
<b>CHAPTER 6. CONCLUSIONS AND FUTURE WORK .....</b>		<b>201</b>
<b>APPENDIX. INVESTIGATION OF QUENCHING MECHANISM.....</b>		<b>207</b>
A.1	Determination of Fluorescence Lifetimes .....	207
A.2	Determination of Redox Potentials .....	207
A.3	Determination of Singlet Excited-State Energies.....	211

## LIST OF TABLES

Table 1.1	Common nomenclature for explosives and related compounds.....	9
Table 1.2	Twelve common military explosives and formulations.....	12
Table 2.1	Spectral properties of fluorophores .....	69
Table 2.2	Quenching constants ( $K_d$ ) for pyrene ( <b>1</b> ) with target and interfering quenchers in methanol at room temperature .....	74
Table 2.3	Quenching constants ( $K_d$ ) for fluorophores with nitrobenzene and 4-nitrotoluene in methanol at room temperature .....	77
Table 2.4	Quenching constants ( $K_d$ ) for purpurin ( <b>5</b> ) with target and interfering quenchers in methanol at room temperature .....	79
Table 2.5	Quenching constants ( $K_d$ ) for malachite green ( <b>8</b> ) with target and interfering quenchers in methanol at room temperature.....	82
Table 2.6	Quenching constants ( $K_d$ ) for phenol red ( <b>9</b> ) with target and interfering quenchers in methanol at room temperature.....	86
Table 2.7	Fluorescence lifetimes ( $\tau_f^0$ ) determined for each of the fluorophores at the wavelengths listed in Table 2.1 ( $n = 6$ ). All values determined in methanol at room temperature .....	91
Table 2.8	Quenching rate constants ( $k_d$ ) calculated for each of the fluorophores in methanol at room temperature .....	92
Table 2.9	Electrochemical data for fluorophores and quenchers in methanol at room temperature.....	93
Table 2.10	Spectroscopic data for fluorophores in methanol at room temperature.....	95
Table 2.11	Free energy for electron-transfer ( $\Delta G_{et}$ , eV) from excited-state fluorophore to ground-state quencher (Mechanism I) and electron-transfer from ground-state quencher to excited-state fluorophore (Mechanism II). Boldface type indicates the more thermodynamically favorable mechanism .....	97
Table 3.1	Optimized fluorescence excitation and emission parameters .....	113

Table 4.1	Correlation coefficient ( $R^2$ ) and parameters of fit (a-d) for test acids to sigmoidal function (Equation 4.1) (top) and the corresponding correlation to the sigmoid transform function (Equation 4.2) (bottom).....	146
Table 4.2	Summary of retention factors (k) and $pK_a$ values for standard acids in water .....	150
Table 4.3	Optimization of the flow rate of a 10 mM sodium hydroxide solution. Mobile phase: 0.5 mL/min, pH = 3. Fluorescein: $10^{-4}$ M, 50 $\mu$ L/min .....	153
Table 4.4	Optimization of the PMT voltage. Mobile phase: 0.5 mL/min, pH = 3. Fluorescein: $10^{-4}$ M, 100 $\mu$ L/min. Sodium hydroxide: $10^{-2}$ M, 75 $\mu$ L/min. Integration time: 0.2 s. Slit widths: 0.2 mm. ....	155
Table 4.5	Optimization of the PMT integration time. Mobile phase: 0.5 mL/min, pH = 3. Fluorescein: $10^{-4}$ M, 100 $\mu$ L/min. Sodium hydroxide: $10^{-2}$ M, 75 $\mu$ L/min. PMT: 700 V. Slit widths: 0.1 mm .....	157
Table 4.6	Optimization of the entrance and exit slit widths. Mobile phase: 0.5 mL/min, pH = 3. Fluorescein: $10^{-4}$ M, 100 $\mu$ L/min. Sodium hydroxide: $10^{-2}$ M, 75 $\mu$ L/min. PMT: 700 V. Integration time: 0.2 s .....	158
Table 5.1	Summary of alcoholic and non-alcoholic beverages used in this study .....	183
Table A.1	Parameters used for determination of fluorescence lifetimes.....	208

## LIST OF FIGURES

Figure 1.1	Jablonski diagram depicting absorption (A), vibrational relaxation (VR), fluorescence (F), and static ( $K_s$ ) and dynamic ( $K_d$ ) fluorescence quenching. Solid lines represent radiative transitions, whereas broken lines represent nonradiative transitions. The electronic states shown are for a fluorophore in its singlet ground ( $^1F_0$ ) and excited ( $^1F_1$ ) states and for a fluorophore-quencher complex in its ground ( $(FQ)_0$ ) and excited states for static ( $(FQ)_1$ ) and dynamic ( $^1F_1Q$ ) quenching... .. 3
Figure 1.2	Structures of common nitroaliphatic and nitroaromatic explosives and degradation products. NM (A), DMNB (B), NB (C), $\alpha$ -DNB (D), TNB (E), 2-NT (F), 2,6-DNT (G), 2-am-DNT (H), TNT (I), Picric acid (J), and Tetryl (K) ..... 10
Figure 1.3	Structures of common nitramine, nitrate ester, peroxide, and inorganic explosives. RDX (L), HMX (M), NGU (N), NG (O), PETN (P), EGDN (Q), TATP (R), HMTD (S), and AN (T) ..... 11
Figure 2.1	Structure of fluorophores under investigation. Pyrene (1); 4-Hydroxycoumarin (2); 4-Bromomethyl-7-methoxycoumarin (3); 7-Diethylamino-4-methylcoumarin (4); Purpurin (5), Acridine orange (6); Methylene blue (7); Malachite green (8); Phenol red (9); Rhodamine 6G (10); Fluorescein (11)..... 65
Figure 2.2	Fluorescence spectra of $5 \times 10^{-5}$ M pyrene in methanol at room temperature in the presence of increasing concentrations of 2,6-dinitrotoluene (top) and the resulting Stern-Volmer plot (bottom). The Stern-Volmer constant for this data set is $450 \text{ M}^{-1}$ with a correlation coefficient of 0.9988 ..... 75
Figure 2.3	Fluorescence spectra of $5 \times 10^{-4}$ M purpurin in methanol at room temperature in the presence of increasing concentrations of 2,6-dinitrotoluene (top) and the resulting Stern-Volmer plot (bottom). The Stern-Volmer constant for this data set is $129 \text{ M}^{-1}$ with a correlation coefficient of 0.9907 ..... 80
Figure 2.4	Fluorescence spectra of $2 \times 10^{-4}$ M malachite green in methanol at room temperature in the presence of increasing concentrations of 2,6-dinitrotoluene (top) and the resulting Stern-Volmer plot (bottom). The Stern-Volmer constant for this data set is $56 \text{ M}^{-1}$ with a correlation coefficient of 0.9958 ..... 83
Figure 2.5	Fluorescence spectra of $6 \times 10^{-4}$ M phenol red in methanol at room temperature in the presence of increasing concentrations of 2,6-

	dinitrotoluene (top) and the resulting Stern-Volmer plot (bottom). The Stern-Volmer constant for this data set is $98 \text{ M}^{-1}$ with a correlation coefficient of 0.9979 .....	87
Figure 2.6	Comparison of experimental quenching rate constants for pyrene ( $\diamond$ ), purpurin ( $\circ$ ), malachite green ( $\Delta$ ), and phenol red ( $\square$ ) with target quenchers (filled) and interfering quenchers (unfilled) in methanol with Rehm-Weller theory (-) .....	100
Figure 3.1	Fluorescence spectra of $10^{-4} \text{ M}$ purpurin in water (—), methanol (---), dioxane (—), and hexane (—) at room temperature. Excitation: 325 nm .....	109
Figure 3.2	Fluorescence spectra of $10^{-3} \text{ M}$ malachite green in water (—), methanol (---), dioxane (—), and hexane (—) at room temperature. Excitation: 325 nm.....	110
Figure 3.3	Fluorescence spectra of $10^{-4} \text{ M}$ phenol red in water (—), methanol (---), dioxane (—), and hexane (—) at room temperature. Excitation: 310 nm.....	111
Figure 3.4	Structures of malachite green. Left: Neutral form. Right: Ionic form.....	114
Figure 3.5	Fluorescence spectra of $2 \times 10^{-4} \text{ M}$ malachite green in dioxane at room temperature in the presence of increasing concentrations of nitrobenzene (top) and the resulting Stern-Volmer plot (bottom). The Stern-Volmer constant for this data set is $120 \text{ M}^{-1}$ with a correlation coefficient of 0.9997 .....	116
Figure 3.6	Fluorescence spectra of a KBr pellet (—) and a KBr pellet containing malachite green (—). Excitation: 325 nm .....	117
Figure 3.7	Fluorescence spectra of a Kimwipe (---), filter paper (—), a Grab-it cloth (—), and fiberglass filter paper (—) at room temperature. Excitation: 325 nm. Slit width: 1 mm (top), 5 mm (bottom).....	120
Figure 3.8	Fluorescence spectra of a Kimwipe (---), filter paper (—), and fiberglass filter paper (—) coated with $10^{-3} \text{ M}$ malachite green solution at room temperature. Excitation: 325 nm. Slit width: 5 mm .....	121
Figure 3.9	Fluorescence spectra of filter paper coated with various concentrations of malachite green solutions at room temperature. Excitation: 325 nm. Slit width: 5 mm .....	122

- Figure 3.10** Fluorescence spectra of a glass slide coated with 1 mg malachite green in 2 g PEG 1500 (—) and PEG 2000 (—). Films prepared by using the melting technique. Spectra acquired at room temperature. Excitation: 325 nm. Slit width: 5 mm ..... 125
- Figure 3.11** Fluorescence spectra of filter paper coated with 0.17 mg malachite green and 0.8% (—), 1.6% (—), 4.1% (—), 5.4% (—), 8.1% (—), 16.3% (—), and 40.6% (---) PEG 2000. Percentages refer to the ratio of polymer mass to filter paper mass. Spectra collected at room temperature. Excitation: 325 nm. Slit width: 5 mm. PMT: 950 V (top), 700 V (bottom)..... 127
- Figure 3.12** Fluorescence spectra of 0.1 g silica particles coated with 30% (---) PEG 2000 (w/w), and 0.17 mg malachite green and 10% (---), 20% (—), and 30% (—) PEG 2000 (w/w). Spectra acquired at room temperature. Excitation: 325 nm. Slit width: 0.1 mm. Integration time: 0.1 s ..... 128
- Figure 4.1** Structures of common low-molecular-weight organic acids. Formic acid (1), Acetic acid (2), Lactic acid (3), Oxalic acid (4), Succinic acid (5), Malic acid (6), Tartaric acid (7), Citric acid (8)..... 133
- Figure 4.2** Acid-base equilibria of fluorescein in aqueous solution at room temperature. Molar absorptivity ( $\epsilon$ ) and quantum yield ( $\Phi$ ) are given for each form at the wavelength of maximum absorbance..... 137
- Figure 4.3** Schematic diagram of the experimental system used for determination of LMW organic acids in beverages by liquid chromatography with pH-dependent fluorescence detection. Pump A: Delivery of sample. Pump B: Delivery of 10 mM sodium hydroxide. Pump C: Delivery of 5 mM fluorescein. I = injection valve, L = lens, F = filter, PMT = photomultiplier tube, CCD = charge-coupled device. Dark lines indicate 1/16" stainless steel tubing. Light lines indicate 340- $\mu$ m o.d. capillary tubing ..... 140
- Figure 4.4** Sigmoidal calibration curve for four test acids in water, determined from the fluorescence power of fluorescein at 510 nm. Test acids: hydrochloric acid (●), benzoic acid (○), maleic acid (■), citric acid (□). Non-linear correlation coefficient ( $R^2$ ) = 0.9921 ..... 144
- Figure 4.5** Linear calibration curve following sigmoid transform for four test acids in water, determined from the fluorescence power of fluorescein at 510 nm. Test acids: hydrochloric acid (●), benzoic acid (○), maleic acid (■), citric acid (□). Linear correlation coefficient ( $R^2$ ) = 0.9729..... 147

- Figure 4.6** Chromatogram of common LMW organic acids obtained by UV-absorbance detection (A) and laser-induced fluorescence detection (B). Column: Hypersil ODS, 5- $\mu$ m particles, 250 mm x 4.6 mm. Mobile phase: 99:1 water:methanol, pH 3. Flow rate: 1.0 mL/min. Laser-induced fluorescence detection: 325-nm excitation, 510-nm emission, 10-nm bandpass. UV-absorbance detection: 215 nm. Solutes: oxalic acid (1), tartaric acid (2), formic acid (3), malic acid (4), lactic acid (5), acetic acid (6), citric acid (7), succinic acid (8)..... 149
- Figure 4.7** Chromatogram of grape juice obtained by UV-absorbance detection (A) and laser-induced fluorescence detection (B). Chromatographic conditions as described in Figure 4.6. Solutes: oxalic acid (1), tartaric acid (2), unknown (3), malic acid (4), citric acid (5). ..... 160
- Figure 4.8** Chromatogram of red wine obtained by UV-absorbance detection (A) and laser-induced fluorescence detection (B). Chromatographic conditions as described in Figure 4.6. Solutes: oxalic acid (1), tartaric acid (2), malic acid (3), unknown (4), lactic acid (5), succinic acid (6) ..... 162
- Figure 4.9** Chromatogram of white wine obtained by UV-absorbance detection (A) and laser-induced fluorescence detection (B). Chromatographic conditions as described in Figure 4.6. Solutes: oxalic acid (1), tartaric acid (2), malic acid (3)..... 163
- Figure 4.10** Chromatogram of red wine vinegar obtained by UV-absorbance detection (A) and laser-induced fluorescence detection (B). Chromatographic conditions as described in Figure 4.6. Solutes: oxalic acid (1), tartaric acid (2), malonic acid (3), acetic acid (4), succinic acid (5) ..... 165
- Figure 4.11** Chromatogram of white wine vinegar obtained by UV-absorbance detection (A) and laser-induced fluorescence detection (B). Chromatographic conditions as described in Figure 4.6. oxalic acid (1), tartaric acid (2), unknown (3), acetic acid (4), succinic acid (5)..... 166
- Figure 4.12** Chromatogram of balsamic vinegar obtained by UV-absorbance detection (A) and laser-induced fluorescence detection (B). Chromatographic conditions as described in Figure 4.6. oxalic acid (1), tartaric acid (2), formic acid (3), malonic acid (4), unknown (5), acetic acid (6), fumaric acid (7) ..... 167
- Figure 4.13** Chromatogram of white vinegar obtained by UV-absorbance detection (A) and laser-induced fluorescence detection (B).

	Chromatographic conditions as described in Figure 4.6. oxalic acid (1), acetic acid (2) .....	169
Figure 4.14	Chromatogram of malt vinegar obtained by UV-absorbance detection (A) and laser-induced fluorescence detection (B). Chromatographic conditions as described in Figure 4.6. oxalic acid (1), unknown (2), unknown (3), acetic acid (4) .....	170
Figure 4.15	Chromatogram of rice vinegar obtained by UV-absorbance detection (A) and laser-induced fluorescence detection (B). Chromatographic conditions as described in Figure 4.6. oxalic acid (1), tartaric acid (2), formic acid (3), lactic acid (4), acetic acid (5), succinic acid (6) .....	171
Figure 5.1	Structures of GHB and related compounds. $\gamma$ -hydroxybutyric acid, GHB (1), $\gamma$ -aminobutyric acid, GABA (2), $\gamma$ -butyrolactone, GBL (3), 1,4-butanediol, 1,4-BD (4), $\gamma$ -valerolactone, GVL (5) .....	178
Figure 5.2	Calibration curve for GHB measured in water, calculated by using peak height (●) and peak area (○). Linear regression for peak height: $y = -1.0121x - 0.0165$ ( $R^2 = 0.9961$ ). Linear regression for peak area: $y = -1.0470x - 0.0678$ ( $R^2 = 0.9946$ ). Error bars represent standard deviation of three measurements .....	186
Figure 5.3	Chromatogram of common organic acids and GHB obtained by UV-absorbance detection (A) and laser-induced fluorescence detection (B). Column: Hypersil ODS, 5- $\mu$ m particles, 250 mm x 4.6 mm. Mobile phase: 99:1 water:methanol, pH 3. Flow rate: 1.0 mL/min. Laser-induced fluorescence detection: 325-nm excitation, 510-nm emission, 10-nm bandpass. UV-absorbance detection: 215 nm. Solutes: oxalic acid (1), tartaric acid (2), formic acid (3), malic acid (4), lactic acid (5), acetic acid (6), citric acid (7), GHB (8), succinic acid (9) .....	187
Figure 5.4	Chromatogram of a 12-oz (360-mL) serving of beer spiked with 0.75 g GHB obtained by UV-absorbance detection (A) and laser-induced fluorescence detection (B). Chromatographic conditions as described in Figure 5.3. Solutes: oxalic acid (1), phosphoric acid (2), GHB (3) .....	189
Figure 5.5	Chromatogram of a 6-oz (180-mL) serving of red wine spiked with 0.75 g GHB obtained by UV-absorbance detection (A) and laser-induced fluorescence detection (B). Chromatographic conditions as described in Figure 5.3. Solutes: oxalic acid (1), tartaric acid (2), malic acid (3), lactic acid (4), unknown (5), GHB (6). .....	190



Figure 5.6	Chromatogram of a 1.5-oz (45-mL) serving of rum spiked with 0.25 g GHB obtained by UV-absorbance detection (A) and laser-induced fluorescence detection (B). Chromatographic conditions as described in Figure 5.3. Solutes: oxalic acid (1), lactic acid (2), GHB (3).....	191
Figure 5.7	Chromatogram of a 12-oz (360-mL) serving of cola spiked with 0.75 g GHB obtained by UV-absorbance detection (A) and laser-induced fluorescence detection (B). Chromatographic conditions as described in Figure 5.3. Solutes: phosphoric acid (1), GHB (2).....	192
Figure 5.8	Chromatogram of an 8-oz (240-mL) serving of coffee spiked with 0.75 g GHB obtained by UV-absorbance detection (A) and laser-induced fluorescence detection (B). Chromatographic conditions as described in Figure 5.3. Solutes: oxalic acid (1), formic acid (2), unknown (3), GHB (4) .....	193
Figure 5.9	Chromatogram of 50 mM each GHB and GBL in water obtained by UV-absorbance detection (A) and laser-induced fluorescence detection (B). Chromatographic conditions as described in Figure 5.3.....	197
Figure A.1	Fluorescence decay curves for pyrene (top) and purpurin (bottom). For pyrene (top), $F_0 = 4477$ , $C = 89.88$ , $\tau = 15.3$ ns, $R^2 = 0.9975$ . For purpurin (bottom), $F_0 = 1607$ , $C = 146.8$ , $\tau = 4.00$ ns, $R^2 = 0.9933$ .....	209
Figure A.2	Fluorescence decay curves for malachite green (top) and phenol red (bottom). For malachite green (top), $F_0 = 2157$ , $C = 38.30$ , $\tau = 1.05$ ns, $R^2 = 0.9887$ . For phenol red (bottom), $F_0 = 1554$ , $C = 48.82$ , $\tau = 1.97$ ns, $R^2 = 0.9936$ .....	210
Figure A.3	Cyclic voltammograms for pyrene in 0.1 M $\text{NaNO}_3$ in methanol, with potential scanned cathodically (top) and anodically (bottom).....	212
Figure A.4	Cyclic voltammograms for purpurin in 0.1 M $\text{NaNO}_3$ in methanol, with potential scanned cathodically (top) and anodically (bottom).....	213
Figure A.5	Cyclic voltammograms for malachite green in 0.1 M $\text{NaNO}_3$ in methanol, with potential scanned cathodically (top) and anodically (bottom).....	214

Figure A.6	Cyclic voltammograms for phenol red in 0.1 M NaNO <sub>3</sub> in methanol, with potential scanned cathodically (top) and anodically (bottom).....	215
Figure A.7	Cyclic voltammograms for nitromethane in 0.1 M NaNO <sub>3</sub> in methanol, with potential scanned cathodically (top) and anodically (bottom).....	216
Figure A.8	Cyclic voltammograms for nitrobenzene in 0.1 M NaNO <sub>3</sub> in methanol, with potential scanned cathodically (top) and anodically (bottom).....	217
Figure A.9	Cyclic voltammograms for 2-nitrotoluene in 0.1 M NaNO <sub>3</sub> in methanol, with potential scanned cathodically (top) and anodically (bottom).....	218
Figure A.10	Cyclic voltammograms for 2,6-dinitrotoluene in 0.1 M NaNO <sub>3</sub> in methanol, with potential scanned cathodically (top) and anodically (bottom).....	219
Figure A.11	Cyclic voltammograms for aniline in 0.1 M NaNO <sub>3</sub> in methanol, with potential scanned cathodically (top) and anodically (bottom).....	220
Figure A.12	Cyclic voltammograms for benzoic acid in 0.1 M NaNO <sub>3</sub> in methanol, with potential scanned cathodically (top) and anodically (bottom).....	221
Figure A.13	Cyclic voltammograms for phenol in 0.1 M NaNO <sub>3</sub> in methanol, with potential scanned cathodically (top) and anodically (bottom).....	222
Figure A.14	Normalized absorbance (—) and emission (—) spectra for pyrene (top) and purpurin (bottom). Emission spectra are collected by using the wavelength of maximum absorbance as the excitation wavelength. Singlet excitation energies are determined from the crossing point of the two spectra.....	223
Figure A.15	Normalized absorbance (—) and emission (—) spectra for malachite green (top) and phenol red (bottom). Emission spectra are collected by using the wavelength of maximum absorbance as the excitation wavelength. Singlet excitation energies are determined from the crossing point of the two spectra.....	224

## **CHAPTER 1**

### **INTRODUCTION AND BACKGROUND**

Fluorescence is a sensitive and selective analytical tool that is widely applied in the analytical chemistry community, but is somewhat underutilized among chemists in the forensic science community. Luminescence-based methods have been used in a limited capacity in the determination of drugs of abuse and in trace evidence analysis. One area in which luminescence-based methods are widely used is in the detection of explosives and their degradation products in complex matrices. Direct detection methods utilize the inherent fluorescence of explosive molecules or the luminescence generated from chemical reactions. These methods include high-energy excitation techniques such as gamma-ray and x-ray fluorescence, detection of decomposition products by fluorescence or chemiluminescence, and detection following reduction to amines or other reactions that produce fluorescent products from the explosive. Indirect detection methods utilize the interference with traditional processes of fluorescence caused by the presence of explosive compounds. Indirect detection methods include quenching of solution-phase, immobilized, and solid-state fluorophores, fluorophore displacement, fluorescence immunoassay, and reactions that produce fluorescent products other than the explosive.

#### **1.1 Fluorescence and Fluorescence Quenching**

Fluorescence can be described as the excitation and radiative relaxation of an electron between orbitals of different energies and is traditionally depicted by the Jablonski diagram (Figure 1.1, center). The first step in a fluorescence

event is the absorption of an incident photon of sufficient energy to promote an electron to a higher energy orbital. The molecule releases the excess energy first through vibrational relaxation and then by emission of a photon, leaving the molecule in its ground electronic state. At low concentrations, where the absorbance ( $\epsilon bC$ ) of the fluorophore is less than 0.05, the fluorescence power (F) can be described by

$$F = 2.3K\epsilon bCP_0 \quad (1.1)$$

The constant K is related to the quantum efficiency of the fluorescence process and the efficiency of optical irradiation and collection,  $\epsilon$  is the molar absorptivity of the fluorophore, C is the concentration of the fluorophore, and  $P_0$  is the source power.<sup>2</sup> When the source power is constant, Equation 1.1 is simplified to

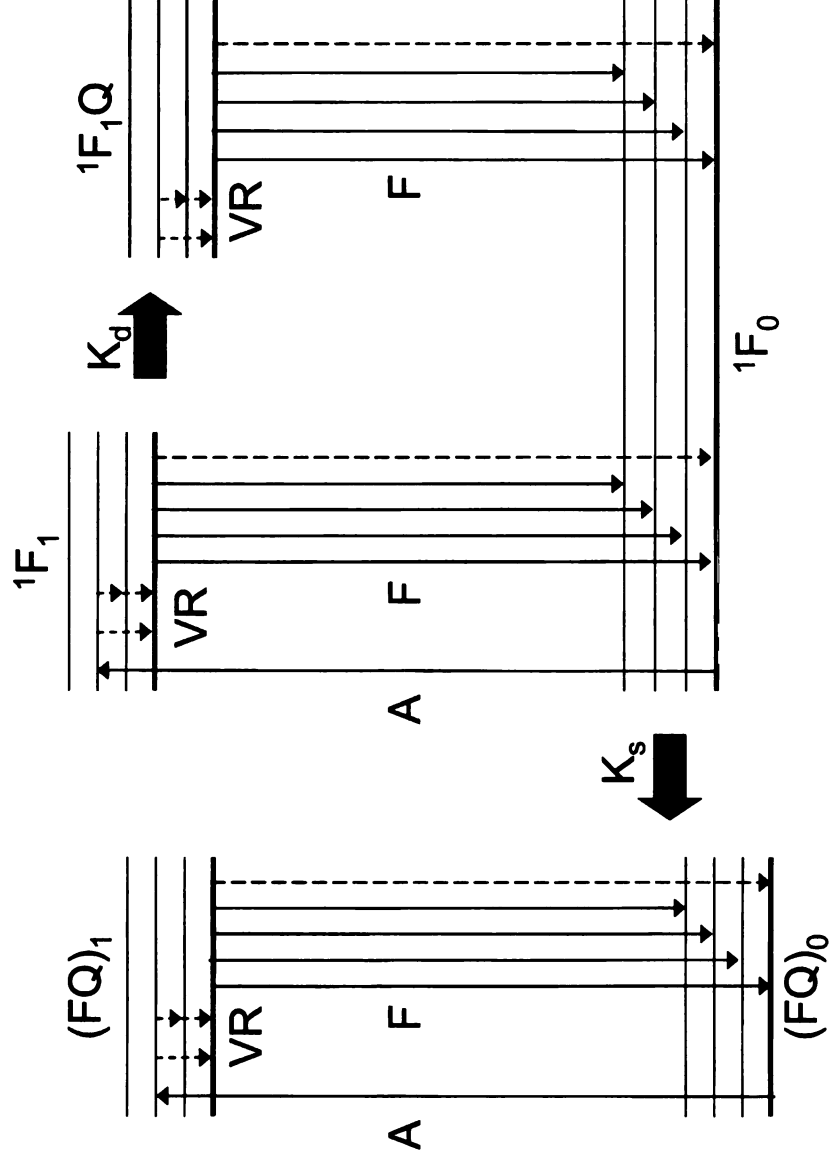
$$F = K'C \quad (1.2)$$

by defining a new constant  $K'$

$$K' = 2.3K\epsilon bP_0 \quad (1.3)$$

When the absorbance is greater than 0.05, the assumptions made in Equations 1.1 and 1.2 are no longer valid and the fluorescence power must be represented by an exponential function.<sup>2</sup>

Fluorescence- or luminescence-based methods offer many benefits over other commonly used techniques. Generally, fluorescence is measured against a low or zero background, as native fluorescence is not common to most chemical species. Fluorescence also demonstrates enhanced sensitivity with



**Figure 1.1.** Jablonski diagram depicting absorption (A), vibrational relaxation (VR), fluorescence (F), and static ( $K_s$ ) and dynamic ( $K_d$ ) fluorescence quenching. Solid lines represent radiative transitions, whereas broken lines represent nonradiative transitions. The electronic states shown are for a fluorophore in its singlet ground ( $1F_0$ ) and excited ( $1F_1$ ) states and for a fluorophore-quencher complex in its ground ( $(FQ)_0$ ) and excited states for static ( $(FQ)_1$ ) and dynamic ( $1F_1Q$ ) quenching.

respect to absorbance methods because the fluorescence power, which is dependent on concentration, is also dependent on the source power.<sup>2</sup> Absorbance methods, in contrast, relate concentration to a ratio of the source power before and after sample interaction. Therefore, the sensitivity of a fluorescence technique can be increased by use of a higher power source, such as a laser. For these reasons, fluorescence methods are typically one to three orders of magnitude more sensitive with expanded linear ranges relative to absorbance-based methods.

Fluorescence quenching is a related technique that allows detection of non-fluorescent species while taking advantage of many of the benefits discussed above. The term "fluorescence quenching" describes any event in which the observed fluorescence signal is decreased.<sup>3</sup> When the decrease in fluorescence results from a change in the optical properties of the sample, the quenching is considered trivial and nonselective.<sup>4</sup> Trivial quenching typically arises from refractive index effects or from primary and secondary absorption, which can be reduced by using a small optical path length of the sample.<sup>5</sup> More selective quenching arises from specific interactions between a non-fluorescent compound, such as an explosive, and a carefully chosen fluorophore. Dynamic quenching involves the transient collisional interaction between an excited-state fluorophore and a ground-state quencher (Figure 1.1, right). In contrast, static quenching involves the formation of a ground-state fluorophore-quencher complex (Figure 1.1, left). Because complex formation between the fluorophore and quencher is required, both dynamic and static quenching are more selective

and, thus, more analytically useful than the trivial mechanisms. By careful choice of fluorophore, the quenching interaction can be tuned to provide selectivity for a variety of analytes and to reduce potential interferences.

Dynamic quenching is described mathematically by the Stern-Volmer equation<sup>6</sup>

$$\frac{\Phi_f^0}{\Phi_f} \approx \frac{F^0}{F} = 1 + k_d \tau_f^0 C_q = 1 + K_d C_q \quad (1.4)$$

where the quantum efficiency of the fluorophore in the absence ( $\Phi_f^0$ ) and presence ( $\Phi_f$ ) of a quencher is related to the Stern-Volmer constant ( $K_d$ ) and the concentration of the quencher ( $C_q$ ). The measured fluorescence power ratio ( $F^0/F$ ) is directly proportional to the quantum efficiency ratio ( $\Phi_f^0 / \Phi_f$ ) when the source power, efficiency of optical irradiation and collection, and fluorophore absorbance remain constant.<sup>4</sup> A graph of the fluorescence power ratio versus the quencher concentration is linear, with a slope equal to the Stern-Volmer quenching constant and an intercept of unity. A similar relationship is observed for static quenching, but the quenching constant is the equilibrium constant for ground-state complex formation between the fluorophore and quencher. The Stern-Volmer constant ( $K_d$ ) can also be expressed as the product of the second-order rate constant for quenching ( $k_d$ ) and the lifetime of the fluorophore in the absence of quencher ( $\tau_f^0$ ). Because dynamic quenching is a collisional process that occurs during the excited-state lifetime of the fluorophore, the fluorescence lifetime changes in the presence of quencher molecules. Hence, measurement

of the fluorescence lifetime in the presence and absence of a quencher can be used to elucidate whether the mechanism is static or dynamic.

## **1.2 Luminescence-Based Methods in Forensic Science**

Luminescence techniques are widely used by forensic biologists, but very few of these methods have been adopted by forensic chemists. One well-known luminescence technique is the detection of blood and body fluids by the oxidation of luminol to produce chemiluminescence.<sup>7</sup> A solution of luminol is sprayed in areas where bloodstains are suspected to occur, and the reaction of iron from heme with luminol is observed at 425 nm in the absence of ambient light. Another common use of fluorescence in forensic science is the visualization of latent fingerprints. When sprayed with a ninhydrin solution, the amino acids contained in the fingerprint residue react to form a ninhydrin dimer that is purple in color.<sup>8</sup> In the presence of a metal salt such as  $\text{ZnCl}_2$  or  $\text{CaCl}_2$ , the dimer forms a metal complex that is fluorescent under visible light (500 – 530 nm).<sup>8</sup> Other reagents for fluorescence detection of latent fingerprints have been developed and include magnetic powders,<sup>9</sup> CdSe–ZnS quantum dots,<sup>10</sup> and 1,2-indanedione.<sup>11</sup> The visualization mechanism has also been adapted for determination of latent lip prints using a solution of Nile Red.<sup>12</sup>

In addition to these commonly used tools, a limited amount of work has investigated the utility of fluorescence-based techniques for analysis of other forensic samples. A number of methods have been identified for determination of drugs of abuse such as amphetamines,<sup>13-20</sup> opiates,<sup>21,22</sup> and hallucinogens<sup>23-26</sup> using native fluorescence,<sup>14-17,24,25</sup> derivatization,<sup>17-23,26-29</sup> and fluorescence



quenching.<sup>13</sup> Although these methods have been reported in the scientific literature, traditional gas chromatography-mass spectrometry and infrared spectroscopy methods are more commonly used in routine forensic analysis of these drugs of abuse. Several luminescence-based methods have also been introduced for trace evidence analysis. Some other unique applications include fluorescence imaging of trace evidence (paints, tapes, adhesives, inks, firearm propellants),<sup>30</sup> age determination from fluorescence of dentin in teeth,<sup>31</sup> and fluorescence imaging of accelerants<sup>32</sup> and gunshot residue.<sup>33</sup> Despite the wide use of luminescence-based methods by analytical chemists, the forensic science community has yet to fully utilize these techniques within state and local laboratories. The analysis of explosives and related compounds, however, is one area in which a variety of luminescence-based techniques have been explored and applied with great success.

### **1.3 Explosives**

The analysis of nitrated explosives is of great importance in a variety of fields.<sup>1</sup> In forensic science, detection of these explosives and their degradation products can be used to identify persons in recent contact with an explosive device.<sup>34</sup> In addition, in environmental chemistry, explosives present in undetonated landmines can leach into and persist in the soil and groundwater, posing a threat to the environment and any living inhabitants.<sup>35,36</sup> In industrial quality control, manufacturers of explosive materials must assure consumers that their products are safe, effective, and free from contamination by monitoring the composition throughout the manufacturing process. Because the requirements

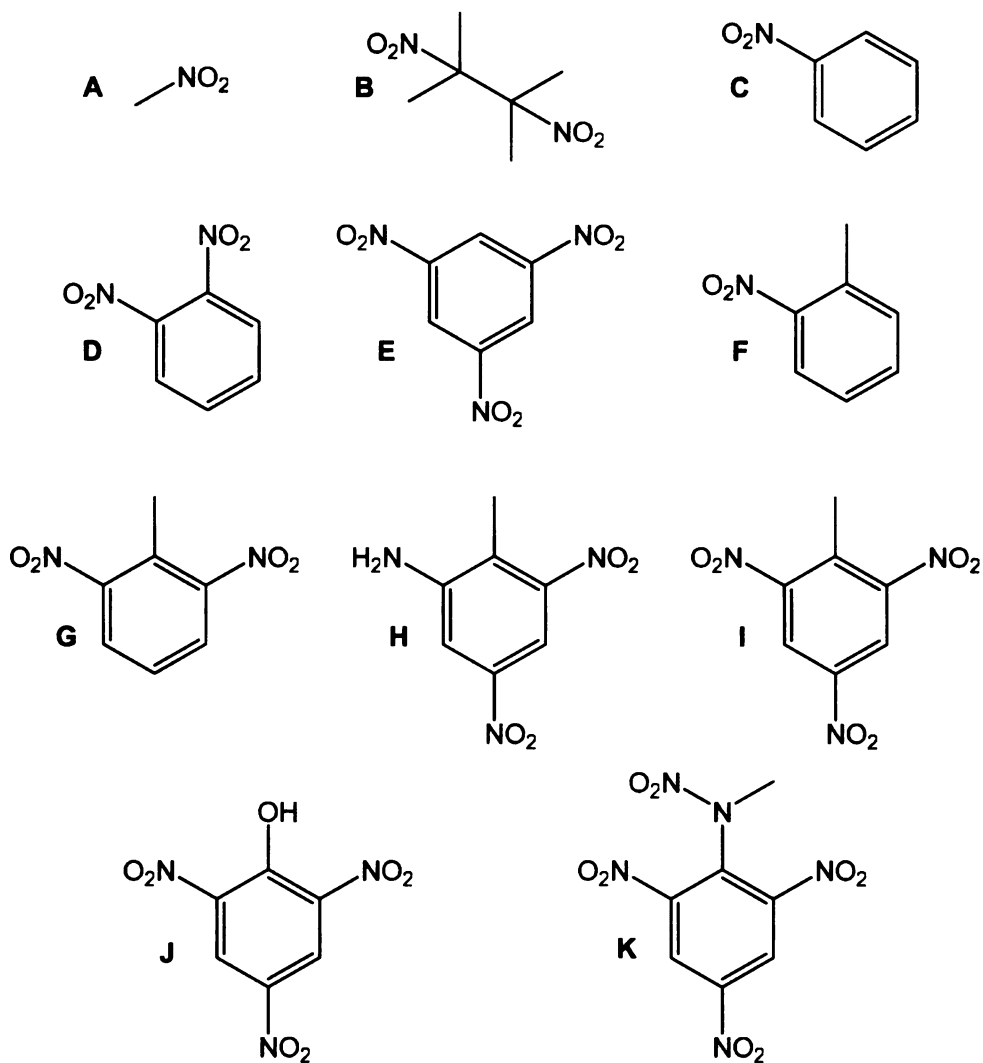
in each of these fields are diverse, a versatile method is needed for the analysis of nitrated explosives.

Of these, the most widely studied are nitrated explosives, including nitroaromatics such as TNT, nitramines such as RDX, and nitrate esters such as PETN (Table 1.1, Figures 1.2-1.3). Military explosives are often composite materials consisting of several of these explosives together with fuels and other excipients (Table 1.2).<sup>1</sup> Extensive characterization of these explosives has led to extremely low detection limits in a laboratory setting. In the field, however, where untrained personnel must identify explosive compounds in the presence of abundant contamination, a simple and effective system is needed to detect these compounds at trace levels. Frequently, detection of hidden explosive devices is difficult owing to the low vapor pressures of many explosives.

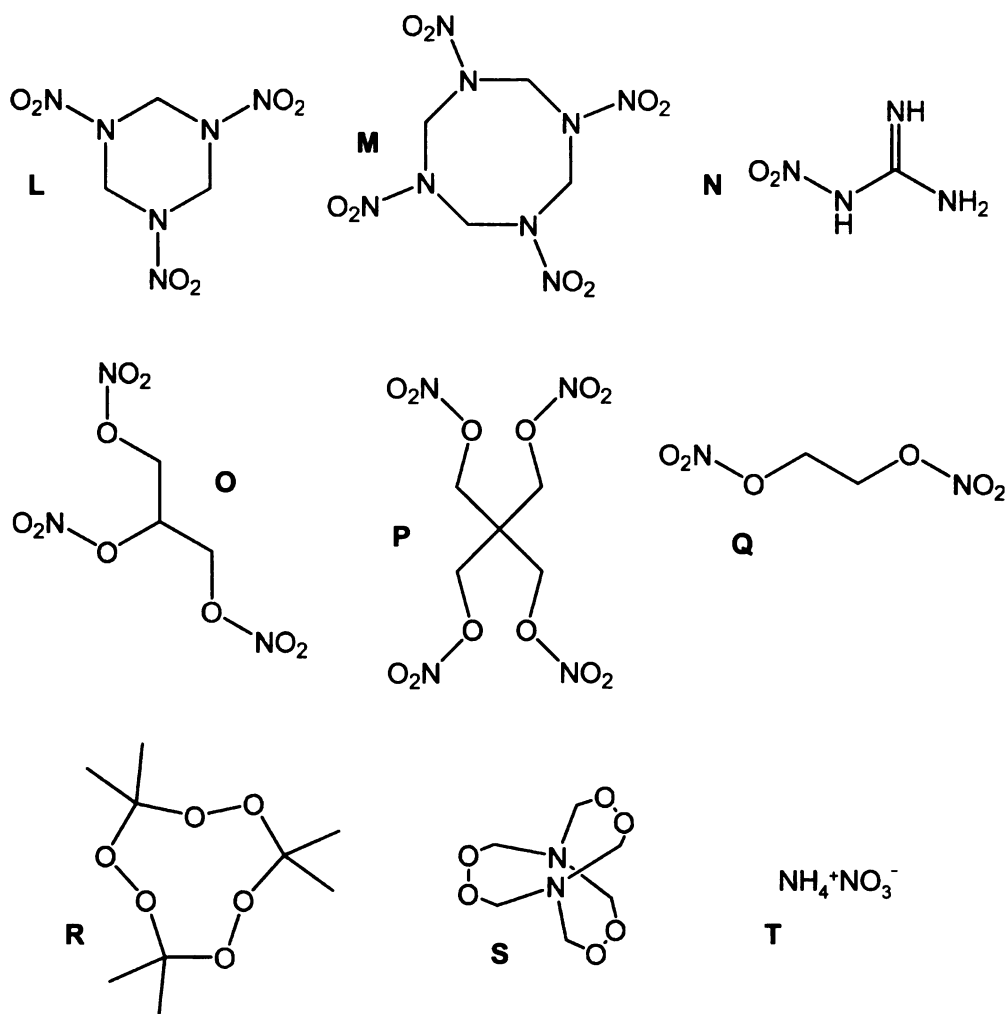
Rising interest in defense and homeland security has led to improved technologies for military explosives detection. These improvements have, in turn, led to increased use of non-nitrated explosive materials.<sup>37</sup> Most recently, liquid or peroxide-based explosives such as TATP and HMTD have been involved in cases of terrorism or drug-related crime (Table 1.1, Figure 1.3).<sup>37-39</sup> Although these compounds are easily synthesized from readily available materials and are comparable in power to TNT, their instability and rapid sublimation make them of little use in military applications. Because these materials are new and significantly different from other classes of explosives, the best methods for their determination have yet to be identified.

**Table 1.1.** Common nomenclature for explosives and related compounds.

Compound	Structural Class	Abbreviation
Nitromethane (A)	Nitroaliphatic	NM
2,3-Dimethyl-2,3-dinitrobutane (B)	Nitroaliphatic	DMNB
Nitrobenzene (C)	Nitroaromatic	NB
<i>o</i> -Dinitrobenzene, <i>m</i> -Dinitrobenzene, <i>p</i> -Dinitrobenzene (D)	Nitroaromatic	DNB
1,3,5-Trinitrobenzene (E)	Nitroaromatic	TNB
2-Nitrotoluene, 3-Nitrotoluene, 4-Nitrotoluene (F)	Nitroaromatic	NT
2,4-Dinitrotoluene, 2,6-Dinitrotoluene (G)	Nitroaromatic	DNT
2-Amino-4,6-dinitrotoluene, 4-Amino-2,6-dinitrotoluene (H)	Nitroaromatic	am-DNT
2,4,6-Trinitrotoluene (I)	Nitroaromatic	TNT
2,4,6-Trinitrophenol (J)	Nitroaromatic	Picric Acid
2,4,6,N-Tetranitro-N-methylaniline (K)	Nitroaromatic/Nitramine	Tetryl
1,3,5-Trinitro-1,3,5-triazacyclohexane (L)	Nitramine	RDX
1,3,5,7-Tetranitro-1,3,5,7-tetraazacyclooctane (M)	Nitramine	HMX
Nitroguanidine (N)	Nitramine	NGU
Nitroglycerin (O)	Nitrate Ester	NG
Pentaerythritol tetranitrate (P)	Nitrate Ester	PETN
Ethylene glycol dinitrate (Q)	Nitrate Ester	EGDN
Triacetone triperoxide (R)	Peroxide	TATP
Hexamethylene triperoxide diamine (S)	Peroxide	HMTD
Ammonium nitrate (T)	Inorganic	AN



**Figure 1.2.** Structures of common nitroaliphatic and nitroaromatic explosives and degradation products. NM (A), DMNB (B), NB (C), *o*-DNP (D), TNB (E), 2-NT (F), 2,6-DNT (G), 2-am-DNT (H), TNT (I), Picric acid (J), and Tetryl (K).



**Figure 1.3.** Structures of common nitramine, nitrate ester, peroxide, and inorganic explosives. RDX (L), HMX (M), NGU (N), NG (O), PETN (P), EGDN (Q), TATP (R), HMTD (S), and AN (T).

**Table 1.2.** Twelve common military explosives and formulations.<sup>1</sup>

<b>Common Name</b>	<b>Formulation</b>
Amatol	TNT + ammonium nitrate
Composition B (Comp B)	RDX + TNT + wax
Composition C-2 (C2)	RDX + TNT +DNT + NT + nitrocellulose + dimethylformamide
Composition C-3 (C3)	RDX + TNT +DNT + NT + Tetryl + nitrocellulose
Composition C-4 (C4)	RDX + polyisobutylene + di(2-ethylhexyl)sebacate + fuel oil
Cyclotol	RDX + TNT
Detasheet	PETN + plasticizer
Octol	HMX + TNT
Pentolite	PETN + TNT
PTX-1	RDX + TNT + Tetryl
PTX-2	RDX + TNT + PETN
Tetrytol	TNT + Tetryl

In the laboratory, nitrated explosives have been separated by thin-layer chromatography,<sup>1,40</sup> gas chromatography,<sup>1,40-45</sup> supercritical fluid chromatography,<sup>1,46</sup> liquid chromatography,<sup>1,5,35,40,47-50</sup> ion chromatography,<sup>1,51</sup> capillary electrophoresis,<sup>34,52</sup> capillary electrochromatography,<sup>53</sup> and micellar electrokinetic chromatography.<sup>36,54</sup> Detection and characterization of nitrated explosives have been accomplished by colorimetric reactions,<sup>1,40,55</sup> densitometry,<sup>1,40</sup> UV absorbance,<sup>1,35,40,47,48,50</sup> infrared spectroscopy,<sup>40,56,57</sup> nuclear magnetic resonance,<sup>1,40</sup> electrochemistry,<sup>1,40,50</sup> immunoassay,<sup>1,40,58-60</sup> mass spectrometry,<sup>1,61,62</sup> ion mobility spectrometry,<sup>1,43,61,62</sup> chemiluminescence,<sup>43-45,58,63</sup> indirect laser-induced fluorescence,<sup>36,53,54,64</sup> and fluorescence quenching.<sup>5,65-74</sup> Unfortunately, many of these methods are difficult to adapt for field use owing to the size of laboratory-scale instrumentation and the need for other accessories that limit portability.

In view of these limitations, explosives are most frequently detected on-site by trained canines<sup>75</sup> or by ion mobility spectrometry.<sup>61</sup> Canines require extensive training and continuous care, and IMS is a destructive technique. Because forensic analyses require confirmation by a second independent technique, sample preservation is critical in cases involving trace quantities of explosive residue. In addition, IMS is plagued by a limited linear dynamic range, interferences from complex matrixes, and poor resolution. Further advances in non-destructive detection techniques for explosives screening will overcome the disadvantages of many of these methods, and can only serve to improve current technology.

## **1.4 Luminescence-Based Methods for Explosives Detection**

As discussed previously, fluorescence- or luminescence-based methods for explosives detection offer many benefits over other common techniques. For example, fluorescence methods are typically one to three orders of magnitude more sensitive than absorbance-based methods. Although mass-spectral techniques are also common for explosives detection, instruments with the required sensitivity have not been developed as field-ready and user-friendly. Fluorescence methods require only a source and detector, both of which can be incorporated easily into a handheld device for field detection of explosives.

Unfortunately, many explosive compounds are not inherently fluorescent. Explosives such as nitramines, nitrate esters, and peroxides have non-conjugated structures that allow efficient vibrational relaxation. Nitroaromatic explosives, despite having aromatic structure, do not fluoresce as a result of the strong electron-withdrawing nature of the nitro substituents. This lack of native fluorescence notwithstanding, many techniques have been proposed in recent years for explosives detection using luminescence-based methods. Several direct techniques have been investigated, such as high-energy excitation methods including gamma resonance technology and x-ray fluorescence. Other direct methods involve reactions to form fluorescent and chemiluminescent products. Indirect methods have also been used in which the fluorescence of a secondary species is quenched by the explosive. Quenching methods have been utilized with solution-phase, immobilized, and solid-state fluorophores. Other indirect methods rely on changes in concentration of a secondary



fluorescent species, including indirect laser-induced fluorescence and fluorescence immunoassay. These methods, as summarized below, have contributed significantly to the current status of field detection of explosives.

#### **1.4.1 Direct Detection Methods**

As discussed previously, explosive compounds are not inherently fluorescent upon excitation by UV or visible light. Despite this limitation, many direct methods have been explored for the determination of explosives. Some techniques utilize high-energy excitation sources, such as x-rays or gamma rays to generate luminescence. Other direct methods involve a chemical reaction resulting in decomposition or the formation of fluorescent products. Decomposition products are detected by fluorescence emission following excitation at deep-UV wavelengths or by using a chemiluminescence reaction with ozone. In all of these methods, the explosive compound or its products are detected as the source of the fluorescence signal.

##### **1.4.1.1 High-Energy Techniques**

X-ray fluorescence (XRF) is a high-energy excitation method that has been investigated for determination of nitrated explosives from a distance without direct contact (i.e., "standoff detection").<sup>76</sup> In this method, a tungsten x-ray source excites the sample and the return fluorescence signature is captured by a germanium crystal detector. Fluorescence profiles are generated by nitro functionalities, where the XRF results from the ejection of an outer-shell electron of a nitrogen atom and replacement by an electron from a higher energy shell ( $E \approx 0.4$  keV). The XRF is increased above the background level of soil or other

components in the surrounding environment in the presence of excess nitrogen atoms from explosives or their residues. XRF spectra have been used for identification of TNT, RDX, PETN, tetryl, C4, Comp B, black powder, smokeless powder, flash powder, ammonium nitrate-fuel oil, detonator cord, and several landmine types. Blair and coworkers report 100% accuracy in field testing for identification of 10 newly buried landmines, and the method is not affected by environmental factors such as wind or presence of vegetation.<sup>76</sup> Explosives residues are also detectable up to six months after removal of the landmine. The current technology allows detection of these explosives from a distance of 2 m.

Gamma resonance technology (GRT) is another high-energy excitation method for detection of nitrated explosives that involves nuclear resonance fluorescence.<sup>77-79</sup> In GRT, monoenergetic gamma rays that match excited levels of  $^{14}\text{N}$  ( $E \approx 9 \text{ MeV}$ ) are produced by in-flight annihilation of fast positrons. When focused on a suspect object, gamma rays are absorbed and reemitted as nuclear fluorescence in areas containing high nitrogen concentrations, such as near the location of a buried landmine. This technology is most useful for scanning large cargo by generation of a real-time, three-dimensional map of nitrogen content as cargo is passed between the source and detector. Although nuclear resonance fluorescence is a potential method for explosives detection, a similar absorbance-based technique has dominated field studies as a result of the higher resonance cross section.<sup>77</sup> Overall, the GRT method is limited by the size of the required instrumentation, namely a particle accelerator and nuclear reaction chambers. Handheld XRF instrumentation is commercially available

(e.g., Thermo Fisher Scientific, Bruker Biosciences, Innov-X Systems, and Oxford Instruments), making XRF the most promising tool of the high-energy excitation methods for explosives detection.

#### 1.4.1.2 Reaction-Based Methods

Another approach to direct luminescence detection is to decompose or fragment the explosive prior to detection. Many of these methods involve decomposition using UV photolysis (220 – 272 nm) or pyrolysis (675 – 1000 K) of the nitrated explosive to NO, followed by measurement of laser-induced fluorescence. The ( $A^2\Sigma^+(v'=0) \leftarrow X^2\Pi_{3/2}(v''=2)$ ) transition of NO is monitored from 245 – 248 nm with excitation at 226 nm by using a frequency-tripled Nd:YAG laser in conjunction with a frequency-doubled dye laser.<sup>80-86</sup> Using photolytic decomposition, reported vapor-phase detection limits are 25 ppb NB,<sup>84</sup> 13 ppb DNB,<sup>82</sup> 3.7 ppb DNT,<sup>82</sup> and 8 ppb TNT.<sup>85</sup> A laboratory detection limit of 40 ppb TNT<sup>81</sup> and a field detection limit of 4 ppm TNT<sup>80</sup> are reported for spiked soil samples. Swayambunathan and coworkers report similar detection limits for TNT, but no signal for RDX and PETN.<sup>86</sup> The authors speculate that the lack of signal is a result of preferential decomposition of RDX and PETN to NO<sub>2</sub> instead of NO. By using low-temperature pyrolysis (300 – 473 K) instead of photolysis to generate NO radicals, low ppm detection limits are reported for RDX and PETN.<sup>86</sup>

Chemiluminescence is an alternative method for NO determination following decomposition of an explosive. Chemiluminescence detection of explosives is most commonly performed with thermal energy analysis (TEA).

The TEA method involves high-temperature pyrolysis (675 – 1000 K) of explosives vapors to produce an NO radical that is oxidized by ozone to form electronically excited nitrogen dioxide ( $\text{NO}_2^*$ ).<sup>87</sup> Upon relaxation, the  $\text{NO}_2^*$  emits at near-infrared wavelengths (600 – 800 nm). Portable explosives detectors based on this technology have been developed at Thermo Electron Corporation and are commercially available.<sup>87-92</sup> The utility of TEA-based field detectors has been reviewed recently,<sup>63,93</sup> and initial studies report ppb and sub-ppb detection limits for nitrated compounds and a linear range extending five orders of magnitude.<sup>44,87-89,94-96</sup> Detection of nitrated explosives in post-blast debris, air samples, solvent extracts of handswabs, and spiked blood has also been successful.<sup>45,90,91,97</sup> Miller and coworkers have also used this technique to map contamination of work areas after sampling with Teflon wipes.<sup>43</sup>

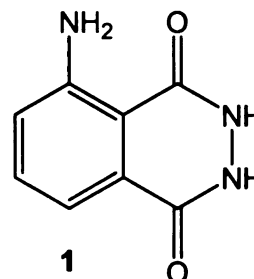
The utility of TEA for detection of explosives following chromatographic separation has also been investigated. Following gas chromatography (GC), a detection limit of 2.6 ppb DNT in a supercritical fluid extract of soil is reported by Francis and coworkers.<sup>98</sup> Crowson and coworkers report low ng detection limits for NG, PETN, TNT, and RDX in solvent extracts of handswabs analyzed by GC-TEA.<sup>99</sup> To further improve sensitivity and selectivity following GC, the blue-green chemiluminescent emission observed upon heating of explosive vapors, rather than the near-infrared emission, has also been investigated.<sup>100</sup> Signals are enhanced in the presence of helium or nitrogen carrier gases. Although no signal is observed for TNT, detection of PETN, RDX, and NG, as well as a

number of related nitrated compounds such as isopropyl nitrate, *n*-propyl nitrate, and ethylnitrate is reported.<sup>100</sup>

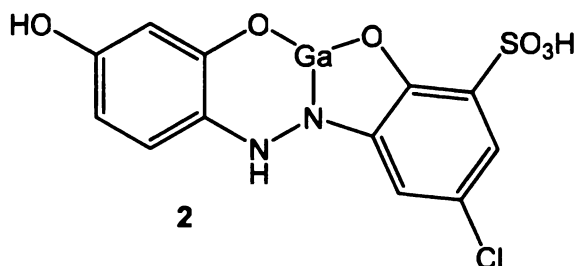
TEA has also been utilized following chromatographic separations using condensed mobile phases. Bowerbank and coworkers report the coupling of TEA with solvating GC, utilizing a packed column with a carbon dioxide mobile phase for determination of DNT, TNT, NG, and PETN.<sup>42</sup> Using TEA, NG detection limits of NG are 10-fold less than those of the common flame-ionization detector, with a linear range from 0.1 – 0.5 ppb NG. Coupling of TEA with capillary supercritical fluid chromatography (SFC) has been investigated by Francis and coworkers<sup>101</sup> and Douse.<sup>46</sup> Following SFC, TEA detection limits are reported in the pg range for TNB, DNT, TNT, tetryl, HMX, RDX, PETN, and NG, with linearity from 1 – 10,000 ppm.<sup>46,101</sup> Explosives detection using TEA has also been adapted for use following liquid chromatography (LC) by Lafleur and Morriseau<sup>102</sup> and Selavka and coworkers.<sup>103</sup> Detection limits of 4 ng RDX and 6 ng PETN are reported, with a linear range extending three orders of magnitude.<sup>102</sup> The major limitation of LC-TEA is that the high temperatures required for pyrolysis of explosives result in increased background noise and decreased sensitivity and selectivity.<sup>103</sup> Selavka and coworkers demonstrate that NO radicals generated by using UV photolysis, rather than pyrolysis, have reduced baseline noise and increased sensitivity for nitroaromatic compounds.<sup>103</sup> Using UV photolysis with LC-TEA, a detection limit of 50 pg TNT is reported.

Detection of nitrite ions ( $\text{NO}_2^-$ ) has also been utilized for determination of nitrated explosives.<sup>104,105</sup> In a method described by Nguyen and coworkers,

nitrite ions are generated by pyrolysis of RDX at temperatures above 673 K. Gaseous nitrite ions oxidize luminol (1) to aminophthalic acid in the presence of sodium sulfite to produce chemiluminescence at 425 nm.<sup>104</sup> The



system is currently designed to signal an alarm in the presence of TNT, RDX, PETN, NG, EGDN, DMNB, and AN. The pyrolysis of TATP also produces oxidizing agents, resulting in the same chemiluminescent reaction and signal generation. In another approach, Lapat and coworkers generate nitrite ions by decomposition of RDX in basic solution at elevated temperature (333 K). In one method, aqueous nitrite ions are reacted with 6-amino-4-chloro-1-phenol-2-sulfonic acid to form a diazonium salt, which reacts with resorcinol and  $\text{Ga}^{3+}$  to form a highly fluorescent lumogallion- $\text{Ga}^{3+}$  complex (2) ( $\lambda_{\text{EX}} = 495 \text{ nm}$ ,  $\lambda_{\text{EM}} = 608 \text{ nm}$ ).<sup>105</sup> Using the fluorescence of this complex, RDX is detectable from

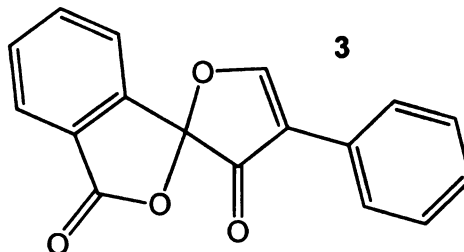


10 ppb to 3 ppm.<sup>105</sup> In a second method, aqueous nitrite ions are reacted with 4-aminofluorescein to form a diazonium salt, which is converted to a highly fluorescent diazotate ( $\lambda_{\text{EX}} = 492 \text{ nm}$ ,  $\lambda_{\text{EM}} = 518 \text{ nm}$ ) in the presence of base. Using this derivatization, RDX is detectable from 5 ppb to 3 ppm.<sup>105</sup>

Another direct method involves reduction of electron-withdrawing nitro substituents on explosives to electron-donating amine substituents, without further decomposition or fragmentation. Replacement with amine groups increases native fluorescence by increasing the electron density of the aromatic

system. Eastwood and coworkers use carbon-nanotube supported Pd particles for reduction of nitroaromatic compounds followed by laser-induced fluorescence ( $\lambda_{\text{EX}} \approx 287 \text{ nm}$ ,  $\lambda_{\text{EM}} \approx 342 \text{ nm}$ ).<sup>106,107</sup>

Alternatively, the amines can be derivatized with fluorescamine (**3**) for more sensitive fluorescence detection ( $\lambda_{\text{EX}} \approx 394 \text{ nm}$ ,  $\lambda_{\text{EM}} \approx$



487 nm).<sup>106,107</sup> Limits of detection as low as 1 pM DNT are achieved by using fluorescamine derivatization.<sup>106</sup>

Bruno and coworkers utilize electrochemiluminescence after complexation to  $\text{Au}^+$  or  $\text{Cu}^{2+}$  ions for determination of diaminotoluenes (DATs).<sup>108</sup> When a current is passed through a solution containing Au-DAT or Cu-DAT, emission from the complex is observed. Detection limits reported for this method are less than 1 ppb for various DATs related to TNT.<sup>108</sup> Mohammadzai and coworkers have developed an extraction and detection method for aminonitroaromatic compounds based on reverse micelle-mediated chemiluminescence (RMM-CL).<sup>109</sup> In this method, the pH of the sample is increased to protonate the amine groups, and chloraurate ions,  $\text{AuCl}_4^-$ , are added as ion pairing agents. The ion pairs are extracted into dichloromethane and introduced into a micelle/luminol mixture. Oxidation of luminol (**1**) to aminophthalic acid by  $\text{AuCl}_4^-$  generates a chemiluminescence signal at 445 nm that is proportional to both the  $\text{AuCl}_4^-$  and aminonitrotoluene concentrations. The detection limits for aminonitrotoluene and dinitroaniline are 0.1  $\mu\text{M}$  with a linear range of 100  $\mu\text{M}$  – 10 mM.

### 1.4.2 Indirect Detection Methods

An alternative approach to luminescence detection of non-fluorescent explosive compounds is measurement of an indirect effect on a secondary fluorescent species. In these indirect methods, the explosive is not involved in the fluorescence process, but affects the fluorescence of another compound. One type of indirect detection method is fluorescence quenching, in which the explosive reduces the fluorescence power of a compound through a collisional interaction or formation of a ground-state complex. Fluorescence quenching has been investigated in both the solution phase and solid phase. Solid-phase materials include fluorescent molecules immobilized on a non-fluorescent support as well as inherently fluorescent solids such as polymers and quantum dots. Other indirect methods have also been used for detection of explosives, including simple spatial or charge-based displacement of a fluorophore, as well as competitive antigen-antibody displacement. Finally, the explosive may undergo reaction with another compound that subsequently becomes fluorescent. In each of these methods, the explosive is not the source of the fluorescence emission, but instead alters the fluorescence of another species.

#### 1.4.2.1 Quenching of Solution-Phase Fluorophores

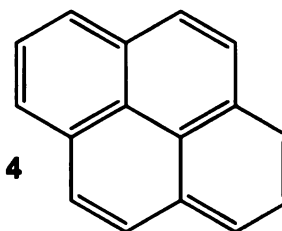
A variety of inorganic and organic fluorophores have been studied in the solution phase for fluorescence quenching detection of nitrated explosives. Bock and coworkers have investigated the quenching of ruthenium tris-bipyridine ( $\text{Ru}(\text{bpy})_3^{2+}$ ) fluorescence ( $\lambda_{\text{EM}} = 620 \text{ nm}$ ) by nitroaromatic compounds in acetonitrile using a standard fluorimeter.<sup>110-112</sup> Quenching is greatest for *m*-DNB



and *p*-DNB, with rate constants of  $10^9 - 10^{10} \text{ M}^{-1} \text{ s}^{-1}$ , but is also observed for NB and *o*-DNB, with rate constants of  $10^3 - 10^5 \text{ M}^{-1} \text{ s}^{-1}$ .<sup>110</sup> The static quenching mechanism involves electron transfer from  $\text{Ru}(\text{bpy})_3^{2+}$  to the nitroaromatic quencher. Although the focus of this work is on the measurement of excited-state redox potentials of  $\text{Ru}(\text{bpy})_3^{2+}$ , the potential of this inorganic fluorophore for the detection of nitrated explosives has clearly been demonstrated.

Glazier and coworkers have expanded on the solution-phase work of Bock and coworkers<sup>110-112</sup> by incorporating  $\text{Ru}(\text{bpy})_3^{2+}$  into poly(amidoamine) (PAMAM) dendrimers.<sup>113</sup> The fluorescence of a solution of  $\text{Ru}(\text{bpy})_3^{2+}$ -modified PAMAM in ethanol ( $\lambda_{\text{EX}} = 450 \text{ nm}$ ,  $\lambda_{\text{EM}} = 575 - 640 \text{ nm}$ ) is quenched by TNT, with a quenching constant of  $2500 \text{ M}^{-1}$ . Relative to TNT, the quenching constant for DNT is 3 to 4 times less at  $700 \text{ M}^{-1}$ , and no quenching is observed for NT. Although this approach may be useful for TNT detection, the inability to detect other related compounds is limiting for field applications.

The solution-phase quenching of organic fluorophores has also been studied.<sup>5,65</sup> Goodpaster and McGuffin report that nitrated explosives are effective quenchers of pyrene (4) fluorescence ( $\lambda_{\text{EX}} = 325 \text{ nm}$ ,  $\lambda_{\text{EM}} = 375 \text{ nm}$ ).



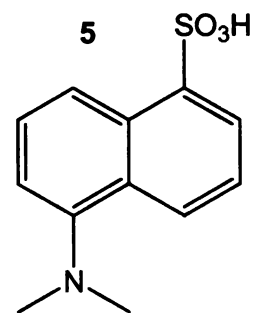
Nitroaromatics are the most efficient quenchers, with rate constants of  $3 \times 10^{10} \text{ M}^{-1} \text{ s}^{-1}$ , as a result of the stable charge-transfer complex that is formed with pyrene.<sup>5</sup> Nitramine and aliphatic explosives also quench the fluorescence of pyrene, but to a lesser extent with rate constants from  $5 \times 10^9 - 1.5 \times 10^{10} \text{ M}^{-1} \text{ s}^{-1}$ . Quenching of pyrene is used as a detection method following

LC with detection limits of 44 ng explosive. Focsaneanu and Scaiano also studied fluorescence quenching of excited-state pyrene by nitrated compounds.<sup>65</sup> These authors compared the quenching of monomer fluorescence ( $\lambda_{\text{EX}} = 355 \text{ nm}$ ,  $\lambda_{\text{EM}} < 400 \text{ nm}$ ) and excimer fluorescence ( $\lambda_{\text{EX}} = 355 \text{ nm}$ ,  $\lambda_{\text{EM}} = 470 \text{ nm}$ ) by nitroaromatic compounds. Similar to the results of Goodpaster and McGuffin, nitroaromatic explosives demonstrate greater quenching than aliphatic explosives. Another solution-phase organic fluorophore with promise for detection of explosives is meso-tetra(4-sulfonatophenyl)porphyrin (TPPS).<sup>114</sup> The fluorescence of TPPS ( $\lambda_{\text{EX}} = 413 \text{ nm}$ ,  $\lambda_{\text{EM}} = 645 \text{ nm}$ ) in pH 7 buffer decreases in the presence of TNT, with a quenching constant on the order of  $10^3 \text{ M}^{-1}$  and a detection limit of 200 ppb TNT. The proposed static quenching mechanism involves binding of TNT to TPPS in a 1:1 ratio. Although pyrene has been identified as the most sensitive and selective fluorophore for quenching detection of nitrated explosives, the less toxic alternatives are more favorable for routine use.

#### 1.4.2.2 Quenching of Immobilized Fluorophores

For greater utility in field detection of explosives by fluorescence quenching, it is beneficial for the fluorophore to be in the solid state. The use of solid-state materials avoids possible leakage and evaporation that can occur when working with solutions.

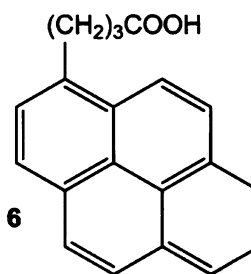
Fang and coworkers have investigated the quenching behavior of dimethylaminonaphthalenesulfonic acid (dansyl) and pyrene



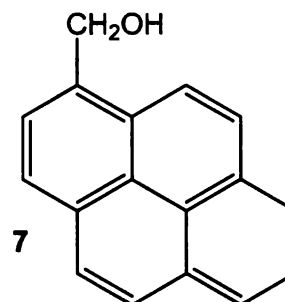
immobilized on glass substrates coated with a self-assembled monolayer for

detection of nitrated explosives.<sup>69,115</sup> The fluorescence of a dansyl (**5**) film ( $\lambda_{\text{EX}} = 340 \text{ nm}$ ,  $\lambda_{\text{EM}} = 505 \text{ nm}$ ) is quenched by aqueous solutions of NB, NT, DNB, and TNT, but not by NM or aromatic compounds such as benzene.<sup>115</sup> The response of this sensor is fast and reversible, with a detection limit of  $1 \mu\text{M}$  TNT in aqueous solution. The fluorescence of a pyrene (**3**) film ( $\lambda_{\text{EX}} = 355 \text{ nm}$ ,  $\lambda_{\text{EM}} = 500 \text{ nm}$ ) is quenched by gaseous TNT, but more significantly by gaseous NB.<sup>69</sup> Again, no interference is observed for the vapors of common organic solvents. In both cases, a static mechanism is proposed based on electron transfer from dansyl or pyrene to the nitrated explosive.

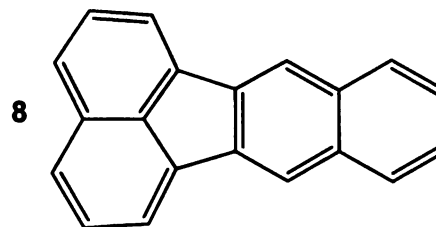
Other pyrene-related compounds have also been utilized for explosives detection by incorporation into membranes or thin films. Jian and Seitz utilized a cellulose acetate polymer membrane containing pyrenebutyric acid (PBA, **6**) for fluorescence quenching detection of explosives.<sup>116</sup> The fluorescence of PBA ( $\lambda_{\text{EX}} = 354 \text{ nm}$ ,  $\lambda_{\text{EM}} = 412 \text{ nm}$ ) is quenched in the presence of aqueous TNT, DNT, and RDX. Despite a slight sensitivity to dissolved oxygen, these sensors are reusable and have detection limits of 2 ppm TNT and DNT and 10 ppm RDX. Because the membrane acts as an extraction device, additional selectivity is gained in the analysis of complex natural water samples. The response time is quite long, however, with a 40-min sample exposure required for constant signal. Pyrenebutyric acid is photostable for 8 hours of continuous exposure to the light source, but some leaching into water is observed after 72 hours. Kumar and coworkers have incorporated



pyrene-based fluorophores into electrospun polymer films for detection of nitroaromatic compounds.<sup>117,118</sup> For PBA ( $\lambda_{\text{EX}} = 275 \text{ nm}$ ,  $\lambda_{\text{EM}} = 395 \text{ nm}$ ) immobilized in poly(4-hydroxybenzyl alcohol), a solution of DNT in dimethylsulfoxide reduces the fluorescence with a quenching constant of approximately  $10^4 \text{ M}^{-1}$ .<sup>118</sup> For 1-pyrenemethanol (**7**,  $\lambda_{\text{EX}} = 350 \text{ nm}$ ,  $\lambda_{\text{EM}} = 450 \text{ nm}$ ) copolymerized with poly(acrylic acid) in an electrospun thin film on a glass slide, the quenching constant for aqueous DNT is even larger at  $10^6 \text{ M}^{-1}$ .<sup>117</sup> For both systems, the quenching is proposed to occur through electron transfer from the pyrene compound to DNT. Of all membrane-bound organic fluorophores, the PBA membrane developed by Jian and Seitz reports the lowest detection limits and is the most useful for aqueous explosive detection.



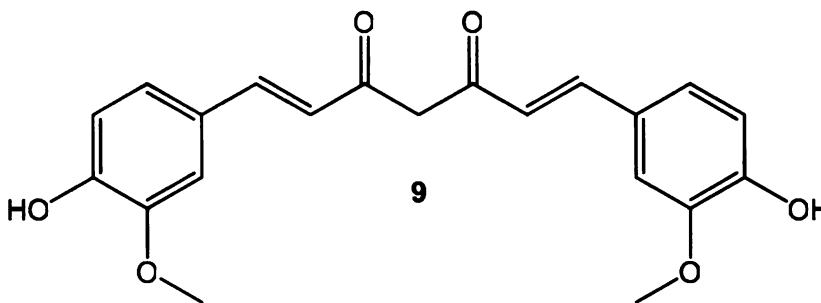
Quenching of benzo[*k*]fluoranthene (**8**), an organic fluorophore similar in structure to pyrene (**4**), is used for explosives detection by Patra and Mishra.<sup>119</sup> Poly(vinyl alcohol) films



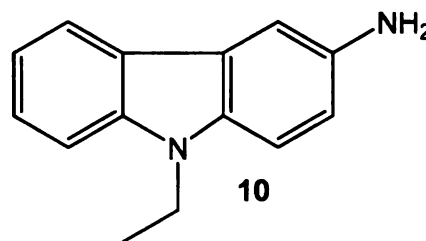
containing benzo[*k*]fluoranthene ( $\lambda_{\text{EX}} = 308 \text{ nm}$ ,  $\lambda_{\text{EM}} = 435 \text{ nm}$ ) supported on a glass slide have been developed. These sensors give a reproducible and reversible response for nitrated explosives, with strong quenching from 0.1 – 1 mM solutions of DNB, NT, nitrobenzoic acid, nitroaniline, nitrobenzobenzene, and nitrophenol in methanol. The sensors are most sensitive to *p*-nitrophenol, with a detection limit of 10  $\mu\text{M}$  in methanol. The greatest interferences are from

acetone (51.6 % quenching relative to 60 mM NB), benzylalcohol (15.6 %), and acrylic acid (11.0 %). The sensors have a response time of 2 – 10 s and some photobleaching of benzo[*k*]fluoranthene is observed after 1 h of constant source exposure.

Other organic fluorophores have also been investigated in an immobilized form for the determination of nitrated explosives. Yu and coworkers have incorporated curcumin (**9**) into a poly(vinyl chloride) membrane for the detection of



nitrophenols such as picric acid.<sup>120</sup> The fluorescence of curcumin ( $\lambda_{\text{EX}} = 426$  nm,  $\lambda_{\text{EM}} = 512$  nm) is quenched most effectively by aqueous *o*-nitrophenol because ground-state complex formation is more sterically hindered by other nitrophenols. The detection limit for this sensor is 0.08 mM *o*-nitrophenol with a linear range of 0.15 – 10 mM. Other nitrophenols are also detected to a lesser degree, including *m*- and *p*-nitrophenol, 2,4-dinitrophenol, and picric acid. Preparation of the sensing film can be simplified by incorporation of a fluorophore directly into the polymer structure. This has been demonstrated by incorporating 3-amino-9-



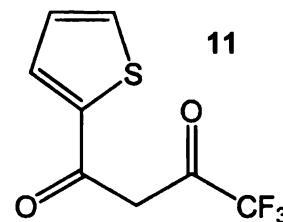
ethylcarbazole (AEC, **10**) ( $\lambda_{\text{EX}} = 275$  nm,  $\lambda_{\text{EM}} = 384$  nm) into the monomer 3-(*N*-methacryloyl) amino-9-ethylcarbazole (MEAC).<sup>121</sup> A thin film is prepared on a

glass slide by copolymerization of MEAC with 2-hydroxypropyl methacrylate. The fluorescence of the film is quenched in the presence of aqueous picric acid through formation of a 1:1 ground-state complex between picric acid and AEC. The quenching response is linear from 10  $\mu$ M – 10 mM picric acid, and no signal is observed for a number of common interferences. In addition, the sensor is stable for more than two months, and leaching of the dye into water is not observed.

Another approach for fluorophore immobilization is by incorporation into a silica monolith. Li and coworkers have developed optical sensors for TNT and related compounds by using this method.<sup>122-124</sup> Using polymer beads as a template, a monolith with a bimodal pore structure is formed on a glass slide. During monolith growth, a porphyrin dye is incorporated into the silica gel matrix, yielding a fluorescent thin film. Upon exposure to saturated TNT vapor (10 ppb), the fluorescence from the porphyrin dye ( $\lambda_{\text{EX}} = 420$  nm,  $\lambda_{\text{EM}} = 660$  nm) is decreased by 50% after 10 s, and is decreased by 97% within 2 min.<sup>124</sup> Quenching is also observed upon exposure to DNT and NB vapors.<sup>123,124</sup> The quenching mechanism is believed to involve hydrogen bonding between porphyrin and the nitro group on the explosives. Incorporation of metallic character into the porphyrin-doped films improves the quenching response of TNT by increasing the binding constant with the film. Films containing Cd are superior for TNT sensing, with 56% quenching within 10 s.<sup>124</sup> In comparison, Zn-containing films demonstrate 43% quenching and undoped films demonstrate 33% quenching in the same amount of time. In all cases, the quenching is

reversible and the fluorescence can be regenerated by purging with nitrogen to remove explosive vapors.

Polymer and silica beads have also been used as a solid support for metal-doped organic fluorophores. Lu and Zhang have developed an optical sensor for aqueous picric acid based on fluorescence quenching of thenoyltrifluoroacetone (TTA, **11**) complexed



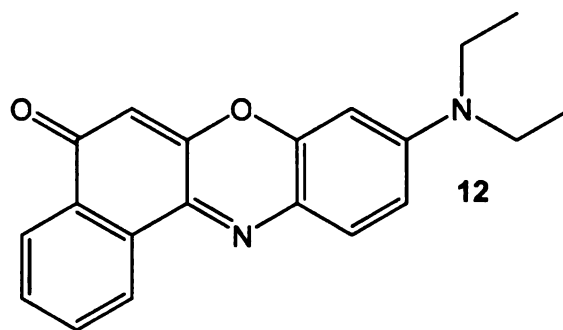
with  $\text{Eu}^{3+}$  immobilized on a chelating resin, Chelex 100.<sup>125</sup>

By coordination of  $\text{Eu}^{3+}$  to the carboxylic acid groups on the poly(styrene-divinylbenzene) resin, water ligands are removed and the luminescence of the film ( $\lambda_{\text{EX}} = 352 \text{ nm}$ ,  $\lambda_{\text{EM}} = 612 \text{ nm}$ ) is increased. Chelation of the hydroxyl group on picric acid to Eu-TTA results in static quenching and fluorescence is decreased. A detection limit of  $2 \mu\text{M}$  picric acid is reported. Sensors utilizing Eu-TTA fluorescence quenching have a lifetime of more than one month and are insensitive to a wide range of interferents including organic acids and inorganic salts.

Sensors containing immobilized fluorophores for analysis of volatile organic compounds<sup>126-129</sup> have been adapted for vapor-phase explosives detection by Walt and coworkers.

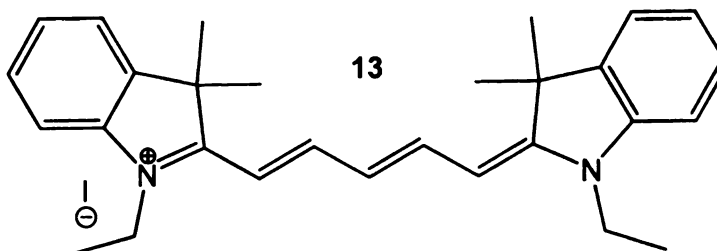
These sensors incorporate Nile Red (**12**) ( $\lambda_{\text{EX}} = 500 \text{ nm}$ ,  $\lambda_{\text{EM}} = 580 \text{ nm}$ ),<sup>130-</sup>

<sup>133</sup> indodicarbocyanine Cy5 (**13**) ( $\lambda_{\text{EX}} = 577 \text{ nm}$ ,  $\lambda_{\text{EM}} = 670 \text{ nm}$ ),<sup>134</sup> and

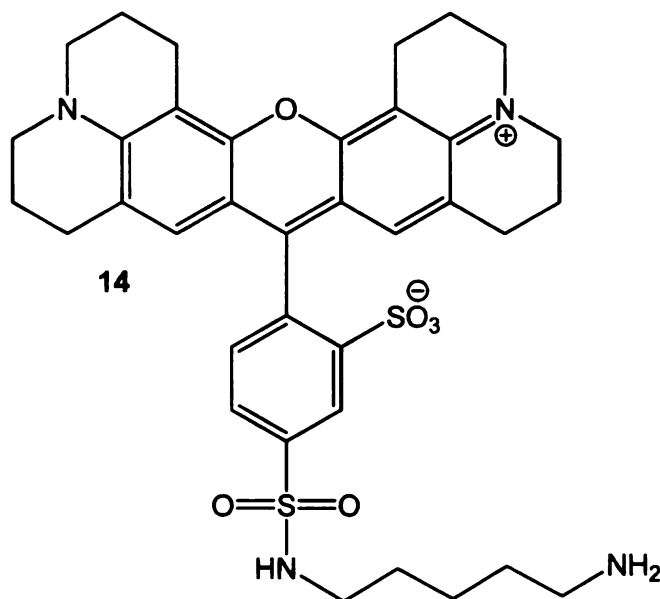


Texas red cadaverine (**14**) ( $\lambda_{\text{EX}} = 577 \text{ nm}$ ,  $\lambda_{\text{EM}} = 610 \text{ nm}$ )<sup>134</sup> into polymer

are fixed onto a glass slide<sup>130,133,135</sup> or onto the end of an optical fiber,<sup>130,131,133,134</sup> which is



exposed to the explosive vapor. The response of the sensor is related to the diffusion of the vapor into the particles and the resulting decrease in fluorescence with time, generating a unique profile for each analyte.<sup>133,134</sup>



complex samples. Using an array of particles allows signal averaging that dramatically decreases the detection limits for explosive compounds.<sup>133</sup> In addition, an array of particles containing several different fluorophores in an electronic nose configuration increases specificity and allows simultaneous detection of multiple explosives.<sup>66,134</sup> These sensors detect nitroaromatic compounds in spiked soil and groundwater samples with detection limits of 50 – 80 ppb DNT.<sup>66</sup> For buried landmine detection, these sensors give no false



positives and have a detection limit of 120 ppb DNT.<sup>66,132</sup> The sensor arrays are also very stable, with a shelf life greater than 10 months.<sup>133</sup>

#### **1.4.2.3 Quenching by Solid-State Fluorophores**

Detection of explosives by quenching of inorganic and organic fluorescent materials is another method under investigation. Quenching of these intrinsically fluorescent materials is similar to quenching of immobilized fluorophores. One example of this method is the visualization of explosives on thin-layer chromatography (TLC) plates containing a fluorescent stationary phase. Fisco describes a portable explosives identification kit based on such visualization.<sup>137</sup> Many commercially-available TLC plates contain a manganese-activated zinc silicate fluorophore ( $\lambda_{\text{EX}} = 254 \text{ nm}$ ,  $\lambda_{\text{EM}} = 525 \text{ nm}$ ). Upon application of explosives to the plate, the explosive absorbs UV light and appears as a dark spot on the fluorescent green background. This mechanism is consistent with trivial quenching, and although it is less selective than other mechanisms, it has been widely utilized in the forensic community for qualitative analysis. Recent work by Meaney and McGuffin describes a quantitative TLC detection method using hand-held UV lamps and digital camera imaging.<sup>138,139</sup> This method yields low microgram detection limits of 12 nitrated explosives and degradation products.

Quenching of photoluminescence from Si nanocrystals, another inorganic material, by nitroaromatic compounds has also been reported.<sup>140</sup> Germanenko and coworkers measure quenching of Si nanocrystals ( $\lambda_{\text{EX}} = 355 \text{ nm}$ ,  $\lambda_{\text{EM}} = 590 - 720 \text{ nm}$ ) in a methanol suspension by adding an aliquot of 0.042

M quencher solution. Quenching is observed for DNB and DNT with rate constants on the order of  $10^6 - 10^7 \text{ M}^{-1} \text{ s}^{-1}$ , but no quenching is observed for NB or NT. A static quenching mechanism is proposed in which an electron is transferred from the conduction band of the Si nanocrystals to the vacant orbitals of the quencher molecules. As a laboratory detection method for nitrated explosives, quenching of Si nanocrystals is very promising. However, because these measurements are made in solution and require a frequency-tripled Nd:YAG laser, the utility of this technique for field detection and sensing of explosives is limited.

Quantum dots are another type of inorganic fluorescent material that has been investigated for detection of explosives. Nieto and coworkers investigated the fluorescence quenching of CdSe quantum dots ( $\lambda_{\text{EX}} = 400 \text{ nm}$ ,  $\lambda_{\text{EM}} = 534 \text{ nm}$ ) in toluene by TNT.<sup>141</sup> The quenching constant for TNT is estimated to be  $10^7 \text{ M}^{-1}$ , and the detection limit using this method is approximately 5 ng TNT. In addition to a decrease in fluorescence, a change in the maximum emission wavelength of the quantum dots is also described. Based on these observations, an energy-transfer mechanism of static quenching is proposed. Similar to the limitations of Si nanocrystals methods, quantum dot quenching measurements are made in solution and require a femtosecond laser, therefore decreasing the utility for field detection and sensing of explosives.

Functionalized carbon nanotubes are another example of nanoparticles that can be used for fluorescence quenching detection of nitrated explosives. Kose and coworkers functionalize well-dispersed carbon nanotubes with a

poly(propionylethylenimine–ethylenimine) copolymer and report fluorescence ( $\lambda_{\text{EX}} = 400 \text{ nm}$ ,  $\lambda_{\text{EM}} = 510 \text{ nm}$ ) as a result of excited-state energy trapping by passivated surface defects.<sup>68</sup> A decrease in the photoluminescence of these nanotubes in methanol is observed in the presence of nitroaromatic compounds such as NB, NT, and DNT. Quenching constants increase from NB to NT to DNT, but the magnitude of quenching constants is small, from  $67 - 132 \text{ M}^{-1}$ . Measurements of fluorescence lifetime indicate a significant contribution from static quenching.

An organometallic material that has been utilized for the fluorescence quenching detection of explosives is a polymetallole or polymeric metallocyclopentadiene.<sup>142</sup> The incorporation of a heavy element from Group 14 into the polymer backbone reduces the band gap and increases fluorescence power. Trogler and coworkers have investigated the potential of porous silicon<sup>143</sup> as well as polymetalloles containing silicon and germanium<sup>70,142,144-146</sup> for the detection of nitrated explosives such as TNT. The fluorescence of porous silicon thin films ( $\lambda_{\text{EX}} = 480 \text{ nm}$ ,  $\lambda_{\text{EM}} = 650 \text{ nm}$ ) is decreased in the presence of explosive vapors in a flowing air stream.<sup>143</sup> Vapor detection limits of 500 ppb NB, 2 ppb DNT, and 1 ppb TNT are reported based on 5 min exposure. The quenching mechanism is believed to be electron transfer from the silicon to the explosive, which is most effective for TNT and DNT as a result of their more positive reduction potentials relative to NB. Because this electron transfer occurs upon adsorption to the silicon surface, high concentrations of NB result in quenching despite the less favorable reduction potential. The authors speculate

that any compound in sufficient concentration is a potential interference and sought improved selectivity for nitrated compounds. Additional specificity, but decreased sensitivity, is observed by incorporation of a  $\text{PtO}_2$  or  $\text{PdO}$  catalyst in the vapor stream to decompose explosives to  $\text{NO}_2$  prior to detection.

Thin films of polymetalloles are more sensitive to quenching than porous silicon films because the conjugated, delocalized structure of the polymer is interrupted by the explosive vapors.<sup>142,144-146</sup> For thin films of poly(tetraphenylsilole) ( $\lambda_{\text{EX}} = 340 \text{ nm}$ ,  $\lambda_{\text{EM}} = 513 \text{ nm}$ ), Trogler and coworkers report quenching constants on the order of  $10^3 \text{ M}^{-1}$  with NB, DNT, and TNT in seawater.<sup>144</sup> Limited interference is reported from organic solvents or inorganic salts. Picric acid demonstrates greater quenching than other nitroaromatics, but the quenching is nonlinear with concentration. Nonetheless, the detection limit for picric acid is 6 ppb in seawater. Modification of the polymetallole to contain a germanium backbone or an alternating Si-Ge backbone leads to comparable or decreased sensitivity relative to the polysilole described above.<sup>145</sup> Fluorescence lifetime studies of these systems indicate that a static mechanism is most probable, and no interferences are observed from organic solvents or inorganic salts. Other polymetallole configurations have also been investigated by Trogler and coworkers for the determination of nitrated explosives.<sup>70,146</sup> By organizing oligomers of polymetalloles into colloidal nanoparticles, quenching efficiency by aqueous TNT is improved, with a detection limit of 100 ppb.<sup>146</sup> As with other polymetalloles, the mechanism for nanoparticle quenching is also static and occurs because TNT disrupts colloidal aggregation. Polymetalloles have also

been sprayed onto non-porous substrates containing explosive contamination and, upon illumination, quenching is observed.<sup>70</sup> These devices are highly portable and field-ready with limited toxicity once prepared. They offer detection limits of 10 ng TNT, 50 ng DNT, and 50 ng picric acid.

Polysiloles have also been modified to contain extensive fluorination, thereby increasing the positive charge on the Si center and increasing attraction to NO<sub>2</sub> groups on explosive molecules.<sup>73,147</sup> Saxena and coworkers report quenching constants for fluorinated polysiloles ( $\lambda_{\text{EX}} = 280 \text{ nm}$ ,  $\lambda_{\text{EM}} = 335 \text{ nm}$ ) on the order of  $10^2 - 10^3 \text{ M}^{-1}$  for picric acid, DNT, TNB, and DNB in tetrahydrofuran solution. For fluorinated polysiloles in a thin film, quenching constants increase to  $10^4 \text{ M}^{-1}$  for picric acid in water.<sup>73,147</sup> Trends in quenching constants for both solutions and thin films of fluorinated polysiloles are consistent with those observed by Trogler and coworkers.<sup>70,142,144-146</sup> The quenching is reversible, and no interference is observed from organic solvents or inorganic acids.

The most widely studied fluorescent materials for detection of nitrated explosives are conjugated fluorescent polymers, first developed by Swager and coworkers.<sup>71,72,148-162</sup> The performance of fluorescent polymers is a result of the “molecular wire” effect, in which the conjugated backbone of the polymer promotes delocalization of electron density and migration of excited-state electrons over large distances.<sup>148,149</sup> The result is an amplified sensor response, where a single molecule of the target analyte can result in quenching of numerous polymer units. The amplified response was verified initially using paraquat, an herbicide and well-known electron-transfer quenching agent.<sup>148</sup>

Many of the original fluorescent polymer materials are iptycene-based and are utilized in a thin film construction. The quenching response of these polymer films to TNT and DNT vapors is dependent on the vapor pressure of the analyte<sup>71,150,151</sup> as well as the charge distribution of both the polymer and analyte.<sup>71,155</sup> Changes to the polymer backbone and side chains cause corresponding changes in the fluorescence properties as well as the quenching response of nitrated explosives. Incorporation of a pentyptycene backbone into the structure of poly(*p*-phenylene ethynylene) (PPE) ( $\lambda_{\text{EX}} = 450 \text{ nm}$ ,  $\lambda_{\text{EM}} = 460 \text{ nm}$ ) and poly(*p*-phenylene butadiynylene) ( $\lambda_{\text{EX}} = 400 \text{ nm}$ ,  $\lambda_{\text{EM}} = 430 \text{ nm}$ ) polymers further amplifies the response, increasing sensitivity and selectivity for TNT.<sup>71,152,161,162</sup> Poly(phenylene) ( $\lambda_{\text{EX}} = 405 \text{ nm}$ ,  $\lambda_{\text{EM}} = 413 \text{ nm}$ ) polymers have also been investigated with some success for the detection of the taggant 2,3-dimethyl-2,3-dinitrobutane (DMNB), which is a required additive in all legally manufactured plastic explosives.<sup>160</sup> Sensitivity is also increased by pumping the polymer films with a nitrogen laser (337 nm) to generate stimulated emission at 535 nm.<sup>72,159</sup> The stimulated emission is disrupted in the presence of TNT vapor, and sub-ppb detection limits are reported.<sup>72,159</sup> In all cases, the quenching of these films is reversible and demonstrates little interference from other aromatic compounds.<sup>71,150-152</sup> Quenching occurs through an electron-transfer mechanism and is dominated by a static interaction between the analyte and the polymer film.<sup>71,72</sup> These polymers have been incorporated into a field-deployable sniffer device (FIDO) through collaboration with Nomadics, Inc.<sup>153-159</sup> The sniffer responds to TNT and degradation products in approximately 5 s, with a detection

limit reported as low as 1 fg TNT in air and soil.<sup>154-158</sup> The sniffer also demonstrates similar selectivity to a trained canine, accurately identifying the presence or absence of a buried mine in 90% of field tests.<sup>154,158</sup> The success of further adaptation of the FIDO device for minefield edge detection is unknown, as appropriate field testing is yet to be completed.<sup>157</sup> Overall, conjugated fluorescent polymers are the state-of-the-art for field detection of explosives and are currently being used by the U.S. military in Iraq.<sup>163</sup> Other conjugated fluorescent polymers have been utilized for detection of explosives with similar reports of sensitivity and detection limits.<sup>67,74,164-166</sup>

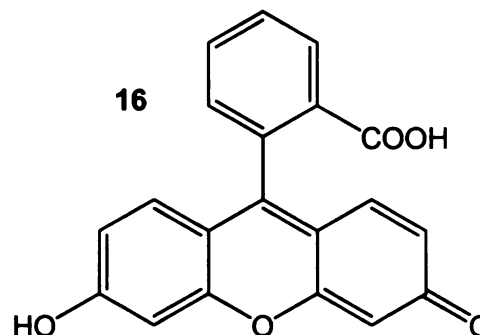
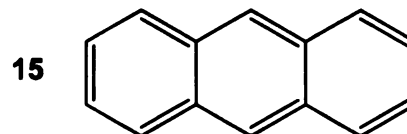
Other developments in the area of conjugated fluorescent polymers have improved the range of applications of these systems for explosives sensing. Simonson and coworkers have developed fluorescent particle sensors for standoff detection of explosives in minefields.<sup>167</sup> Poly(styrene-divinylbenzene) copolymer particles are embedded with a patented PPE polymer as well as *p*-bis(*o*-methylstyryl)-benzene (MSB) as an internal standard. The fluorescence of the PPE component ( $\lambda_{\text{EX}} = 355 \text{ nm}$ ,  $\lambda_{\text{EM}} = 460 \text{ nm}$ ) is generated by using a frequency-tripled Nd:YAG laser and is quenched in the presence of explosives vapors. These fluorescent particles are designed for distribution over soil in areas where contamination is suspected. Quenching of the fluorescence is observed using light detection and ranging (LIDAR) technology, in which decreases in PPE polymer fluorescence (normalized to MSB) indicate the presence of nitroaromatic compounds. The limit of detection using these fluorescent particles is 1 ppm TNT in soil from a distance of 0.5 km, but fresh

particles must be distributed frequently as photodegradation is observed in direct sunlight.

Chen and coworkers found that addition of a cationic surfactant to poly(2,5-methoxypropyloxysulfonate phenylene vinylene), an anionic conjugated polymer, enhances quenching by nitroaromatics while decreasing interference from cationic molecules.<sup>168</sup> Irreversible quenching by DNT is observed down to 1 nM for polymer thin films containing the surfactant, but quenching is more reversible when the polymer and surfactant are arranged in a bilayer structure. These investigations of conjugated polymer modifications broaden the range of polymers that can be used for explosives sensing devices.

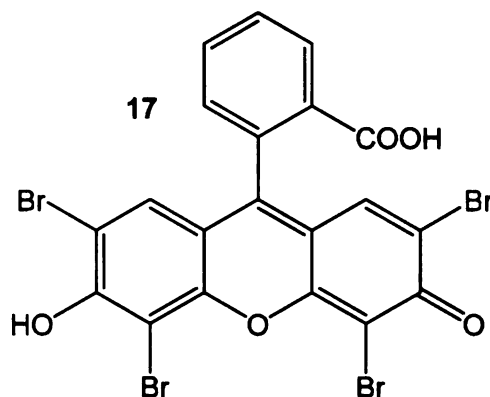
#### 1.4.2.4 Indirect Laser-Induced Fluorescence

Several authors have used indirect laser-induced fluorescence (ILIF) for the determination of various explosives. In this approach, the fluorophore is displaced by the explosive based on either space or charge considerations, leading to a local decrease in fluorescence. Kennedy and coworkers have separated NG, PETN, NGU, EGDN, RDX, HMX, TNT and tetryl using micellar electrokinetic chromatography (MEKC) with detection by ILIF.<sup>54</sup> Four organic fluorophores are investigated for utility as the background fluorophore, including anthracene (15), fluorescein (16), eosin (17) and rhodamine B (18). The fluorophores are added to the



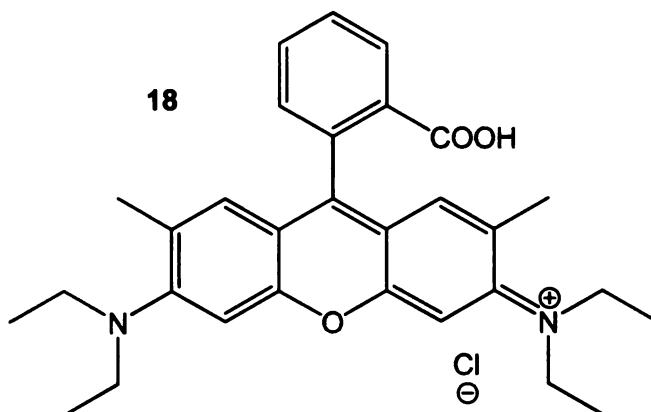


background electrolyte, producing a constant fluorescence upon excitation with an Ar<sup>+</sup> laser at 488 nm and detection at 520 nm. When the fluorophore is contained within the sodium dodecyl sulfate (SDS) micelle, radiative relaxation processes are




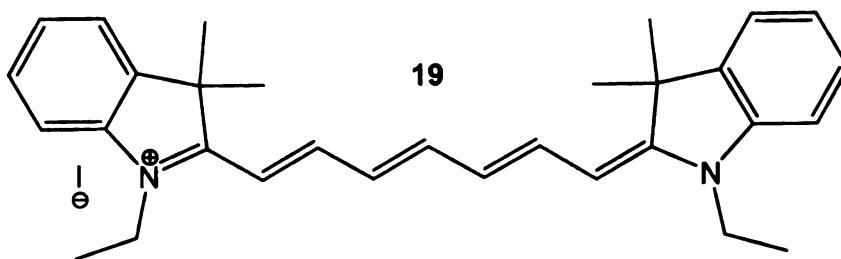
favorable and lead to increased fluorescence. In aqueous solution, explosives preferentially reside within the hydrophobic micelle environment as well. Thus, the presence of the explosives will perturb the equilibrium between the fluorophore and the micelle,

resulting in a change in fluorescence. The authors suggest that some decrease in fluorescence may be the result of quenching by the explosives



in the aqueous phase. The decrease in fluorescence is proportional to the concentration of explosive. To determine the most favorable fluorophore, the quantum yield upon excitation at 488 nm and the effect of the SDS solution on the fluorescence signal is first considered. Anthracene (15) is unsuitable for this application because no fluorescence is observed at 520 nm upon excitation at 488 nm. The fluorescence of eosin (17) decreases in the presence of SDS, while that of fluorescein (16) and rhodamine B (18) increase in the presence of SDS. The authors conclude that because rhodamine B exhibits a more stable baseline,

Bailey and Wallenborg have also developed an ILIF method for detection of explosives following MEKC and capillary electrochromatography (CEC) using cyanine dyes Cy5 (13) and Cy7 (19) to generate the fluorescence


CN(C)C1=C(C2=CC=CC=C2C3=C1C(C)(C)C(C)(C)C3)C=CC=CC=CC=CC=C4C5=CC=CC=C5N(CCC)C4

#### 1.4.2.5 Fluorescence Immunoassay

40

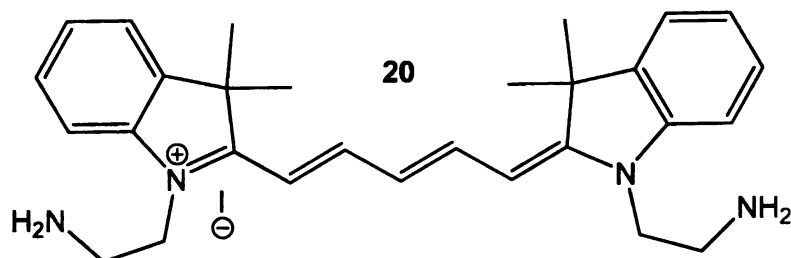
labeled analog of the explosive molecule (antigen). The fluorescence signal changes when explosives in the sample compete for the antibody binding site, thereby displacing the labeled antigen.

Detection of TNT and degradation products has been explored by Bromberg and Mathies by using a solution-phase fluorescence immunoassay in conjunction with capillary electrophoresis (CE) on a microchip or microchannel plate.<sup>52,59</sup> In these studies, anti-TNT antibodies and fluorescein-labeled TNB antigens (**16**) ( $\lambda_{\text{EX}} = 488 \text{ nm}$ ,  $\lambda_{\text{EM}} = 520 \text{ nm}$ ) are added to each sample at constant concentration. For TNT-containing samples, unlabeled TNT binds selectively with the antibody, displacing the labeled antigen. Following separation by CE, the relative intensities of the peaks corresponding to the labeled antigen and the labeled antigen-antibody complex are compared and the amount of displaced antigen is determined. The amount of displaced antigen is directly proportional to the concentration of TNT in the sample, with a detection limit of 1 ppb TNT and a linear range of 1 – 300 ppb TNT.

A similar competitive immunoassay has been utilized for explosive detection by immobilization of the antibody on a solid substrate. Work at the U.S. Naval Research Laboratory (NRL) by Ligler and coworkers has focused on the development of specific and sensitive sensors for TNT and RDX,<sup>169</sup> with detection limits as low as 15 ppt TNT<sup>170</sup> and 10 ppt RDX.<sup>171</sup> Antigens used in these studies are labeled with fluorescein-coupled cadaverine (**16**) ( $\lambda_{\text{EX}} = 490 \text{ nm}$ ,  $\lambda_{\text{EM}} = 520 \text{ nm}$ ), Texas Red cadaverine (**14**) ( $\lambda_{\text{EX}} = 583 \text{ nm}$ ,  $\lambda_{\text{EM}} = 607 \text{ nm}$ ), or cyanine-5-ethylenediamine (**20**) ( $\lambda_{\text{EX}} = 640 \text{ nm}$ ,  $\lambda_{\text{EM}} = 665 \text{ nm}$ ). These

immunoassay systems have been incorporated into a number of field devices. In addition to traditional plate-based

immunosensors,<sup>172</sup> flow immunosensors have

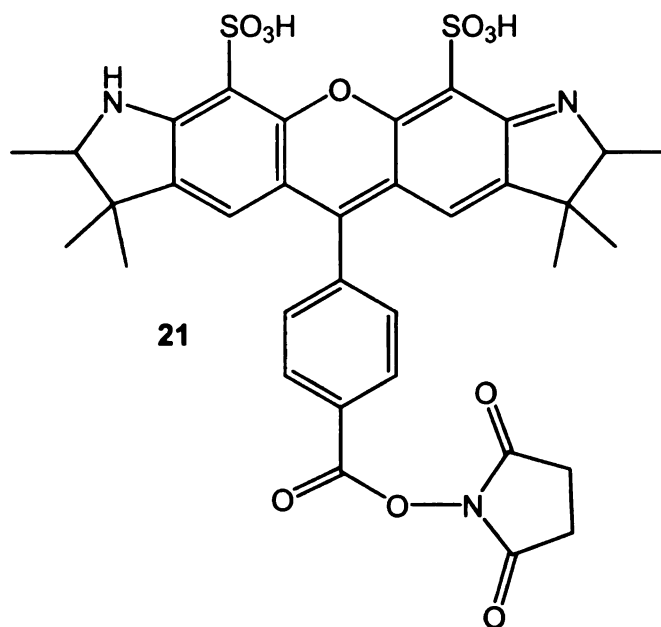


been developed in which the antibody is immobilized on a bead and then packed in a cylindrical tube<sup>169,173-181</sup> or bound to the inner wall of a capillary<sup>60,170,171,181-184</sup> or microchip.<sup>185</sup> Fiber optic probes have also been developed in which the antibody is bound to the surface of an optical fiber, allowing the fluorescence signal to be detected in real time.<sup>186-192</sup> These devices have been tested on real samples including river, harbor, and bilge water,<sup>183,186</sup> tap water,<sup>183</sup> groundwater,<sup>172,178-181,192-195</sup> seawater,<sup>60,175,176,181,195</sup> and soil extracts<sup>172,182,190,196</sup> at low cost and with minimal interference. Improvement in background stability and response of the biosensors is achieved through sample pretreatment by solid-phase extraction.<sup>195</sup> Two devices have been designed and marketed commercially by Research International, Inc. for TNT and RDX detection, including a membrane-based device (FAST 2000) for water analysis<sup>181,193,194,196</sup> and a fiber optic sensor (Analyte 2000).<sup>192</sup> The U.S. Environmental Protection Agency (EPA) has approved Method 4655 for detection of TNT and RDX using the continuous flow immunosensor developed at the NRL.<sup>197</sup> This work has been extended to the detection of PETN utilizing an anti-PETN antibody, with detection limits of 1 ppb.<sup>174,177,183</sup> All flow-based immunosensors have response times less than 1 min. Despite the fast response time and low detection limits,

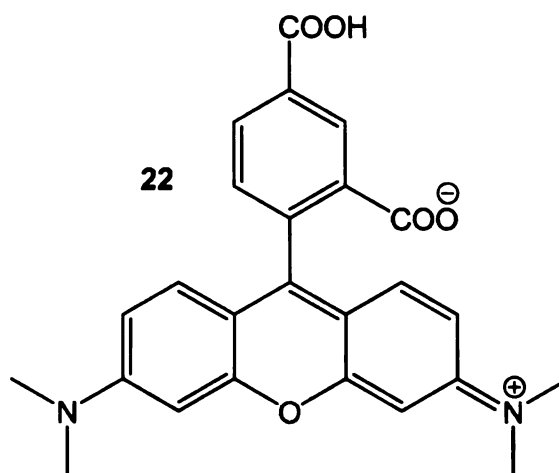
improvements in antibody and antigen stability at elevated temperatures and over long periods of time are necessary to increase the utility of immunosensors.

More recently, work at the NRL by Medintz and coworkers has exploited the strong binding between biotin and avidin for improvements in competitive TNT immunoassay.<sup>198</sup> In these

devices, the anti-TNT antibody and TNB antigen are both contained in a DNA arm, biotinylated, and bound to an avidin surface. In addition, the antibody fragment is labeled with an AlexaFluor 532 donor dye (**21**) ( $\lambda_{\text{EX}} = 520 \text{ nm}$ ,  $\lambda_{\text{EM}} = 555$

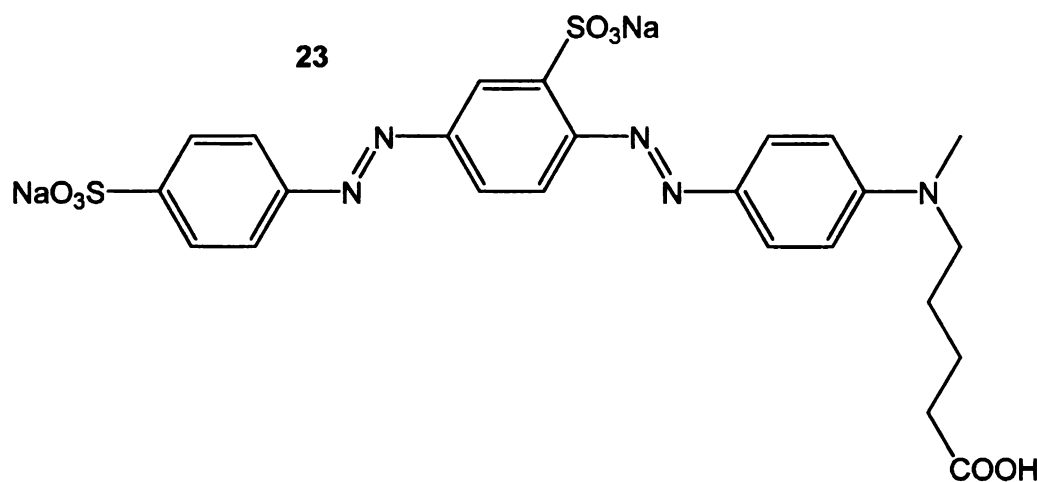


nm) while the antigen fragment is labeled with a carboxytetramethylrhodamine (TAMRA) acceptor dye (**22**) ( $\lambda_{\text{EX}} = 565 \text{ nm}$ ,  $\lambda_{\text{EM}} = 590 \text{ nm}$ ). The fluorescence emission of the system is monitored with excitation at 510 nm and emission at 600 nm. In the absence of TNT, the baseline fluorescence is high due to fluorescence resonance energy transfer (FRET) between the two dye molecules. In the presence of TNT, however, FRET is interrupted and a decrease in the fluorescence signal is



observed. Using this method, TNT degradation products such as TNB, am-DNT, and DNT are also detectable due to their structural similarity to TNT and consequent affinity for the anti-TNT antibody. Limits of detection of 1 ppm TNT and am-DNT, 5 ppb RDX, and 7.5 ppb DNT are reported, with a linear range of 1 – 25 ppm TNT.

A further extension of this work at the NRL by Goldman and coworkers involves the use of CdSe–ZnS quantum dots as the substrate to which the antibody is bound for competitive immunoassay.<sup>199-201</sup> In these sensors, quantum dots ( $\lambda_{\text{EX}} = 400 \text{ nm}$ ,  $\lambda_{\text{EM}} = 530 \text{ nm}$ ) are derivatized with anti-TNT or anti-RDX antibodies, and the TNB antigen is labeled with a dye such as the Black Hole Quencher 10 acceptor (**23**) ( $\lambda_{\text{ABS}} = 530 \text{ nm}$ ).<sup>201</sup> The antibody sites are



saturated with the labeled antigen prior to introduction of the sample. In the absence of TNT, FRET occurs between the quantum dot and the labeled antigen and no fluorescence is observed. In the presence of TNT, however, the labeled antigen is displaced, resulting in an increase in fluorescence from the quantum dot. A small increase in fluorescence is observed for am-DNT and tetryl with the

anti-TNT antibody, although no response is observed for DNT. The sensors are operational in both simulated seawater and soil extracts, with detection limits of 1 ppb RDX<sup>200</sup> and 20 ppt TNT.<sup>199,201</sup>

An electrochemiluminescence enzyme immunoassay for TNT and PETN detection has also been developed.<sup>58</sup> In this method, antibodies corresponding to each explosive are labeled with horseradish peroxidase (HRP) and bound to high-affinity paramagnetic beads through an avidin-biotin linkage. The beads are mixed with a sample containing luminol (1) and are concentrated magnetically onto the gold-coated iron working electrode. Hydrogen peroxide is generated electrochemically by HRP from dissolved oxygen in the solution. As hydrogen peroxide is generated, luminol is oxidized to aminophthalic acid, producing chemiluminescence at 445 nm. When TNT or PETN are present in the sample and bind to their respective antibodies, the activity of HRP is decreased and peroxide generation is suppressed, resulting in a decrease in luminol chemiluminescence. Detection limits for this method are 0.11 ppb TNT and 19.8 ppb PETN.

Another unique approach to a fluorescence immunoassay for the detection of TNT is based on a comparison of the photosynthetic activity of two groups of algae.<sup>202</sup> In this method developed by Altamirano and coworkers, the control algae strain exhibits reduced photosynthetic activity in the presence of TNT, as determined by the fluorescence of chlorophyll. A second strain has been made resistant to TNT and maintains a constant level of chlorophyll production in the presence or absence of TNT. The relative fluorescence of the

two strains can be related to the concentration of TNT with a detection limit of 500 ppb. Although the response time of 3 min is comparable to other immunoassays, this method is less sensitive and less durable than conventional immunoassays.

Another potential immunoassay for determination of nitrated explosives is based on a yeast strain engineered by Radhika and coworkers.<sup>203,204</sup> Preliminary reports indicate that this yeast strain couples olfactory receptor signaling to green fluorescent protein production for detection of DNT.<sup>203</sup> In the presence of DNT, a rat olfactory protein is triggered and increased levels of cyclic adenosine monophosphate (cAMP) are produced. The yeast strain has been engineered to recognize the increased concentration of cAMP and respond through production of a green fluorescent protein ( $\lambda_{\text{EX}} = 485 \text{ nm}$ ,  $\lambda_{\text{EM}} = 535 \text{ nm}$ ). This pioneering work is promising for development of artificial nose technology and field detection of explosives.

#### **1.4.2.6 Reactions Producing Fluorescent Species**

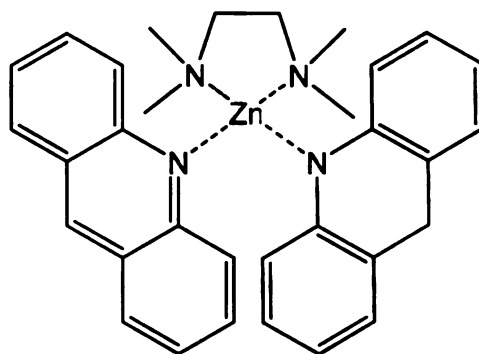
An alternative method for detection of explosives involves the redox reaction of a secondary species by nitrated explosives to generate a fluorescent product. Woltman and coworkers have developed a method in which nitrated explosives are electrochemically reduced to amines following LC separation.<sup>64</sup> These amines are combined post-column with a solution of  $\text{Ru}(\text{bpy})_3^{3+}$ , which is reduced to the highly fluorescent  $\text{Ru}(\text{bpy})_3^{2+}$  ( $\lambda_{\text{EX}} = 488 \text{ nm}$ ,  $\lambda_{\text{EM}} = 600 \text{ nm}$ ). This method is demonstrated using both isocratic and gradient mobile phases with  $\text{Ar}^+$



laser-induced fluorescence, yielding sub-nM TNT detection limits and a linear range from 1 nM to 20  $\mu$ M TNT.

Another related mechanism for detecting explosives involves the use of an analogue of nicotinamide adenine dinucleotide (NADH). Andrew and Swager have designed a sensor material for detection of RDX and PETN based on the fluorescence activation of a Zn analogue of 10-methyl-9,10-dihydroacridine (AcrH<sub>2</sub>).<sup>205,206</sup> The fluorescence of Zn-AcrH<sub>2</sub> increases 80-fold in the presence of

RDX and 25-fold in the presence of PETN upon hydride abstraction to form Zn-AcrH<sup>+</sup> (**24**) ( $\lambda_{\text{EX}} = 313$  nm,  $\lambda_{\text{EM}} = 480$



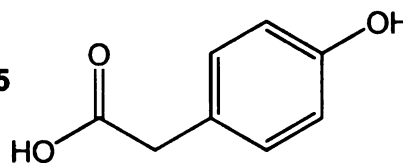
nm). The proposed mechanism involves photoreduction of RDX and PETN by excited-state Zn-AcrH<sub>2</sub> to form Zn-AcrH<sup>+</sup>, which releases a photon upon relaxation.<sup>205</sup> The quantum yield increases linearly with increasing [AcrH<sub>2</sub>], indicating that a single Zn-complexed AcrH<sup>+</sup> is involved in the photoreduction. The reduced forms of RDX and PETN formed during the photoreaction have not been identified, but N-nitroso forms are proposed.<sup>205</sup> The sensor shows no response to nitroaromatic explosives such as TNT, and has no interference from other aromatic organic compounds.

Fluorescence detection of peroxide-based explosives TATP and HMTD has been investigated through the formation of catalytic hydrogen peroxide.<sup>38,39</sup> Schulte-Ladbeck and coworkers use irradiation at 254 nm to decompose aqueous explosive standards or extracts of exploded samples to hydrogen

peroxide. The generated hydrogen peroxide

catalyzes the dimerization of *p*- 25

hydroxyphenylacetic acid (25) in the presence



of horseradish peroxidase. This dimer is highly fluorescent at 405 nm upon excitation with 320 – 325 nm light.<sup>38,39</sup> Detection limits for this method are 0.8

μM TATP and HMTD with a linear dynamic range from 3 – 50 μM TATP and 3 – 100 μM HMTD.<sup>38</sup> Using this method, no false positives or false negatives are

observed among 30 real samples containing potential contaminants such as soil, dust, and cleaning agents.

## 1.5 Research Objectives

Luminescence-based methods are of great importance in the search for a sensitive and selective detector for explosives and other forensically important compounds. A more detailed understanding of the mechanism of interaction between explosives and sensor materials is necessary. This information will aid in the development of new fluorescent materials with an improved ability to detect explosives in complex field settings. The focus of this research has been the identification of new fluorescence quenching interactions that can be used to advance the field of forensic science. The fluorescence quenching response of several solution-phase fluorophores in the presence of nitrated explosives is presented in Chapter 2. For those fluorophores with a sensitive response for nitrated explosives, the quenching mechanism is explored. The most promising fluorophores are incorporated into solid-state materials and their fluorescence properties explored further in Chapter 3. In a second application, the pH-

sensitivity of fluorescein is exploited for the post-column detection of acids in beverages and food products in Chapter 4. This method is expanded to include the forensic detection of GHB in adulterated beverages for alleged sexual assault cases in Chapter 5. This fluorescence quenching work will introduce more luminescence-based applications into the forensic science community and improve current technologies for determination of explosives and drugs of abuse.

## 1.6 References

1. Yinon, J.; Zitrin, S. *Modern Methods and Applications in Analysis of Explosives*; Wiley: Chichester, UK, 1993.
2. Skoog, D. A.; Holler, F. J.; Nieman, T. A. *Principles of Instrumental Analysis*, 5th ed.; Saunders College Publishing: Philadelphia, PA, 1998.
3. Lakowicz, J. *Principles of Fluorescence Spectroscopy*; Plenum Press: New York, NY, 1983.
4. McGuffin, V. L.; Goodpaster, J. V. In *Encyclopedia of Environmental Analysis and Remediation*; Meyers, R., Ed.; Wiley: New York, NY, 1998, pp 3815-3831.
5. Goodpaster, J. V.; McGuffin, V. L. *Anal. Chem.* **2001**, 73, 2004-2011.
6. Goodpaster, J. V.; Harrison, J. F.; McGuffin, V. L. *J. Phys. Chem. A* **2002**, 106, 10645-10654.
7. Lee, H. C. In *Forensic Science Handbook*; Saferstein, R., Ed.; Prentice-Hall, Inc.: Englewood Cliffs, NJ, 1982; Vol. 2.
8. Almog, J.; Levinton-Shamuilov, G.; Cohen, Y.; Azoury, M. *J. Forensic Sci.* **2007**, 52, 330-334.
9. Seah, L. K.; Dinish, U. S.; Phang, W. F.; Chao, Z. X.; Murukeshan, V. M. *Forensic Sci. Int.* **2005**, 152, 249-257.
10. Sametband, M.; Shweky, I.; Banin, U.; Mandler, D.; Almog, J. *Chem. Comm.* **2007**, 1142-1144.
11. Alaoui, I. M.; Menzel, E. R.; Farag, M.; Cheng, K. H.; Murdock, R. H. *Forensic Sci. Int.* **2005**, 152, 215-219.
12. Castello, A.; Alvarez-Segui, M.; Verdu, F. *Forensic Sci. Int.* **2005**, 155, 185-187.
13. Kochana, J.; Wilamowski, J.; Parczewski, A. *Chromatographia* **2004**, 60, 481-484.
14. Concheiro, M.; de Castro, A.; Quintela, O.; Lopez-Rivadulla, M.; Cruz, A. *Forensic Sci. Int.* **2005**, 150, 221-226.
15. Caslavaska, J.; Thormann, W. *Electrophoresis* **2004**, 25, 1623-1631.
16. Nakamura, S.; Tomita, M.; Wada, M.; Chung, H.; Kuroda, N.; Nakashima, K. *Biomed. Chromatogr.* **2006**, 20, 622-627.

17. Alnajjar, A.; Butcher, J. A.; McCord, B. *Electrophoresis* **2004**, *25*, 1592-1600.
18. Wada, M.; Nakamura, S.; Tomita, M.; Nakashima, M. N.; Nakashima, K. *Luminescence* **2005**, *20*, 210-215.
19. Nakamoto, A.; Namera, A.; Nishida, M.; Yashiki, M.; Kuramoto, T.; Takei, Y.; Furuno, M.; Minakuchi, H.; Nakanishi, K.; Kimura, K. *Forensic Toxicol.* **2006**, *24*, 75-79.
20. Tomita, M.; Nakashima, M. N.; Wada, M.; Nakashima, K. *Biomed. Chromatogr.* **2006**, *20*, 1380-1385.
21. Ghazi-Khansari, M.; Zendehdel, R.; Pirali-Hamedani, M.; Amini, M. *Clin. Chim. Acta* **2006**, *364*, 235-238.
22. Pulli, T.; Hoyhtya, M.; Soderlund, H.; Takkinen, K. *Anal. Chem.* **2005**, *77*, 2637-2642.
23. Kato, N.; Kojima, T.; Yoshiyagawa, S.; Ohta, H.; Toriba, A.; Nishimura, H.; Hayakawa, K. *J. Chromatogr. A* **2007**, *1145*, 229-233.
24. Huhn, C.; Pütz, M.; Martin, N.; Dahlenburg, R.; Pyell, U. *Electrophoresis* **2005**, *26*, 2391-2401.
25. Pietsch, J.; Schulz, K.; Körner, B.; Trauer, H.; Dreßler, J.; Gey, M. *Chromatographia* **2004**, *60*, 89-92.
26. Saito, K.; Toyo'oka, T.; Kato, M.; Fukushima, T.; Shirota, O.; Goda, Y. *Talanta* **2005**, *66*, 562-568.
27. Yang, X.; Wang, X.; Zhang, X. *Anal. Chim. Acta* **2005**, *549*, 81-87.
28. Zhou, J.; Xu, X.; Wang, Y. *J. Chromatogr. B* **2007**, *848*, 226-231.
29. Matsuda, K.; Asakawa, N.; Iwanaga, M.; Gohda, A.; Fukushima, S.; Ishii, Y.; Yamada, H. *Forensic Toxicol.* **2006**, *24*, 41-47.
30. Payne, G.; Wallace, C.; Reedy, B.; Lennard, C.; Schuler, R.; Exline, D.; Roux, C. *Talanta* **2005**, *67*, 334-344.
31. Yekkala, R.; Meers, C.; Van Schepdael, A.; Hoogmartens, J.; Lambrichts, I.; Willems, G. *Forensic Sci. Int.* **2006**, *159*, S89-S94.
32. Saitoh, N.; Takeuchi, S. *Forensic Sci. Int.* **2006**, *163*, 38-50.
33. Bird, D. K.; Agg, K. M.; Barnett, N. W.; Smith, T. A. *J. Microsc.* **2007**, *226*, 18-25.

34. Casamento, S.; Kwok, B.; Roux, C.; Dawson, M.; Doble, P. J. *Forensic Sci.* **2003**, *48*, 1075-1083.
35. Gholamian, F.; Chaloosi, M.; Husain, S. W. *Prop. Expl. Pyrotech.* **2002**, *27*, 31-33.
36. Wallenborg, S. R.; Bailey, C. G. *Anal. Chem.* **2000**, *72*, 1872-1878.
37. Schulte-Ladbeck, R.; Vogel, M.; Karst, U. *Anal. Bioanal. Chem.* **2006**, *386*, 559-565.
38. Schulte-Ladbeck, R.; Kolla, P.; Karst, U. *Analyst* **2002**, *127*, 1152-1154.
39. Schulte-Ladbeck, R.; Kolla, P.; Karst, U. *Anal. Chem.* **2003**, *75*, 731-735.
40. Yinon, J.; Zitrin, S. *The Analysis of Explosives*; Pergamon: Elmsford, NY, 1981.
41. Oxley, J.; Smith, J.; Resende, E.; Pearce, E. J. *Forensic Sci.* **2003**, *48*, 742-753.
42. Bowerbank, C. R.; Smith, P. A.; Fetterolf, D. D.; Lee, M. L. *J. Chromatogr. A* **2000**, *902*, 413-419.
43. Miller, C. J.; Glenn, D. F.; Hartenstein, S. D. *Proc. SPIE-Int. Soc. Opt. Eng.* **1998**, *3575*, 335-341.
44. Douse, J. M. F. *J. Chromatogr. A* **1987**, *410*, 181-189.
45. Batlle, R.; Carlsson, H.; Tollback, P.; Colmsjo, A.; Crescenzi, C. *Anal. Chem.* **2003**, *75*, 3137-3144.
46. Douse, J. M. F. *J. Chromatogr. A* **1988**, *445*, 244-250.
47. US Environmental Protection Agency **1994**, Method 8330: Nitroaromatics and Nitramines by High-Performance Liquid Chromatography (HPLC).
48. Gates, P.; Furlong, E.; Dorsey, T.; Burkhardt, M. *Trends Anal. Chem.* **1996**, *15*, 319-325.
49. Doali, J.; Juhasz, A. *J. Chromatogr. Sci.* **1974**, *12*, 51-56.
50. Spiegel, K.; Welsch, T. *Fresenius J. Anal. Chem.* **1997**, *357*, 333-337.
51. Reutter, D.; Buechele, R.; Rudolph, T. *Anal. Chem.* **1983**, *55*, 1468A-1472A.
52. Bromberg, A.; Mathies, R. A. *Anal. Chem.* **2003**, *75*, 1188-1195.

53. Bailey, C. G.; Wallenborg, S. R. *Electrophoresis* **2000**, 21, 3081-3087.
54. Kennedy, S.; Caddy, B.; Douse, J. M. F. *J. Chromatogr. A* **1996**, 726, 211-222.
55. Stevanovic, S.; Mitrovic, M. *Int. J. Environ. Anal. Chem.* **1990**, 40, 69-76.
56. Pristera, F.; Halik, M.; Castelli, A.; Fredericks, W. *Anal. Chem.* **1960**, 32, 495-508.
57. Conduit, C. P. *J. Chem. Soc.* **1959**, 3273-3277.
58. Wilson, R.; Clavering, C.; Hutchinson, A. *Anal. Chem.* **2003**, 75, 4244-4249.
59. Bromberg, A.; Mathies, R. A. *Electrophoresis* **2004**, 25, 1895-1900.
60. Charles, P. T.; Rangasammy, J. G.; Anderson, G. P.; Romanoski, T. C.; Kusterbeck, A. W. *Anal. Chim. Acta* **2004**, 525, 199-204.
61. Eiceman, G. A.; Stone, J. A. *Anal. Chem.* **2004**, 76, 390A-397A.
62. Buryakov, I. A. *J. Chromatogr. B* **2004**, 800, 75-82.
63. Jimenez, A. M.; Navas, M. J. *J. Hazard. Mater.* **2004**, 106, 1-8.
64. Woltman, S. J.; Even, W. R.; Sahlin, E.; Weber, S. G. *Anal. Chem.* **2000**, 72, 4928-4933.
65. Focsaneanu, K.-S.; Scaiano, J. C. *Photochem. Photobiol. Sci.* **2005**, 4, 817-821.
66. Albert, K. J.; Myrick, M. L.; Brown, S. B.; James, D. L.; Milanovich, F. P.; Walt, D. R. *Environ. Sci. Technol.* **2001**, 35, 3193-3200.
67. Kim, T. H.; Kim, H. J.; Kwak, C. G.; Park, W. H.; Lee, T. S. *J. Polym. Sci., Part A: Polym. Chem.* **2006**, 44, 2059-2068.
68. Kose, M. E.; Harruff, B. A.; Lin, Y.; Veca, L. M.; Lu, F.; Sun, Y. P. *J. Phys. Chem. B* **2006**, 110, 14032-14034.
69. Zhang, S.; Lu, F.; Gao, L.; Ding, L.; Fang, Y. *Langmuir* **2007**, 23, 1584-1590.
70. Toal, S. J.; Sanchez, J. C.; Dugan, R. E.; Trogler, W. C. *J. Forensic Sci.* **2007**, 52, 79-83.
71. Yang, J. S.; Swager, T. M. *J. Am. Chem. Soc.* **1998**, 120, 11864-11873.

72. Rose, A.; Zhu, Z.; Madigan, C. F.; Swager, T. M.; Bulovic, V. *Nature* **2005**, *434*, 876-879.
73. Saxena, A.; Fujiki, M.; Rai, R.; Kwak, G. *Chem. Mater.* **2005**, *17*, 2181-2185.
74. Naddo, T.; Che, Y.; Zhang, W.; Balakrishnan, K.; Yang, X.; Yen, M.; Zhao, J.; Moore, J. S.; Zang, L. *J. Am. Chem. Soc.* **2007**, *129*, 6978-6979.
75. Furton, K. G.; Myers, L. J. *Talanta* **2001**, *54*, 487-500.
76. Blair, H. M.; Poteet, W. M. *Proc. SPIE-Int. Soc. Opt. Eng.* **2000**, *4129*, 494-502.
77. Guardala, N. A.; Farrell, J. P.; Dudnikov, V.; Merkel, G. *AIP Conf. Proc.* **2003**, *680*, 905-908.
78. Brondo, J.; Wielopolski, L.; Thieberger, P.; Alessi, J.; Vartsky, D.; Sredniawski, J. *AIP Conf. Proc.* **2003**, *680*, 931-934.
79. Wielopolski, L.; Thieberger, P.; Alessi, J.; Brondo, J.; Vartsky, D.; Sredniawski, J. *AIP Conf. Proc.* **2003**, *680*, 919-923.
80. Boudreaux, G. M.; Miller, T. S.; Kunefke, A. J.; Singh, J. P.; Yueh, F.-Y.; Monts, D. L. *Appl. Opt.* **1999**, *38*, 1411-1417.
81. Wu, D.; Singh, J. P.; Yueh, F. Y.; Monts, D. L. *Appl. Opt.* **1996**, *35*, 3998-4003.
82. Shu, J.; Bar, I.; Rosenwaks, S. *Appl. Phys. B* **2000**, *70*, 621-625.
83. Shu, J.; Bar, I.; Rosenwaks, S. *Appl. Phys. B* **2000**, *71*, 665-672.
84. Shu, J.; Bar, I.; Rosenwaks, S. *Appl. Opt.* **1999**, *38*, 4705-4710.
85. Arusi-Parpar, T.; Heflinger, D.; Lavi, R. *Appl. Opt.* **2002**, *40*, 6677-6681.
86. Swayambunathan, V.; Singh, G.; Sausa, R. C. *Appl. Opt.* **1999**, *38*, 6447-6454.
87. Fine, D. H.; Lieb, D.; Rufeh, F. *J. Chromatogr.* **1975**, *107*, 351-357.
88. Fine, D. H.; Rounbehler, D. P. *J. Chromatogr.* **1975**, *109*, 271-279.
89. Fine, D. H.; Rufeh, F.; Lieb, D.; Rounbehler, D. P. *Anal. Chem.* **1975**, *47*, 1188-1191.
90. Fine, D. H.; Wendel, G. J. *Proc. SPIE-Int. Soc. Opt. Eng.* **1993**, *2092*, 131-136.



91. Fine, D. H.; Yu, W. C.; Goff, E. U.; Bender, E. C.; Reutter, D. J. *J. Forensic Sci.* **1984**, 29, 732-746.
92. Conrad, F. J.; Kenna, B. T.; Hannum, D. W. *Nucl. Mat. Man.* **1990**, 19, 902-905.
93. Moore, D. S. *Rev. Sci. Instrum.* **2004**, 75, 2499-2512.
94. Lafleur, A. L.; Mills, K. M. *Anal. Chem.* **1981**, 53, 1202-1205.
95. Douse, J. M. F. *J. Chromatogr. A* **1983**, 256, 359-362.
96. Collins, D. A. *J. Chromatogr. A* **1989**, 483, 379-383.
97. Douse, J. M. F. *J. Chromatogr. A* **1985**, 328, 155-165.
98. Francis, E. S.; Wu, M.; Farnsworth, P. B.; Lee, M. L. *J. Microcol. Sep.* **1995**, 7, 23-28.
99. Crowson, C. A.; Cullum, H.; Hiley, R. W.; Lowe, A. *J. Forensic Sci.* **1996**, 41, 980-989.
100. Crowson, A.; Hiley, R. W.; Ingham, T.; McCreedy, T.; Pilgrim, A. J.; Townshend, A. *Anal. Comm.* **1997**, 34, 213-216.
101. Francis, E. S.; Eatough, D. J.; Lee, M. L. *J. Microcol. Sep.* **1994**, 6, 395-401.
102. Lafleur, A. L.; Morriseau, B. D. *Anal. Chem.* **1980**, 52, 1313-1318.
103. Selavka, C. M.; Tontarski Jr., R. E.; Strobel, R. A. *J. Forensic Sci.* **1987**, 32, 941-952.
104. Nguyen, D. H.; Locquiao, S.; Huynh, P.; Zhong, Q.; He, W.; Christensen, D.; Zhang, L.; Bilkhu, B. In *Electronic Noses and Sensors for the Detection of Explosives*; Gardner, J. W., Yinon, J., Eds.; Kluwer Academic Publishers: Norwell, MA, 2004, pp 71-80.
105. Lapat, A.; Székelyhidi, L.; Hornyák, I. *Biomed. Chromatogr.* **1997**, 11, 102-104.
106. Eastwood, D.; Fernandez, C.; Yoon, B. Y.; Sheaff, C. N.; Wai, C. M. *Appl. Spectrosc.* **2006**, 60, 958-963.
107. Sheaff, C. N.; Eastwood, D.; Wai, C. M. *Appl. Spectrosc.* **2007**, 61, 68-73.
108. Bruno, J. G.; Cornette, J. C. *Microchem. J.* **1997**, 56, 305-314.

109. Mohammadzai, I. U.; Ashiuchi, T.; Tsukahara, S.; Okamoto, Y.; Fujiwara, T. *J. Chin. Chem. Soc.* **2005**, *52*, 1037-1042.
110. Bock, C. R.; Connor, J. A.; Gutierrez, A. R.; Meyer, T. J.; Whitten, D. G.; Sullivan, B. P.; Nagle, J. K. *J. Am. Chem. Soc.* **1979**, *101*, 4815-4824.
111. Bock, C. R.; Connor, J. A.; Gutierrez, A. R.; Meyer, T. J.; Whitten, D. G.; Sullivan, B. P.; Nagle, J. K. *Chem. Phys. Lett.* **1979**, *61*, 522-525.
112. Bock, C. R.; Meyer, T. J.; Whitten, D. G. *J. Am. Chem. Soc.* **1975**, *97*, 2909-2911.
113. Glazier, S.; Barron, J. A.; Morales, N.; Ruschak, A. M.; Houston, P. L.; Abruna, H. D. *Macromolecules* **2003**, *36*, 1272-1278.
114. Rahman, M.; Harmon, H. J. *Spectrochim. Acta A* **2006**, *65*, 901-906.
115. Kang, J.; Ding, L.; Lu, F.; Zhang, S.; Fang, Y. *J. Phys. D: Appl. Phys.* **2006**, *39*, 5097-5102.
116. Jian, C.; Seitz, W. R. *Anal. Chim. Acta* **1990**, *237*, 265-271.
117. Wang, X.; Lee, S.-H.; Drew, C.; Senecal, K. J.; Kumar, J.; Samuelson, L. A. *Polymer Preprints* **2002**, *43*, 130-131.
118. Kumar, V.; Dhawan, A.; Wang, X.; Parmar, V. S.; Samuelson, L. A.; Kumar, J.; Cholli, A. *Polymer Preprints* **2003**, *44*, 1224-1225.
119. Patra, D.; Mishra, A. K. *Sensor Actuat. B - Chem* **2001**, *80*, 278-282.
120. Wang, Y.; Wang, K.-M.; Shen, G.-I.; Yu, R.-Q. *Talanta* **1997**, *44*, 1319-1327.
121. Hu, X.; Jiao, K.; Sun, W.; You, J.-Y. *Electroanalysis* **2006**, *18*, 613-620.
122. Tao, S.; Li, G.; Zhu, H. *J. Mater. Chem.* **2006**, *16*, 4521-4528.
123. Tao, S.; Li, G. *Colloid Polym. Sci.* **2007**, *285*, 721-728.
124. Tao, S.; Shi, Z.; Li, G.; Li, P. *Angew. Chem. Int. Ed.* **2006**, *7*, 1902-1905.
125. Lu, J.; Zhang, Z. *Anal. Chim. Acta* **1996**, *318*, 175-179.
126. Barnard, S. M.; Walt, D. R. *Environ. Sci. Technol.* **1991**, *25*, 1301-1304.
127. Barnard, S. M.; Walt, D. R. *Nature* **1991**, *353*, 338-340.
128. White, J.; Kauer, J. S.; Dickinson, T. A.; Walt, D. R. *Anal. Chem.* **1996**, *68*, 2191-2202.

129. Johnson, S. R.; Sutter, J. M.; Engelhardt, H. L.; Jurs, P. C.; White, J.; Kauer, J. S.; Dickinson, T. A.; Walt, D. R. *Anal. Chem.* **1997**, *69*, 4641-4648.
130. Albert, K. J.; Dickinson, T. A.; Walt, D. R. *Proc. SPIE-Int. Soc. Opt. Eng.* **1998**, *3392*, 426-431.
131. Dickinson, T. A.; Michael, K. L.; Kauer, J. S.; Walt, D. R. *Anal. Chem.* **1999**, *71*, 2192-2198.
132. Albert, K. J.; Myrick, M. L.; Brown, S. B.; Milanovich, F. P.; Walt, D. R. *Proc. SPIE-Int. Soc. Opt. Eng.* **1999**, *3710*, 308-314.
133. Albert, K. J.; Walt, D. R. *Anal. Chem.* **2000**, *72*, 1947-1955.
134. Michael, K. L.; Taylor, L. C.; Schultz, S. L.; Walt, D. R. *Anal. Chem.* **1998**, *70*, 1242-1248.
135. Stitzel, S. E.; Cowen, L. J.; Albert, K. J.; Walt, D. R. *Anal. Chem.* **2001**, *73*, 5266-5271.
136. Bakken, G. A.; Kauffman, G. W.; Jurs, P. C.; Albert, K. J.; Stitzel, S. S. *Sensor Actuat. B - Chem* **2001**, *79*, 1-10.
137. Fisco, W. J. *Forensic Sci.* **1975**, *20*, 141-148.
138. Meaney, M. S.; McGuffin, V. L. *J. Forensic Sci.* **2007** (submitted).
139. Meaney, M. S., Michigan State University, East Lansing, MI, 2007.
140. Germanenko, I. N.; Li, S.; El-Shall, M. S. *J. Phys. Chem. B* **2001**, *105*, 59-66.
141. Nieto, S.; Santana, A.; Hernandez, S. P.; Lareau, R.; Chamberlain, R. T.; Castro, M. E. *Proc. SPIE-Int. Soc. Opt. Eng.* **2004**, *5403*, 256-260.
142. Toal, S. J.; Trogler, W. C. *J. Mater. Chem.* **2006**, *16*, 2871-2883.
143. Content, S.; Trogler, W. C.; Sailor, M. J. *Chem. Eur. J.* **2000**, *6*, 2205-2213.
144. Sohn, H.; Calhoun, R. M.; Sailor, M. J.; Trogler, W. C. *Angew. Chem. Int. Ed.* **2001**, *40*, 2104-2105.
145. Sohn, H.; Sailor, M. J.; Magde, D.; Trogler, W. C. *J. Am. Chem. Soc.* **2003**, *125*, 3821-3830.
146. Toal, S. J.; Magde, D.; Trogler, W. C. *Chem. Comm.* **2005**, 5465-5467.

147. Saxena, A.; Rai, R.; Kim, S.-Y.; Fujiki, M.; Naito, M.; Okoshi, K.; Kwak, G. *J. Polym. Sci., Part A: Polym. Chem.* **2006**, *44*, 5060-5075.
148. Zhou, Q.; Swager, T. M. *J. Am. Chem. Soc.* **1995**, *117*, 12593-12602.
149. Swager, T. M. *Acc. Chem. Res.* **1998**, *31*, 201-207.
150. Yang, J. S.; Swager, T. M. *J. Am. Chem. Soc.* **1998**, *120*, 5321-5322.
151. Williams, V. E.; Yang, J. S.; Lugmair, C. G.; Miao, Y. J.; Swager, T. M. *Proc. SPIE-Int. Soc. Opt. Eng.* **1999**, *3710*, 402-408.
152. Rose, A.; Lugmair, C. G.; Miao, Y. J.; Kim, J.; Levitsky, I. A.; Williams, V.; Swager, T. M. *Proc. SPIE-Int. Soc. Opt. Eng.* **2000**, *4038*, 512-518.
153. la Grone, M. J.; Cumming, C. J.; Fisher, M.; Reust, D.; Taylor, L. C. *Proc. SPIE-Int. Soc. Opt. Eng.* **1999**, *3710*, 409-420.
154. la Grone, M. J.; Cumming, C. J.; Fisher, M.; Fox, M.; Jacob, S.; Reust, D.; Rockley, M. G.; Towers, E. *Proc. SPIE-Int. Soc. Opt. Eng.* **2000**, *4038*, 553-562.
155. Cumming, C. J.; Aker, C.; Fisher, M.; Fok, M.; la Grone, M. J.; Reust, D.; Rockley, M. G.; Swager, T. M.; Towers, E.; Williams, V. *IEEE T. Geosci. Remote* **2001**, *39*, 1119-1128.
156. Swager, T. M.; Wosnick, J. H. *MRS Bulletin* **2002**, *27*, 446-450.
157. Fisher, M.; Sikes, J. *Proc. SPIE-Int. Soc. Opt. Eng.* **2003**, *5089*, 1078-1087.
158. Cumming, C. J.; Fisher, M.; Sikes, J. In *Electronic Noses & Sensors for the Detection of Explosives*; Gardner, J. W., Yinon, J., Eds.; Kluwer Academic Publishers: Norwell, MA, 2004, pp 53-69.
159. Henry, C. *Chem. Eng. News* **2005**, *83*(16), 11.
160. Thomas III, S. W.; Amara, J. P.; Bjork, R. E.; Swager, T. M. *Chem. Comm.* **2005**, 4572-4574.
161. Zhao, D.; Swager, T. M. *Polymer Preprints* **2005**, *46*, 1194-1195.
162. Zhao, D.; Swager, T. M. *Macromolecules* **2005**, *38*, 9377-9384.
163. Wang, L. *Chem. Eng. News* **2007**, *85*(15), 11.
164. Liu, Y.; Mills, R. C.; Boncella, J. M.; Schanze, K. S. *Langmuir* **2001**, *17*, 7452-7455.

165. Chang, C.-P.; Chao, C.-Y.; Huang, J. H.; Li, A.-K.; Hsu, C.-S.; Lin, M.-S.; Hsieh, B. R.; Su, A.-C. *Synth. Met.* **2004**, *144*, 297-301.
166. Levitsky, I. A.; Euler, W. B.; Tokranova, N.; Rose, A. *Appl. Phys. Lett.* **2007**, *90*, 041904-041903.
167. Simonson, R. J.; Hance, B. G.; Schmitt, R. L.; Johnson, M. S.; Hargis Jr., P. J. *Proc. SPIE-Int. Soc. Opt. Eng.* **2001**, *4394*, 879-889.
168. Chen, L.; McBranch, D.; Wang, R.; Whitten, D. *Chem. Phys. Lett.* **2000**, *330*, 27-33.
169. Whelan, J. P.; Kusterbeck, A. W.; Wemhoff, G. A.; Bredehorst, R.; Ligler, F. S. *Anal. Chem.* **1993**, *65*, 3561-3565.
170. Narang, U.; Gauger, P. R.; Ligler, F. S. *Anal. Chem.* **1997**, *69*, 1961-1964.
171. Charles, P. T.; Kusterbeck, A. W. *Biosens. Bioelect.* **1999**, *14*, 387-396.
172. Goldman, E. R.; Cohill, T. J.; Patterson, C. H.; Anderson, G. P.; Kusterbeck, A. W.; Mauro, J. M. *Environ. Sci. Technol.* **2003**, *37*, 4733-4736.
173. Judd, L. L.; Kusterbeck, A. W.; Charles, P. T.; Ligler, F. S.; Whelan, J. P.; Foster, K. E. *The Flow Immunosensor Used to Detect the Small Molecular Weight Molecule TNT*; Air and Waste Management Association: Pittsburgh, PA, 1993.
174. Kusterbeck, A. W.; Gauger, P. R.; Charles, P. T. *Proc. SPIE-Int. Soc. Opt. Eng.* **1997**, *2937*, 191-196.
175. Green, T. M.; Charles, P. T.; Anderson, G. P. *Anal. Biochem.* **2002**, *310*, 36-41.
176. Goldman, E. R.; Pazirandeh, M. P.; Charles, P. T.; Balighian, E. D.; Anderson, G. P. *Anal. Chim. Acta* **2002**, *457*, 13-19.
177. Kusterbeck, A. W.; Judd, L. L.; Yu, H.; Myles, J.; Liger, F. S. *Proc. SPIE-Int. Soc. Opt. Eng.* **1993**, *2092*, 218-226.
178. Charles, P. T.; Bart, J. C.; Judd, L. L.; Gauger, P. R.; Ligler, F. S.; Kusterbeck, A. W. *Proc. SPIE-Int. Soc. Opt. Eng.* **1997**, *3105*, 80-87.
179. Bart, J. C.; Judd, L. L.; Kusterbeck, A. W. *Sensor Actuat. B - Chem* **1997**, *39*, 411-418.
180. Bart, J. C.; Judd, L. L.; Hoffman, K. E.; Wilkins, A. M.; Kusterbeck, A. W. *Environ. Sci. Technol.* **1997**, *31*, 1505-1511.

181. Shriver-Lake, L.; Charles, P.; Kusterbeck, A. *Anal. Bioanal. Chem.* **2003**, 377, 550-555.
182. Narang, U.; Gauger, P. R.; Ligler, F. S. *Anal. Chem.* **1997**, 69, 2779-2785.
183. Judd, L. L.; Kusterbeck, A. W.; Conrad, D. W.; Yu, H.; Jr., H. L. M.; Ligler, F. S. *Proc. SPIE-Int. Soc. Opt. Eng.* **1995**, 2388, 198-204.
184. Narang, U.; Gauger, P. R.; Kusterbeck, A. W.; Ligler, F. S. *Anal. Biochem.* **1998**, 255, 13-19.
185. Holt, D. B.; Gauger, P. R.; Kusterbeck, A. W.; Ligler, F. S. *Biosens. Bioelect.* **2002**, 17, 95-103.
186. Shriver-Lake, L. C.; Breslin, K. A.; Charles, P. T.; Conrad, D. W.; Golden, J. P.; Ligler, F. S. *Anal. Chem.* **1995**, 67, 2431-2435.
187. Bakaltcheva, I. B.; Shriver-Lake, L. C.; Ligler, F. S. *Sensors and Actuators B: Chemical* **1998**, 51, 46-51.
188. Bakaltcheva, I. B.; Ligler, F. S.; Patterson, C. H.; Shriver-Lake, L. C. *Anal. Chim. Acta* **1999**, 399, 13-20.
189. Shriver-Lake, L. C.; Donner, B. L.; Ligler, F. S. *Environ. Sci. Technol.* **1997**, 31, 837-841.
190. Shriver-Lake, L. C.; Patterson, C. H.; van Bergen, S. K. *Field Anal. Chem. Tech.* **2000**, 4, 239-245.
191. Shriver-Lake, L. C.; Breslin, K. A.; Golden, J. P.; Judd, L. L.; Choi, J.; Ligler, F. S. *Proc. SPIE-Int. Soc. Opt. Eng.* **1994**, 2367, 52-58.
192. van Bergen, S. K.; Bakaltcheva, I. B.; Lundgren, J. S.; Shriver-Lake, L. C. *Environ. Sci. Technol.* **2000**, 34, 704-708.
193. Kusterbeck, A. W.; Charles, P. T. *Field Anal. Chem. Tech.* **1998**, 2, 341-350.
194. Charles, P. T.; Gauger, P. R.; Patterson, C. H.; Kusterbeck, A. W. *Environ. Sci. Technol.* **2000**, 34, 4641-4650.
195. Charles, P. T.; Dingle, B. M.; Van Bergen, S.; Gauger, P. R.; Patterson Jr., C. H.; Kusterbeck, A. W. *Field Anal. Chem. Tech.* **2001**, 5, 272-280.
196. Gauger, P. R.; Holt, D. B.; Patterson Jr., C. H.; Charles, P. T.; Shriver-Lake, L.; Kusterbeck, A. W. *J. Hazard. Mater.* **2001**, 83, 51-63.
197. Lesnik, B. *Environ. Test. Anal.* **1999**, 8, 8.

198. Medintz, I. L.; Goldman, E. R.; Lassman, M. E.; Hayhurst, A.; Kusterbeck, A. W.; Deschamps, J. R. *Anal. Chem.* **2005**, 77, 365-372.
199. Medintz, I. L.; Goldman, E. R.; Clapp, A. R.; Uyeda, H. T.; Lassman, M. E.; Hayhurst, A.; Mattoussi, H. *Proc. SPIE-Int. Soc. Opt. Eng.* **2005**, 5705, 166-174.
200. Tran, P. T.; Goldman, E. R.; Anderson, G. P.; Mauro, J. M.; Mattoussi, H. *Proc. SPIE-Int. Soc. Opt. Eng.* **2002**, 4636, 23-30.
201. Goldman, E. R.; Medintz, I. L.; Whitley, J. L.; Hayhurst, A.; Clapp, A. R.; Uyeda, H. T.; Deschamps, J. R.; Lassman, M. E.; Mattoussi, H. *J. Am. Chem. Soc.* **2005**, 127, 6744-6751.
202. Altamirano, M.; Garcia-Villada, L.; Agrelo, M.; Sanchez-Martin, L.; Martin-Otero, L.; Flores-Moya, A.; Rico, M.; Lopez-Rodas, V.; Costas, E. *Biosens. Bioelect.* **2004**, 19, 1319-1323.
203. Radhika, V.; Proikas-Cezanne, T.; Jayaraman, M.; Onesime, D.; Ha, J. H.; Dhanasekaran, D. N. *Nat. Chem. Biol.* **2007**, 3, 325-330.
204. Everts, S. *Chem. Eng. News* **2007**, 85(20), 10.
205. Andrew, T. L.; Swager, T. M. *J. Am. Chem. Soc.* **2007**, 129, 7254-7255.
206. Science & Technology Concentrates. *Chem. Eng. News* **2007**, 85(23), 32.

## **CHAPTER 2**

### **SOLUTION-PHASE INVESTIGATIONS OF COMMON FLUOROPHORES FOR THE DETECTION OF NITRATED EXPLOSIVES**

Previous studies indicated that nitrated explosives may be detected by fluorescence quenching of pyrene and related compounds. The use of pyrene, however, invokes numerous health and waste disposal hazards. In this chapter, ten safer fluorophores are identified for quenching detection of target nitrated compounds. Initially, Stern-Volmer constants are measured for each fluorophore with nitrobenzene and 4-nitrotoluene to determine the sensitivity of the quenching interaction. For fluorophores with quenching constants greater than  $50 \text{ M}^{-1}$ , sensitivity and selectivity are investigated further using an extended set of target quenchers. Nitromethane, nitrobenzene, 4-nitrotoluene, and 2,6-dinitrotoluene are chosen to represent nitrated explosives and their degradation products; aniline, benzoic acid, and phenol are chosen to represent potential interfering compounds. Among the fluorophores investigated, purpurin, malachite green, and phenol red demonstrate the greatest sensitivity and selectivity for nitrated compounds. Correlation of the quenching rate constants for these fluorophores to Rehm-Weller theory suggests an electron-transfer quenching mechanism. As a result of the large quenching constants, purpurin, malachite green, and phenol red are the most promising for future detection of nitrated explosives via fluorescence quenching.



## **2.1 Introduction and Background**

### **2.1.1 Analysis of Nitrated Explosives**

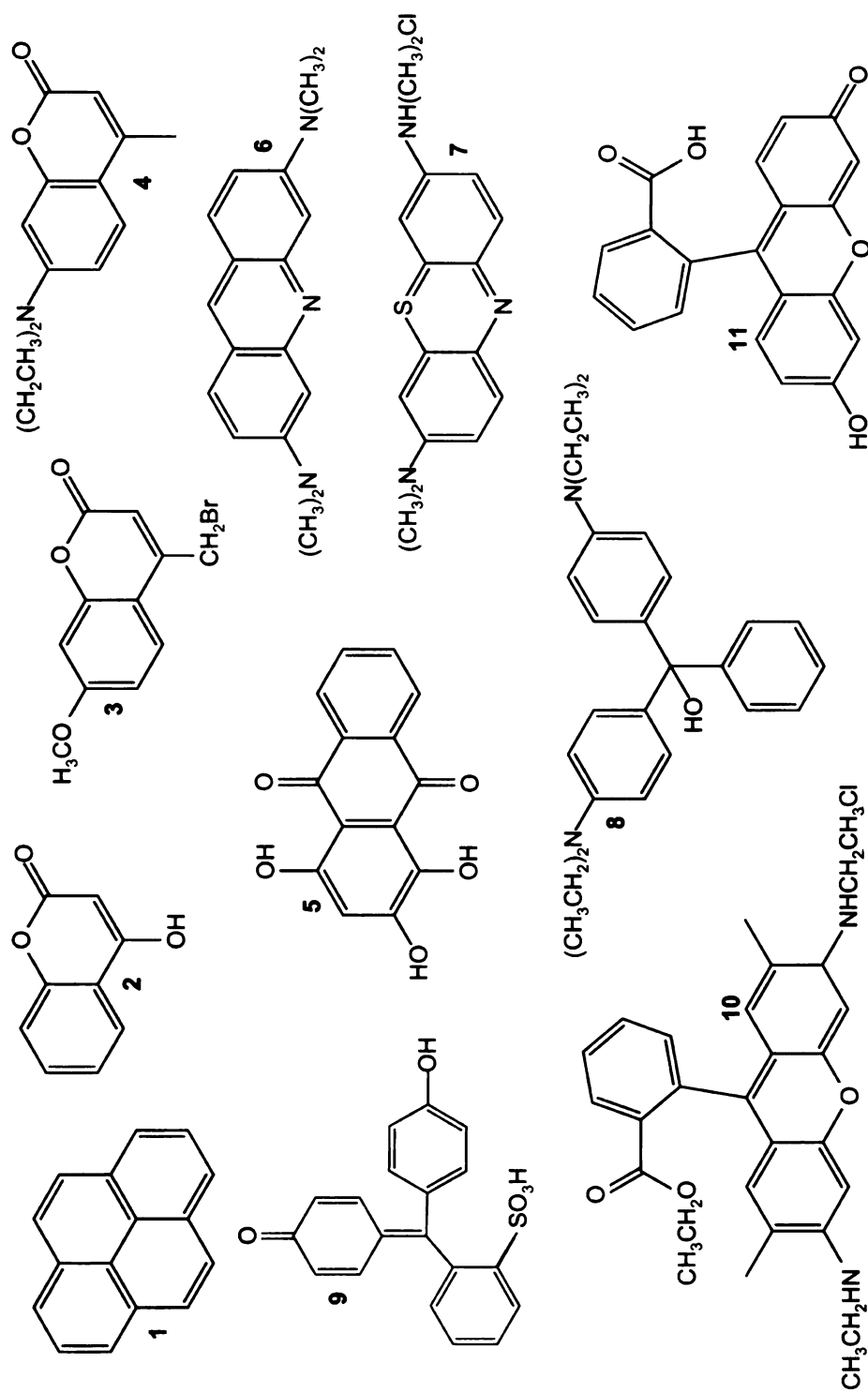
The analysis of nitrated explosives is of great importance in a variety of fields.<sup>1</sup> In forensic science, as discussed in Chapter 1, identification of these explosives and their degradation products can be used to identify persons in recent contact with an explosive device.<sup>2</sup> In addition, in environmental chemistry, explosives present in undetonated landmines can leach into and persist in the soil and groundwater, posing a threat to the environment and any living inhabitants.<sup>3,4</sup> For industrial quality control, manufacturers of explosive materials must assure consumers that their products are safe, effective, and free from contamination by monitoring the composition throughout the manufacturing process. Because the requirements in each of these fields are so diverse, a versatile method is needed for the analysis of nitrated explosives.

#### **2.1.2 Solution-Phase Fluorescence Quenching**

As discussed briefly in Chapter 1, the fluorescence quenching of pyrene and related compounds by nitrated explosives and degradation products has been explored.<sup>5-8</sup> Goodpaster and McGuffin report that nitroaromatic compounds are more efficient quenchers than their aliphatic counterparts, with quenching constants up to three times greater.<sup>7</sup> In addition, measured quenching constants increase with increasing nitration of the molecules. These experimental results support the *ab initio* calculations of Goodpaster and coworkers, which suggest that the fluorescence quenching mechanism involves the formation of an excited-state ion pair.<sup>7</sup> Upon collision of excited-state pyrene and ground-state

nitromethane, an electron is transferred from pyrene to nitromethane. As the molecules separate, the electron is transferred back to pyrene and the excitation energy is dissipated by vibrational relaxation of nitromethane. A similar mechanism can be postulated for the nitrated explosives.<sup>7</sup> Aliphatic explosives may accept the transferred electron with similar efficiency to nitromethane. However, aromatic explosives have a large number of resonance structures that can stabilize the resulting ion and enhance the efficiency of electron transfer. Because of the higher efficiency, Stern-Volmer quenching constants are expected to be greater for aromatic than aliphatic explosives, as confirmed experimentally.<sup>7</sup> Increasing the number of electron-withdrawing nitro groups further enhances the ability of the aromatic explosive to accept an electron from pyrene. Consequently, the Stern-Volmer constants are expected to be greater with increasing degree of nitration, as confirmed experimentally.<sup>7</sup> In direct comparison to UV absorbance detection, the fluorescence quenching method of Goodpaster and McGuffin demonstrates a 40-fold improvement in signal-to-noise ratio.<sup>7</sup> Although pyrene offers excellent sensitivity and selectivity for nitrated explosives, the hazards associated with pyrene discourage its routine use.

In this study, several alternative fluorophores (Figure 2.1) have been selected based on the proposed quenching mechanism and other criteria essential to their incorporation into a new or existing field-ready device. The selected fluorophores have lower toxicity than pyrene to reduce health and waste disposal concerns that may arise from their routine use. These molecules are selected for testing because they have conjugated, electron-rich structures with



**Figure 2.1.** Structure of fluorophores under investigation. Pyrene (**1**); 4-Hydroxycoumarin (**2**); 4-Bromomethyl-7-methoxycoumarin (**3**); 7-Diethylamino-4-methylcoumarin (**4**); Purpurin (**5**), Acridine orange (**6**); Methylene blue (**7**); Malachite green (**8**); Phenol red (**9**); Rhodamine 6G (**10**); Fluorescein (**11**).

significant electron-donating capabilities to facilitate ion-pair formation during the quenching process.<sup>7,9</sup> Another relevant selection criterion is a high quantum efficiency, which allows high sensitivity to be achieved with a low fluorophore concentration. The excitation and emission wavelength of the fluorophore are also important when considering potential field applications. Because handheld UV lamps (254 and 366 nm) are readily available in the forensic community, fluorophores with excitation wavelengths in the UV region are beneficial. In a field device, detection may be achieved visually or through the use of a digital camera or similar imaging device. In the latter approach, where glass optics may be involved, fluorophores with emission wavelengths in the visible region are of greatest utility. Finally, good physical, chemical, and photolytic stability of the fluorophore are desirable features that will maximize durability and longevity of a field-ready device.

The goal of this study is to evaluate the selected fluorophores with regard to their potential utility for on-site explosives detection. Stern-Volmer constants for each fluorophore are measured with target nitrated compounds as well as potential interfering compounds to determine sensitivity and selectivity. Of the target quenchers, nitromethane and nitrobenzene are models of aliphatic and aromatic nitrated explosives, respectively, while 4-nitrotoluene and 2,6-dinitrotoluene are models of degradation products. Behavior of specific explosives and their degradation products is not investigated in this preliminary work, but will likely be consistent with the chosen models. Of the interfering quenchers, aniline is representative of bases, while benzoic acid and phenol are

representative of acids. These functional groups and aromatic molecules, in general, are found ubiquitously in the environment. Through the Stern-Volmer constants, the sensitivity and selectivity of the selected fluorophores for the compounds of interest are evaluated and compared directly to those for pyrene. Promising fluorophores identified from this study may be useful in a variety of field-ready devices, including sensors, wipes, and air sampling tubes.

## **2.2 Experimental Methods**

### **2.2.1 Reagents**

Reagent-grade fluorophores are used as received and include 4-hydroxycoumarin (Aldrich), 4-bromomethyl-7-methoxycoumarin (Aldrich), 7-diethylamino-4-methylcoumarin (Aldrich), acridine orange (Eastman Kodak), fluorescein (Eastman Kodak), phenol red (Aldrich), purpurin (National Aniline Division), malachite green (Sigma), methylene blue (Coleman and Bell), pyrene (MCB), and rhodamine 6G (MCB). Target quenchers, selected to model nitroaromatic explosives and their degradation products, are used as received and include nitromethane (Aldrich), nitrobenzene (Mallinckrodt), 4-nitrotoluene (Aldrich), and 2,6-dinitrotoluene (Aldrich). Interfering quenchers are used as received and include aniline (Fisher), benzoic acid (Spectrum), and phenol (Mallinckrodt).

### **2.2.2 Determination of Quenching Constants**

Fluorescence power measurements are performed by using a flow-injection laser-induced fluorescence spectrometer. The sample is introduced by

a helium gas-displacement pump (30 psi) into a 50- $\mu\text{m}$  i.d. fused-silica capillary flow cell. The excitation source, a continuous-wave He-Cd laser (Melles Griot, model 3074-40M, 325 nm, 38 mW), is filtered and focused onto a section of the capillary where the polyimide coating has been removed to allow UV transmission. The fluorescence emission is collimated, filtered to remove scattered laser light, and refocused onto the entrance slit of a 0.34-m Czerny-Turner monochromator (Instruments SA, model 340E, 300 groove/mm grating, 2-nm band-pass). The emission is collected by a thermoelectrically-cooled charge-coupled device (CCD) detector (Instruments SA, model (A)TECCD-2000x800-7) operated at 240 K. A commercially available electronic interface (Instruments SA, models Datascan 2 and CCD 2000) and associated software (Instruments SA, Spectramax for Windows, version 3.1) are used for instrument control and data acquisition.

Stock solutions of the fluorophores ( $10^{-3}$  M) and quenchers ( $10^{-2}$  M) are prepared in high-purity spectroscopic-grade methanol (Honeywell Burdick & Jackson). For preliminary studies, dilute solutions of each fluorophore are prepared at concentrations ranging from  $10^{-3}$  to  $10^{-6}$  M. Fluorescence spectra are measured and the peak heights at the maximum emission wavelength (Table 2.1) are used to determine the linearity of the fluorescence response. Linearity is necessary to ensure accuracy of the measured quenching constant, as the addition of quencher is equivalent to a reduction in the active fluorophore concentration. For quenching studies, stock solutions are combined and diluted in methanol to prepare working solutions of constant fluorophore and varied

**Table 2.1.** Spectral properties of fluorophores.

<b>Fluorophore</b>	<b><math>\lambda_{\text{max (EM)}}</math> (nm)<sup>a</sup></b>	<b>Relative Fluorescence Power<sup>b</sup></b>
Pyrene (1)	397.2	0.345
4-Hydroxycoumarin (2)	381.0	0.00151
4-Bromomethyl-7-methoxycoumarin (3)	408.1	0.206
7-Diethylamino-4-methylcoumarin (4)	448.4	0.764
Purpurin (5)	412.6	0.0802
Acridine Orange (6)	556.0	0.0757
Methylene Blue (7)	716.9	0.136
Malachite Green (8)	379.1	0.0225
Phenol Red (9)	368.6	0.00840
Rhodamine 6G (10)	585.8	1.00
Fluorescein (11)	559.1	0.0283

<sup>a</sup> Maximum emission wavelengths ( $\lambda_{\text{max (EM)}}$ ) are given in methanol with excitation at 325 nm.

<sup>b</sup> Relative fluorescence power is normalized with respect to concentration, integration time of the CCD detector, and to the fluorescence of Rhodamine 6G.

quencher concentrations. Fluorophore concentrations are selected to obtain approximately equal fluorescence power for each fluorophore while maintaining linearity, and are generally on the order of  $10^{-4}$  to  $10^{-5}$  M. Quencher concentrations are varied over the range of  $10^{-2}$  to  $10^{-4}$  M.

For each solution, five replicates of the fluorescence spectrum are acquired over a 220-nm range. From the average peak height at the maximum emission wavelength, the fluorescence power is determined for the fluorophore solution in the absence of quencher ( $F^0$ ) and in the presence of quencher ( $F$ ). The fluorescence power ratio ( $F^0/F$ ) is then graphed against the quencher concentration to generate a Stern-Volmer plot, as described in Equation 1.4. Using a spreadsheet program (Microsoft Excel, version 2003), the slope (Stern-Volmer constant) and intercept are determined by linear regression. The Stern-Volmer constant for each fluorophore with a given quencher is compared to that for pyrene, the reference fluorophore. This ratio of Stern-Volmer constants allows a direct comparison of the relative sensitivity of the fluorophore with respect to that of pyrene. The Stern-Volmer constant for each fluorophore with a given quencher is also compared to that for nitrobenzene, the reference quencher. This ratio of Stern-Volmer constants allows a direct comparison of the selectivity of the fluorophore for the target and interfering compounds.

### **2.2.3 Determination of Fluorescence Lifetimes**

Fluorescence lifetimes are determined in collaboration with Dr. Gary Blanchard of Michigan State University by using a time-correlated single-photon-counting spectrometer.<sup>10</sup> In this system, the second harmonic of a continuous-



wave mode-locked Nd:YAG laser (Coherent, model Antares 76-S) is used to excite a cavity-dumped, synchronously pumped dye laser (Coherent, model 702-2, 325 nm, 1 mW). Fluorescence emission is collected and focused on a subtractive double monochromator of Czerny-Turner design (American Holographic, model DB10-S, 10-nm bandpass). The emission is detected with a cooled two-stage microchannel plate photomultiplier (Hamamatsu, model R3809U-51) operated at 273 K. Single-photon counting is performed with commercially available electronic instrumentation (Tennelec, models TC454, TC864, TC412A, TC525, and PCA-II) and associated software (National Instruments, Labview, version 7.1). Six replicate measurements of the fluorescence time decay are acquired by single-photon counting. The data are fit by nonlinear regression to a single-exponential function using a peak-fitting program (Table Curve 2D, Jandel Scientific, version 2.02). Because the fluorescence lifetimes range from 1 to 15 ns, deconvolution of the instrument response function (~35 ps full width at half-maximum) from the experimental data is not necessary. A more detailed description of the data analysis is given in the Appendix.

#### **2.2.4 Determination of Redox Potentials**

To investigate the quenching mechanism, oxidation ( $E_{\text{ox}}$ ) and reduction ( $E_{\text{red}}$ ) potentials are determined for each fluorophore and quencher by using cyclic voltammetry in collaboration with Dr. Elizabeth McGaw of Michigan State University. Solutions are prepared containing  $10^{-3}$  M fluorophore or quencher and 0.1 M  $\text{NaNO}_3$  as the supporting electrolyte in methanol. All solutions are

degassed by nitrogen purge for 5 minutes prior to measurement. The electrochemical measurements are performed using a glassy carbon working electrode ( $0.07\text{ cm}^2$  area), a Pt counter electrode, and a nonaqueous “no leak” Ag/AgCl reference electrode (Cypress Systems, model EE009, 3 M KCl fill solution). A potentiostat (CH Instruments, model 650A) is used to scan the potential from 0.0 to +1.5 V at 0.5 V/s for determination of oxidation potentials and from 0.0 to -1.5 V at 0.5 V/s for determination of reduction potentials. For reversible systems,  $E_{\text{ox}}$  and  $E_{\text{red}}$  are calculated as the average of the anodic and cathodic peak potentials. For irreversible systems,  $E_{\text{ox}}$  is reported as the anodic peak potential and  $E_{\text{red}}$  is reported as the cathodic peak potential. A more detailed description of the data analysis is given in the Appendix.

### **2.2.5 Determination of Singlet Excitation Energies**

Also needed to investigate the quenching mechanism are the singlet excitation energies ( $E_{0,0}$ ) for each fluorophore. UV-visible absorbance and fluorescence emission spectra are acquired by using commercially available spectrophotometers (Hitachi, models U-4001 and F-4500, respectively). Because the absorbance and emission spectra for each fluorophore are mirror images, the energy of the singlet excited state is determined from the wavelength at which the normalized absorption and emission spectra intersect.<sup>9</sup> A more detailed description of the data analysis is given in the Appendix.

## **2.3 Results and Discussion**

### **2.3.1 Fluorophore Characterization**

Table 2.1 summarizes the emission wavelengths and relative

fluorescence powers of the fluorophores as determined on the flow-injection laser-induced fluorescence spectrometer. All fluorophores have excitation wavelengths in the ultraviolet region, which is desirable for the development of a field detection device. These fluorophores demonstrate a wide range of maximum emission wavelengths, from phenol red at 369 nm to methylene blue at 717 nm. Most fluorophores have sufficient emission in the visible region to be useful in a field detection device. The relative fluorescence power with 325-nm excitation is also variable, with rhodamine 6G having the highest fluorescence and with phenol red and 4-hydroxycoumarin having the lowest, approximately 100- and 1000-fold less than that of rhodamine 6G, respectively.

### **2.3.2 Quenching of Pyrene by Nitrated Explosives**

Because the quenching of pyrene by nitrated compounds is well documented,<sup>7</sup> pyrene is used as a reference fluorophore throughout these studies. Quenching constants determined for pyrene with the target and interfering quenchers, as well as correlation data for Stern-Volmer plots, are given in Table 2.2. An example spectral data set and Stern-Volmer plot are shown in Figure 2.2. As noted previously by Goodpaster and McGuffin,<sup>7</sup> the Stern-Volmer constant for the target aliphatic quencher, nitromethane, is less than those for its aromatic counterparts, such as nitrobenzene (Table 2.2). Moreover, the addition of an electron-donating methyl group slightly decreases the quenching constant for 4-nitrotoluene compared to nitrobenzene. Conversely, the addition of an electron-withdrawing nitro group significantly increases the quenching constant for 2,6-dinitrotoluene compared to

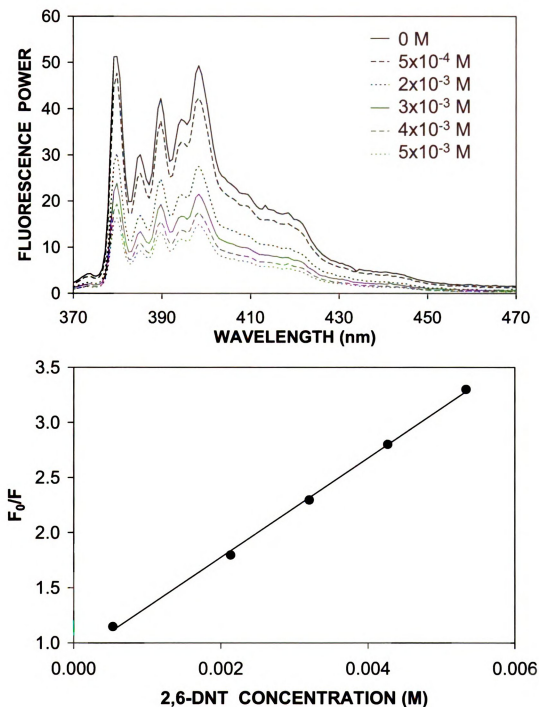
**Table 2.2.** Quenching constants ( $K_d$ ) for pyrene (1) with target and interfering quenchers in methanol at room temperature.<sup>a</sup>

	Quencher	$K_d$ ( $M^{-1}$ )	Intercept	$R^2$	Quencher Selectivity <sup>b</sup>
<b>Target Quenchers</b>	Nitromethane	$103 \pm 7$	$1.04 \pm 0.05$	0.999	0.33
	Nitrobenzene	$315 \pm 8$	$1.04 \pm 0.01$	0.999	1.00
	4-Nitrotoluene	$297 \pm 5$	$0.94 \pm 0.08$	0.996	0.94
	2,6-Dinitrotoluene	$450 \pm 20$	$0.9 \pm 0.2$	0.994	1.43
<b>Interfering Quenchers</b>	Aniline	$74 \pm 8$	$0.95 \pm 0.05$	0.976	0.23
	Benzoic Acid	$20 \pm 20$	$1.008 \pm 0.002$	0.816	0.06
	Phenol	$-3 \pm 5$	$0.99 \pm 0.01$	0.508	NA <sup>c</sup>

<sup>a</sup> Determined from Equation 1.4, with correlation coefficient  $R^2$ .

<sup>b</sup> Quencher selectivities are calculated relative to nitrobenzene.

<sup>c</sup> NA = not available. Value cannot be calculated from a negative Stern-Volmer constant.



**Figure 2.2.** Fluorescence spectra of  $5 \times 10^{-5}$  M pyrene in methanol at room temperature in the presence of increasing concentrations of 2,6-dinitrotoluene (top) and the resulting Stern-Volmer plot (bottom). The Stern-Volmer constant for this data set is  $450 \text{ M}^{-1}$  with a correlation coefficient of 0.9988.

4-nitrotoluene.

The Stern-Volmer constants determined for the interfering aromatic compounds are significantly less than those for the target aromatic compounds. Benzoic acid and phenol have quenching constants that are statistically indistinguishable from zero. The correlation coefficients for these regressions deviate significantly from unity as a direct result of the small quenching constant and, therefore, there is greater uncertainty in the data. The quenching constant for aniline, however, is comparable to that measured for nitromethane. Consequently, the presence of amines in the environment could cause interference in the detection of nitromethane or other aliphatic nitrated explosives. At higher concentrations, such amines may even cause interference in the detection of nitroaromatic explosives. However, the ability to detect selected amines may be beneficial, as the degradation of nitrated explosives can result in reduction of the nitro groups to amine groups (e.g., 2,4,6-trinitrotoluene to 2-amino-4,6-dinitrotoluene or 4-amino-2,6-dinitrotoluene).

The selectivity of pyrene for each quencher is calculated with respect to nitrobenzene, as summarized in Table 2.2. Ideally, the selectivity for nitrated compounds is near or greater than unity and the selectivity for interfering compounds is much less than unity. All of the target quenchers demonstrate a greater selectivity with pyrene than all of the interfering quenchers. The selectivities for the nitroaromatic compounds are near or greater than unity, although the value for nitromethane is significantly less and more similar to that for aniline.

**Table 2.3.** Quenching constants ( $K_d$ ) for fluorophores with nitrobenzene and 4-nitrotoluene in methanol at room temperature.<sup>a</sup>

Fluorophore	Nitrobenzene			4-Nitrotoluene		
	$K_d$ ( $M^{-1}$ )	Intercept	$R^2$	$K_d$ ( $M^{-1}$ )	Intercept	$R^2$
Pyrene (1)	315 ± 8	1.04 ± 0.01	0.999	297 ± 5	0.94 ± 0.08	0.996
4-Hydroxycoumarin (2)	4.4 ± 0.6	1.02 ± 0.05	1.000	6.3 ± 0.3	1.04 ± 0.02	0.940
4-Bromomethyl-7-methoxycoumarin (3)	39 ± 2	1.09 ± 0.03	0.990	43 ± 4	1.09 ± 0.04	0.987
7-Diethylamino-4-methylcoumarin (4)	38 ± 3	0.98 ± 0.03	0.997	40 ± 1	0.97 ± 0.01	0.994
Purpurin (5)	143 ± 6	0.97 ± 0.06	0.999	140 ± 3	1.01 ± 0.01	0.995
Acridine Orange (6)	30 ± 7	1.01 ± 0.02	0.986	40 ± 1	0.99 ± 0.01	0.997
Methylene Blue (7)	1 ± 2	1.03 ± 0.01	0.580	3.3 ± 0.1	1.02 ± 0.02	0.989
Malachite Green (8)	48 ± 1	0.97 ± 0.05	0.998	53 ± 6	1.027 ± 0.005	0.995
Phenol Red (9)	79 ± 2	1.01 ± 0.03	0.997	100 ± 13	1.01 ± 0.04	0.997
Rhodamine 6G (10)	21 ± 7	0.94 ± 0.06	0.996	16.1 ± 0.8	0.97 ± 0.03	0.996
Fluorescein (11)	20 ± 10	1.01 ± 0.05	0.957	32 ± 3	1.00 ± 0.02	0.959

<sup>a</sup> Determined from Equation 1.4, with correlation coefficient  $R^2$ .

### **2.3.3 Preliminary Investigation of Selected Fluorophores**

Quenching constants are measured for the selected fluorophores with nitrobenzene and 4-nitrotoluene (Table 2.3). The magnitude of the Stern-Volmer constant is representative of the sensitivity of the quenching interaction, and the values can be directly compared for a given quencher. The quenching constants for all of the selected fluorophores with nitrobenzene and 4-nitrotoluene are significantly less than those for pyrene. Purpurin demonstrates the greatest quenching constant, with a value half that of pyrene. In addition, malachite green and phenol red exhibit satisfactory quenching, with measured Stern-Volmer constants of nearly  $50 \text{ M}^{-1}$  or greater. The other fluorophores show very little sensitivity for nitrobenzene or 4-nitrotoluene, as illustrated by the small quenching constants for 4-hydroxycoumarin, methylene blue, rhodamine 6G, and fluorescein. Based on the values of the quenching constants, only purpurin, malachite green, and phenol red are chosen for further investigation.

### **2.3.4 Quenching of Purpurin by Nitrated Explosives**

The Stern-Volmer constants and rate constants measured for purpurin with the extended set of target and interfering quenchers are shown in Table 2.4. An example spectral data set and Stern-Volmer plot are shown in Figure 2.3. As with pyrene, the quenching constant for the target aliphatic compound is less than those for the target aromatic compounds. The quenching constants for nitrobenzene, 4-nitrotoluene, and 2,6-dinitrotoluene are all approximately the same value,  $140 \text{ M}^{-1}$ , within experimental error. This similarity indicates that, in the presence of a nitro group, the addition of other functional groups to the



**Table 2.4.** Quenching constants ( $K_d$ ) for purpurin (5) with target and interfering quenchers in methanol at room temperature.<sup>a</sup>

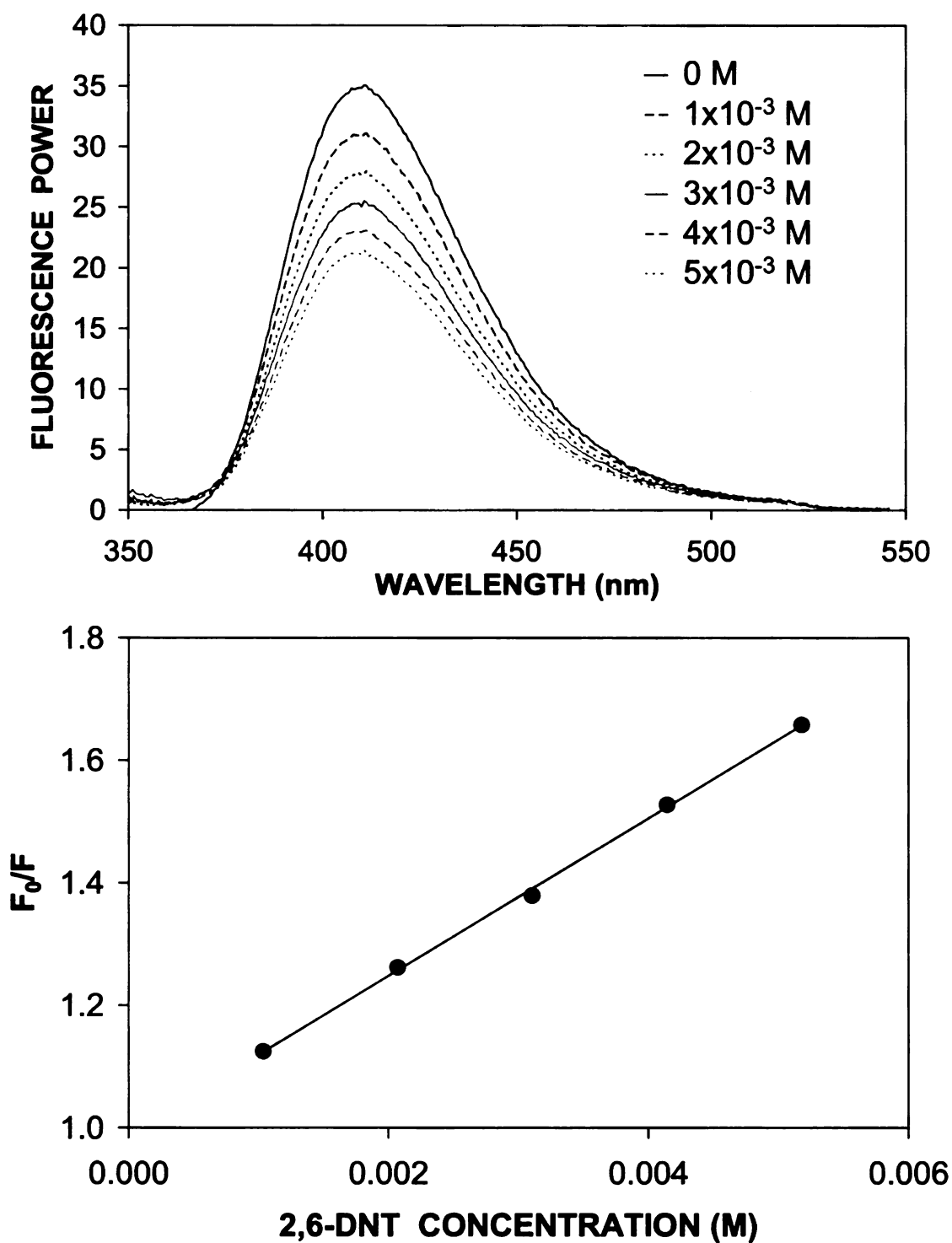
	Quencher	$K_d$ ( $M^{-1}$ )	Intercept	$R^2$	Quencher Selectivity <sup>b</sup>	Fluorophore Selectivity <sup>c</sup>
<b>Target Quenchers</b>	Nitromethane	$86 \pm 1$	$1.02 \pm 0.01$	0.998	0.60	0.83
	Nitrobenzene	$143 \pm 6$	$0.97 \pm 0.06$	0.999	1.00	0.45
	4-Nitrotoluene	$140 \pm 3$	$1.01 \pm 0.01$	0.995	0.98	0.47
	2,6-Dinitrotoluene	$130 \pm 10$	$1.02 \pm 0.03$	0.998	0.91	0.29
<b>Interfering Quenchers</b>	Aniline	$-2 \pm 1$	$1.02 \pm 0.01$	0.620	NA <sup>d</sup>	NA
	Benzoic Acid	$21 \pm 7$	$1.001 \pm 0.002$	0.855	0.15	1.05
	Phenol	$9 \pm 7$	$1.00 \pm 0.02$	0.908	0.06	NA

<sup>a</sup> Determined from Equation 1.4, with correlation coefficient  $R^2$ .

<sup>b</sup> Quencher selectivities are calculated relative to nitrobenzene.

<sup>c</sup> Fluorophore selectivities are calculated relative to pyrene.

<sup>d</sup> NA = not available. Value cannot be calculated from a negative Stern-Volmer constant.



**Figure 2.3.** Fluorescence spectra of  $5 \times 10^{-4}$  M purpurin in methanol at room temperature in the presence of increasing concentrations of 2,6-dinitrotoluene (top) and the resulting Stern-Volmer plot (bottom). The Stern-Volmer constant for this data set is  $129 \text{ M}^{-1}$  with a correlation coefficient of 0.9907.

aromatic ring, whether electron-donating or -withdrawing, does little to alter the quenching of purpurin. These quenching constants for purpurin are approximately three-fold less than those for pyrene (Table 2.2).

The Stern-Volmer constants for the interfering compounds are significantly less than those for the target compounds. Aniline and phenol have quenching constants near zero, while benzoic acid has a quenching constant that is small but statistically indistinguishable from zero at the 95% confidence level. Interestingly, the quenching constant for aniline with purpurin is significantly less than that with pyrene and, hence, has less potential for interference.

The selectivity of purpurin for each quencher is also calculated with respect to nitrobenzene, as summarized in Table 2.4. All of the target quenchers demonstrate a greater selectivity with purpurin than all of the interfering quenchers, with values near or greater than unity. In contrast to pyrene, purpurin exhibits a selectivity for nitromethane that is more similar to the target quenchers than the interfering quenchers. This suggests that purpurin may be more effective for detection of nitrated explosives than pyrene.

### **2.3.5 Quenching of Malachite Green by Nitrated Explosives**

The Stern-Volmer constants and rate constants measured for malachite green with the extended set of target and interfering quenchers are shown in Table 2.5. An example spectral data set and Stern-Volmer plot are shown in Figure 2.4. As with pyrene, the quenching constant for the target aliphatic compound is less than those of the target aromatic compounds. The quenching constants increase only slightly upon the addition of electron-donating and

**Table 2.5.** Quenching constants ( $K_d$ ) for malachite green (8) with target and interfering quenchers in methanol at room temperature.<sup>a</sup>

	Quencher	$K_d$ (M <sup>-1</sup> )	Intercept	R <sup>2</sup>	Quencher Selectivity <sup>b</sup>	Fluorophore Selectivity <sup>c</sup>
<b>Target Quenchers</b>	Nitromethane	36 ± 5	1.04 ± 0.01	0.997	0.75	0.35
	Nitrobenzene	48 ± 1 <sup>d</sup>	0.97 ± 0.05 <sup>d</sup>	0.998 <sup>d</sup>	1.00 <sup>d</sup>	0.15 <sup>d</sup>
		49 ± 2 <sup>e</sup>	1.10 ± 0.02 <sup>e</sup>	0.995 <sup>e</sup>	1.00 <sup>e</sup>	0.16 <sup>e</sup>
	4-Nitrotoluene	53 ± 6	1.027 ± 0.005	0.995	1.10	0.18
	2,6-Dinitrotoluene	64 ± 3	1.04 ± 0.01	0.993	1.33	0.14
<b>Interfering Quenchers</b>	Aniline	-16 ± 1 <sup>d</sup>	1.00 ± 0.02 <sup>d</sup>	0.998 <sup>d</sup>	NA <sup>f</sup>	NA
		-20 ± 2 <sup>e</sup>	1.04 ± 0.05 <sup>e</sup>	0.988 <sup>e</sup>	NA	NA
	Benzoic Acid	170 ± 30 <sup>d</sup>	1.4 ± 0.1 <sup>d</sup>	0.988 <sup>d</sup>	3.54 <sup>d</sup>	8.50 <sup>d</sup>
		23 ± 7 <sup>e</sup>	1.04 ± 0.06 <sup>e</sup>	0.941 <sup>e</sup>	0.47 <sup>e</sup>	1.15 <sup>e</sup>
	Phenol	0 ± 3	0.99 ± 0.02	0.758	0.00	NA

<sup>a</sup> Determined from Equation 1.4, with correlation coefficient R<sup>2</sup>.

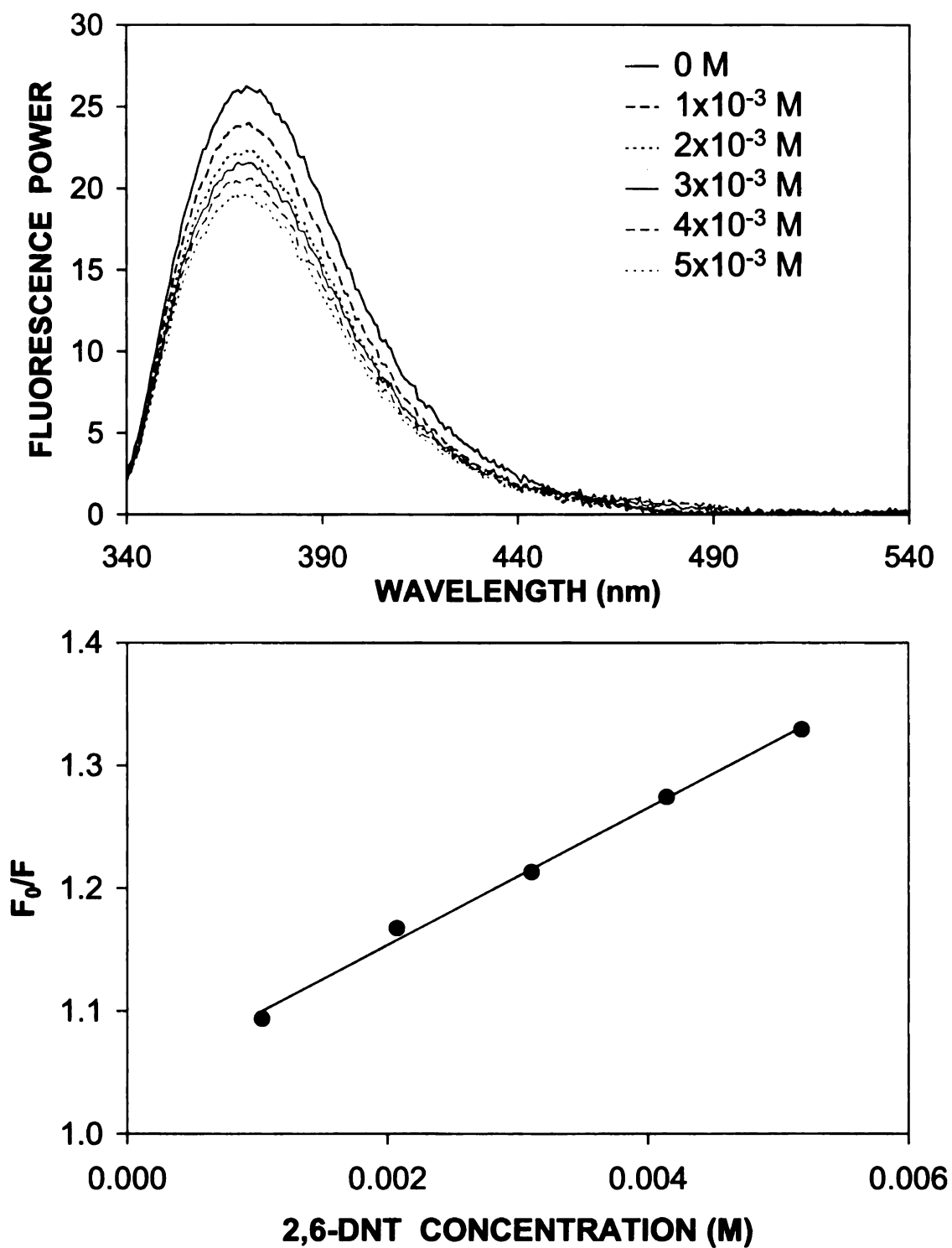
<sup>b</sup> Quencher selectivities are calculated relative to nitrobenzene.

<sup>c</sup> Fluorophore selectivities are calculated relative to pyrene.

<sup>d</sup> Unbuffered solution.

<sup>e</sup> Solution buffered with 0.25 M acetic acid:triethylamine (2:1) in methanol.

<sup>f</sup> NA = not available. Value cannot be calculated from a negative Stern-Volmer constant.



**Figure 2.4.** Fluorescence spectra of  $2 \times 10^{-4}$  M malachite green in methanol at room temperature in the presence of increasing concentrations of 2,6-dinitrotoluene (top) and the resulting Stern-Volmer plot (bottom). The Stern-Volmer constant for this data set is  $56 \text{ M}^{-1}$  with a correlation coefficient of 0.9958.

-withdrawing groups. These quenching constants for malachite green are approximately an order of magnitude less than those for pyrene (Table 2.2).

The Stern-Volmer constants for the interfering compounds with malachite green, however, are less straight-forward. The quenching constant for phenol is zero, for aniline is less than zero, and for benzoic acid is substantially greater than any of the target quenchers. During preparation of the malachite green solutions, the color is visibly changed upon addition of both aniline and benzoic acid, and becomes more intense as the concentration of quencher increases. The color change and unexpected quenching behavior is believed to be a pH effect, resulting from the addition of the acidic and basic quenchers. Malachite green is known to change color with pH,<sup>11</sup> and there is some evidence for a decrease in quantum yield in acidic solution.<sup>12</sup> This decrease in fluorescence power may be considered as a form of trivial quenching, which can be minimized by proper buffering of the solutions.

To minimize the pH change, malachite green solutions are buffered using acetic acid and triethylamine (2:1) in methanol. The quenching constants are measured for benzoic acid and aniline, and for nitrobenzene as a control (Table 2.5). The quenching constants for nitrobenzene and aniline are statistically equivalent in the buffered and unbuffered solutions, whereas the quenching constant for benzoic acid decreases significantly upon buffering. In fact, the quenching constant for benzoic acid is statistically indistinguishable from zero at the 95% confidence level. Clearly, these results indicate that the large quenching constant observed for benzoic acid in unbuffered solution is the

consequence of trivial and not dynamic quenching.

The negative quenching constant determined for malachite green and aniline, however, is not the consequence of trivial quenching, as the value does not change upon buffering the solution. Based on this result, the interaction between malachite green and aniline is not related to a simple proton transfer. The negative value may arise from the formation of a ground-state complex between malachite green and aniline that has a greater absorbance or quantum yield than malachite green alone. The resulting increase in fluorescence power relative to a solution in the absence of aniline yields a negative Stern-Volmer constant.

The selectivity of malachite green for each quencher is also calculated with respect to nitrobenzene, as summarized in Table 2.5. Selectivities for the target compounds, including nitromethane, are all near or greater than unity, and are greater than those measured for the interfering quenchers. The selectivity for benzoic acid in unbuffered solution, however, is three times greater than for the target quenchers, indicating a large potential for interference. When the fluorophore solution is buffered, the selectivity for benzoic acid decreases dramatically, to a value less than 0.5. This clearly indicates the importance of buffering malachite green solutions to avoid interference from acidic species.

### **2.3.6 Quenching of Phenol Red by Nitrated Explosives**

The Stern-Volmer constants and rate constants measured for phenol red with the extended set of target and interfering quenchers are shown in Table 2.6. An example spectral data set and Stern-Volmer plot are shown in Figure 2.5. As

**Table 2.6.** Quenching constants ( $K_d$ ) for phenol red (9) with target and interfering quenchers in methanol at room temperature.<sup>a</sup>

	Quencher	$K_d$ ( $M^{-1}$ )	Intercept	$R^2$	Quencher Selectivity <sup>b</sup>	Fluorophore Selectivity <sup>c</sup>
<b>Target Quenchers</b>	Nitromethane	$47 \pm 2$	$1.02 \pm 0.01$	0.997	0.59	0.46
	Nitrobenzene	$79 \pm 2^d$	$1.01 \pm 0.03^d$	0.997 <sup>d</sup>	1.00 <sup>d</sup>	0.25 <sup>d</sup>
		$83 \pm 2^e$	$0.98 \pm 0.02^e$	0.998 <sup>e</sup>	1.00 <sup>e</sup>	0.26 <sup>e</sup>
	4-Nitrotoluene	$100 \pm 10$	$1.01 \pm 0.04$	0.997	1.27	0.34
	2,6-Dinitrotoluene	$96 \pm 2$	$1.040 \pm 0.005$	0.997	1.22	0.21
<b>Interfering Quenchers</b>	Aniline	$-6.8 \pm 0.5^d$	$0.94 \pm 0.05^d$	0.970 <sup>d</sup>	NA <sup>f</sup>	NA
		$-8 \pm 4^e$	$1.00 \pm 0.04^e$	0.923 <sup>e</sup>	NA	NA
	Benzoic Acid	$11 \pm 5$	$1.01 \pm 0.01$	0.946	0.14	0.55
	Phenol	$-2 \pm 2$	$1.00 \pm 0.04$	0.472	NA	NA

<sup>a</sup> Determined from Equation 1.4, with correlation coefficient  $R^2$ .

<sup>b</sup> Quencher selectivities are calculated relative to nitrobenzene.

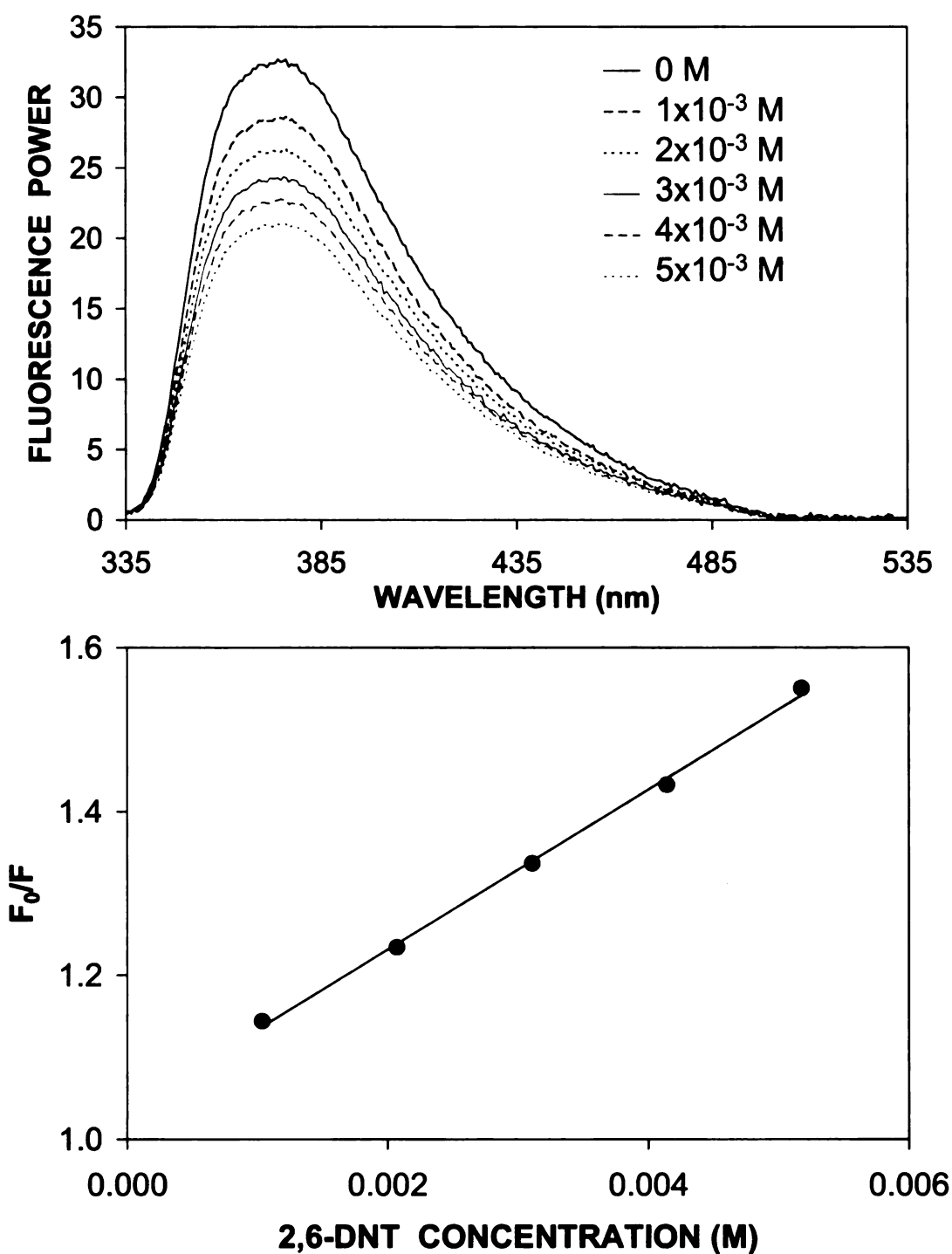
<sup>c</sup> Fluorophore selectivities are calculated relative to pyrene.

<sup>d</sup> Unbuffered solution.

<sup>e</sup> Solution buffered with 0.25 M acetic acid:triethylamine (2:1) in methanol.

<sup>f</sup> NA = not available. Value cannot be calculated from a negative Stern-Volmer constant.





**Figure 2.5.** Fluorescence spectra of  $6 \times 10^{-4}$  M phenol red in methanol at room temperature in the presence of increasing concentrations of 2,6-dinitrotoluene (top) and the resulting Stern-Volmer plot (bottom). The Stern-Volmer constant for this data set is  $98 \text{ M}^{-1}$  with a correlation coefficient of 0.9979.

with pyrene, the quenching constant for the target aliphatic compound is less than those of the target aromatic compounds. The quenching constants increase only slightly upon the addition of an electron-donating methyl group but remain constant for an additional electron-withdrawing nitro group. These quenching constants for phenol red are three- to four-fold less than those for pyrene (Table 2.2).

Consistent with the trends of the other fluorophores, the Stern-Volmer constants for the interfering compounds are significantly less than those for the target compounds. In fact, these quenching constants with phenol red are statistically indistinguishable from zero at the 95% confidence level. A negative quenching constant is measured for phenol red and aniline, similar to that observed for malachite green. Phenol red ( $pK_a = 7.9$ ) is a common pH indicator, so the addition of aniline increases solution pH and causes a color change. However, solutions of phenol red and aniline buffered with acetic acid and triethylamine (2:1) give statistically equivalent quenching constants to those measured in unbuffered solutions (Table 2.6). Hence, the negative quenching constant is not the result of trivial quenching and may arise from the formation of a ground-state complex between the fluorophore and quencher, as with malachite green.

The selectivity of phenol red for each quencher is calculated with respect to nitrobenzene, as summarized in Table 2.6. All of the target quenchers demonstrate a larger selectivity with phenol red than all of the interfering quenchers. The selectivities for the nitroaromatic compounds are all near or

greater than unity. The value for nitromethane is significantly less, but is still greater than that for the interfering quenchers. Although selectivities could not be calculated for aniline and phenol because the quenching constants were less than zero, there is little potential interference from these or related compounds in the detection of nitrated explosives.

### 2.3.7 Proposed Quenching Mechanism

As discussed previously, fluorescence quenching of pyrene is believed to occur by electron transfer from the excited-state fluorophore to the ground-state quencher.<sup>13</sup> This mechanism can be examined in more detail by using the empirical model of Rehm and Weller.<sup>14</sup> The free energy change for an outer-sphere electron-transfer process ( $\Delta G_{et}$ ) is given by

$$\Delta G_{et} = E_{ox} - E_{red} - E_{0,0} - C \quad (2.1)$$

where  $E_{ox}$  and  $E_{red}$  are the ground-state oxidation and reduction potentials of the electron donor and acceptor, respectively,  $E_{0,0}$  is the energy of the singlet excited-state fluorophore, and  $C$  is a Coulombic term relating the energy of the separated ions. In polar solvents such as methanol, the Coulombic term of Equation 2.1 is less than 2% of  $\Delta G_{et}$  and can be neglected in the determination of  $\Delta G_{et}$ .<sup>15</sup> The rate constant for fluorescence quenching,  $k_d$ , is related to the free energy for electron transfer by

$$k_d = \frac{k_0}{1 + 0.25 \left[ \exp(\Delta G_{et}^* / RT) + \exp(\Delta G_{et} / RT) \right]} \quad (2.2)$$

where  $k_0$  represents the diffusion-limited rate constant ( $1.4 \times 10^{10} \text{ M}^{-1} \text{ s}^{-1}$  in methanol),<sup>16</sup>  $R$  is the gas constant,  $T$  is the absolute temperature, and  $\Delta G_{et}^*$  is

the activation energy for the electron-transfer process, which is given as a monotonic function of  $\Delta G_{\text{et}}$ .<sup>14</sup>

$$\Delta G_{\text{et}}^* = \left[ \left( \frac{\Delta G_{\text{et}}}{2} \right)^2 + (\Delta G_{\text{et}}(0))^2 \right]^{1/2} + \frac{\Delta G_{\text{et}}}{2} \quad (2.3)$$

In Equation 2.3,  $\Delta G_{\text{et}}(0)$  is the activation free energy when  $\Delta G_{\text{et}} = 0$  and has been determined experimentally to be 0.104 eV.<sup>14</sup> In general, agreement between calculated and experimental values of  $k_d$  within a factor of two is considered evidence in favor of an outer-sphere electron-transfer quenching mechanism.

### 2.3.7.1 Fluorescence Lifetimes

To compare Stern-Volmer constants with Rehm-Weller theory, calculation of quenching rate constants is necessary. Fluorescence lifetimes are determined in methanol for pyrene, purpurin, malachite green, and phenol red, at wavelengths listed in Table 2.1. Fluorescence lifetimes are determined from nonlinear regression to a single-exponential function, and are given in Table 2.7. Typical correlation coefficients ( $R^2$ ) for the nonlinear regression ranged from 0.9887 to 0.9975 (see Appendix). The Stern-Volmer constants (Tables 2.2 and 2.4-2.6), together with the fluorescence lifetimes, are used to calculate second-order rate constants according to Equation 1.4, and are given in Table 2.8. The rate constants for pyrene, purpurin, malachite green, and phenol with all quenchers are  $10^9$  to  $10^{10} \text{ M}^{-1} \text{ s}^{-1}$ , approaching the diffusion-limited value of  $1.4 \times 10^{10} \text{ M}^{-1} \text{ s}^{-1}$  in methanol.<sup>16</sup>

**Table 2.7.** Fluorescence lifetimes ( $\tau_f^0$ ) determined for each of the fluorophores at the wavelengths listed in Table 2.1 ( $n = 6$ ). All values determined in methanol at room temperature.

<b>Fluorophore</b>	<b><math>\tau_f^0</math> (ns)</b>
Pyrene	$15.32 \pm 0.06$
Purpurin	$3.93 \pm 0.05$
Malachite Green	$1.050 \pm 0.007$
Phenol Red	$1.99 \pm 0.02$

**Table 2.8.** Quenching rate constants ( $k_d$ ) calculated for each of the fluorophores in methanol at room temperature.

Quenching Rate Constant, $k_d$ ( $10^{10} \text{ M}^{-1} \text{ s}^{-1}$ ) <sup>a</sup>				
	Quencher	Pyrene	Purpurin	Phenol Red
<b>Target Quenchers</b>	Nitromethane	0.67 ± 0.05	2.19 ± 0.04	2.4 ± 0.1
	Nitrobenzene	2.06 ± 0.05	3.6 ± 0.2	4.0 ± 0.1 <sup>d</sup>
	4-Nitrotoluene	1.94 ± 0.03	3.56 ± 0.09	4.2 ± 0.1 <sup>e</sup>
	2,6-Dinitrotoluene	2.9 ± 0.1	3.3 ± 0.3	5.0 ± 0.5
<b>Interfering Quenchers</b>	Aniline	0.48 ± 0.05	NA	4.8 ± 0.1
	Benzoic Acid	0.1 ± 0.1	0.5 ± 0.2	NA
	Phenol	NA <sup>b</sup>	0.2 ± 0.2	0.6 ± 0.3
				NA

<sup>a</sup> Determined from Equation 1.4 with uncertainty calculated by propagation of error.

<sup>b</sup> NA = not available. Value cannot be calculated from a negative Stern-Volmer constant.

<sup>c</sup> Unbuffered solution.

<sup>d</sup> Solution buffered with 0.50 M acetic acid:triethylamine (2:1) in methanol.

**Table 2.9.** Electrochemical data for fluorophores and quenchers in methanol at room temperature.

		<b>E<sub>ox</sub> (V)</b>	<b>E<sub>red</sub> (V)</b>
<b>Fluorophore</b>	Pyrene	0.41	-0.96
	Purpurin	0.89	-0.99
	Phenol Red	1.22	-0.35
	Malachite Green	0.75	-0.51
<b>Quencher</b>	Nitromethane	NA <sup>a</sup>	-1.03
	Nitrobenzene	1.23	-0.50
	4-Nitrotoluene	1.24	-0.53
	2,6-Dinitrotoluene	1.20	-0.37
	Aniline	0.41	-1.04
	Benzoic Acid	0.41	-1.01
	Phenol	0.63	-1.03

<sup>a</sup> NA = not available. No oxidation potential is observed for nitromethane.

### **2.3.7.2 Redox Potentials**

Oxidation and reduction potentials for each fluorophore and quencher are also needed for comparison of quenching data to Rehm-Weller theory (Equation 2.1). Redox potentials for each fluorophore and quencher are determined in methanol from cyclic voltammograms (see Appendix) and are summarized in Table 2.9. Based on the redox potentials, general trends can be hypothesized about the electron-donating or -accepting ability of the fluorophores and quenchers. Pyrene and phenol red are more likely to be reduced, or accept an electron. Conversely, purpurin and malachite green are more likely to be oxidized, or donate an electron. Of the quenchers, no oxidation potential is measurable for nitromethane over the range investigated, indicating that nitromethane is more likely to be reduced. The target quenchers are all more likely to be reduced, with reduction potentials that are closer to zero. The opposite is true for the interfering quenchers, in that all are more likely to be oxidized.

### **2.3.7.3 Singlet Excitation Energies**

Singlet excitation energies for each fluorophore are also needed for comparison of quenching data to Rehm-Weller theory (Equation 2.1). Singlet excitation energies ( $E_{0,0}$ ) are determined in methanol from absorbance and fluorescence spectra (see Appendix) and are summarized in Table 2.10. Phenol red has the largest singlet excitation energy (3.70 eV), while purpurin has the smallest (3.22 eV). Because the emission of all of the fluorophores occurs within the same spectral region, the range of singlet excitation energies is narrow, less



**Table 2.10.** Spectroscopic data for fluorophores in methanol at room temperature.

Fluorophore	$E_{0,0}$ (eV)
Pyrene	3.44
Purpurin	3.22
Phenol Red	3.70
Malachite Green	3.63

than 0.5 eV.

#### 2.3.7.4 Comparison to Rehm-Weller Theory

In order to examine the quenching mechanism for each fluorophore, measured rate constants are compared with Rehm-Weller theory. The relevant electrochemical ( $E_{\text{ox}}$ ,  $E_{\text{red}}$ ) and spectroscopic ( $E_{0,0}$ ) parameters for the fluorophores and quenchers are used to evaluate Equation 2.1 for each fluorophore-quencher pair. The  $\Delta G_{\text{et}}$  values calculated for each fluorophore-quencher pair are compared in Table 2.11 for each of the possible electron-transfer mechanisms. Mechanism I involves the transfer of an electron from the excited-state fluorophore ( $F^*$ ) to the ground-state quencher (Q), denoted as  $F^* + Q \rightarrow (F^+Q^-)^*$ . Mechanism II involves the transfer of an electron from the ground-state quencher to the excited-state fluorophore, denoted as  $F^* + Q \rightarrow (F^-Q^+)^*$ . Of the two, the mechanism that yields the more negative value of  $\Delta G_{\text{et}}$  is more thermodynamically favorable.

The  $\Delta G_{\text{et}}$  values for pyrene with each of the target quenchers (Table 2.11) suggest that the most probable quenching mechanism is via transfer of an electron from excited-state pyrene to the ground-state quencher (Mechanism I). This mechanism is consistent with that previously demonstrated by *ab initio* calculations with nitromethane.<sup>13</sup> This mechanism is also consistent with the trends in electron-donating and -accepting ability of the quencher molecules. During ion-pair formation with pyrene, the aromatic structure of nitrobenzene allows greater stabilization of the incurred negative charge than nitromethane, as reflected in their reduction potentials (Table 2.9). The result is a greater rate

**Table 2.11.** Free energy for electron-transfer ( $\Delta G_{\text{et}}$ , eV) from excited-state fluorophore to ground-state quencher (Mechanism I) and electron-transfer from ground-state quencher to excited-state fluorophore (Mechanism II). Boldface type indicates the more thermodynamically favorable mechanism.

Quencher	Pyrene		Purpurin		Phenol Red		Malachite Green	
	I	II	I	II	I	II	I	II
Nitromethane	<b>-2.00</b>	NA <sup>a</sup>	<b>-1.30</b>	NA	<b>-1.45</b>	NA	<b>-1.85</b>	NA
Nitrobenzene	<b>-2.53</b>	-1.25	<b>-1.83</b>	-1.00	-1.98	<b>-2.12</b>	<b>-2.38</b>	-1.85
4-Nitrotoluene	<b>-2.50</b>	-1.24	<b>-1.80</b>	-0.99	-1.95	<b>-2.11</b>	<b>-2.35</b>	-2.38
2,6-Dinitrotoluene	<b>-2.66</b>	-1.28	<b>-1.96</b>	-1.03	-2.11	<b>-2.15</b>	<b>-2.51</b>	-2.35
Aniline	-1.99	<b>-2.07</b>	-1.29	<b>-1.82</b>	-1.44	<b>-2.94</b>	-1.84	<b>-2.51</b>
Benzoic Acid	-2.02	<b>-2.07</b>	-1.32	<b>-1.82</b>	-1.47	<b>-2.94</b>	-1.87	<b>-1.84</b>
Phenol	<b>-2.00</b>	-1.85	-1.30	<b>-1.60</b>	-1.45	<b>-2.72</b>	-1.85	<b>-1.87</b>

<sup>a</sup> NA = not available. No oxidation potential is observed for nitromethane, so  $\Delta G_{\text{et}}$  values cannot be determined.

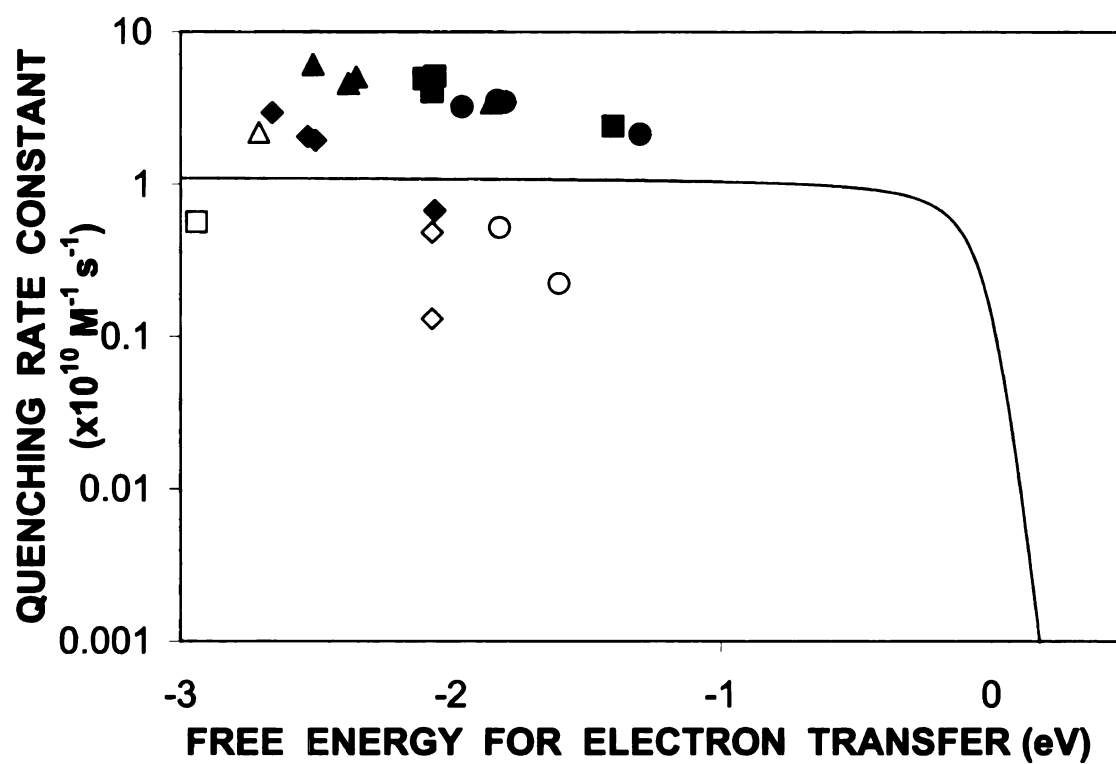
constant for quenching by nitrobenzene compared to nitromethane (Table 2.2). Similarly, the electron-donating methyl group of nitrotoluene increases the electron density of the aromatic ring compared to nitrobenzene. The increase in electron density results in less stabilization of the negatively charged ion, as reflected in the reduction potential, and a smaller rate constant. Finally, the additional nitro group of 2,6-dinitrotoluene significantly decreases the electron density on the aromatic ring, resulting in a substantially greater rate constant compared to 4-nitrotoluene. Because the electron-withdrawing capacity of the nitro group is much greater than the electron-donating capacity of the methyl group, the effect on the magnitude of the rate constant is not equal and opposite. Each of these trends is consistent with the measured Stern-Volmer quenching constants, rate constants, and the predicted  $\Delta G_{et}$  values for pyrene with the target quenchers.

The calculated  $\Delta G_{et}$  values (Table 2.11) indicate that Mechanism I is most likely for purpurin and malachite green with the target quenchers. It is noteworthy that the mechanism is similar to that for pyrene, despite the presence of functional groups on these fluorophores that may alter the electronic structure and interactions with the quenchers. In the case of phenol red, however, the alternative mechanism involving electron-transfer from the ground-state quencher to the excited-state fluorophore (Mechanism II) is more likely for the target quenchers. Regardless of the direction of electron transfer, all of the quenching rate constants are approximately equal to the diffusion limit of  $1.4 \times 10^{10} \text{ M}^{-1} \text{ s}^{-1}$  in methanol.<sup>16</sup> It is interesting that Mechanism II is also most

probable for all of the fluorophores with the interfering quenchers (Table 2.11). The values of  $\Delta G_{et}$  are relatively large and comparable to those for the target quenchers. However, the rate constants are substantially less than those for the target quenchers (Table 2.8).

Quenching rate constants for each fluorophore-quencher pair are compared to the  $\Delta G_{et}$  values predicted by Rehm-Weller theory in Figure 2.6. As a result of their shorter fluorescence lifetimes, the rate constants for all fluorophores with the target quenchers are comparable. In general, the magnitude of the rate constants is directly related to the magnitude of the  $\Delta G_{et}$  values according to Rehm-Weller theory. For the target quenchers, many of the measured rate constants are within a factor of two, and all are within a factor of five, of the predicted values.

In contrast, the rate constants for the fluorophores with the interfering quenchers are notably less than the values predicted by Rehm-Weller theory. A possible explanation for this discrepancy is that Rehm-Weller theory assumes the kinetic behavior is simply related to the thermodynamic behavior (i.e.,  $\Delta G^*_{et}$  is a monotonic function of  $\Delta G_{et}$ , Equation 2.3). This may not be true if steric or statistical considerations are important in the collisional interaction between the fluorophore and quencher. Another possibility is that Rehm-Weller theory assumes the redox potential of the excited-state fluorophore is simply related to that of the ground state (i.e.,  $E^*_{ox} = E_{ox} - E_{0,0}$  or  $E^*_{red} = E_{red} + E_{0,0}$ ). This may not be true if the excited and ground states differ substantially in electron distribution and density. Finally, it is possible that the model of simple outer-sphere electron



**Figure 2.6.** Comparison of experimental quenching rate constants for pyrene ( $\diamond$ ), purpurin ( $\circ$ ), malachite green ( $\Delta$ ), and phenol red ( $\square$ ) with target quenchers (filled) and interfering quenchers (unfilled) in methanol with Rehm-Weller theory (-).

transfer does not accurately describe the interaction between the fluorophore and the interfering quenchers.

## **2.4 Conclusions**

Of the extended group of fluorophores investigated in this study, pyrene, purpurin, malachite green, and phenol red are shown to have sensitive and selective quenching interactions with a target group of nitrated quenchers. The remaining fluorophores under investigation demonstrate little or no response to nitrated compounds. Because each fluorophore may interact with the quenchers through a different mechanism, various degrees of sensitivity and selectivity are observed. Of the fluorophores studied, pyrene demonstrates the greatest sensitivity for nitrated molecules, but its routine use presents health and waste disposal hazards. Purpurin, malachite green, and phenol red demonstrate less sensitivity but comparable or greater selectivity for nitrated molecules. Both malachite green and phenol red exhibit pH-dependent fluorescence, but only malachite green shows quenching behavior that is a function of pH. With buffering, the interference of acidic species on the quenching of malachite green fluorescence can be reduced. In general, pH-sensitive fluorophores are not ideal for application in the detection of explosives on-site, as various matrices may be encountered that could lead to erroneous results. Thus, among these potential fluorophores, purpurin shows the most promise for detection of nitrated explosives by fluorescence quenching.

Based on the results reported herein, purpurin, malachite green, or phenol red are suitable for a variety of applications. For example, they can be

used in the laboratory detection of nitrated explosives separated by using liquid chromatography. Following LC, the fluorophore can be added post-column and quenching monitored with a standard fluorescence detector.<sup>7</sup> In addition, field-ready devices can be developed by incorporation of these fluorophores into optical fiber sensors, wipes, air and water sampling tubes, etc. The use of handheld UV lamps and digital cameras is appropriate for these applications. The detection limits of the explosives must be determined and optimized for each of these applications.

In this work, only a limited number of potential fluorophores have been selected based on their structural similarities to pyrene. From these results, however, it is evident that mechanistic similarities do not follow directly from structural similarities. Consequently, a more broad and diverse selection of fluorophores may prove essential for the development of a fluorescence quenching method for the detection of nitrated explosives.



## 2.5 References

1. Yinon, J.; Zitrin, S. *Modern Methods and Applications in Analysis of Explosives*; Wiley: Chichester, UK, 1993.
2. Casamento, S.; Kwok, B.; Roux, C.; Dawson, M.; Doble, P. *J. Forensic Sci.* **2003**, *48*, 1075-1083.
3. Gholamian, F.; Chaloosi, M.; Husain, S. W. *Prop. Expl. Pyrotech.* **2002**, *27*, 31-33.
4. Wallenborg, S. R.; Bailey, C. G. *Anal. Chem.* **2000**, *72*, 1872-1878.
5. Jian, C.; Seitz, W. R. *Anal. Chim. Acta* **1990**, *237*, 265-271.
6. Zhang, S.; Lu, F.; Gao, L.; Ding, L.; Fang, Y. *Langmuir* **2007**, *23*, 1584-1590.
7. Goodpaster, J. V.; McGuffin, V. L. *Anal. Chem.* **2001**, *73*, 2004-2011.
8. Focsaneanu, K.-S.; Scaiano, J. C. *Photochem. Photobiol. Sci.* **2005**, *4*, 817-821.
9. Goodpaster, J. V.; McGuffin, V. L. *Anal. Chem.* **2000**, *72*, 1072-1077.
10. DeWitt, L.; Blanchard, G. J.; LeGoff, E.; Benz, M. E.; Liao, J. H.; Kanatzidis, M. G. *J. Am. Chem. Soc.* **1993**, *115*, 12158-12164.
11. Chernyak, V.; Reisfeld, R. *Chem. Phys. Lett.* **1991**, *181*, 39-44.
12. Hu, X.; Jiao, K.; Sun, W.; You, J.-Y. *Electroanalysis* **2006**, *18*, 613-620.
13. Goodpaster, J. V.; Harrison, J. F.; McGuffin, V. L. *J. Phys. Chem. A* **2002**, *106*, 10645-10654.
14. Rehm, D.; Weller, A. *Isr. J. Chem.* **1970**, *8*, 259-&.
15. Tachiya, M.; Murata, S. *J. Phys. Chem.* **1992**, *96*, 8441-8444.
16. Zanini, G. P.; Montejano, H. A.; Previtali, C. M. *J. Chem. Soc., Faraday Trans.* **1995**, *91*, 1197-1202.

### **CHAPTER 3**

#### **INVESTIGATION OF POTENTIAL FIELD-READY DEVICES FOR THE DETECTION OF NITRATED EXPLOSIVES VIA FLUORESCENCE QUENCHING**

Field-ready devices for explosives detection based on fluorescence quenching are currently being used in Iraq, and the improvement of such devices will inevitably increase the security of soldiers and other law enforcement agents. Because solid-state devices are most desirable for such applications, this chapter examines immobilization of the fluorophores identified in the solution-phase fluorescence quenching studies described in Chapter 2. The goal of fluorophore incorporation is to determine the viability of solid-state devices such as wipes and air sampling tubes for explosives detection. To identify the most appropriate matrix polarity, fluorescence of the dyes is first compared in a variety of solvents, including water, methanol, dioxane, and hexane. The most promising fluorescence is observed for malachite green and phenol red in dioxane, and for purpurin in methanol. Fluorescence of immobilized dyes is compared in matrices including filter paper and poly(ethylene glycol) of various molecular weights. For malachite green, incorporation into a poly(ethylene glycol) matrix yields the greatest fluorescence. Poly(ethylene glycol) containing malachite green is coated on filter paper, glass slides, and silica particles and the resulting devices compared with regard to their fluorescence and fluorescence quenching behavior. Ideally, stable fluorescence with UV excitation and visible emission would be observed in a matrix that could be easily incorporated into field devices such as wipes or air sampling tubes.

### **3.1 Experimental Methods**

The experiments related to the incorporation of fluorophores into solid-state devices are conducted with the assistance of Ms. Heidi Bonta, an undergraduate research assistant.

#### **3.1.1 Reagents**

Reagent-grade fluorophores are used as received and include purpurin (Fisher Scientific), phenol red (Aldrich), and malachite green (Sigma). Stock solutions of each fluorophore ( $10^{-3}$  to  $10^{-4}$  M) are prepared in dioxane (Sigma-Aldrich), hexane (Mallinckrodt), methanol (Sigma-Aldrich), methylene chloride (Mallinckrodt), and distilled, deionized water (Corning Glass Works, model MP-3A). Stock solutions are diluted to give working solutions of concentrations varying from  $10^{-3}$  to  $10^{-7}$  M. Poly(ethylene glycol) (Sigma-Aldrich) is obtained in molecular weights of 750, 1000, 1500, and 2000 g/mol. Malachite green is added into the melted polymer or into a solution of the polymer in dioxane or methylene chloride.

#### **3.1.2 Fluorescence Measurements**

Fluorescence of dye-containing substrates is visually observed by using a 366-nm handheld UV lamp (Mineralight Lamp, Multiband UV-254/366nm, Model UVGL-58) in the absence of ambient light. A conventional fluorimeter (Hitachi F-4500) is utilized for measurement of excitation and emission spectra. Quartz cuvettes with a 1-cm path length (Starna Cells) are used for solution-phase measurements, while a reflectance attachment is utilized for solid-phase

measurements (Hitachi Solid Sample Holder #650-0161). To use this reflectance attachment, the substrates must be attached to a support such as a microscope slide. Initially, fluorescence spectra are collected by using an excitation wavelength of 325 nm based on previous results (Chapter 2). Emission wavelengths are scanned at 240 nm/min from 330 – 500 nm. Excitation and emission wavelengths are optimized through iterative comparison of maxima in the emission and excitation spectra, respectively. Entrance and exit slit widths of 5 mm and a photomultiplier tube voltage of 950 V are employed for most measurements. Background fluorescence of each solvent or substrate is also measured for comparison. Analysis of the resulting data is completed using a spreadsheet program (Microsoft Excel, version 2003).

For quenching studies, solutions are prepared by combining stock solutions of malachite green and quencher in dioxane. The concentration of malachite green in each solution is  $2 \times 10^{-4}$  M, and the concentrations of quenchers nitromethane and nitrobenzene vary from  $2 \times 10^{-3}$  –  $1 \times 10^{-2}$  M. The fluorescence emission of these solutions is measured by using the spectroscopic system described previously (Section 2.2.2). Stern-Volmer constants for malachite green in dioxane are compared to those determined previously in methanol (Section 2.3.5).

### **3.1.3 Preparation of Solid Substrates**

To verify the fluorescence in the solid state, solid malachite green is mixed with potassium bromide (Spectrum, IR grade), ground, pressed into a pellet, and analyzed in the fluorimeter by using the reflectance attachment (*vide*

*infra*). Fluorophores are also examined on substrates including filter paper (Whatman), fiberglass filter paper (Hurlbut Paper Co.), Kimwipe sheets (Kimberly-Clark), and Grab-it dust cloths (S.C. Johnson & Son, Inc.). The fluorescence of the substrates before and after methanol pretreatment is compared. Pretreatment includes soaking in 3 mL of methanol and drying at 100 °C in an oven for 10 minutes and is designed to remove adsorbed compounds from the substrate. Fluorophores are adsorbed to paper-based substrates by soaking in 10 mL of fluorophore solution in an open Petri dish. The Petri dishes are placed in a fume hood the solvent is allowed to evaporate. Other materials including blue cotton cloth, unbleached paper towel, unbleached cardboard, and a sterile bandage pad are also investigated as substrates for malachite green. Fluorophore solution is applied dropwise onto the untreated substrate. Dry substrates are cut to fit onto a support (*vide infra*) and the fluorescence of the mounted substrates is measured by using the reflectance attachment.

Various techniques for mounting of substrates are evaluated, including different supports and adhesives. A glass microscope slide (Fisher Scientific) and black cardboard are investigated as potential support materials. Double-sided tape (3M Scotch Brand Tape), green laboratory tape (Shamrock), and white laboratory tape (Shamrock) are investigated as potential adhesives. Double-sided tape is applied between the substrate and support, whereas single-sided tape is applied on the front edges of the substrate and also with the substrate folded around the support and secured on the opposite side. Tapes and supports are compared to minimize the background fluorescence and

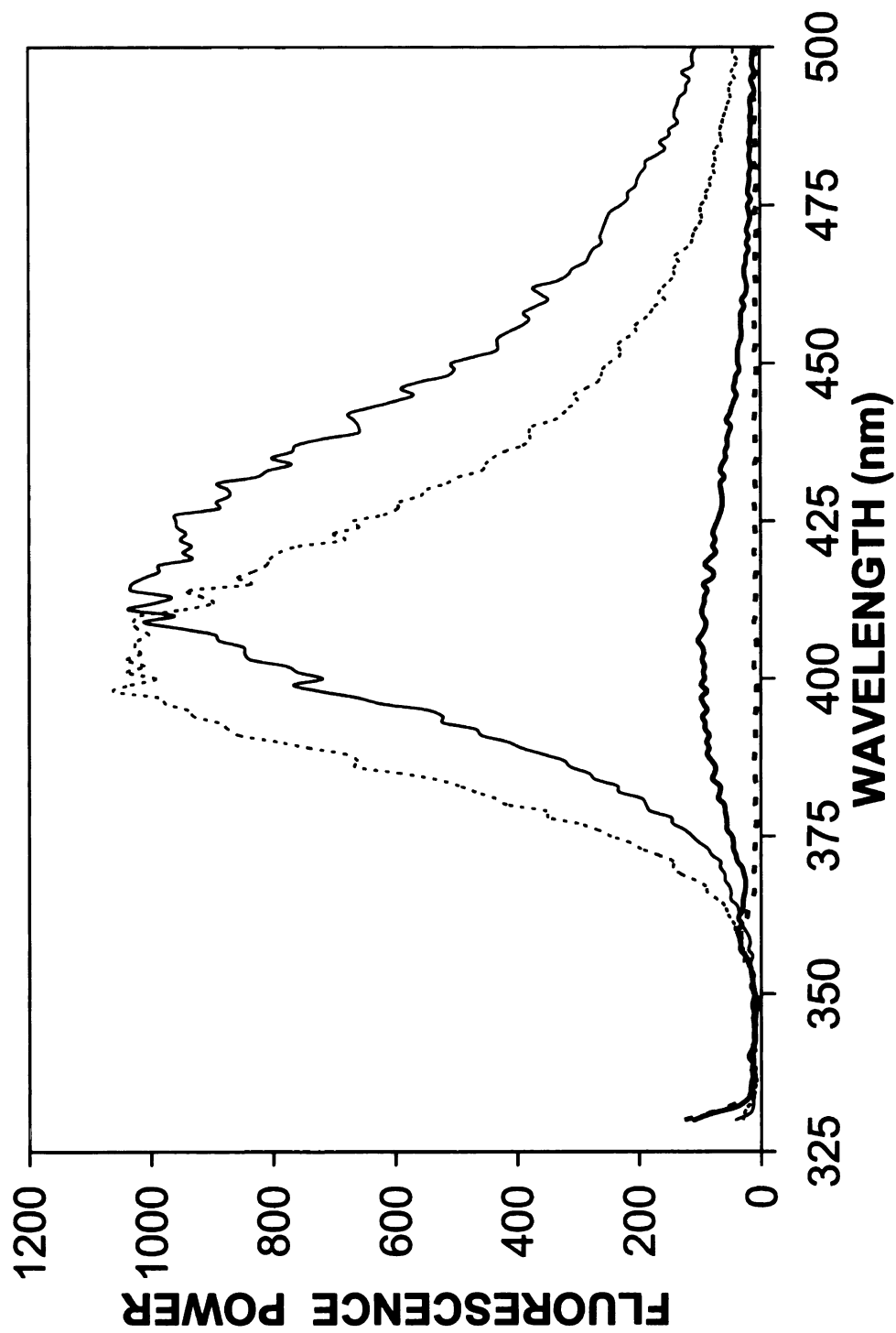
potential interference. For polymer substrates, mixtures of malachite green and poly(ethylene glycol) are poured onto the support. If solvent is used to dissolve the polymer and malachite green, the solvent is allowed to evaporate prior to fluorescence measurement.

Poly(ethylene glycol) is also supported on silica particles (Johns-Manville Products, Chromosorb, hexamethyldisilazane (HMDS) treated, 30/60 mesh). Particles are coated with a solution of poly(ethylene glycol) and  $5 \times 10^{-4}$  M malachite green in methylene chloride. The mixture is placed in a rotary evaporator and the solvent is allowed to evaporate slowly under vacuum. Adjusting the ratio of polymer mass to particle mass from 10 – 30% allows adjustment of the film thickness. The coated particles are packed into a quartz pyrolysis tube (CDS Analytical, Inc., part 10A1-3008) and secured on both ends with quartz wool (Alltech). Fluorescence of the coated particles is measured by using the spectroscopic system described in Chapter 2.

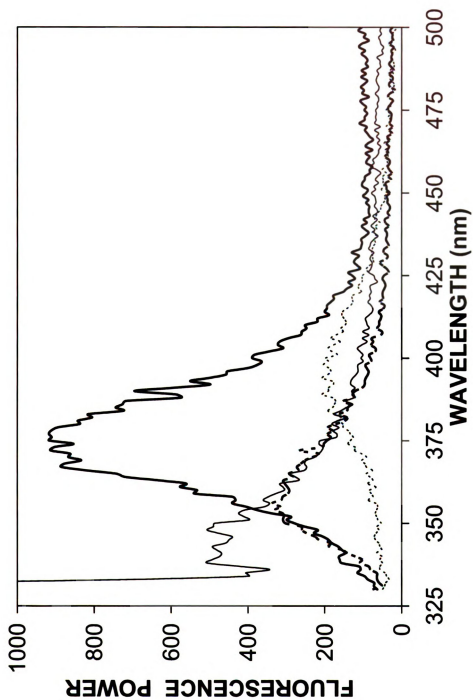
## **3.2 Results and Discussion**

### **3.2.1 Solution-Phase Fluorescence and Quenching**

For solution-phase measurements, solvent polarity is known to directly affect fluorescence emission.<sup>1</sup> Determination of optimum solvent polarity for each fluorophore provides insight into the most appropriate matrix for a solid-state device. For example, if the greatest fluorescence is observed in aqueous solution, polar matrices are most favorable, and a substrate such as cellulose may be ideal. The fluorescence of purpurin, malachite green, and phenol red are measured in water, methanol, dioxane, and hexane, as shown in Figures 3.1-3.3.

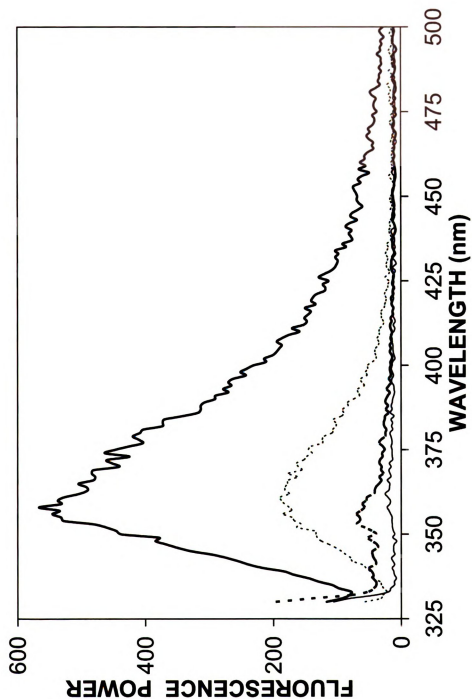


**Figure 3.1.** Fluorescence spectra of  $10^{-4}$  M purpurin in water (—), methanol (-.-), dioxane (---), and hexane (---) at room temperature. Excitation: 325 nm.



**Figure 3.2.** Fluorescence spectra of  $10^{-3}$  M malachite green in water (—), methanol (---), dioxane (· · ·), and hexane (— ·) at room temperature. Excitation: 325 nm.





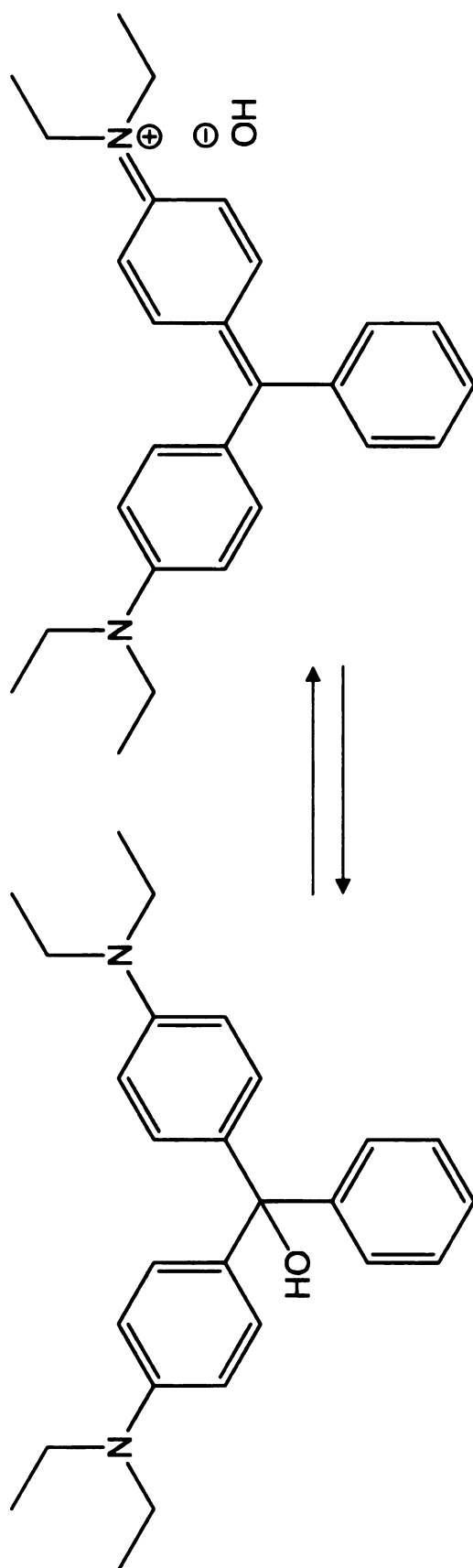
**Figure 3.3.** Fluorescence spectra of  $10^{-4}$  M phenol red in water (—), methanol (---), dioxane (· · ·), and hexane (- · -) at room temperature. Excitation: 310 nm.

The fluorescence power of malachite green and phenol red are greatest in dioxane, while the fluorescence power of purpurin is greatest in methanol and water. This result indicates that the fluorescent forms of malachite green and phenol red require less polar environments, while that of purpurin prefers polar environments. The optimum solvent conditions and maximum emission wavelengths are summarized in Table 3.1. The fluorescence power of both malachite green and purpurin is greater than that of phenol red. In addition, the fluorescence of purpurin is somewhat inconsistent, and spectra could not be measured reproducibly for solutions of similar concentration. Because the fluorescence spectra of malachite green are more reproducible than those of purpurin during the initial studies, malachite green is selected for use in further exploratory studies.

In addition to the fluorescence power, the appearance of malachite green in water, methanol, dioxane, and hexane is used to identify the most ideal environmental polarity. Malachite green is known to exist in two forms in solution, as shown in Figure 3.4. The ionic form, which predominates in polar solution, is blue-green and absorbs strongly at 618 nm. The color observed for solutions of malachite green in water and methanol is characteristic of the ionic form. The neutral form, however, predominates in non-polar solutions and is nearly colorless. The color observed for solutions of malachite green in dioxane and hexane is characteristic of the neutral form. Based on the color of malachite green solutions and the fluorescence spectra in Figure 3.1, the colorless form is the most fluorescent and is desirable for subsequent measurements.

**Table 3.1.** Optimized fluorescence excitation and emission parameters.

	<b>Solvent</b>	<b>Excitation Wavelength (nm)</b>	<b>Emission Wavelength (nm)</b>
Malachite Green	Dioxane	325	375
Purpurin	Methanol	325	405
	Water	325	418
Phenol Red	Dioxane	310	360

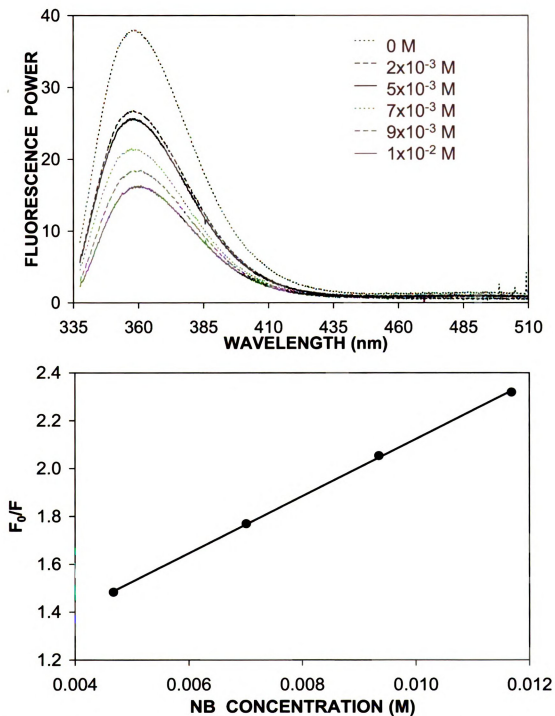


**Figure 3.4.** Structures of malachite green. Left: Neutral form. Right: Ionic form.

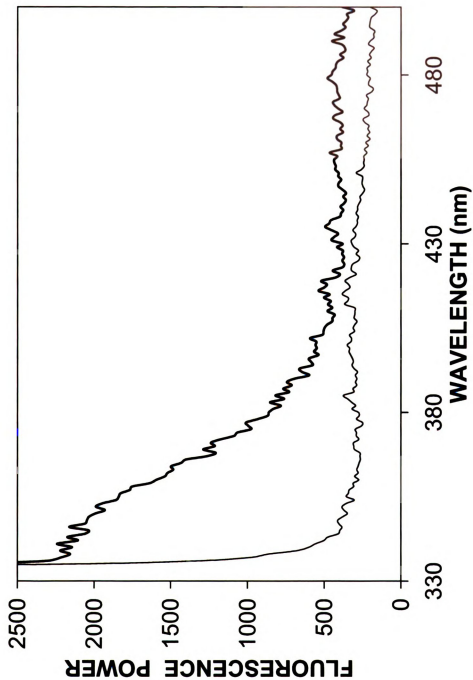
To determine the utility of an explosives detection device based on malachite green, the quenching behavior with model compounds is measured in dioxane. Quenching data for malachite green with nitrobenzene is given in Figure 3.5. The quenching constant for nitrobenzene in dioxane is  $120 \text{ M}^{-1}$ , which is significantly greater than the value measured previously in methanol ( $50 \text{ M}^{-1}$ , Chapter 2). The quenching constant for nitromethane in dioxane is  $5 \text{ M}^{-1}$ , which is significantly less than the value measured previously in methanol ( $36 \text{ M}^{-1}$ ). Despite the decrease in quenching constant for nitromethane, the increase observed for nitrobenzene is promising and indicates that a device based on malachite green in a non-polar matrix could be useful for nitroaromatic explosives detection.

### **3.2.2 Solid-Phase Fluorescence**

For nitrated explosives detection, the use of a solid-state fluorophore is more advantageous than a solution-phase fluorophore to avoid concerns of leakage or evaporation of the solvent. First, to verify that malachite green fluoresces in a solid form, a KBr pellet is prepared containing solid malachite green. The fluorescence of this mixture is measured in the fluorimeter, and the spectra are given in Figure 3.6. The increase in fluorescence that is observed upon addition of malachite green to the KBr indicates that the solid form of malachite green is sufficiently fluorescent. The emission spectrum of malachite green in KBr is similar to that in water, indicating that the polar KBr matrix is not optimal for this application.



**Figure 3.5.** Fluorescence spectra of  $2 \times 10^{-4}$  M malachite green in dioxane at room temperature in the presence of increasing concentrations of nitrobenzene (top) and the resulting Stern-Volmer plot (bottom). The Stern-Volmer constant for this data set is  $120 \text{ M}^{-1}$  with a correlation coefficient of 0.9997.



**Figure 3.6.** Fluorescence spectra of a KBr pellet (—) and a KBr pellet containing malachite green (---). Excitation: 325 nm.

The fluorescence power of malachite green is greatest in dioxane, indicating that a non-polar matrix is most desirable. The structure of poly(ethylene glycol) is similar in polarity to dioxane, as the polymer contains ether groups and only terminal hydroxyl groups. For design of an inexpensive field device, however, a poly(ethylene glycol) polymer will require the use of an additional support material for durability.

The effect of substrate pretreatment is investigated in which the fluorescence from substrates rinsed in methanol is compared to those that are unrinsed. Contaminants such as dust and other particulates that could be adsorbed to the surface may affect the observed fluorescence or the interaction of the fluorophore with the substrate. Overall, pretreatment of substrates has little effect on the fluorescence of the substrate or the fluorophore-coated substrate. Unrinsed substrates are utilized for all subsequent measurements.

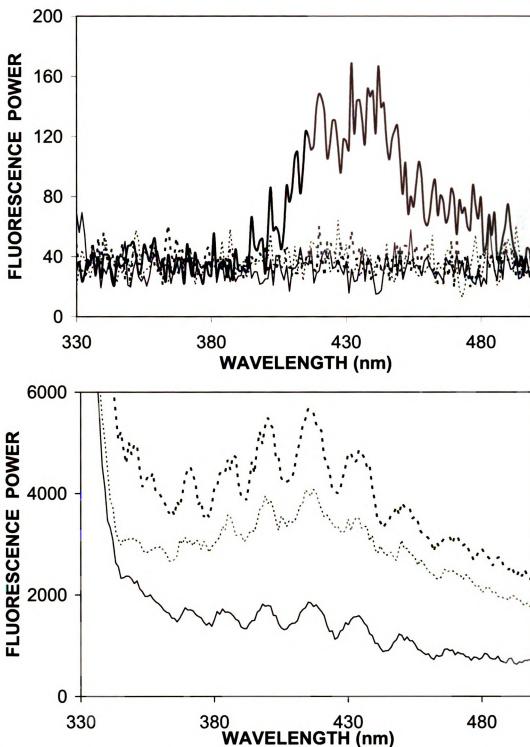
The fluorescence of the support materials is also investigated. Glass slides are found to have lower background fluorescence in the range of 385 – 400 nm compared to black cardboard. The low background is important to ensure that the contribution to the overall signal of the sample is minimal. Mounting of the paper substrates using double-sided tape also minimizes background fluorescence compared to using white or green tape on the back of the support. The orientation of the mounted substrate is also unimportant, as filter paper taped to a glass slide in a variety of possible orientations gives consistent fluorescence. Sufficient reproducibility is also observed, as the fluorescence power is consistent upon removing and reinserting mounted



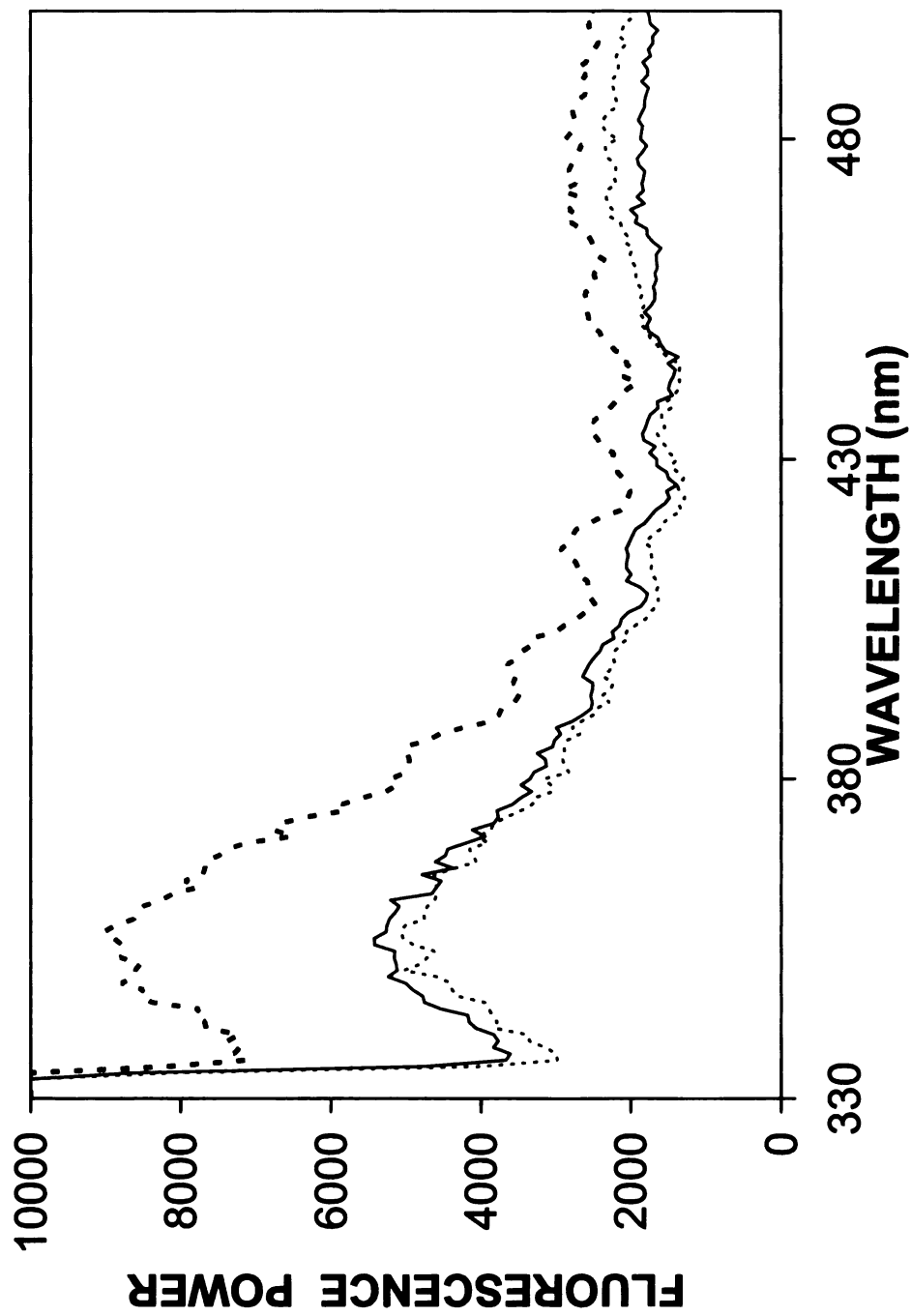
substrates. Based on these initial observations, paper substrates are mounted onto glass slides using double-sided tape for all subsequent measurements.

The fluorescence of malachite green is also studied on various substrates. Of the substrates investigated, fiberglass filter paper has the lowest background fluorescence (Figure 3.7, bottom). The fluorescence of the Grab-it cloth is significantly greater than that of the other substrates (Figure 3.7, top), indicating that interference with malachite green fluorescence may occur. Other substrates such as unbleached cardboard, unbleached paper towel, blue cloth, and sterile bandage pads have greater background fluorescence that is more irregular, also limiting their use in this application. In comparison to fiberglass filter paper and a Kimwipe, coated filter paper demonstrates the greatest fluorescence upon application of  $10^{-3}$  M malachite green in methanol (Figure 3.8). Based on these results, filter paper coated with malachite green is used for subsequent measurements.

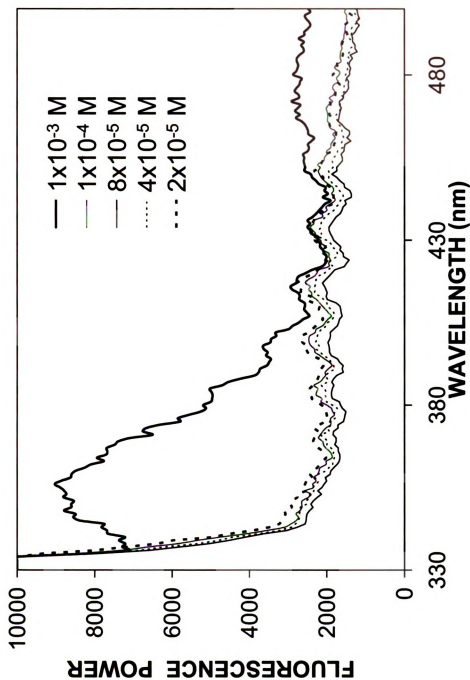
The concentration dependence of malachite green coated on filter paper is also of interest for future development of a field device. Fluorescence spectra for filter paper coated by using 10 mL of various concentrations of malachite green from  $2 \times 10^{-5}$  –  $1 \times 10^{-3}$  M are given in Figure 3.9. The filter paper coated by using the most concentrated solution displays the greatest fluorescence, and yields the only quantifiable peak observed for the different malachite green concentrations. The fluorescence of the filter paper coated with  $10^{-3}$  M malachite green, however, is not reproducible. Repeated studies using  $10^{-3}$  M and greater concentrations on filter paper do not yield measurable fluorescence. In addition,



**Figure 3.7.** Fluorescence spectra of a Kimwipe (---), filter paper (—), a Grab-it cloth (—), and fiberglass filter paper (—) at room temperature. Excitation: 325 nm. Slit width: 1 mm (top), 5 mm (bottom).



**Figure 3.8.** Fluorescence spectra of a Kimwipe (---), filter paper (— · —), and fiberglass filter paper (—) coated with  $10^{-3}$  M malachite green solution at room temperature. Excitation: 325 nm. Slit width: 5 nm.



**Figure 3.9.** Fluorescence spectra of filter paper coated with various concentrations of malachite green solutions at room temperature. Excitation: 325 nm. Slit width: 5 nm.

the fluorescence emission of malachite green on filter paper is more similar to the spectra observed in polar solvents such as water, indicating that greater fluorescence can be obtained in a less polar matrix.

Overall, although malachite green fluoresces in the solid state, the fluorescence cannot be measured reliably when coated on filter paper. Filter paper, like other cellulose-based paper products, contains many hydroxyl groups that contribute to the high polarity of the substrate. The result observed for malachite green on filter paper is consistent with that observed for polar solvents such as water and methanol, indicating that a less polar matrix is required for this application. The low background fluorescence of filter paper before and after coating with malachite green, however, indicates that this material is suitable as a support for poly(ethylene glycol) films containing malachite green.

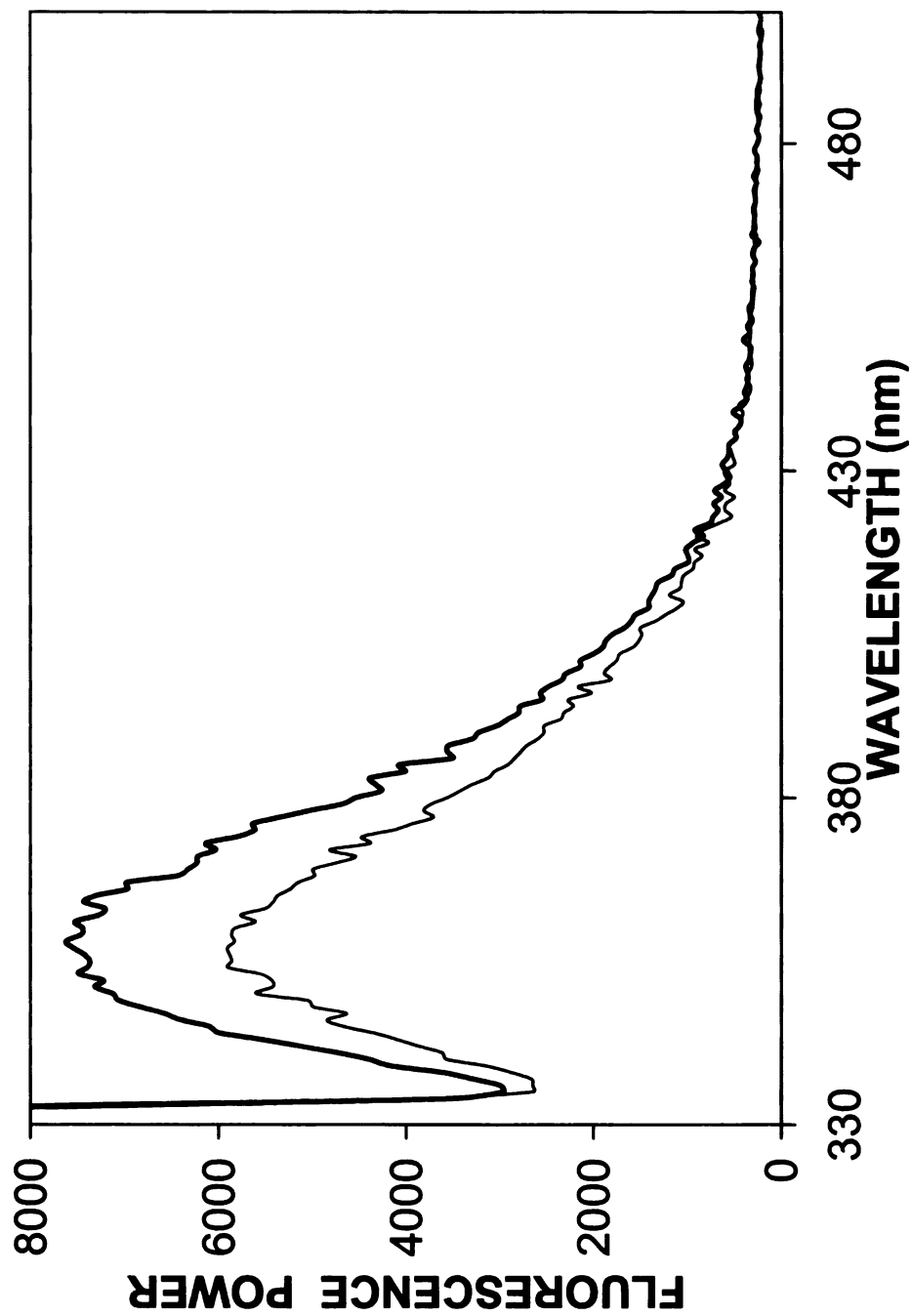
### **3.2.3 Poly(ethylene glycol)-Coated Substrates**

As discussed previously, dioxane and poly(ethylene glycol) (PEG) are comparable in polarity. Various molecular weights of PEG are investigated for utility in a field device for explosives detection, including 750, 1000, 1500, and 2000 g/mol. PEG 750 is a viscous liquid, PEG 1000 is a waxy solid, and PEG 1500 and 2000 are solids. Because a solid-state device is desired, the utility of PEG 750 is limited in this application. In addition, the melting point of PEG 1000 is 37 – 40 °C, indicating that at slightly elevated temperatures, such as in a warm climate, this material would also be liquefied. Based on this, the PEG 1500 and 2000 are utilized for measurements that follow. For incorporation of malachite green into the solid-state polymer, two methods are employed. One method

involves heating of the polymer beyond the melting point followed by addition of solid malachite green. Another method involves combination of solutions of the polymer and malachite green prepared in a suitable solvent. The solubility of PEG in various solvents is investigated, and methylene chloride, a common solvent for stationary phase preparation in gas chromatography, is determined to adequately dissolve both polymers as well as malachite green. The fluorescence of poly(ethylene glycol)-malachite green mixtures is investigated when supported on a glass slide, filter paper, and silica particles.

The fluorescence power of glass slides coated with PEG 1500 and 2000 containing malachite green is measured. The spectra in Figure 3.10 correspond to polymer mixtures prepared by heating the polymer above the melting point followed by addition of solid malachite green. Malachite green completely dissolves in the polymer matrix at slightly elevated temperature. The fluorescence power of malachite green in PEG 2000 is greater than that in PEG 1500 when coated on a glass slide. In addition, the fluorescence emission of malachite green in the polymer matrix is similar to the spectrum observed in dioxane, indicating that this matrix is sufficiently non-polar to allow maximum fluorescence emission. Based on this result, PEG 2000 is utilized for all subsequent measurements.

Malachite green and polymer solutions are coated onto filter paper in various mass ratios to determine the ratio that yields the greatest fluorescence power. Initial studies are performed by applying the polymer-malachite green solution in methylene chloride dropwise onto the filter paper in a Petri dish.



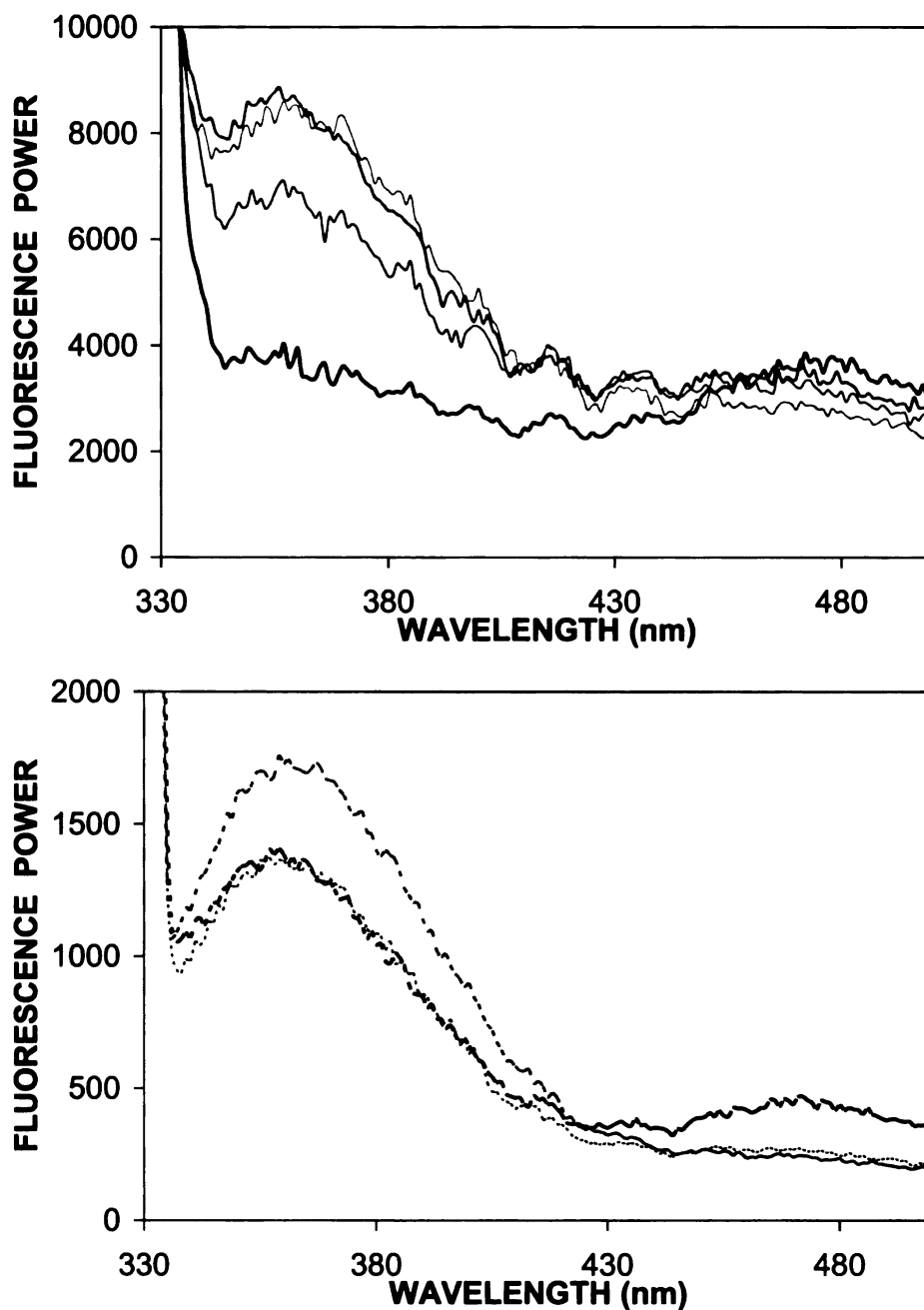
**Figure 3.10.** Fluorescence spectra of a glass slide coated with 1 mg malachite green in 2 g PEG 1500 (—) and PEG 2000 (---). Films prepared by using the melting technique. Spectra acquired at room temperature. Excitation: 325 nm. Slit width: 5 mm.

These studies indicate that this method is not reliable or reproducible because some mass of polymer may be lost to the Petri dish. The amount of polymer lost is inversely related to the amount of polymer present in the solution, as the increased viscosity in solutions of high polymer concentration prevents complete coverage of the filter paper. In addition, the capillary action that causes the polymer mixture to spread to the edges of the filter paper results in preferential migration of the malachite green with the solvent front. Once the solvent has evaporated, regions of higher malachite green concentration are visible by eye.

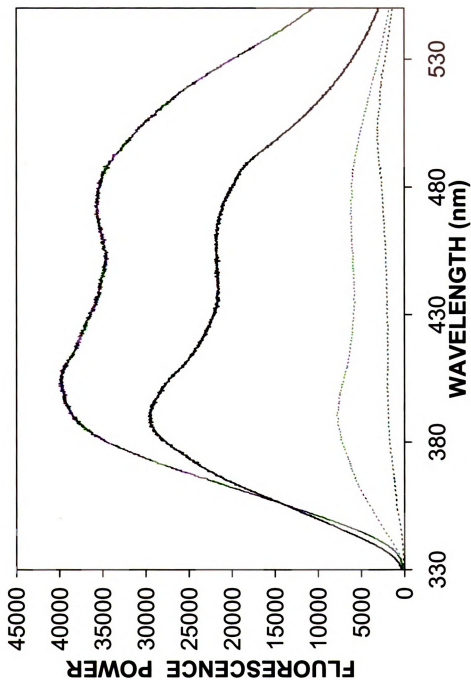
To overcome this problem, an application system based on capillary pressure is developed in which the solution is painted onto the filter paper using a fused-silica capillary. Solutions containing PEG 2000 and malachite green are prepared in methylene chloride and coated on the filter paper by applying 15 psi air pressure to the solution. The applied pressure causes displacement of the polymer solution through the capillary and onto the filter paper. As shown in Figure 3.11, as the proportion of polymer is increased in the solution, the fluorescence power of malachite green also increases.

The malachite green polymer is also coated onto silica particles as a method for explosives detection. The effect of polymer concentration or density is compared for silica particles with polymer-to-particle mass ratios of 10%, 20%, and 30% with incorporation of 0.17 mg malachite green. The fluorescence power for each of these coated particles is given in Figure 3.12. The fluorescence from these coated particles is also visible by eye under irradiation from a handheld UV lamp. As observed for the coated filter paper, the greatest fluorescence power is





**Figure 3.11.** Fluorescence spectra of filter paper coated with 0.17 mg malachite green and 0.8% (—), 1.6% (—), 4.1% (—), 5.4% (—), 8.1% (—), 16.3% (—), and 40.6% (---) PEG 2000. Percentages refer to the ratio of polymer mass to filter paper mass. Spectra collected at room temperature. Excitation: 325 nm. Slit width: 5 mm. PMT: 950 V (top), 700 V (bottom).



**Figure 3.12.** Fluorescence spectra of 0.1 g silica particles coated with 30% (---) PEG 2000 (w/w), and 0.17 mg malachite green and 10% (---), 20% (---), and 30% (—) PEG 2000 (w/w). Spectra acquired at room temperature. Excitation: 325 nm. Slit width: 0.1 nm. Integration time: 0.1 s.

observed for greater mass ratios or film thicknesses of the PEG polymer. Some discoloration of the particles is observed upon exposure to 325-nm laser irradiation, but when removed from the laser beam path the original color returns. An exposure study in which the tube is continuously irradiated with a laser source indicates that the fluorescence decreases rapidly (within 3 min), and only the background fluorescence of the polymer remains. At this point, it is unclear if fluorophore degradation would occur to the same degree if a lower power source is used.

### **3.3 Conclusions and Future Work**

A general protocol for incorporation of a solution-phase fluorophore into a solid-state device has been developed. Initial studies with various substrates indicate that a polar paper-based matrix alone is not sufficient to support the fluorescence of malachite green. In contrast, a less polar PEG solution containing malachite green fluoresces in the solid state when coated on glass slides, filter paper, or silica particles. The paper-based substrate coated with polymer can be developed as a wipe for detection of explosives on surfaces such as luggage or cargo. An air sampling device could be developed based on coated silica particles enclosed in a quartz tube. Malachite green may be a useful fluorophore for these devices if a lower power source is utilized, such as a handheld lamp. Similar procedures could be investigated for devices containing phenol red and purpurin. For any device, the fluorescence must be stable upon source irradiation to prevent false positives from fluorophore degradation. In addition, significant testing with explosive particles and vapors is necessary to

verify that the quenching behavior observed in the solution phase is also observed in the polymer matrices.

### **3.4     References**

1.     Lakowicz, J. *Principles of Fluorescence Spectroscopy*; Plenum Press: New York, NY, 1983.

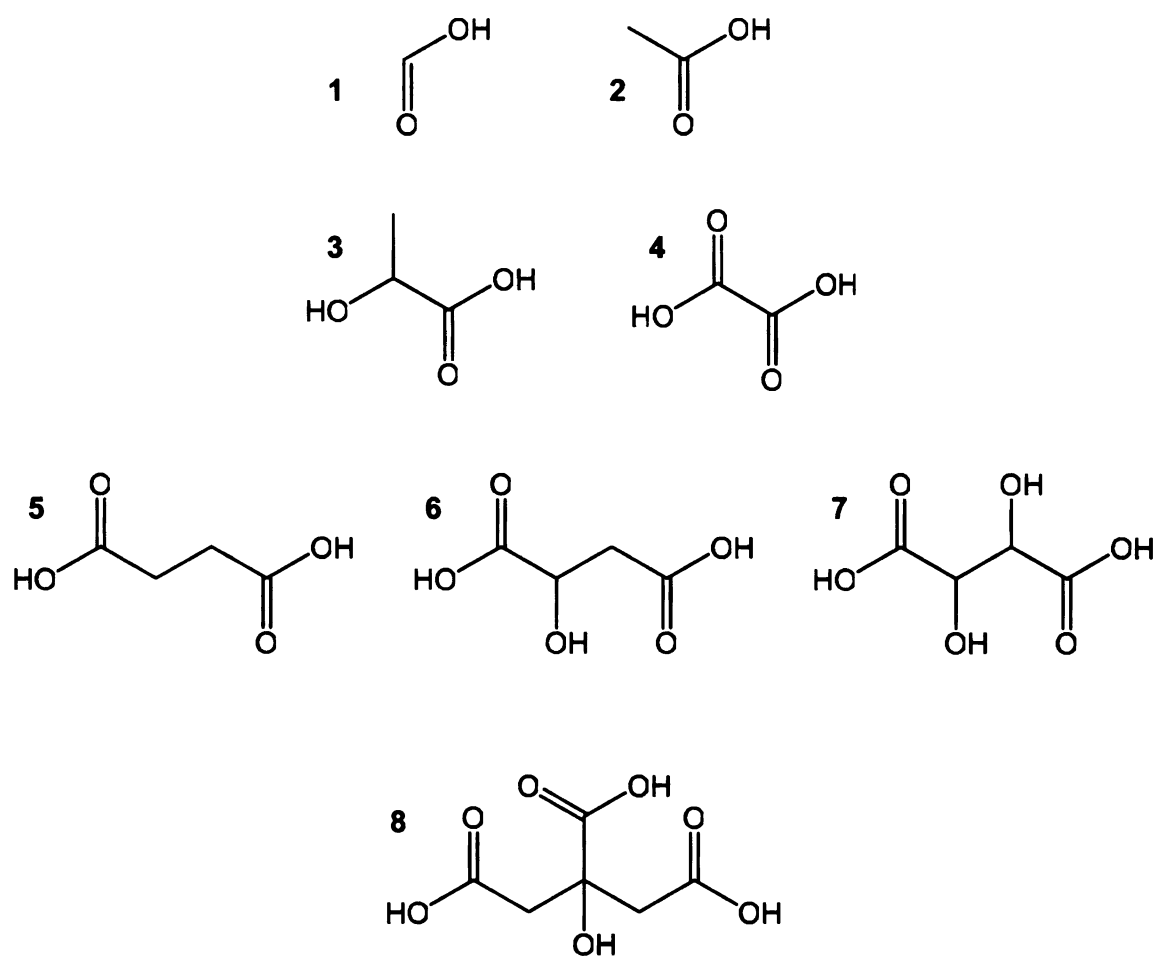
## CHAPTER 4

### pH-ENHANCED FLUORESCENCE DETECTION OF ACIDS

A novel method for determination of acidic species based on the pH-sensitive fluorescence of fluorescein is presented. Fluorescein is a commonly used fluorophore whose quantum yield changes dramatically as a function of protonation state and, therefore, of solution pH. For a compound more acidic than fluorescein ( $pK_a \leq 5.5$ ), proton transfer will lead to a decrease in fluorescence that can be employed in quantitative or qualitative analysis. The fluorescence response of fluorescein is investigated using a series of organic and inorganic acids, and is shown to be sigmoidal with the logarithm of proton concentration. The linear range extends two orders of magnitude and is centered about the fluorescein concentration in solution. The linear range can be extended to four orders of magnitude using a sigmoidal curve fit, and can be shifted to higher or lower concentrations by adjustment of the fluorescein concentration. This method is applied to the analysis of grape juice and a variety of wine and vinegar samples following liquid chromatography. Improvements in sensitivity and selectivity are observed for acids found in these beverages and foods upon direct comparison to UV-absorbance detection.

#### 4.1 Introduction and Background

The determination of low-molecular-weight (LMW) organic acids (Figure 4.1) is important in a variety of fields. These compounds are present in physiological fluids as intermediates or final products in many metabolic pathways. The role of these acids in metabolism of fats, amino acids, and



**Figure 4.1.** Structures of common low-molecular-weight organic acids. Formic acid (1), Acetic acid (2), Lactic acid (3), Oxalic acid (4), Succinic acid (5), Malic acid (6), Tartaric acid (7), Citric acid (8).

carbohydrates makes their determination an important indicator of organ function.<sup>1-3</sup> In the environment, LMW organic acids may originate from combustion of fossil fuels, burning of biomass in incinerators, or from photooxidation of organic compounds.<sup>4</sup> High concentrations of these acids are found in soils and plants, especially at the soil-root interface where nutrient uptake occurs. The presence of these acids affects plant uptake of nutrients and toxins by enhancing the availability of anions to plants.<sup>5,6</sup> In addition, the solubility of toxins such as heavy metals and phosphorous in soil can be affected by LMW organic acids through complexation and acid-base reactions.<sup>7</sup>

Another field in which LMW organic acids are important is food and beverage analysis.<sup>1,8,9</sup> One of the most common applications is in quality control of wines, as the LMW organic acid content is strongly correlated with the color, odor, and flavor of the wine.<sup>8,9</sup> Grapes, the source of many traditional wines, contain numerous acids such as tartaric, citric, and malic acids. The properties of the wine are related to the distribution of these acids, which are often added to wines after fermentation to decrease the pH.<sup>8</sup> In addition, malic acid can undergo bacterial fermentation to form lactic acid during wine production, which results in a pH decrease and decreased wine quality.<sup>8</sup> The complexity of the fermentation process and the dependence of wine quality on pH motivate the analysis of acids in wines and related products in the food and beverage industry

In addition to wine, the quality of several related food and beverage products can also be affected by acid content. For example, grape juice contains acids such as tartaric, citric, and malic acids. As with wine, these acids are often



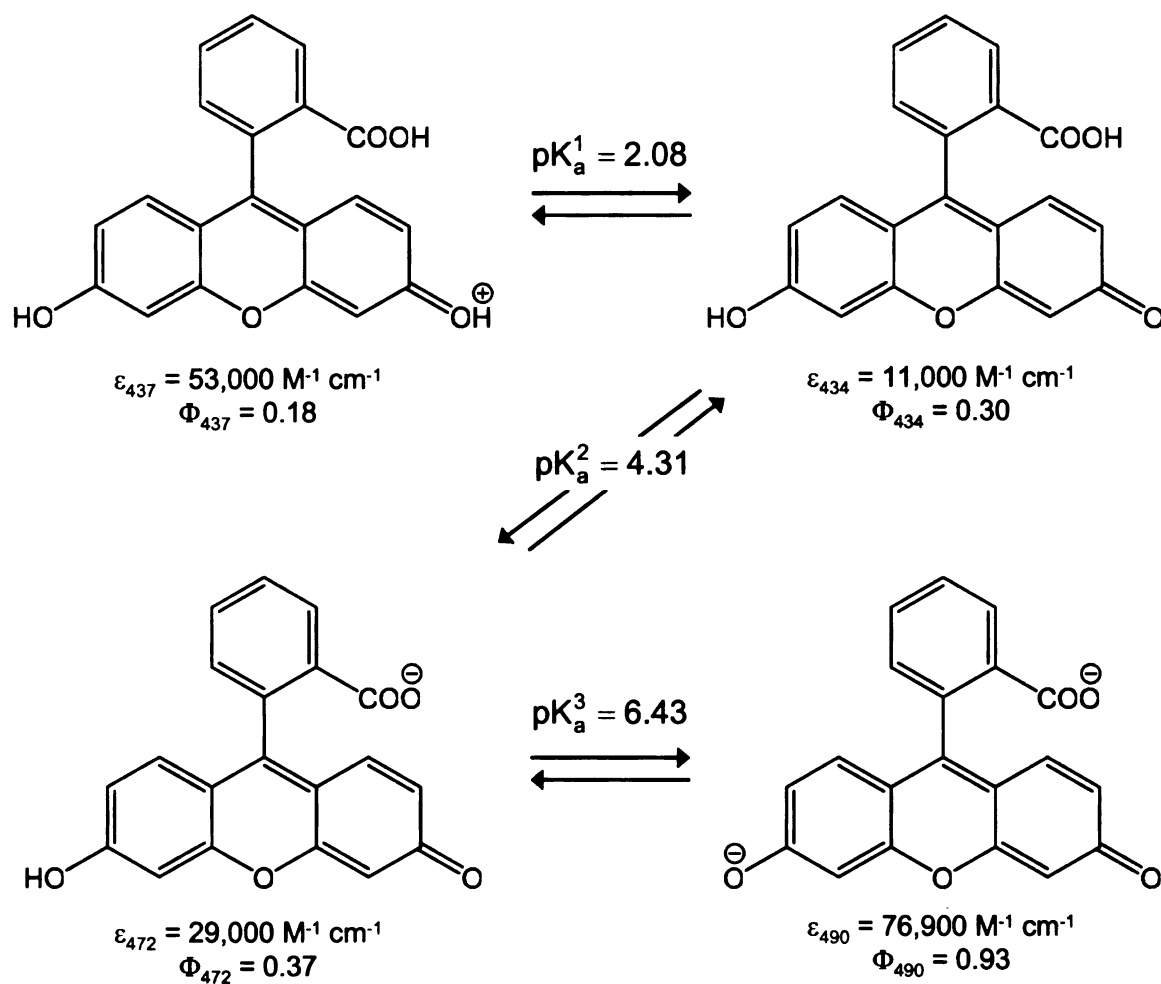
added to grape juice for pH adjustment, and their relative concentrations are important in the overall quality of the product. Upon fermentation, carbohydrates or sugars in the juice are converted to alcohols to produce wine. Further fermentation of wine or grape products involves oxidation of alcohols to acids, producing vinegars. Thus, many types of vinegar also contain a number of acids that are related to the origin of the vinegar as well as the degree of oxidation. To decrease cost, many types of vinegar are produced from acetic acid solutions, in which sugars and colors are added to reproduce the flavor of natural aging and fermentation. Analysis of the acid content of such vinegars can reveal the natural products present only in high quality, aged vinegar.

The most common methods for analysis of LMW organic acids in foods and beverages are liquid chromatography (LC)<sup>9-22</sup> or capillary electrophoresis (CE)<sup>8,18,23-33</sup> with UV-absorbance<sup>8-10,18-32</sup> or conductimetric detection.<sup>9,14-18,24,33</sup> Both LC and CE provide sufficient separation of LMW organic acids in the neutral and ionic forms, respectively. The sensitivity of UV-absorbance and conductimetric detection methods are also sufficient for the primary LMW organic acid components in food and beverage samples. The greatest drawback of UV-absorbance and conductimetric detection, however, lies in the lack of selectivity of these methods. Conductimetric detection responds to all ionic species by measuring the change in current that results from the presence of charged molecules. Similarly, UV-absorbance detection responds to all species with sufficient molar absorptivity at the monitored wavelength. Although UV-absorbance detection is often considered more selective than conductimetric

detection, this is not the case for LMW organic acids. The main UV-absorbing functionality on LMW organic acids is the carboxylic acid group, for which the wavelength of maximum absorbance is from 180 – 220 nm.<sup>1,6,8,9,18,30,31</sup> The potential for interference is great, as many, if not most, other functional groups also absorb in this region. To overcome this limitation, indirect UV-absorbance detection is used with CE and provides greater selectivity than direct detection. The selectivity and sensitivity of indirect UV-absorbance detection arise from the use of a secondary compound that absorbs at a longer wavelength, thereby reducing interferences.<sup>6</sup>

This work describes a new alternative to indirect UV-absorbance detection to improve selectivity in the detection of LMW organic acids. A novel detection method based on pH-dependent fluorescence of fluorescein is presented. Fluorescein is a commonly used fluorophore with desirable properties such as a high molar absorptivity, high fluorescence quantum yield, and good photostability.<sup>34,35</sup> In solution, fluorescein occurs in cationic, neutral, anionic, and dianionic forms, depending on the pH (Figure 4.2). The fluorescence properties, including the molar absorptivity ( $\epsilon$ ) and quantum yield ( $\Phi$ ), change as a function of the degree of protonation.<sup>34</sup> These quantities are greatest for the dianionic form and decrease with increasing protonation to the anionic, neutral, and cationic forms.<sup>34</sup> The pH-sensitivity of fluorescein results in a decrease in fluorescence in the presence of acidic species.

In this study, an experimental system has been developed for separation of neutral LMW organic acids by reversed-phase LC using an unbuffered mobile



**Figure 4.2.** Acid-base equilibria of fluorescein in aqueous solution at room temperature. Molar absorptivity ( $\epsilon$ ) and quantum yield ( $\Phi$ ) are given for each form at the wavelength of maximum absorbance.

phase. After the separation, the pH is adjusted to a more neutral value and fluorescein is introduced post-column. When no acids are present, a constant elevated background of fluorescein is detected by laser-induced fluorescence. In the presence of LMW organic acids, however, the fluorescence is decreased below the background level to yield a negative signal. The decrease in fluorescence arises because the acids transfer protons to the fluorescein molecules, causing a decrease in the fluorescence quantum yield. This method facilitates the determination of LMW organic acids in grape-based juice, wines, and vinegars by simplifying the chromatograms of the complex sample matrices by detecting only acidic species.

## **4.2 Experimental Methods**

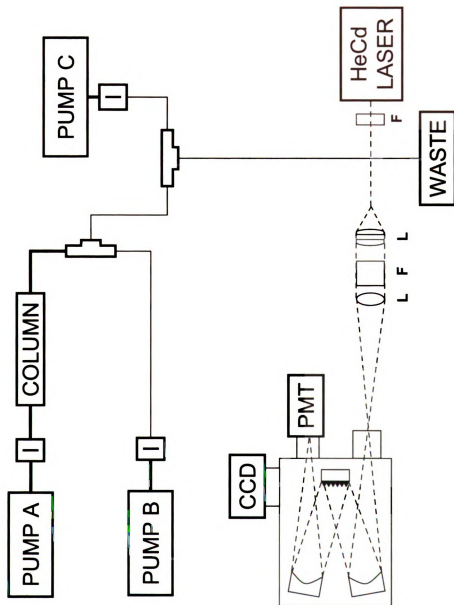
### **4.2.1 Reagents**

Reagent-grade acetic acid (Aldrich), benzoic acid (Spectrum), citric acid (MCB Chemical), formic acid (JT Baker), hydrochloric acid (JT Baker), lactic acid (JT Baker), maleic acid (JT Baker), malic acid (Sigma), oxalic acid (JT Baker), succinic acid (Sigma), and tartaric acid (JT Baker) are used to prepare aqueous stock solutions at 25 mM concentration. Aqueous fluorescein solutions are prepared at 5 mM concentration by using the disodium salt (Sigma). High-purity, spectroscopic grade methanol (Honeywell Burdick and Jackson) and distilled deionized water (Corning Glass Works, model MP-3A) are used for solution preparation and to prepare mobile phases for liquid chromatography. Fresh solutions are prepared daily, and stock solutions are stored in a refrigerator to prevent degradation. Grape juice, wines, and vinegars are purchased from local

supermarkets and are filtered prior to analysis. Sodium nitrate (JT Baker) is used as a void marker for UV-absorbance detection and is added to samples in a final concentration of 0.1 mM.

#### **4.2.2 Chromatographic System**

A system has been designed for the analysis of acids in beverages and other food samples (Figure 4.3). In this system, a reciprocating piston pump delivers the mobile phase at a nominal flow rate of 1.0 mL/min. The mobile phase for separation of acids in beverages consists of 1% methanol in distilled deionized water, adjusted to pH 3.0 using hydrochloric acid. Samples are introduced by using a 20- $\mu$ L injection valve (Valco Instruments, model EC6W) onto the reversed-phase chromatographic column (Supelco Hypersil ODS, 5  $\mu$ m particles, 250 mm x 4.6-mm i.d.). The terminus of the column is connected to a stainless steel tee (Valco Instruments, model ZT1), where the effluent is mixed with an aqueous solution of 10 mM sodium hydroxide (Aldrich) to increase the pH to approximately 8.0. The sodium hydroxide solution is delivered to this tee at 0.15 mL/min by using a syringe pump (Applied Biosystems, model 140) and a 10-mL injection valve (Rheodyne, model 7125). The pH-adjusted effluent is then directed to a second tee where an aqueous solution of 5 mM fluorescein is introduced at 0.30 mL/min by using another syringe pump and 10-mL injection valve. After mixing, the effluent is directed to a fluorescence detector (*vide infra*). For comparison, the column effluent is also directly connected to a UV-visible absorbance detector (Jasco, model UVIDEC-100-V, 215 nm, 1 cm pathlength). The UV-absorbance data are collected by using a commercially available



**Figure 4.3.** Schematic diagram of the experimental system used for determination of LMW organic acids in beverages by liquid chromatography with pH-dependent fluorescence detection. Pump A: Delivery of sample, Pump B: Delivery of 10 mM sodium hydroxide, Pump C: Delivery of 5 mM fluorescein. I = injection valve, L = lens, F = filter, PMT = photomultiplier tube, CCD = charge-coupled device. Dark lines indicate 1/16" stainless steel tubing. Light lines indicate 340- $\mu$ m o.d. capillary tubing.

interface (National Instruments, model BNC 2120) and associated software (National Instruments, Labview, version 5.1). Retention times are consistent for known solutes with each detector, indicating that no correction is needed in order to align chromatograms obtained using UV-absorbance and fluorescence detection.

#### **4.2.3 Spectroscopic System**

Chromatographic detection is achieved by using a laser-induced fluorescence spectrometer as shown in Figure 4.3 and described in detail elsewhere.<sup>36</sup> In this system, a helium-cadmium laser (Melles Griot, model 3074-40M, 325 nm, 20 mW) is focused onto a fused-silica capillary flow cell (Polymicro Technologies, 180- $\mu$ m i.d., 340- $\mu$ m o.d.). Fluorescence emission is collimated, filtered to remove scattered laser light, and refocused onto the entrance slit of a 0.34-m Czerny-Turner monochromator (Instruments SA, model 340E, 300 groove/mm grating). Emission is collected by using a thermoelectrically cooled, charge-coupled device (CCD) detector (Instruments SA, model (A)TECCD-2000x800-7) operated at 240 K, which allows collection of the entire fluorescence spectrum over a 220-nm range. The spectrometer is also equipped with a photomultiplier tube (Hamamatsu, model R-106, 10-nm bandpass) used for chromatographic studies. Instrument control and data acquisition are provided by a commercially available electronic interface (Instruments SA, model Datascan 2) and associated software (Instruments SA, Spectramax for Windows, version 3.1).

For initial steady-state studies with test acids, the CCD detector is used to collect the fluorescein emission spectrum as a function of acid concentration. The peak height at the maximum emission wavelength (510 nm) is used for the construction of a static calibration curve for each test acid. For chromatographic studies, the photomultiplier tube is used to measure the fluorescence emission at 510 nm as a function of time. Peak heights and areas are calculated from the chromatographic peaks and are used for the construction of calibration curves. Peak-fitting software is used for data analysis (Microsoft Excel, version 2003) and non-linear regression (Table Curve 2D, Jandel Scientific, version 2.02).

### **4.3 Results and Discussion**

#### **4.3.1 Method Development and Optimization**

As discussed previously, the decrease in fluorescence is related to the number of protons transferred from the acid to fluorescein. The number of protons available is dependent on the relative strength of the acid compared to the strength of fluorescein. For acids with  $pK_a \leq 5.5$ , approximately 1 pH unit below the  $pK_a$  of the fluorescein dianion, protons are completely transferred to fluorescein and measured as a decrease in fluorescence. For monoprotic acids, the concentration of protons available for donation to fluorescein is equal to the concentration of acid in the sample. For diprotic and triprotic acids with all  $pK_a$  values  $\leq 5.5$ , however, the concentration of protons available is two and three times the concentration of acid in the sample, respectively. In all cases, the behavior of fluorescein and an acid is inherently similar to the titration of a weak base. In a traditional titration of this type, the pH is monitored as a function of the

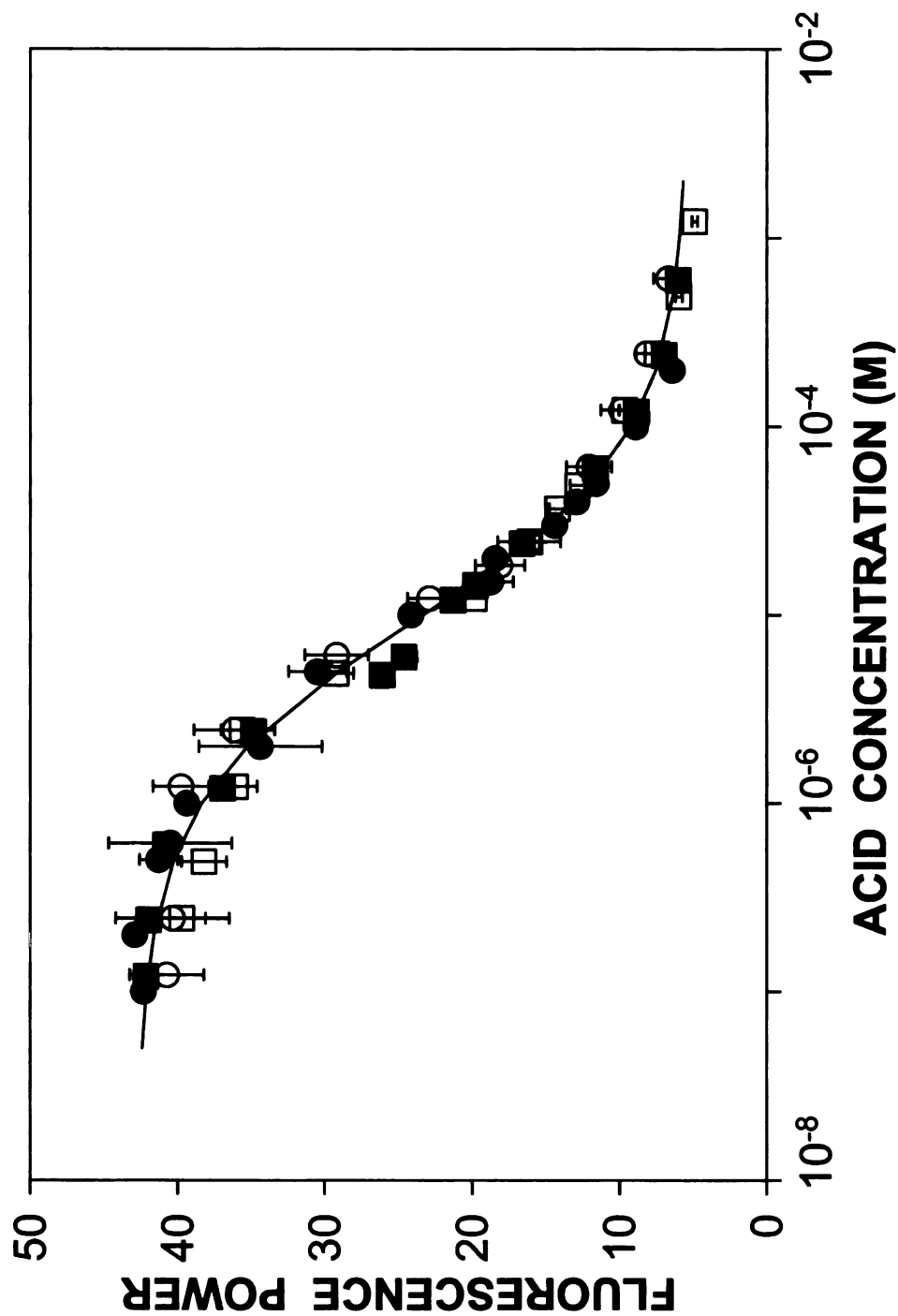


volume of acid added, while in this method the fluorescence is monitored as a function of pH (or  $-\log [\text{acid}]$ ). Thus, the calibration curve is inherently sigmoidal in shape, as demonstrated in Figure 4.4.

#### **4.3.1.1 Analysis of Test Acids**

The response of fluorescein is first investigated by measurement of the solution fluorescence in the presence of various acid concentrations. Four test acids are selected for steady-state studies, including a strong acid (hydrochloric acid), a monoprotic weak acid (benzoic acid,  $\text{pK}_a = 4.21$ ), a diprotic weak acid (maleic acid,  $\text{pK}_a = 1.97, 6.07$ ), and a triprotic weak acid (citric acid,  $\text{pK}_a = 3.15, 4.77, 6.40$ ). The fluorescence of a  $10^{-5}$  M fluorescein solution is measured in the presence of  $10^{-3}$  to  $10^{-7}$  M concentration of each acid (Figure 4.4). As mentioned previously, the number of available protons is dependent on the  $\text{pK}_a$  values for the acids relative to that of disodium fluorescein. Although maleic acid is a diprotic acid, it behaves as a monoprotic acid with fluorescein because the second  $\text{pK}_a$  value is greater than  $\sim 5.5$ . Similarly, citric acid behaves as a diprotic acid with fluorescein because the third  $\text{pK}_a$  value is greater than  $\sim 5.5$ . For this reason, the concentration of available protons in the solution is twice the prepared concentration of citric acid.

After correction of the proton concentration, Figure 4.4 demonstrates that fluorescein has the same sigmoidal response to all four acids, regardless of acid strength for  $\text{pK}_a$  values  $\leq 5.5$ . The resulting advantage is that a single calibration curve can be constructed using a test acid and applied for the quantitation of any acid in an unknown sample. It is also noteworthy that the



**Figure 4.4.** Sigmoidal calibration curve for four test acids in water, determined from the fluorescence power of fluorescein at 510 nm. Test acids: hydrochloric acid (●), benzoic acid (○), maleic acid (■), citric acid (□). Non-linear correlation coefficient ( $R^2$ ) = 0.9921.

inflection point of the sigmoidal curve is centered about  $10^{-5}$  M acid concentration and the curve is linear for two orders of magnitude. At the inflection point, the concentrations of fluorescein and acid are equivalent at  $10^{-5}$  M. Hence, another advantage of this method is that the linear range can be translated to higher or lower concentrations for a variety of applications by adjustment of the fluorescein concentration.

To linearize the calibration curve, the fluorescence power of fluorescein as a function of acid concentration is fit by nonlinear regression to a sigmoidal function.

$$y = a + \frac{b}{1 + \exp\left(\frac{c - x}{d}\right)} \quad (4.1)$$

In this function,  $y$  is the fluorescence power,  $x$  is the logarithm of the acid concentration, and  $a$ ,  $b$ ,  $c$ , and  $d$  are fit parameters determined by least-squares regression (Table 4.1, top). For the test acids, correlation coefficients ( $R^2$ ) for the sigmoidal function are greater than 0.994, indicating a strong correlation. The fit parameters  $a$ ,  $b$ ,  $c$ , and  $d$  are use to predict the fluorescence power resulting from a given concentration by graphing the logarithm of the acid concentration ( $x$ ) as a function of the sigmoid transform function ( $z$ ).

$$z = -\ln\left(\frac{b}{y - a} - 1\right) + c \quad (4.2)$$

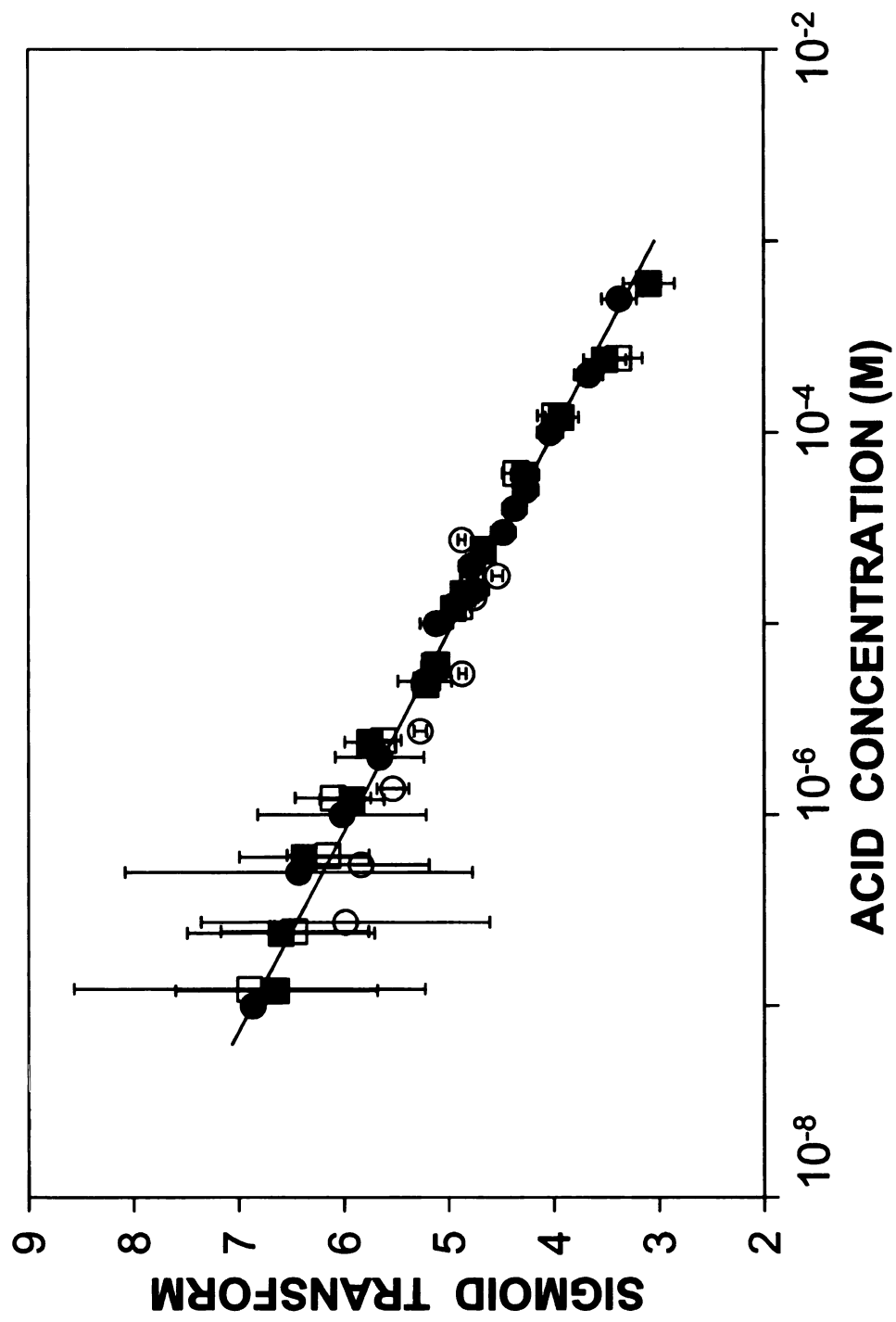
The remaining variables in Equation 4.2 are as defined in Equation 4.1. The resulting calibration curve is linear over four orders of magnitude (Figure 4.5, Table 4.1, bottom).

**Table 4.1.** Correlation coefficient ( $R^2$ ) and parameters of fit (a-d) for test acids to sigmoidal function (Equation 4.1) (top) and the corresponding correlation to the sigmoid transform function (Equation 4.2) (bottom).

Acid	Sigmoidal Function				
	a	b	c	d	$R^2$
Hydrochloric	2912	41420	5.012	0.5587	0.9946
Benzoic	8289	35560	5.027	0.3732	0.9962
Maleic	5153	39290	5.145	0.5384	0.9944
Citric	5389	35380	5.282	0.4646	0.9944

Acid	Linear Sigmoidal Transform		
	m	b	$R^2$
Hydrochloric	0.9854	0.0718	0.9943
Benzoic	0.9432	0.2707	0.9320
Maleic	0.9998	-0.0193	0.9898
Citric	0.9949	0.0213	0.9874



**Figure 4.5.** Linear calibration curve following sigmoid transform for four test acids in water, determined from the fluorescence power of fluorescein at 510 nm. Test acids: hydrochloric acid (●), benzoic acid (○), maleic acid (■), citric acid (□). Linear correlation coefficient ( $R^2$ ) = 0.9729.

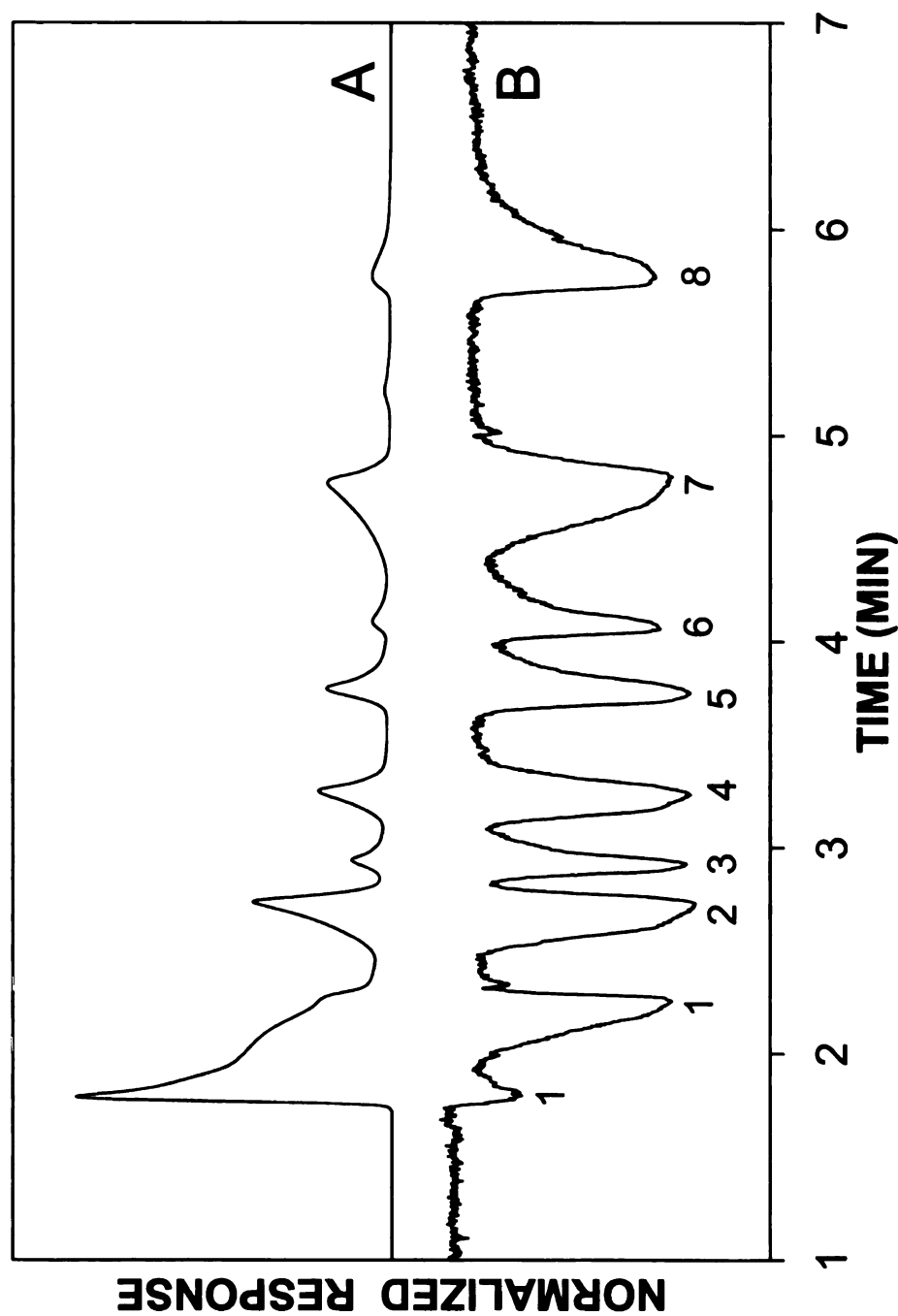
#### 4.3.1.2 Chromatographic Optimization

This pH-sensitive detection method can be practically applied to separations by LC or CE. In order to separate a standard mixture of LMW organic acids by reversed-phase liquid chromatography, the acids must be uncharged. Thus, the pH of the mobile phase is adjusted to pH 3.0 using hydrochloric acid. A buffer cannot be used for acidification as it will interfere with the pH-sensitive detection. A small amount of methanol is included in the mobile phase to solubilize the hydrocarbon stationary phase and prevent collapse.<sup>37</sup> Using a mobile phase of 99:1 water:methanol (pH = 3.0), near baseline resolution of several standard acids is achieved in less than 7 min (Figure 4.6). Retention factors are calculated by

$$k = \frac{t_R - t_0}{t_0} \quad (4.3)$$

where  $t_R$  is the retention time of the standard acid and  $t_0$  is the retention time of sodium nitrate (a non-retained marker). The retention factor for each acid, summarized in Table 4.2, is compared with those in the beverage samples in order to identify the components.

The retention order of these LMW organic acids follows directly from a comparison of their structures (Figure 4.1). The retention factors are precise within 0.5% for all of the acids under these conditions. For a reversed-phase separation, retention depends on the number of carbons in the backbone of the acid, as well as the polarity of the molecule. Polarity is related to the number of acid groups and hydroxyl groups present on the molecule. For compounds with



**Figure 4.6.** Chromatogram of common LMW organic acids obtained by UV-absorbance detection (A) and laser-induced fluorescence detection (B). Column: Hypersil ODS, 5- $\mu$ m particles, 250 mm x 4.6 mm. Mobile phase: 99:1 water:methanol, pH 3. Flow rate: 1.0 mL/min. Laser-induced fluorescence detection: 325-nm excitation, 510-nm emission, 10-nm bandpass. UV-absorbance detection: 215 nm. Solutes: oxalic acid (1), tartaric acid (2), formic acid (3), malic acid (4), lactic acid (5), acetic acid (6), citric acid (7), succinic acid (8).

**Table 4.2.** Summary of retention factors ( $k$ ) and  $pK_a$  values for standard acids in water.

Acid	$k^a$	$pK_a$
Oxalic acid <sup>b</sup>	$-0.006 \pm 0.003$ $0.206 \pm 0.004$	1.23, 4.19
Tartaric acid	$0.5263 \pm 0.0004$	2.98, 4.34
Formic acid	$0.646 \pm 0.002$	3.75
Malic acid	$0.855 \pm 0.001$	3.40, 5.11
Lactic acid	$1.160 \pm 0.006$	3.85
Acetic acid	$1.386 \pm 0.007$	4.76
Citric acid	$1.739 \pm 0.009$	3.15, 4.77, 5.40
Succinic acid	$2.52 \pm 0.01$	4.16, 5.61

<sup>a</sup> Retention factors determined by using sodium nitrate as a void marker. Errors are representative of the standard deviation of replicate measurements ( $n = 3$ ).

<sup>b</sup> Two peaks are often observed for oxalic acid. The first peak may be a decomposition product.



the same polarity, retention increases as the number of carbons increases. For monocarboxylic acids, retention increases from formic to acetic acid, and for dicarboxylic acids, retention increases from oxalic to succinic acid. Increasing the number of acid groups increases the polarity of the molecule, resulting in decreased retention. For acids with the same number of carbons, retention decreases with increasing number of acid groups from acetic to oxalic acid. Addition of hydroxyl groups to the molecule also increases the polarity and decreases the retention. For acids with the same number of carbons and acid groups, retention decreases with increasing number of hydroxyl groups from succinic to malic to tartaric acid. Overall, this column and mobile phase are behaving as expected and the precision of the retention factors allows identification of unknown compounds with confidence.

#### **4.3.1.3 Detector Optimization**

After the separation, the pH is adjusted to ~8.0 and the fluorescein solution is introduced. To avoid corrosion and salt precipitation in chromatographic pumps, the sodium hydroxide and fluorescein solutions are introduced by using large volume (10 mL) injection loops. The solutions are introduced separately to allow independent control of pH and fluorescein concentration. After optimization, introduction of a solution containing fluorescein at high pH could be used to accomplish pH adjustment and fluorescein addition simultaneously.

For this new detection system, several parameters must be optimized. The first consideration is dilution of the sample as a result of the post-column

addition of fluorescein and sodium hydroxide solutions. To this end, high concentrations at low flow rates of each are desirable. Based on the corrosive nature of high concentrations of sodium hydroxide, a high concentration limit is set at 10 mM (pH  $\approx$  12). The optimum flow rate of the sodium hydroxide solution will introduce enough hydroxide ions to neutralize the excess protons contained in the pH 3 mobile phase. The flow rate is varied from 10 – 30% of the mobile phase flow rate, or 50 – 150  $\mu$ L/min with a constant mobile phase flow rate (0.5 mL/min) and fluorescein flow rate (50  $\mu$ L/min). As shown in Table 4.3, the background fluorescence increases dramatically for sodium hydroxide flow rates from 10 – 15% of the mobile phase flow rate, but is relatively constant at flow rates greater than 15%. Therefore, when the flow rate of sodium hydroxide is greater than  $\sim$ 15% of the mobile phase flow rate, the pH has been increased to a level at which fluorescein is completely deprotonated. Above this level, the fluorescence background no longer increases with increasing pH. This result is consistent with combining a mobile phase pH  $\approx$  3 ( $[H^+] = 10^{-3}$  M) with a basic solution of pH  $\approx$  12 ( $[OH^-] = 10^{-2}$  M) in a 10:1 ratio to give a neutral pH.

The optimum fluorescein concentration is directly related to the concentration of acidic species in the sample. At the detector, the concentration of fluorescein should be equal to or greater than the acidic solute concentration. In the region in which the fluorescein concentration is up to an order of magnitude greater than the acid concentration, the change in fluorescence with acid concentration is measurable and quantitative (Figure 4.4). To determine the concentration of the sample at the detector (C), Equation 4.4 is used with a

**Table 4.3.** Optimization of the flow rate of a 10 mM sodium hydroxide solution.  
Mobile phase: 0.5 mL/min, pH = 3. Fluorescein:  $10^{-4}$  M, 50  $\mu$ L/min.

<b>NaOH Flow Rate (<math>\mu</math>L/min)</b>	<b>Relative NaOH Flow Rate (%)<sup>a</sup></b>	<b>Background Fluorescence (<math>\mu</math>A)</b>	<b>Noise (<math>\mu</math>A)</b>	<b>Background/ Noise</b>
50	10	0.0258	0.0037	6.913
55	11	0.0664	0.0168	3.962
60	12	0.4017	0.0099	40.39
75	15	0.4092	0.0098	41.64
100	20	0.4435	0.0099	45.04
125	25	0.4588	0.0099	46.19
150	30	0.5103	0.0111	46.08

<sup>a</sup> Relative sodium hydroxide flow rate is with respect to the mobile phase flow rate of 0.5 mL/min.

sample chromatogram.

$$C = \frac{C_0 V_{inj} N^{1/2}}{V_0 (1+k)(2\pi)^{1/2}} \quad (4.4)$$

In this equation,  $C_0$  is the initial or injected concentration of the solute,  $V_{inj}$  is the injected volume,  $k$  is the retention factor of the solute,  $N$  is the plate number, and  $V_0$  is the void volume of the column. The plate number  $N$  is determined from the retention time ( $t_R$ ) and the width of the chromatographic peak ( $w$ ) by

$$4.3N = 16 \left( \frac{t_R}{w} \right)^2 \quad (4.5)$$

The void volume of the column is determined as the product of the flow rate and the void time from injection of a non-retained solute. Using these equations, a 25-fold dilution factor of the column in this configuration is determined. The fluorescein concentration and flow rate are selected by using the information about dilution of the sample as well as the expected concentrations of acids in real samples to be analyzed. As a result of fluorescein solubility in water, a high concentration limit of 5 mM is established. Using this concentration and a column flow rate of 1.0 mL/min, a flow rate of 300  $\mu$ L/min fluorescein is selected to yield a concentration of ~1 mM fluorescein at the detector.

Detector-related parameters are also optimized, including PMT voltage, integration time, and slit width. The PMT voltage is varied from 500 – 800 V at constant integration time (0.2 s) and slit width (0.2 mm), and the background and noise are given in Table 4.4. A greater PMT voltage provides a greater amplification of the photocurrent, but may also amplify the noise simultaneously.

**Table 4.4.** Optimization of the PMT voltage. Mobile phase: 0.5 mL/min, pH = 3. Fluorescein:  $10^{-4}$  M, 100  $\mu$ L/min. Sodium hydroxide:  $10^{-2}$  M, 75  $\mu$ L/min. Integration time: 0.2 s. Slit widths: 0.2 mm.

<b>PMT Voltage</b>	<b>Background Current (<math>\mu</math>A)</b>	<b>Noise (<math>\mu</math>A)</b>	<b>Background/Noise</b>
500	0.0652	0.0030	21.620
600	0.2302	0.0039	59.649
700	0.8083	0.0120	67.476
800	2.1355	0.0319	66.940

Although the background fluorescence increases with increasing PMT voltage, the noise also increases. Beyond 700 V, no further increase in background/noise ratio is observed. A PMT voltage of 700 V is utilized in all subsequent measurements.

Integration time is another parameter that affects the output signal for analysis of acids by directly affecting the number of data points collected per unit time. The number of data points collected does not affect the background fluorescence level, but does affect the noise (Table 4.5). Therefore, the most beneficial integration time is 1.0 s. However, for the best representation of chromatographic peaks, a sufficient number of data points must be collected during elution. As seen in Figure 4.6, many of the chromatographic peaks are 10 – 15 s in width, and an integration time of 1.0 s may cause loss in information. For this reason, an integration time of 0.2 s is utilized in all subsequent measurements.

The entrance and exit slit widths are also optimized to provide the best enhancement in the background/noise ratio. The slit widths are varied from 0.1 – 1.0 mm at constant PMT voltage (700 V) and integration time (0.2 s), and the background and noise are given in Table 4.6. Increasing the slit widths allows more light to be collected by the photomultiplier tube, increasing the background fluorescence. As with PMT voltage, however, the increased fluorescence is accompanied by increased noise. As the slit widths increase, the background and noise increase as expected. The background/noise ratio also increases over this range. At slit widths of 1.0 mm, the photomultiplier signal is out of range and

**Table 4.5.** Optimization of the PMT integration time. Mobile phase: 0.5 mL/min, pH = 3. Fluorescein:  $10^{-4}$  M, 100  $\mu$ L/min. Sodium hydroxide:  $10^{-2}$  M, 75  $\mu$ L/min. PMT: 700 V. Slit widths: 0.1 mm.

Integration Time (s)	Background Current ( $\mu$ A)	Noise ( $\mu$ A)	Background/Noise
0.1	0.2355	0.0084	26.665
0.2	0.2359	0.0063	35.372
0.25	0.2365	0.0056	40.055
0.5	0.2374	0.0039	57.145
1.0	0.2367	0.0031	71.392

**Table 4.6.** Optimization of the entrance and exit slit widths. Mobile phase: 0.5 mL/min, pH = 3. Fluorescein:  $10^{-4}$  M, 100  $\mu$ L/min. Sodium hydroxide:  $10^{-2}$  M, 75  $\mu$ L/min. PMT: 700 V. Integration time: 0.2 s.

Slit Widths (mm)	Background Current ( $\mu$ A)	Noise ( $\mu$ A)	Background/ Noise
0.1	0.1665	0.0054	31.058
0.2	0.8083	0.0120	67.476
0.5	8.1670	0.0804	101.534
0.8	29.1043	0.2045	142.286



could not be measured. Based on this data, slit widths of 0.8 mm are most beneficial. However, in order to prevent damage to the PMT from continuous exposure to such large background currents, slit widths of 0.2 mm are selected to maintain the current at 1 – 2  $\mu\text{A}$  for all subsequent measurements.

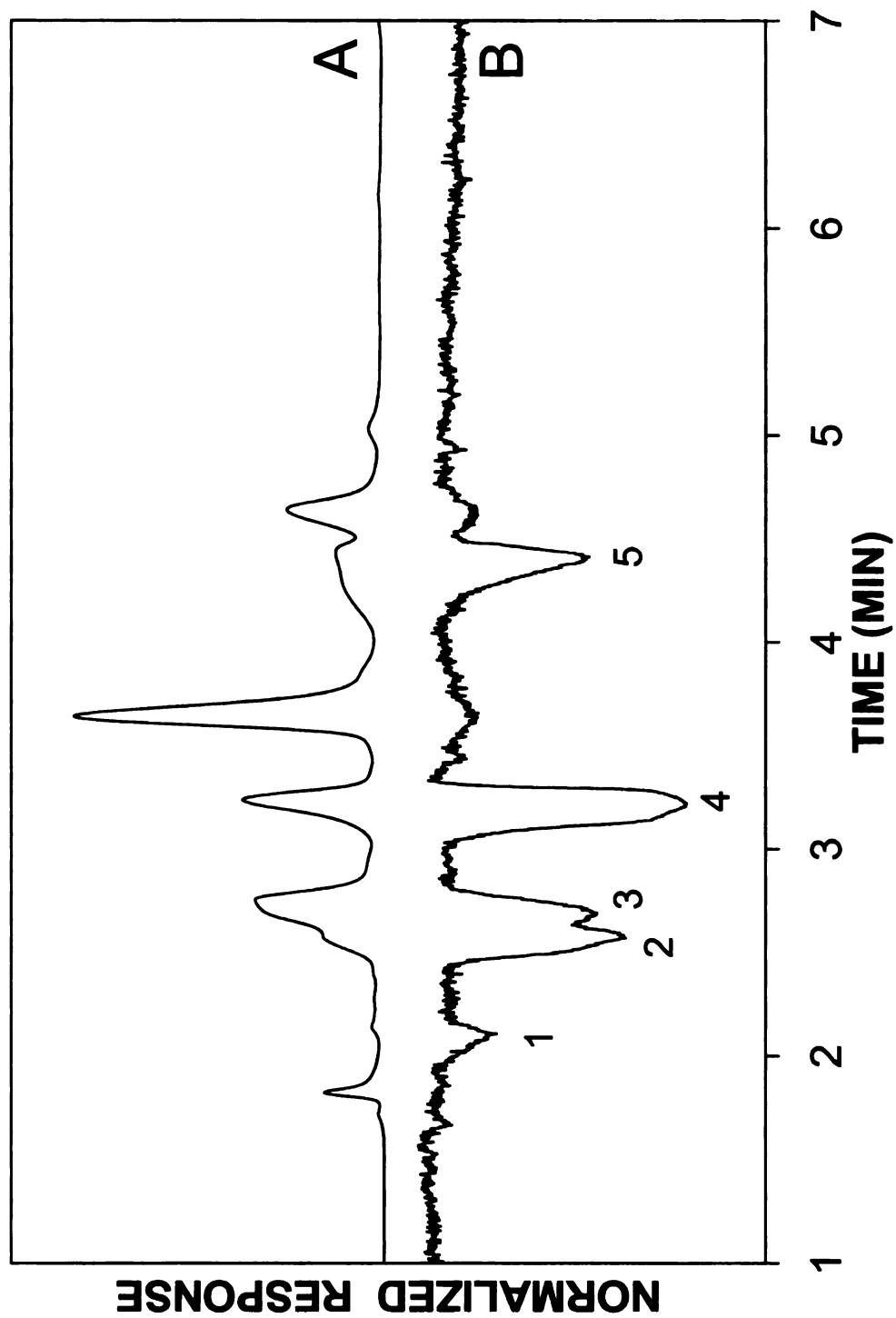
## **4.3.2 Analysis of Real Samples**

### **4.3.2.1 Analysis of Grape Juice**

As discussed previously, grapes and related products contain a number of LMW organic acids. The acids determined in a filtered red grape juice sample are shown in Figure 4.7. By comparison to the standard acid chromatogram (Figure 4.6), the grape juice sample contains oxalic, tartaric, malic, and citric acids. A comparison of the chromatograms in Figure 4.7 indicates that some of the native UV-absorbing compounds in the red grape juice sample are not acidic in nature. As a result, the chromatogram collected by using fluorescence detection is somewhat simplified in comparison to that using UV-absorbance detection. The utility of the proposed method lies in the simplicity of the resulting chromatograms by eliminating potential interferences and improving the ability to correctly identify acidic species in a variety of samples.

### **4.3.2.2 Analysis of Wines**

Red and white wine are alcoholic beverages prepared by the natural fermentation of grapes. Yeast is added to crushed grapes to aid the fermentation process, converting sugars into alcohols. The type of wine produced depends both on the type of grape and yeast used for fermentation, and the quality of the

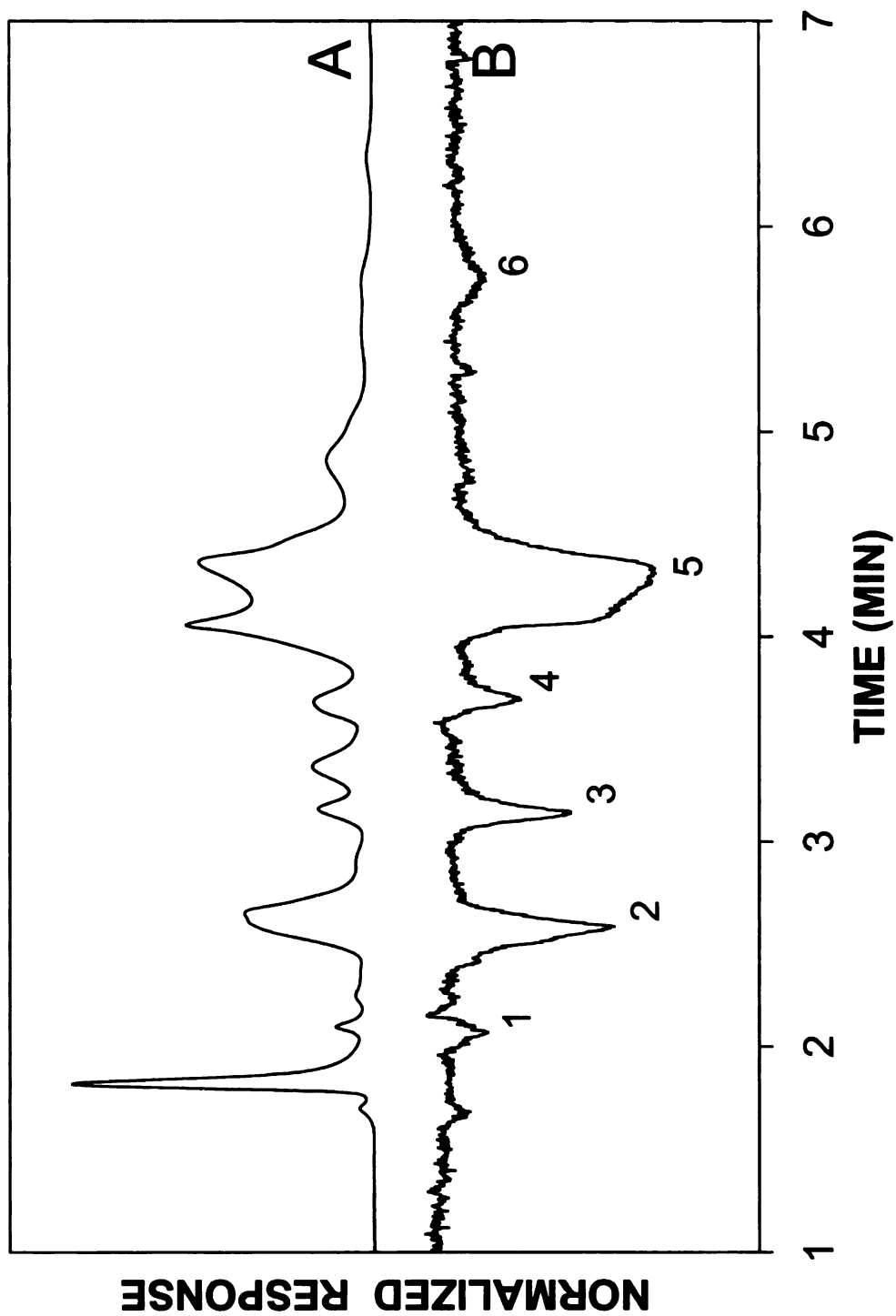


**Figure 4.7.** Chromatogram of grape juice obtained by UV-absorbance detection (A) and laser-induced fluorescence detection (B). Chromatographic conditions as described in Figure 4.6. Solutes: oxalic acid (1), tartaric acid (2), unknown (3), malic acid (4), citric acid (5).

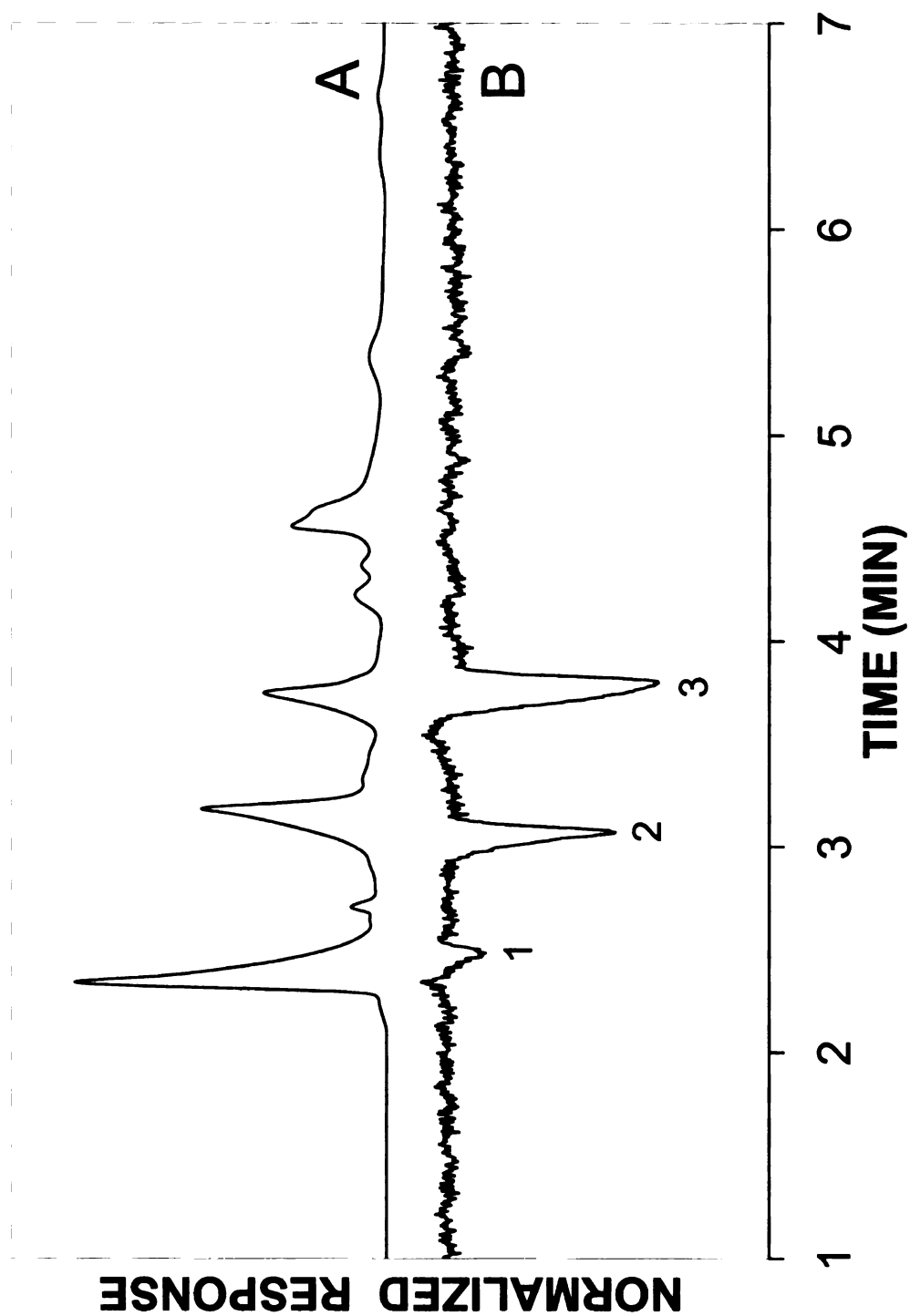
wine is related to the acid content. Because they are prepared directly from grapes, the acid content of wine is expected to be similar to that of grape juice. As shown in Figure 4.8, red wine contains many of the same acidic species as previously identified in red grape juice. By comparison to the standard acid chromatogram (Figure 4.6), the red wine sample contains oxalic, tartaric, malic, lactic, and succinic acids. A comparison of the chromatograms in Figure 4.8 also indicates that some weakly absorbing acids such as succinic acid would be non-detectable using UV-absorbance detection. The fluorescence method may identify acids important to wine quality that could be undetected using UV-absorbance detection. The chromatograms obtained by using UV-absorbance and fluorescence detection for determination of acids in a white wine sample are shown in Figure 4.9. By comparison to the standard acid chromatogram (Figure 4.6), the white wine sample contains oxalic, tartaric, and malic acids. As expected, the acid content of both wine samples is consistent with that of the grape juice sample.

#### **4.3.2.3 Analysis of Vinegars**

Vinegars are the product of further fermentation or oxidation of wines, resulting in the conversion of ethanol into acetic acid. Just as the quality of wine depends on the acid content, the quality and flavor of vinegar is related to the quality of the original grape product. The most flavorful vinegars are allowed to ferment for many months or years and contain a number of acids in addition to acetic acid, the primary component. Because they are prepared directly from wines, the acid content of red and white wine vinegars is expected to be similar



**Figure 4.8.** Chromatogram of red wine obtained by UV-absorbance detection (A) and laser-induced fluorescence detection (B). Chromatographic conditions as described in Figure 4.6. Solutes: oxalic acid (1), tartaric acid (2), malic acid (3), unknown (4), lactic acid (5), succinic acid (6).

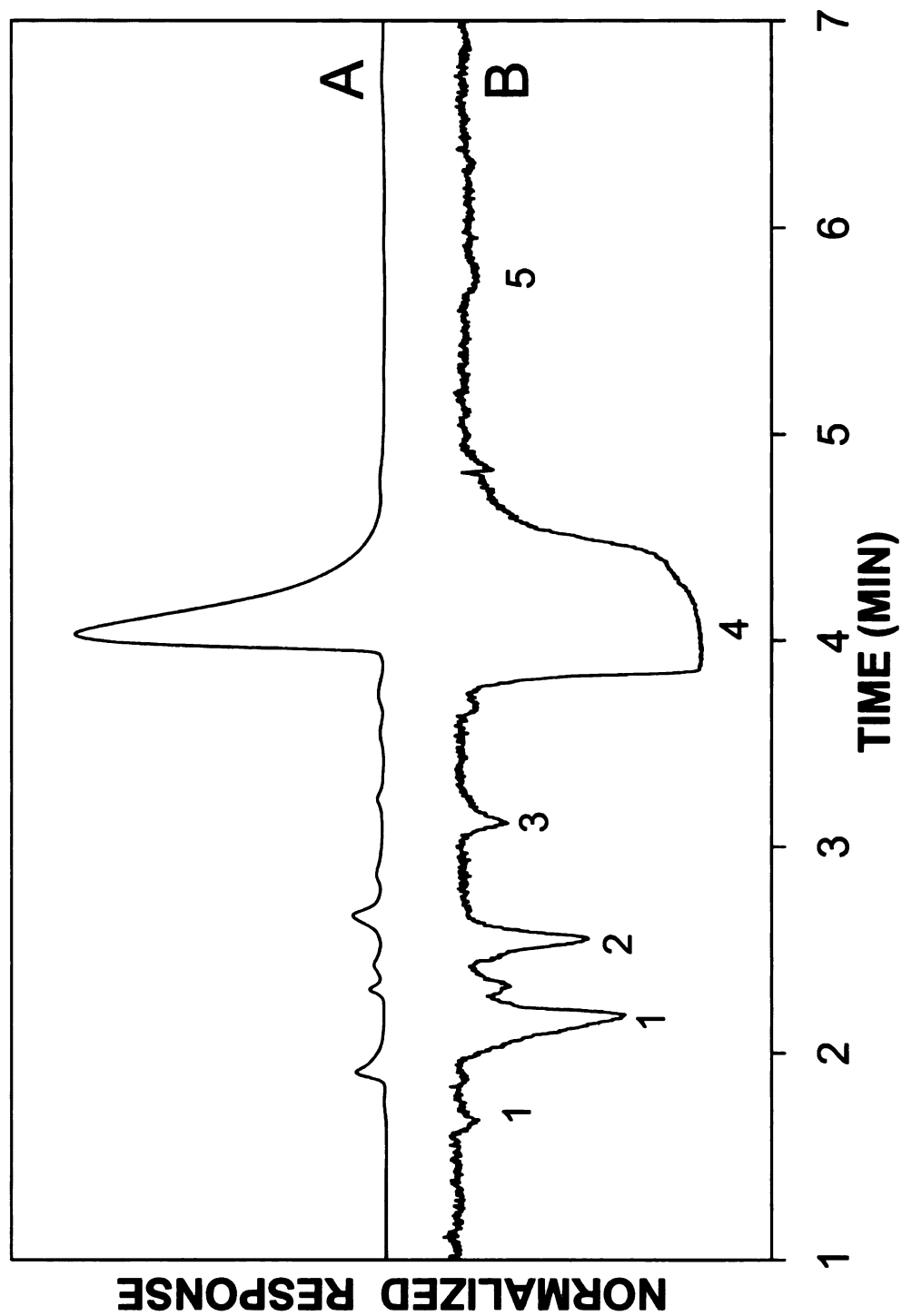


**Figure 4.9.** Chromatogram of white wine obtained by UV-absorbance detection (A) and laser-induced fluorescence detection (B). Chromatographic conditions as described in Figure 4.6. Solutes: oxalic acid (1), tartaric acid (2), malic acid (3).

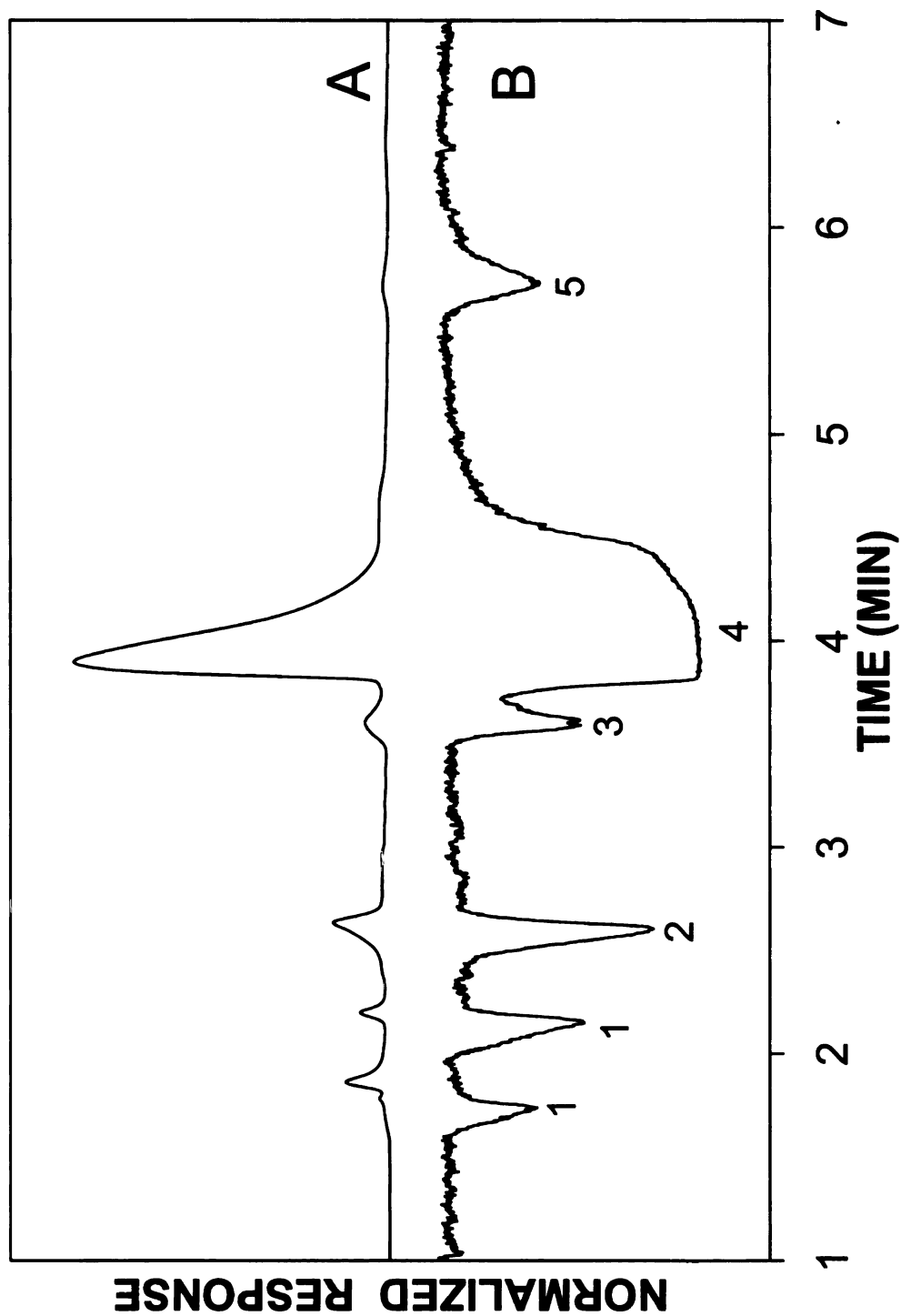
to that of grape juice and wines. As shown in Figure 4.10, red wine vinegar contains many of the same acidic species as previously identified. By comparison to the standard acid chromatogram (Figure 4.6), the red wine vinegar sample contains oxalic, tartaric, malonic, acetic, and succinic acids. As shown in Figure 4.11, the white wine vinegar sample contains oxalic, tartaric, acetic, and succinic acids.

Balsamic vinegar is another type of vinegar prepared from the concentrated juice or must of grapes. Balsamic vinegar is allowed to age for several years and, through the fermentation process, becomes a more viscous, sweet, and flavorful vinegar. The resulting chromatograms from a sample of balsamic vinegar are given in Figure 4.12. By comparison to the standard acid chromatogram (Figure 4.6), the balsamic vinegar sample contains oxalic, tartaric, malonic, acetic, and fumaric acids. As discussed previously for the wine analysis, the succinic and fumaric acids that are detected in the vinegars by the fluorescence method would be undetectable by UV-absorbance detection. For all of the grape-derived foods and beverages, the fluorescence technique is a novel and more selective alternative to traditional UV-absorbance detection.

Many other vinegars are prepared in ways other than from the fermentation of wines or other grape products, as discussed previously. White vinegar, for example, can be prepared by oxidizing a distilled alcohol or from fermentation of grains such as maize. The most common forms of inexpensive white vinegar are prepared directly from acetic acid as a 5% aqueous solution. An analysis of a white vinegar sample reveals only one component in addition to

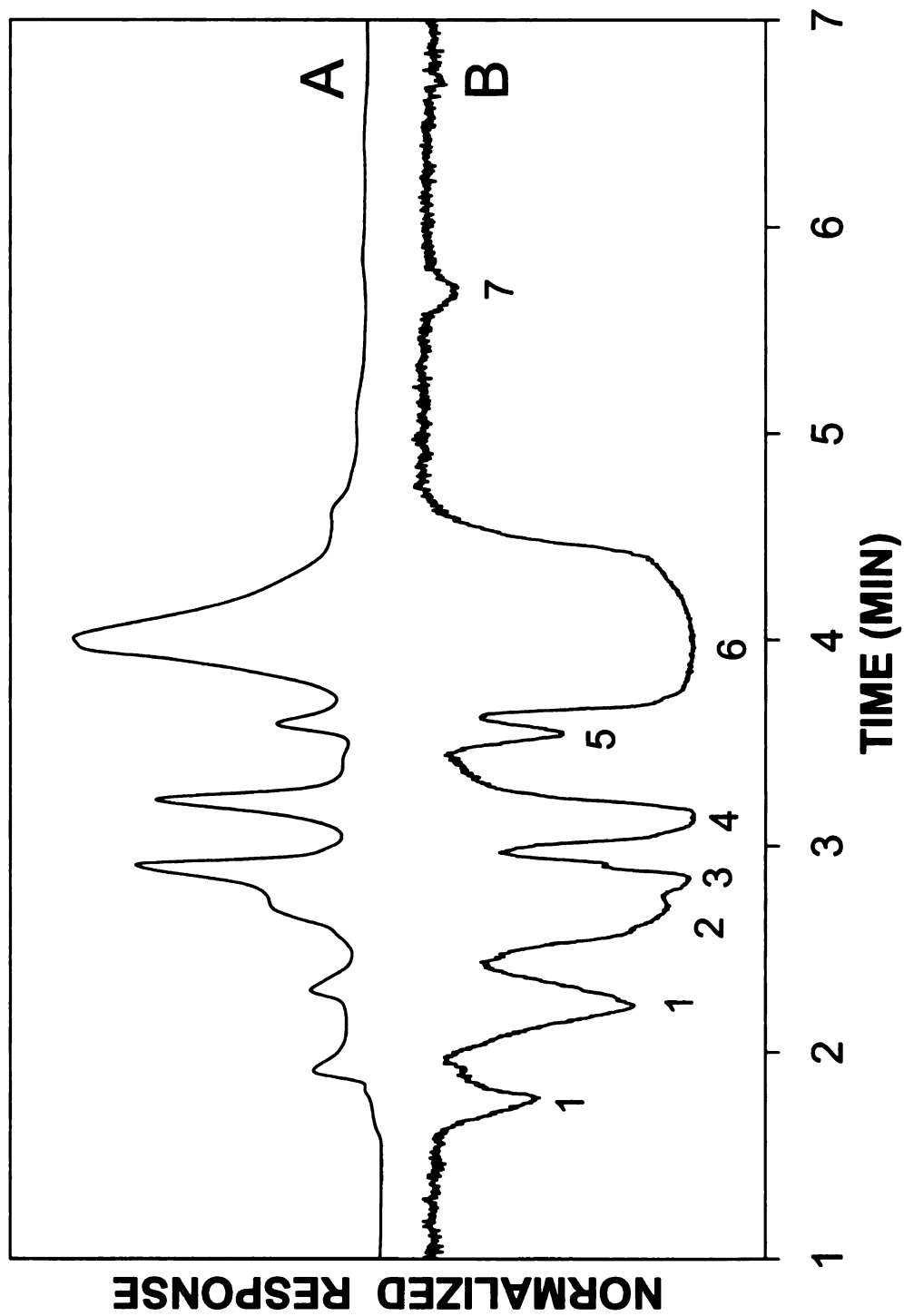


**Figure 4.10.** Chromatogram of red wine vinegar obtained by UV-absorbance detection (A) and laser-induced fluorescence detection (B). Chromatographic conditions as described in Figure 4.6. Solutes: oxalic acid (1), tartaric acid (2), malonic acid (3), acetic acid (4), succinic acid (5).



**Figure 4.11.** Chromatogram of white wine vinegar obtained by UV-absorbance detection (A) and laser-induced fluorescence detection (B). Chromatographic conditions as described in Figure 4.6. oxalic acid (1), tartaric acid (2), unknown (3), acetic acid (4), succinic acid (5).





**Figure 4.12.** Chromatogram of balsamic vinegar obtained by UV-absorbance detection (A) and laser-induced fluorescence detection (B). Chromatographic conditions as described in Figure 4.6. oxalic acid (1), tartaric acid (2), formic acid (3), malonic acid (4), unknown (5), acetic acid (6), fumaric acid (7).

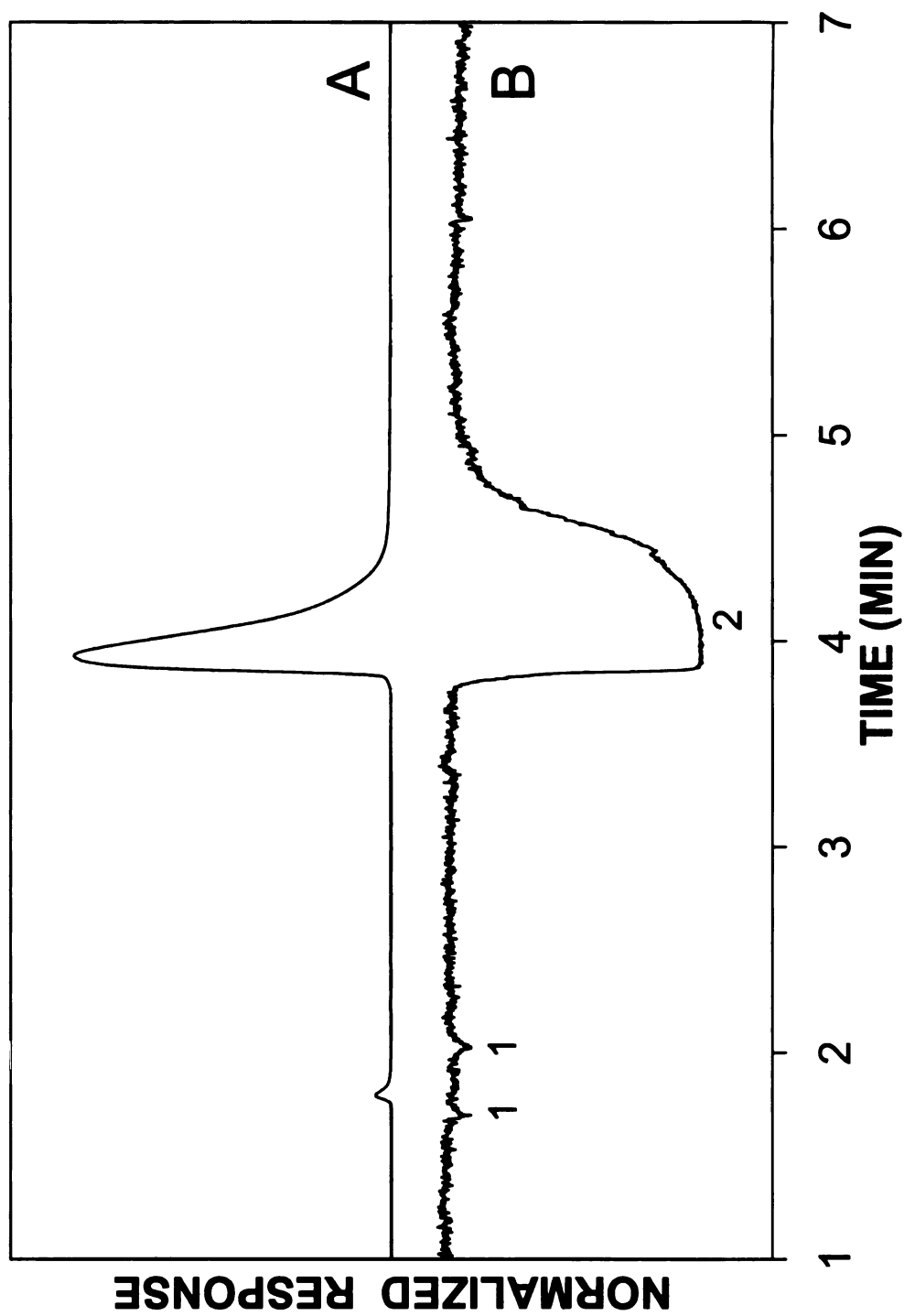
acetic acid (Figure 4.13). A low concentration of oxalic acid is determined, near the detection limit of 3 mM. The simple LWM organic acid profile indicates that this sample is most likely prepared directly from an acetic acid solution.

Malt vinegar is another type of vinegar that is traditionally prepared from malting barley. During this process, the starches in the barley are converted to maltose, which is fermented and aged. As with white vinegar, a more cost-effective malt vinegar can be prepared from an acetic acid solution with added caramel color to reproduce the effects of natural aging. An analysis of a malt vinegar sample reveals numerous acidic components, including oxalic and acetic acids (Figure 4.14). The remaining components could not be identified using the standard set of LMW organic acids. The complexity of the profile, however, indicates that this malt vinegar sample is prepared through the traditional process of malting barley.

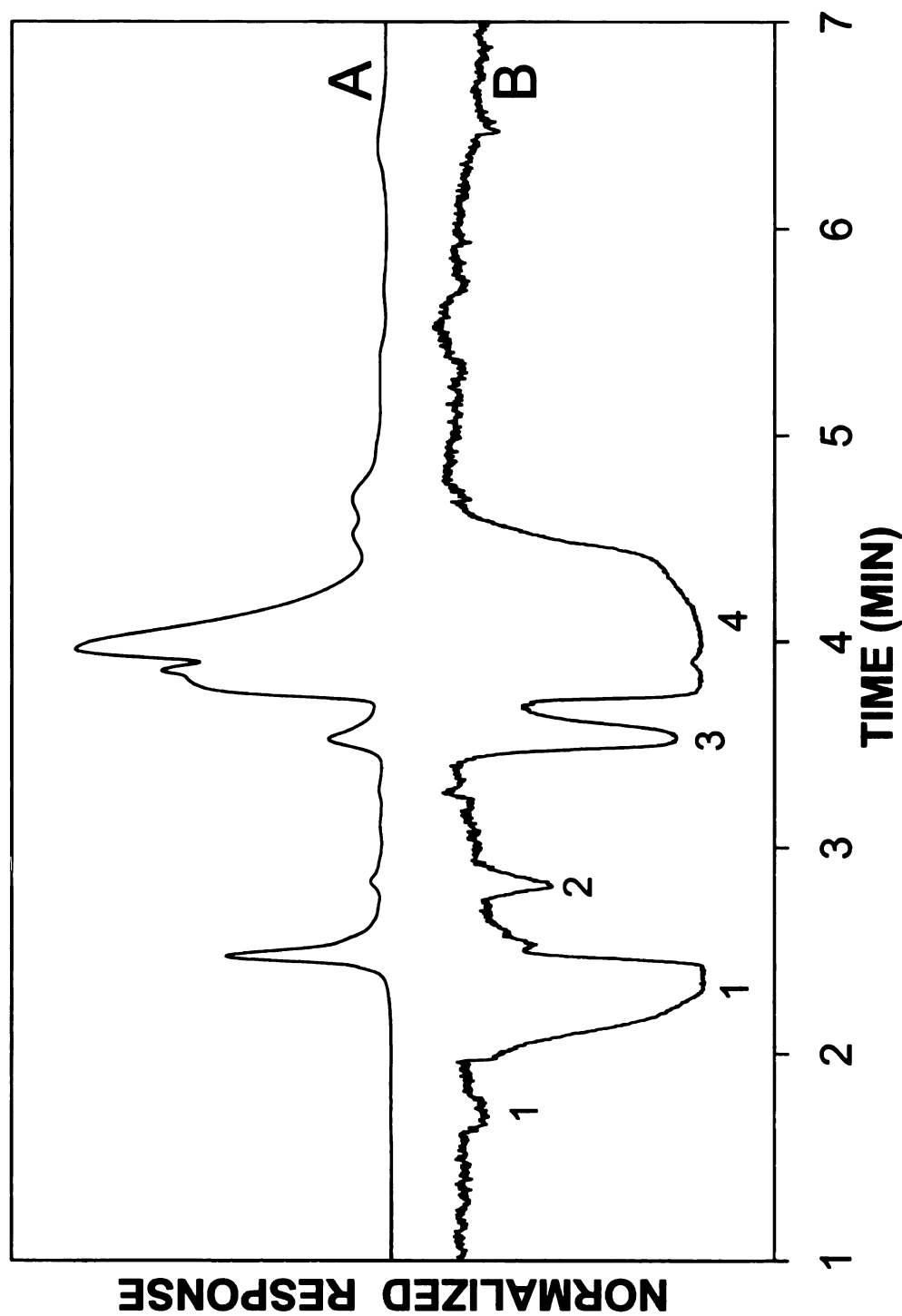
Another common type of vinegar is rice vinegar, prepared from the fermentation of the starches in rice or rice wine. Similar to balsamic or other wine vinegars, the acid profile of rice vinegar is complex (Figure 4.15). By comparison to the standard acid chromatogram (Figure 4.6), oxalic, tartaric, formic, lactic, acetic, and succinic acids are identified in the rice vinegar sample. For all vinegar samples, this method provides a clear profile of the acid content, and allows conclusions to be drawn regarding the origin of the sample.

#### **4.4 Conclusions**

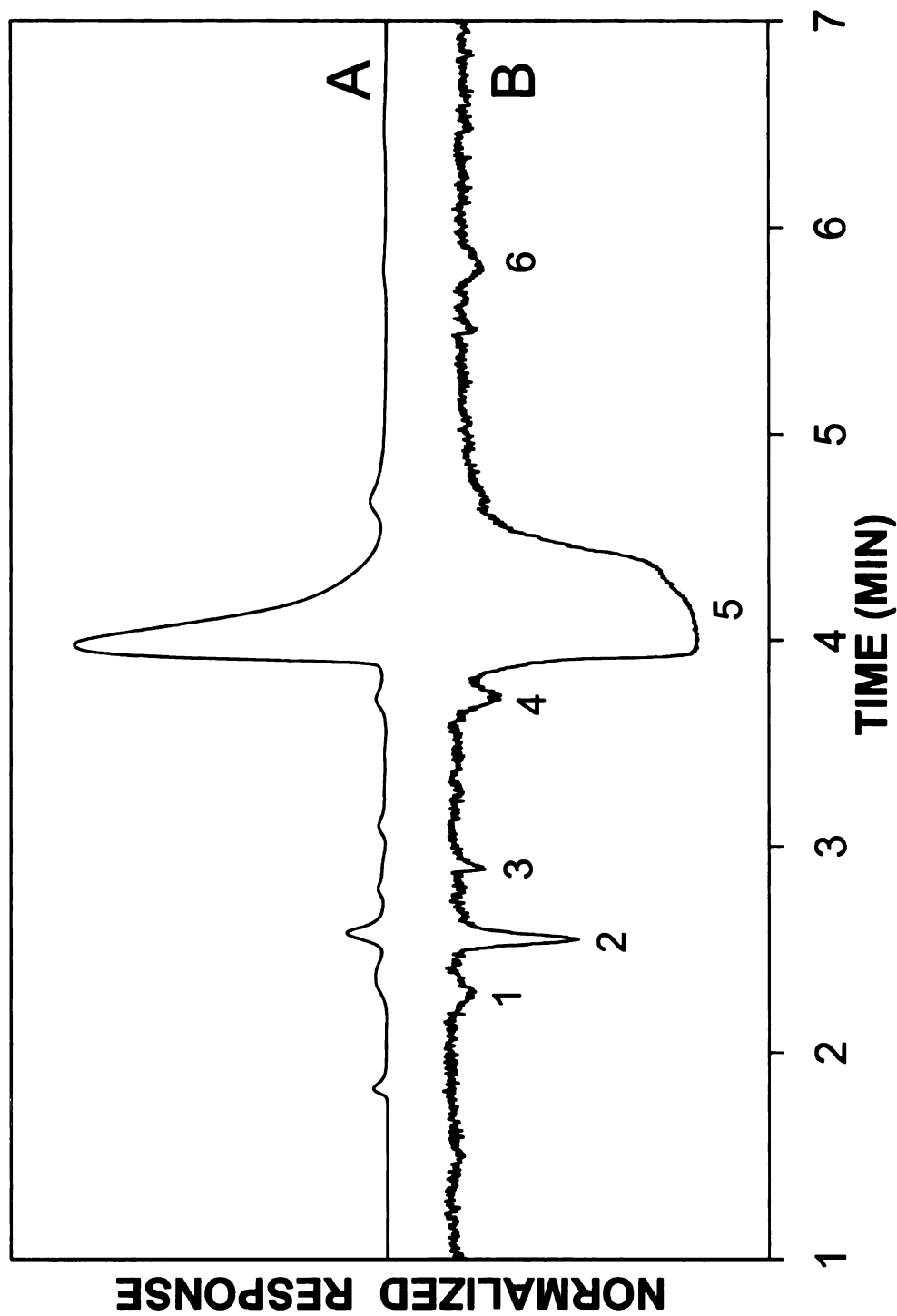
A novel method for determination of acids based on the pH-sensitive fluorescence of fluorescein has been developed. The native acid-base



**Figure 4.13.** Chromatogram of white vinegar obtained by UV-absorbance detection (A) and laser-induced fluorescence detection (B). Chromatographic conditions as described in Figure 4.6. oxalic acid (1), acetic acid (2).



**Figure 4.14.** Chromatogram of malt vinegar obtained by UV-absorbance detection (A) and laser-induced fluorescence detection (B). Chromatographic conditions as described in Figure 4.6. oxalic acid (1), unknown (2), unknown (3), acetic acid (4).



**Figure 4.15.** Chromatogram of rice vinegar obtained by UV-absorbance detection (A) and laser-induced fluorescence detection (B). Chromatographic conditions as described in Figure 4.6. oxalic acid (1), tartaric acid (2), formic acid (3), lactic acid (4), acetic acid (5), succinic acid (6).

properties of fluorescein and the related changes in fluorescence quantum yield are exploited for detection of acidic species in foods and beverages. This method is useful for any compound that is more acidic than fluorescein, allowing sufficient proton transfer in both aqueous and polar organic solvents. The behavior of fluorescein fluorescence is sigmoidal with the logarithm of proton concentration. The linear range extends two orders of magnitude and is centered about the fluorescein concentration in solution. The linear range can be extended to four orders of magnitude using a sigmoidal transform function, and can be shifted to higher or lower concentrations by adjustment of the fluorescein concentration. This method is validated by using a series of test acids, including inorganic and organic acids, strong and weak acids, and acids of varying degrees of protonation. The application of this method to the analysis of grape juice and derivatives, including a variety of wine and vinegar samples, following liquid chromatography is demonstrated. Improvements in sensitivity and selectivity are observed for acids found in these samples upon direct comparison to UV-absorbance detection. This fluorescence method provides a new tool for analysis of acidic species with potential use in a variety of disciplines including forensic, environmental, and clinical analyses.

#### 4.5 References

1. Galli, V.; García, A.; Saavedra, L.; Barbas, C. *Electrophoresis* **2003**, *24*, 1951-1981.
2. Presto Elgstoén, K. B.; Zhao, J. Y.; Anacleto, J. F.; Jellum, E. J. *Chromatogr. A* **2001**, *914*, 265-275.
3. Verhaeghe, B. J.; Lefevère, M. F.; De Leenheer, A. P. *Clin. Chem.* **1988**, *34*, 1077-1083.
4. Tedetti, M.; Kawamura, K.; Charrière, B.; Chevalier, N.; Sempere, R. *Anal. Chem.* **2006**, *78*, 6012-6018.
5. Naidu, R.; Chen, Z. *Chromatographia* **2001**, *54*, 495-500.
6. Xu, J.; Chen, Z.; Yu, J. C.; Tang, C. *J. Chromatogr. A* **2002**, *942*, 289-294.
7. Chen, Z.; Tang, C.; Yu, J. C. *J. High Resolut. Chromatogr.* **1999**, *22*, 379-385.
8. Mato, I.; Huidobro, J. F.; Simal-Lozano, J.; Sancho, M. T. *Anal. Chim. Acta* **2006**, *565*, 190-197.
9. Hayenga, I. In *Analytix: Advances in Analytical Chemistry*, 2006.
10. Dopico-García, M. S.; Valentao, P.; Guerra, L.; Andrade, P. B.; Seabra, R. M. *Anal. Chim. Acta* **2007**, *583*, 15-22.
11. Grayeski, M. L.; DeVasto, J. K. *Anal. Chem.* **1987**, *59*, 1203-1206.
12. Paredes, E.; Maestre, S. E.; Prats, S.; Todolí, J. L. *Anal. Chem.* **2006**, *78*, 6774-6782.
13. Edelmann, A.; Diewok, J.; Baena, J. R.; Lendl, B. *Anal. Bioanal. Chem.* **2003**, *376*, 92-97.
14. Kotani, A.; Miyaguchi, Y.; Tomita, E.; Takamura, K.; Kusu, F. *J. Agric. Food Chem.* **2004**, *52*, 1440-1444.
15. Helaleh, M. I. H.; Tanaka, K.; Taoda, H.; Hu, W.; Hasebe, K.; Haddad, P. R. *J. Chromatogr. A* **2002**, *956*, 201-208.
16. Palma, M.; Barroso, C. G. *Anal. Chim. Acta* **2002**, *458*, 119-130.
17. Poels, I.; Nagels, L. J.; Verreyt, G.; Geise, H. J. *Anal. Chim. Acta* **1998**, *370*, 105-113.

18. Castro, R.; Moreno, M.; Natera, R.; García-Rowe, F.; Hernández, M.; Barroso, C. *Chromatographia* **2002**, *56*, 57-61.
19. Zotou, A.; Loukou, Z.; Karava, O. *Chromatographia* **2004**, *60*, 39-44.
20. Perez-Ruiz, T.; Martinez-Lozano, C.; Tomas, V.; Martin, J. J. *Chromatogr. A* **2004**, *1026*, 57-64.
21. Kerem, Z.; Bravdo, B.-a.; Shoseyov, O.; Tugendhaft, Y. *J. Chromatogr. A* **2004**, *1052*, 211-215.
22. de Villiers, A.; Lynen, F.; Crouch, A.; Sandra, P. *Chromatographia* **2004**, *59*, 403-409.
23. Soga, T.; Ross, G. A. *J. Chromatogr. A* **1999**, *837*, 231-239.
24. Klampfl, C. W.; Katzmayer, M. U.; Buchberger, W. *Electrophoresis* **1998**, *19*, 2459-2464.
25. Xiong, X.; Li, S. F. Y. *J. Chromatogr. A* **1998**, *822*, 125-136.
26. Kaniansky, D.; Masar, M.; Madajova, V.; Marak, J. *J. Chromatogr. A* **1994**, *677*, 179-185.
27. Kenney, B. F. *J. Chromatogr.* **1991**, *546*, 423-430.
28. Arellano, M.; Andrianary, J.; Dedieu, F.; Couderc, F.; Puig, P. J. *Chromatogr. A* **1997**, *765*, 321-328.
29. O'Flaherty, B.; Yang, W.-P.; Sengupta, S.; Cholli, A. L. *Food Chem.* **2001**, *74*, 111-118.
30. Castineira, A.; Pena, R. M.; Herrero, C.; Garcia-Martin, S. *J. High Resolut. Chromatogr.* **2000**, *23*, 647-652.
31. Castineira, A.; Pena, R. M.; Herrero, C.; Garcia-Martin, S. *J. Food Compos. Anal.* **2002**, *15*, 319-331.
32. Nutku, M. S.; Erim, F. B. *J. Microcolumn Sep.* **1999**, *11*, 541-543.
33. Huang, X.; Luckey, J. A.; Gordon, M. J.; Zare, R. N. *Anal. Chem.* **1989**, *61*, 766-770.
34. Sjoback, R.; Nygren, J.; Kubista, M. *Spectrochim. Acta, Part A* **1995**, *51*, L7-L21.
35. Margulies, D.; Melman, G.; Shanzer, A. *Nat. Mater.* **2005**, *4*, 768-771.



36. Goodpaster, J. V.; McGuffin, V. L. *Appl. Spectrosc.* **1999**, 53, 1000-1008.
37. Bidlingmeyer, B. A.; Broske, A. D. *J. Chromatogr. Sci.* **2004**, 42, 100-106.

## **CHAPTER 5**

### **pH-ENHANCED FLUORESCENCE DETECTION OF $\gamma$ -HYDROXYBUTYRIC ACID IN BEVERAGES**

Because of the short half-life of  $\gamma$ -hydroxybutyric acid (GHB) in physiological fluids, an abandoned beverage may be the best source of forensic evidence for the identification of this drug in a sexual assault case. This study presents a novel method for detection of GHB in beverages. The proposed method utilizes separation by liquid chromatography with detection based on the pH-sensitive fluorescence of fluorescein, as described in Chapter 4. This method is sensitive only to acids and, therefore, is a vast improvement over UV-absorbance methods in highly colored, complex beverage matrices. Several alcoholic and non-alcoholic beverages are spiked with GHB and analyzed using the proposed method. Under the conditions used in this study, the limit of detection is 3 mM GHB in beer, red wine, rum, cola, and coffee with a linear range of 1 – 100 mM GHB. This detection limit corresponds to a dose of 90 mg of GHB in an 8-oz beverage, which is an order of magnitude below the therapeutic dose and 20 – 40 times below the typical recreational dose. A dose of GHB administered with malicious intent may further exceed these levels. Variation in GHB retention time is observed for beverages with higher alcohol content (e.g., rum), but identification can be readily confirmed by coinjection of a GHB standard. Using the proposed method, no selective interconversion of GHB and  $\gamma$ -butyrolactone (GBL) is observed, and in samples containing both compounds, GBL is not detected.

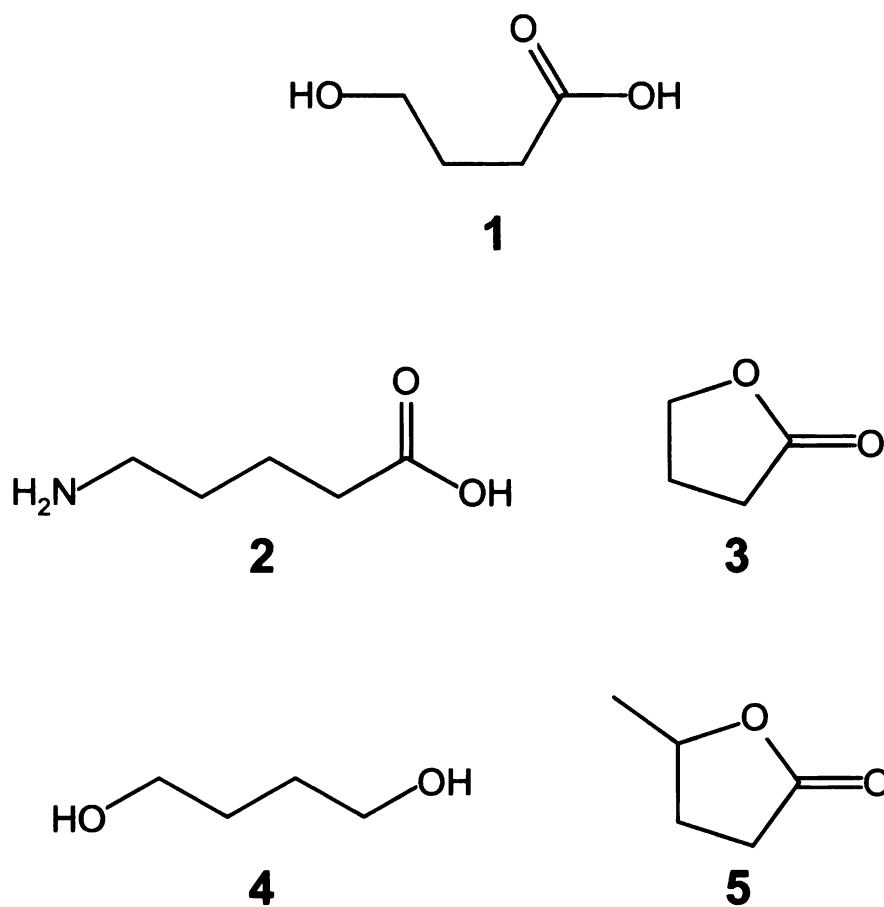
## **5.1 Introduction and Background**

### **5.1.1 GHB**

$\gamma$ -Hydroxybutyric acid (GHB, Figure 5.1) is a minor metabolite of  $\gamma$ -aminobutyric acid (GABA), a neurotransmitter that inhibits uptake of dopamine. At endogenous levels, GHB has only a mild affinity for GABA receptors, but at therapeutic and recreational doses, binding increases dramatically. As a central nervous system depressant, GHB can produce stimulatory effects at low doses (1 – 2 g) and sedative effects at higher doses.<sup>1-4</sup> Clinically, GHB is used to treat narcolepsy, for weight control, as an anesthetic, to induce amnesia, and has been considered for treatment of alcohol and opioid addiction.<sup>2,5-7</sup> The use of GHB has also been promoted in the body-building community as a tool for weight loss and muscle gain. In 1990, GHB was banned by the U.S. Food and Drug Administration due to serious side effects.<sup>8</sup> Some of these side effects include headache, dizziness, disorientation, seizures, nausea, vomiting, respiratory depression, and coma.<sup>7,9,10</sup> In 2000, GHB was added to the list of Schedule I controlled substances,<sup>11</sup> and the main GHB precursor,  $\gamma$ -butyrolactone or GBL, became a List I chemical. Currently, the only legal form of GHB is a prescription drug (Xyrem®) used to treat narcolepsy.<sup>12</sup>

### **5.1.2 Illicit GHB and Forensic Implications**

Illicit GHB is available under street names of Liquid Ecstasy, Liquid X, Grievous Bodily Harm, Georgia Home Boy, G, and Scoop,<sup>7,13</sup> and abuse as a recreational drug has increased in recent years. Doses of 3 – 4 g GHB can



**Figure 5.1.** Structures of GHB and related compounds.  $\gamma$ -hydroxybutyric acid, GHB (1),  $\gamma$ -aminobutyric acid, GABA (2),  $\gamma$ -butyrolactone, GBL (3), 1,4-butanediol, 1,4-BD (4),  $\gamma$ -valerolactone, GVL (5).

cause euphoria, reduced inhibitions, and rapid loss of consciousness. Because GHB is odorless and tasteless, increased use of GHB in sexual assault cases has been reported.<sup>2,3,10,14-16</sup> In addition, the onset of effects is extremely rapid, resulting in loss of consciousness within 10 – 30 min.<sup>7</sup> Analogs of GHB (Figure 5.1) such as GBL (Renewtrient, Revivarant, Blue Nitro),  $\gamma$ -hydroxyvaleric acid (GVL), and 1,4-butanediol (1,4-BD, FX, Thunder Nectar, Zen) are also commonly abused, as *in vivo* conversion to GHB produces similar effects to direct consumption of GHB.<sup>7,17,18</sup> Typically, illicit GHB is manufactured clandestinely from GBL, which can be purchased legally as an industrial solvent or illegally as a health food product.<sup>13</sup> Sodium or potassium hydroxide is then used to hydrolyze GBL to GHB in aqueous solution.<sup>19</sup> The GHB product may be isolated as a powder, partially dried to a paste or wet mass, concentrated, or left in solution. Prior to consumption, the GHB product is dissolved or further diluted in aqueous media such as beverages.

After consumption, the half-life of GHB in physiological fluids is extremely short.<sup>20</sup> Peak plasma concentrations are observed within 20 – 40 min, and peak urine concentrations are observed within 4 h.<sup>7,12</sup> Of the original GHB dose, only about 5% is excreted in urine and is undetectable after 12 hours.<sup>12</sup> Because GHB can induce amnesia and disorientation, many victims of sexual assault may not be aware of the urgency required for determination of GHB in bodily fluids. As a result of these short physiological timeframes, the ability to detect GHB after an extended time in beverages will improve evidentiary procedures related to sexual assault cases.

The potential for interconversion of GHB and GBL between manufacture and consumption has also been a legal concern. Although the overall effect of consumption is the same, a legal distinction exists between possession and consumption of GHB (a Schedule I controlled substance) and GBL (a List I chemical). As a result, any proposed detection methods must distinguish between GHB and GBL, although no method can overcome the problem of interconversion prior to analysis. The stability of aqueous GHB and GBL solutions has been studied as a function of pH and temperature, and a natural equilibrium of GBL:GHB (2:1) has been reported in pure water.<sup>19</sup> Hydrolysis of GBL to GHB is slowest in pure water and in slightly acidic solution (pH 4.0 – 6.5). The rate of hydrolysis increases with decreasing pH and increasing temperature. In basic solution, however, GBL is completely converted to GHB within 15 min.<sup>19</sup> Conversely, GHB is stable for over 200 days in slightly acidic solution, and undergoes esterification to GBL only at extremely low pH. Commercial GBL products have been found to contain ~30% GHB, consistent with the natural equilibrium. In beverages spiked with GBL, GHB is detectable after 1 – 3 days.<sup>19</sup>

### **5.1.3 Determination of GHB**

Preliminary methods for GHB screening are based on colorimetric tests,<sup>21-23</sup> microcrystal tests,<sup>24,25</sup> and enzyme-based assays.<sup>26</sup> Because the beverage matrices in which GHB is administered are complex and often colored, determination based on simple color tests may be difficult or impossible.<sup>25</sup> Fillers and dyes in adulterated beverages as well as the presence of alcohol may interfere with the determination of drugs such as GHB.<sup>17</sup> Isolation of GHB from

aqueous matrices has been accomplished by using liquid-liquid extraction<sup>25,27</sup> and solid-phase microextraction.<sup>28</sup> In forensic laboratories, the most common method for GHB determination is via precipitation of the silver salt from the beverage or solution. This precipitate is then isolated by filtration and identified by infrared (IR) spectroscopy.<sup>19,27,29,30</sup> Although this method is widely available and effective for identification of GHB, quantitation by IR spectroscopy is difficult. Quantitation is important as the amount of GHB present in a beverage may discriminate between recreational ingestion and malicious administration of GHB.

In order to quantitate the amount of GHB present in a sample, a chromatographic method is often necessary to separate GHB from other compounds. Separation methods for GHB analysis in aqueous beverage matrices include gas chromatography,<sup>19,27,28,31-33</sup> liquid chromatography,<sup>19,29,34</sup> and micellar electrokinetic chromatography.<sup>17,35</sup> Detection of GHB has been achieved by using UV-visible absorbance,<sup>17,19,27,29</sup> indirect UV absorbance,<sup>35</sup> mass spectrometry,<sup>19,27,28,33,34</sup> ion mobility spectrometry,<sup>36</sup> nuclear magnetic resonance,<sup>29,37</sup> and flame ionization detection.<sup>33</sup> Some of these methods rely on conversion of GHB to GBL prior to analysis, which may complicate the legal interpretation of the result.<sup>33,38</sup>

Of these methods, only a limited number involve separation of GHB from beverages matrices.<sup>17,19,33</sup> In the current work, a liquid chromatographic method for separation of GHB in beverages is presented together with a novel detection method based on pH-dependent fluorescence. Beverage components and GHB are separated by reversed-phase liquid chromatography using an unbuffered

acidic mobile phase, as described in Chapter 4. After separation, the pH is adjusted to a more neutral value and fluorescein is introduced post-column. When no acids are present, a constant fluorescence background of fluorescein is observed. In the presence of GHB or other acids, however, the fluorescence is decreased below the background level to yield a negative signal. This method facilitates the determination of GHB in beverages by simplifying the chromatograms of complex beverage matrices by detecting only acidic species.

## **5.2 Experimental Methods**

### **5.2.1 Sample Preparation**

Alcoholic and non-alcoholic beverage samples are purchased from local supermarkets and convenience stores (Table 5.1). Ground coffee is purchased from a local supermarket and brewed according to manufacturer's specifications. Carbonated beverages are ultrasonicated for 10 min to remove dissolved carbon dioxide, and all beverages are gravity filtered using filter paper (Whatman) to remove particulates. Sodium nitrate (JT Baker) is used as a void marker for UV-absorbance detection and is added to all solutions in a final concentration of 0.1 mM. Beverages are spiked with GHB (Aldrich) at concentrations determined by using typical serving sizes together with a typical dose of 0.75 g (Table 5.1). For construction of the calibration curves, solutions containing 1 – 100 mM GHB are prepared in distilled deionized water (Corning Glass Works, model MP-3A). For GBL conversion studies, solutions containing 50 mM each of GHB and GBL (Aldrich) are prepared in distilled deionized water. Reagent-grade acetic acid (Aldrich), citric acid (MCB Chemical), formic acid (JT Baker), lactic acid (JT



**Table 5.1.** Summary of alcoholic and non-alcoholic beverages used in this study.

<b>Beverage</b>	<b>Alcohol content (%)</b>	<b>Serving size</b>		<b>[GHB] in 1-3 g dose (mM)</b>
		<b>oz</b>	<b>mL</b>	
Beer	4.2	12	360	27 – 82
Red wine	9	6	180	54 – 162
Rum	35	1.5	45	217 – 650
Cola	0	12	360	27 – 82
Coffee	0	8	240	41 – 122

Baker), malic acid (JT Baker), oxalic acid (JT Baker), succinic acid (Sigma), and tartaric acid (JT Baker) are used to prepare standard solutions at 25 mM concentration in distilled deionized water. Fresh solutions are prepared daily, and stock solutions are stored in the refrigerator to prevent degradation.

### **5.2.2 Experimental System**

A system has been designed for the analysis of acidic species in beverages, and has been described in the previous chapter (Section 4.2.2, Figure 4.3). The mobile phase for separation of GHB in beverages consists of 1% methanol (Honeywell Burdick and Jackson) in distilled deionized water, adjusted to pH 3 by using hydrochloric acid. Post-column, the pH is adjusted to 8.0 by addition of 10 mM sodium hydroxide and fluorescein is introduced from a 5 mM solution. Chromatographic detection is achieved by using a laser-induced fluorescence spectrometer ( $\lambda_{\text{EX}} = 325 \text{ nm}$ ,  $\lambda_{\text{EM}} = 510 \text{ nm}$ ) and UV-absorbance detector ( $\lambda_{\text{ABS}} = 215 \text{ nm}$ ). All other experimental parameters are as described in Chapter 4.

## **5.3 Results and Discussion**

### **5.3.1 GHB Calibration Curve**

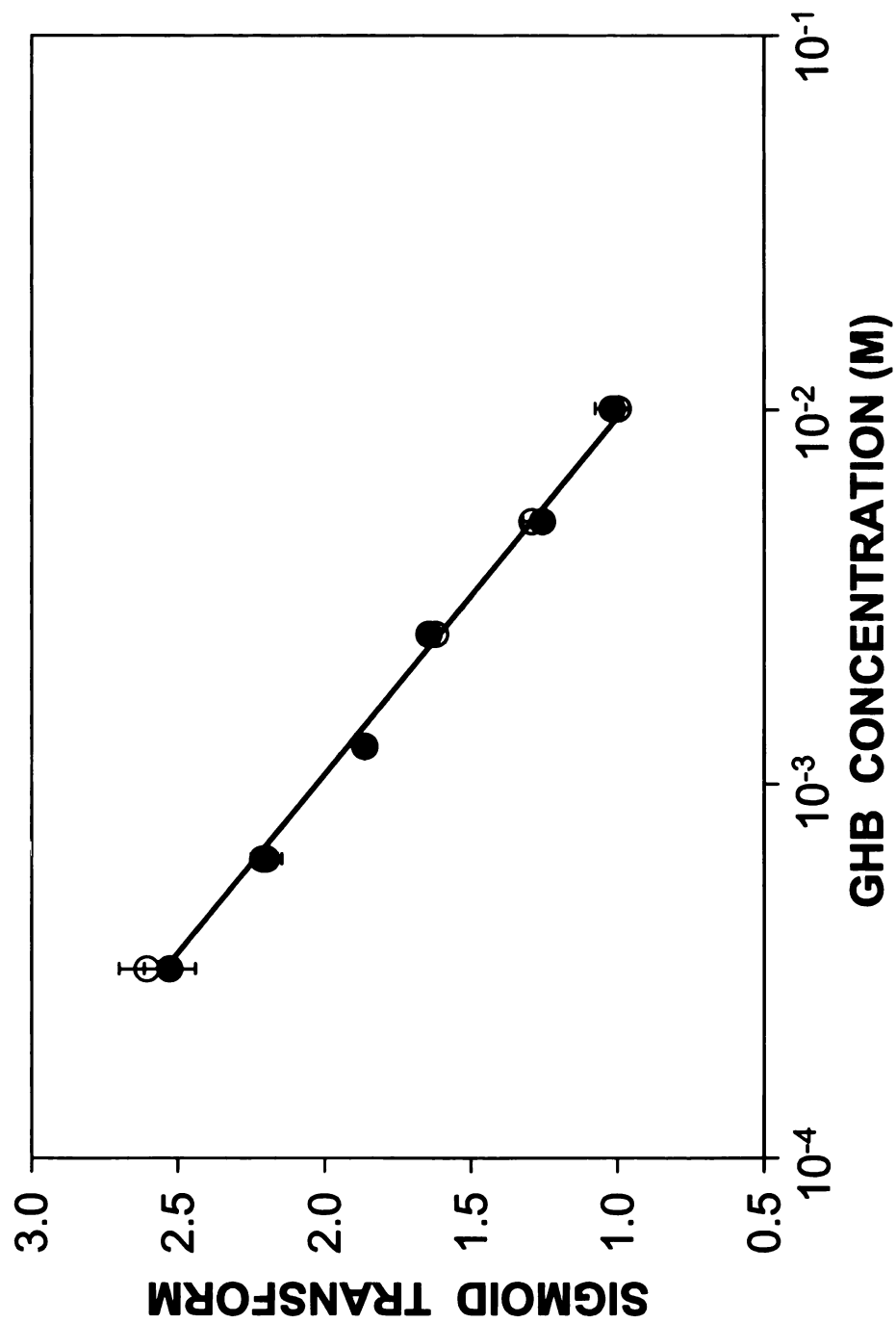
As discussed in Chapter 4, the decrease in fluorescence is related to the number of protons transferred from GHB to fluorescein. Because GHB is a monoprotic acid, the concentration of GHB in the sample is equal to the concentration of protons available for donation to fluorescein. The behavior of fluorescein and GHB is inherently similar to the titration of a weak base with a

weak acid. In this study, calibration curves are generated by injection of GHB solutions of varying concentration from 1 – 100 mM. The chromatographic peak height or area measurements are fit by nonlinear regression to a sigmoidal function (Table Curve 2D, Jandel Scientific, version 2.02). A graph is then prepared of the sigmoidal function of peak height or area versus concentration (Equation 4.1) to yield a linear calibration curve, as shown in Figure 5.2. The correlation coefficient for this curve is related to the quality of sigmoidal fit and is greater than 0.994 for both peak height and area. This indicates that the concentration of GHB in an unknown sample can be determined with good accuracy and precision.

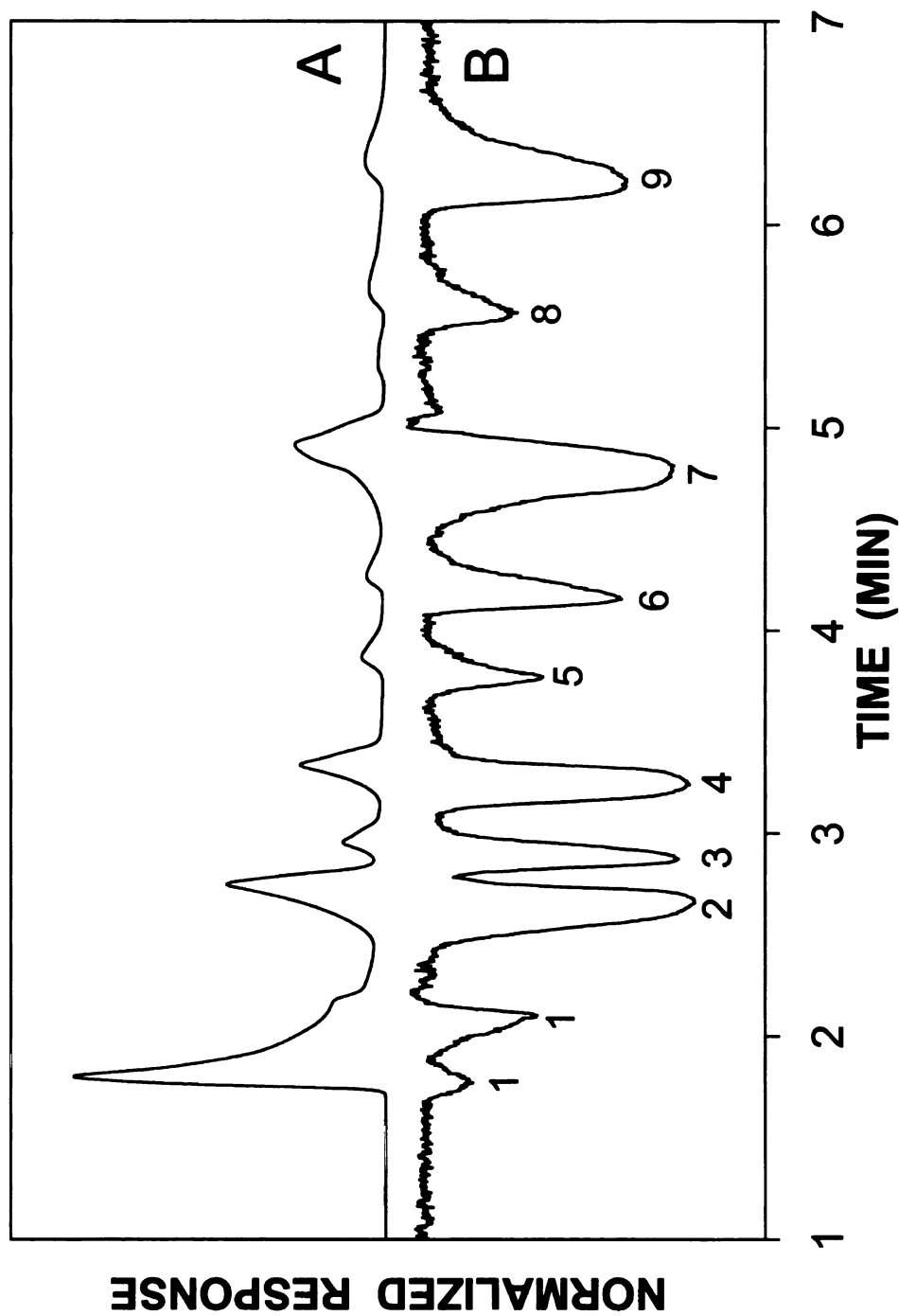
From the calibration curve, the limit of detection of GHB is determined to be 3 mM in aqueous solution ( $S/N = 3$ ) and the linear dynamic range is two orders of magnitude. The detection limit and linear range are sufficient for determination of GHB in adulterated beverages, as demonstrated by the typical concentration ranges in Table 5.1.

### **5.3.2 Beverage Analysis**

For analysis of GHB in beverages, determination of potential interferences is critical. The most probable interferences are low-molecular-weight organic acids such as formic, acetic, lactic, and citric acids. Using the method described in Chapter 4, eight common organic acids are successfully resolved from GHB by using a mobile-phase composition of 99:1 water:methanol adjusted to pH 3 (Figure 5.3). The retention factor for each acid, summarized in Table 4.2, is compared with those in the beverage samples in order to identify



**Figure 5.2.** Calibration curve for GHB measured in water, calculated by using peak height (●) and peak area (○). Linear regression for peak height:  $y = -1.0121x - 0.0165$  ( $R^2 = 0.9961$ ). Linear regression for peak area:  $y = -1.0470x - 0.0678$  ( $R^2 = 0.9946$ ). Error bars represent standard deviation of three measurements.



**Figure 5.3.** Chromatogram of common organic acids and GHB obtained by UV-absorbance detection (A) and laser-induced fluorescence detection (B). Column: Hypersil ODS, 5- $\mu$ m particles, 250 mm x 4.6 mm. Mobile phase: 99:1 water:methanol, pH 3. Flow rate: 1.0 mL/min. Laser-induced fluorescence detection: 325-nm excitation, 510-nm emission, 10-nm bandpass. UV-absorbance detection: 215 nm. Solutes: oxalic acid (1), tartaric acid (2), formic acid (3), malic acid (4), lactic acid (5), acetic acid (6), citric acid (7), GHB (8), succinic acid (9).

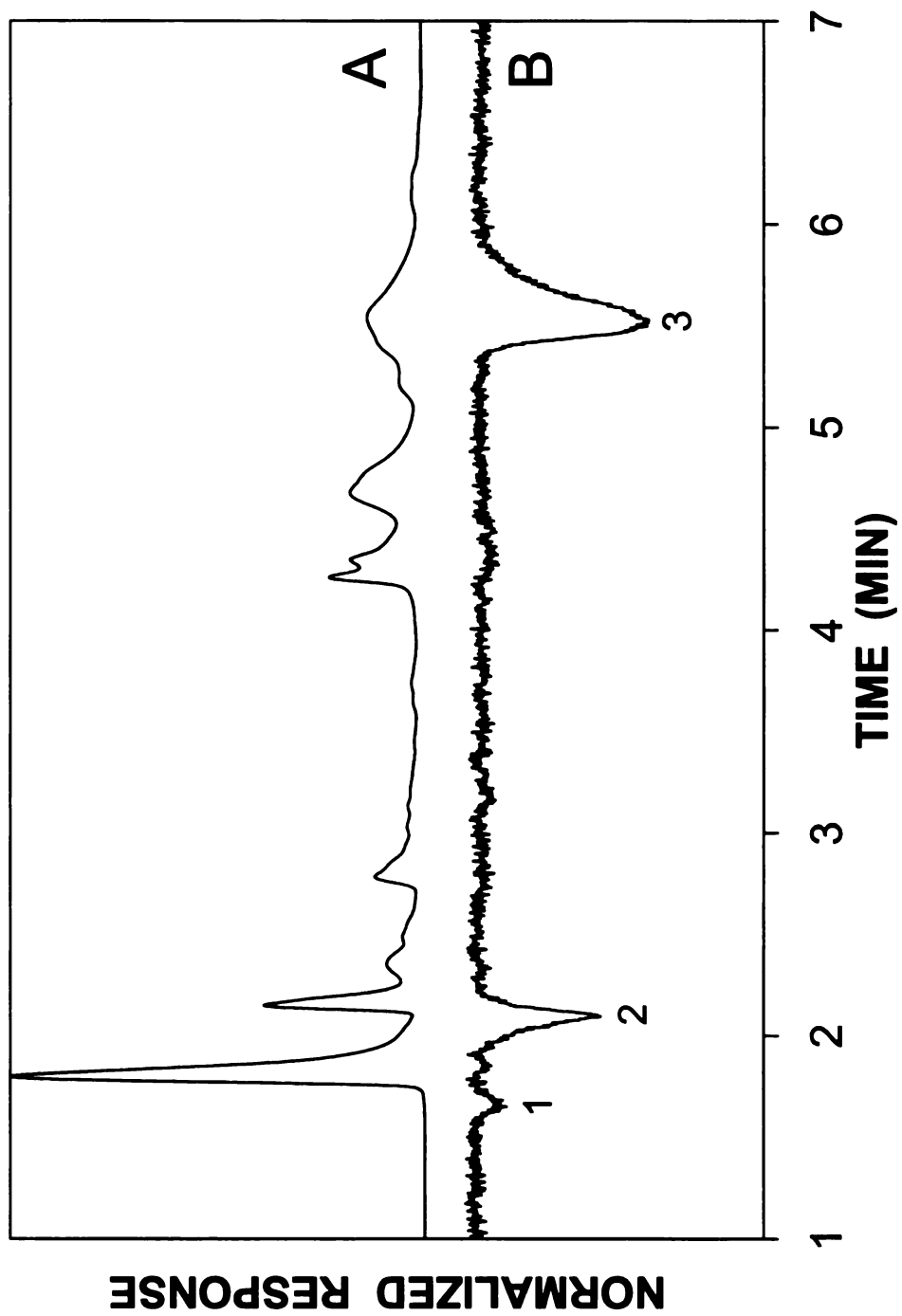
the components.

#### **5.3.2.1 GHB in Alcoholic Beverages**

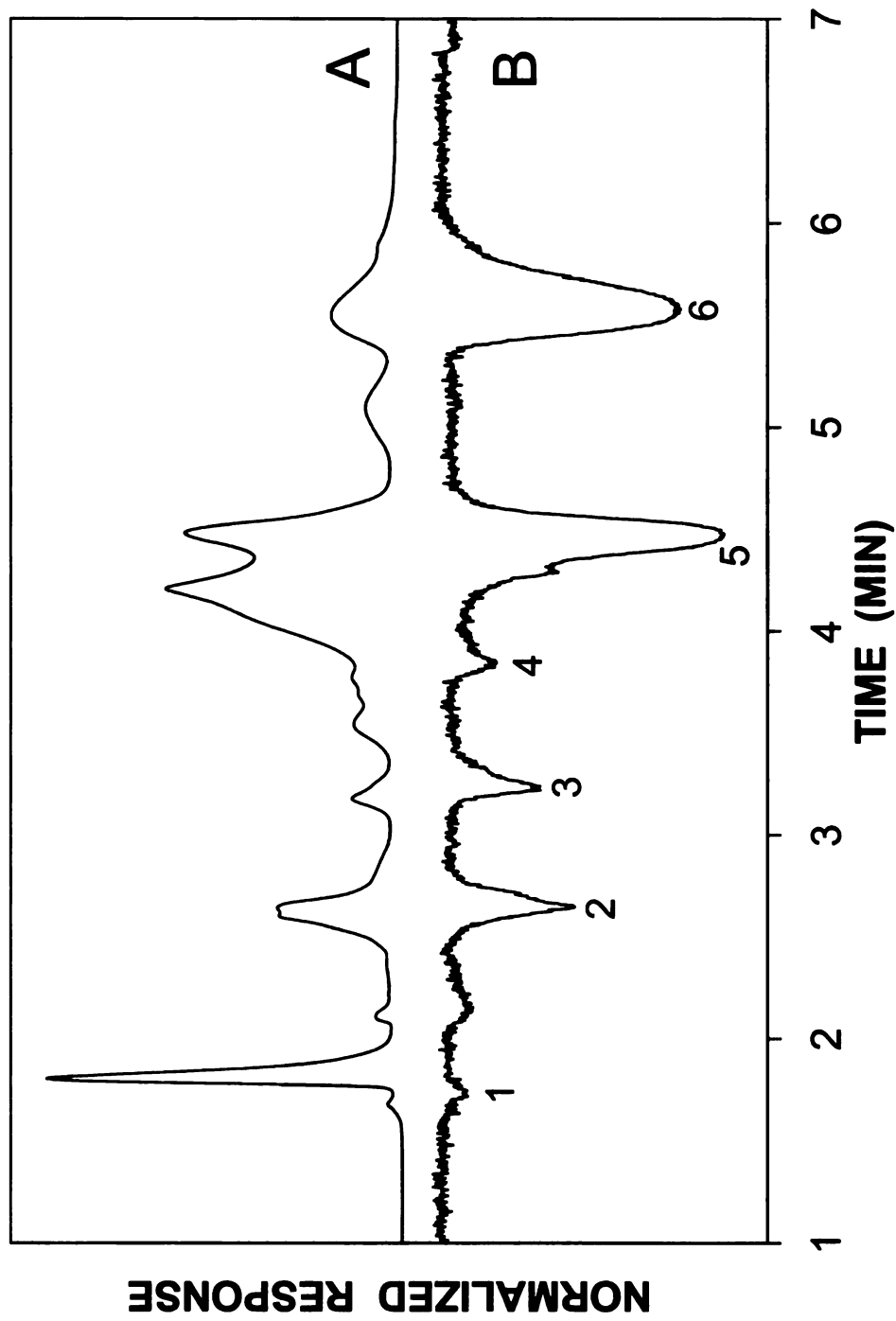
Alcoholic beverages such as beer, red wine, and rum are spiked with GHB as described in Table 5.1, and the resulting chromatograms are shown in Figures 5.4-5.6. For all of the alcoholic beverages, the chromatograms with fluorescence detection are greatly simplified with respect to those with UV-absorbance detection. The UV-absorbance method responds to any compound that absorbs 215-nm light, yielding a complex chromatogram with many peaks that can interfere with GHB determination. The fluorescence method, however, responds only to acids. For selective determination of GHB in beverages, the fluorescence method eliminates potential interferences from non-acidic absorbing species such as fermentation products. By comparison to the chromatogram of standard acids (Figure 5.3), oxalic and phosphoric acids are identified in the beer sample (Figure 5.4). Oxalic, tartaric, malic, and lactic acids are identified in the red wine sample (Figure 5.5), whereas oxalic and lactic acids are identified in the rum sample (Figure 5.6). In all of the alcoholic beverages, the detection limit of GHB is determined to be 3 mM ( $S/N = 3$ ). As mentioned previously, this detection limit is sufficient for determination of GHB in adulterated beverages (Table 5.1).

#### **5.3.2.2 GHB in Non-Alcoholic Beverages**

Non-alcoholic beverages such as cola and coffee are also spiked with GHB and analyzed by using the current method (Figures 5.7 and 5.8). As

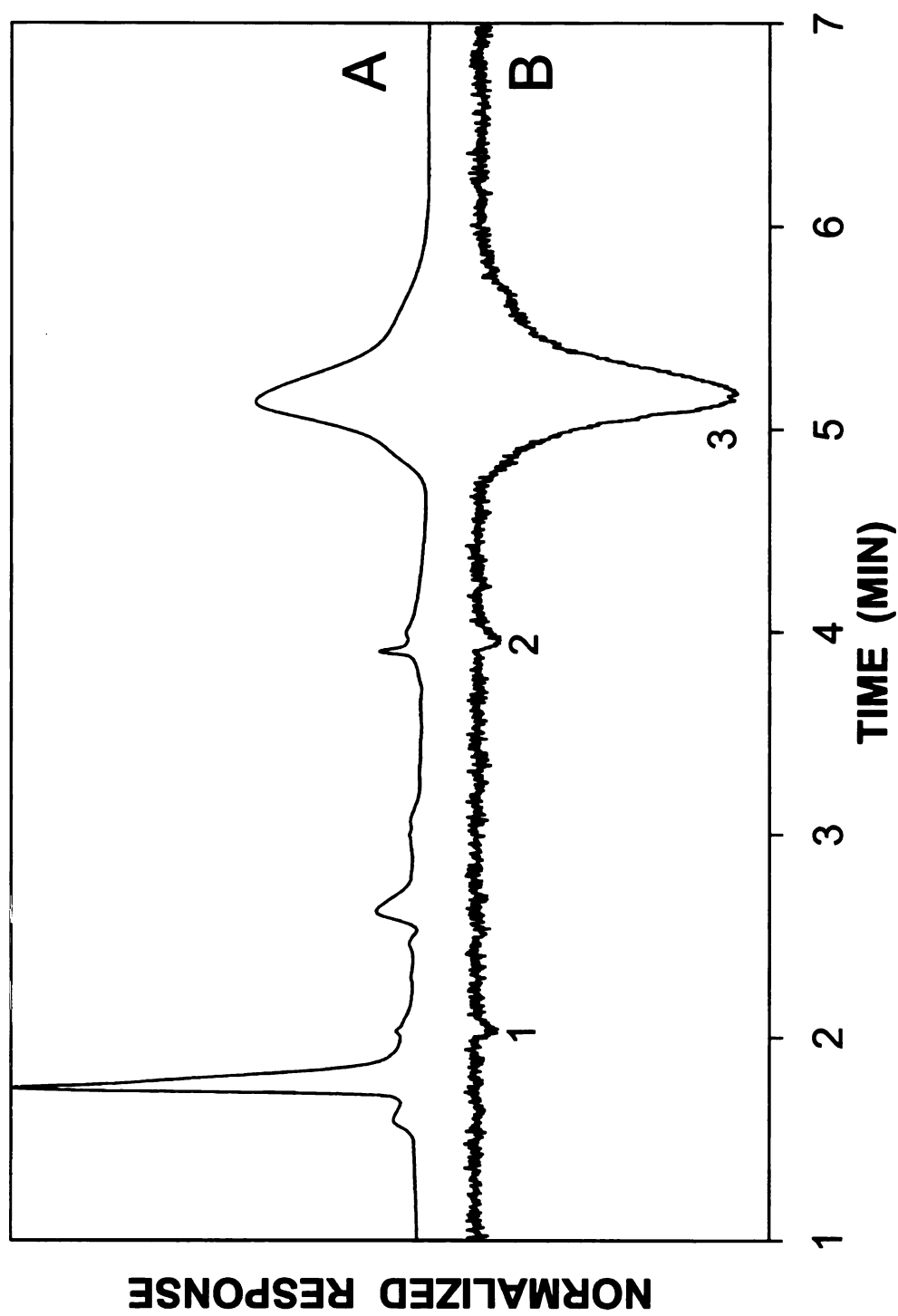


**Figure 5.4.** Chromatogram of a 12-oz (360-mL) serving of beer spiked with 0.75 g GHB obtained by UV-absorbance detection (A) and laser-induced fluorescence detection (B). Chromatographic conditions as described in Figure 5.3. Solutes: oxalic acid (1), phosphoric acid (2), GHB (3).

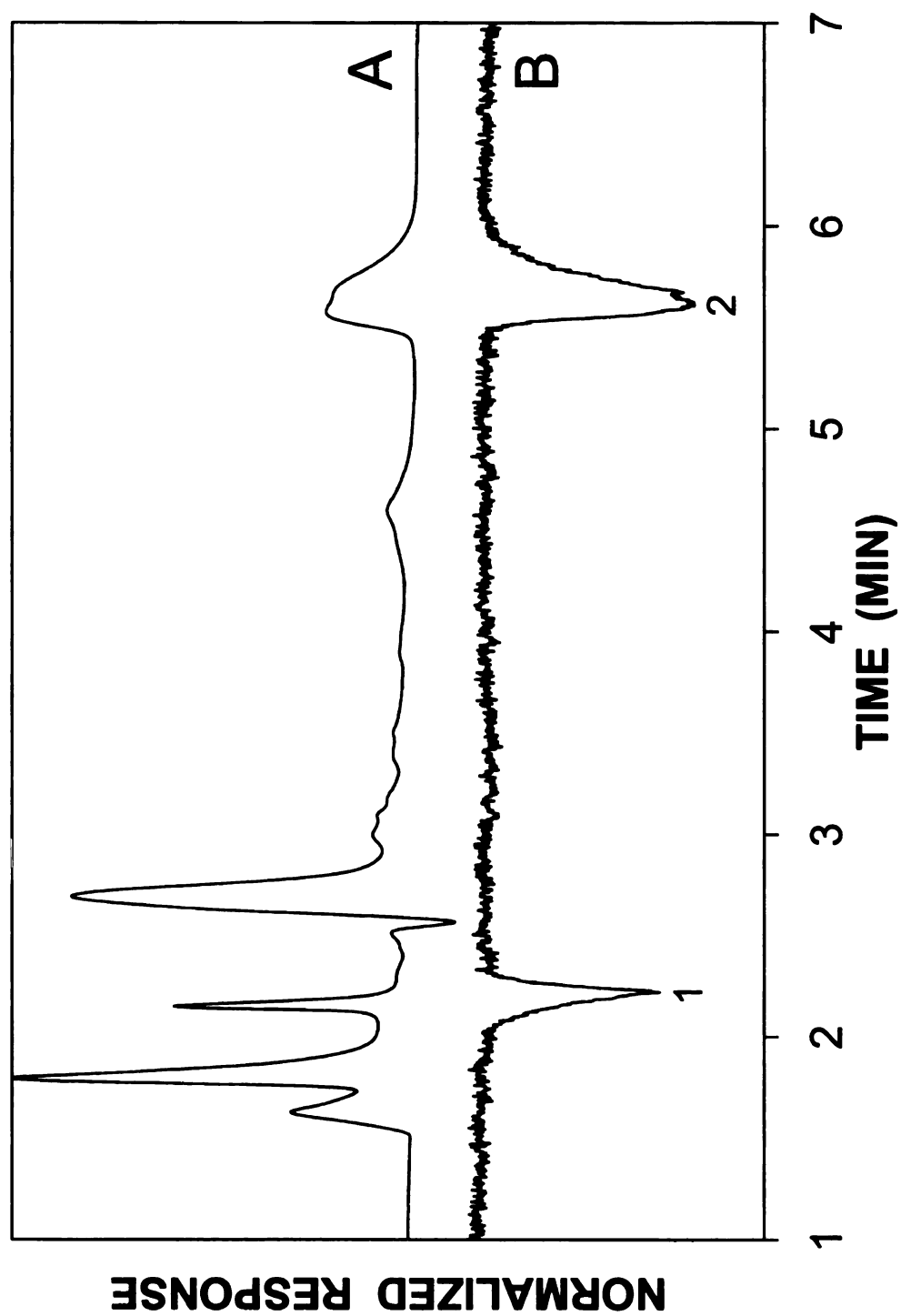


**Figure 5.5.** Chromatogram of a 6-oz (180-mL) serving of red wine spiked with 0.75 g GHB obtained by UV-absorbance detection (A) and laser-induced fluorescence detection (B). Chromatographic conditions as described in Figure 5.3. Solutes: oxalic acid (1), tartaric acid (2), malic acid (3), lactic acid (4), unknown (5), GHB (6).

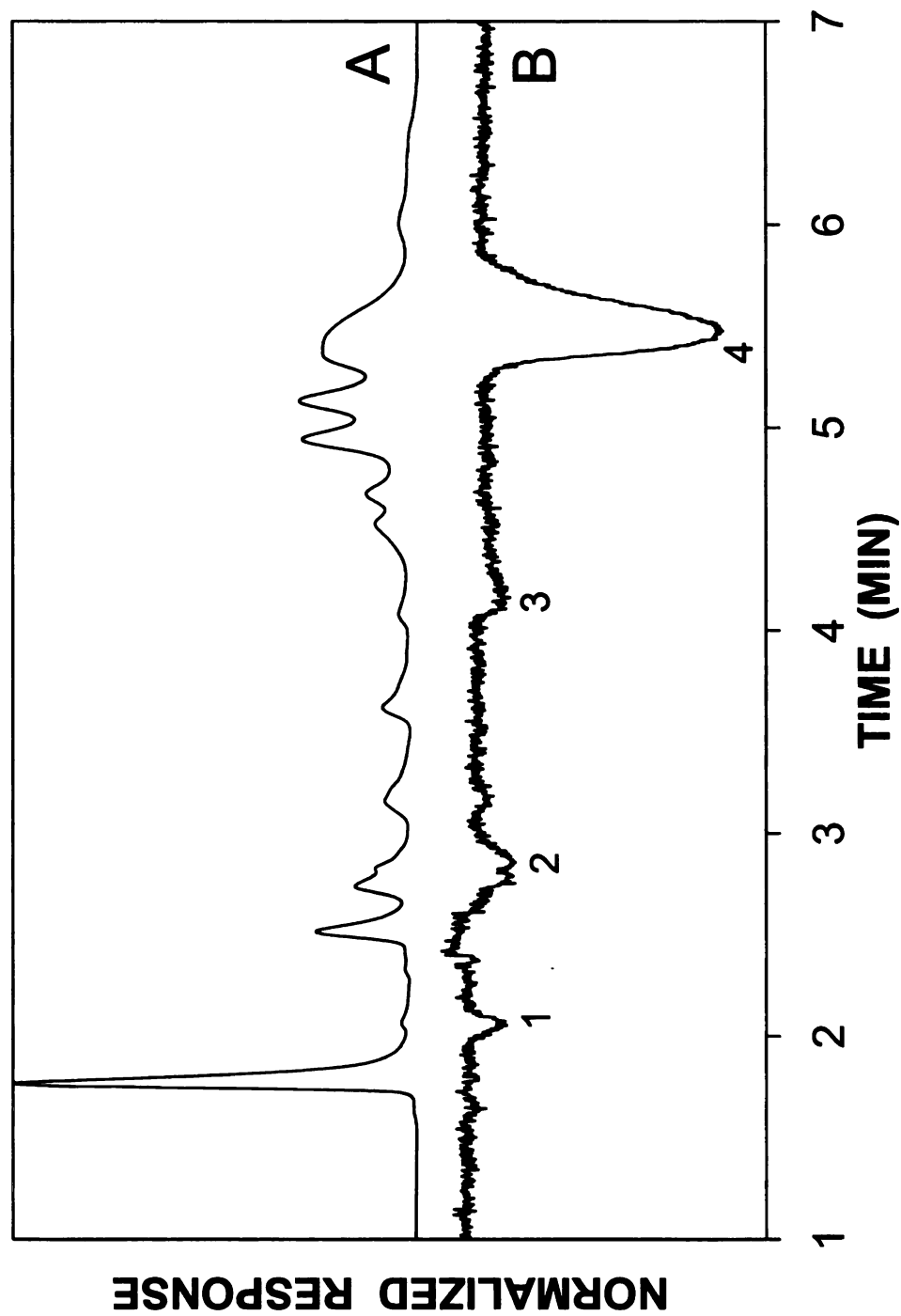




**Figure 5.6.** Chromatogram of a 1.5-oz (45-mL) serving of rum spiked with 0.25 g GHB obtained by UV-absorbance detection (A) and laser-induced fluorescence detection (B). Chromatographic conditions as described in Figure 5.3. Solutes: oxalic acid (1), lactic acid (2), GHB (3).



**Figure 5.7.** Chromatogram of a 12-oz (360-mL) serving of cola spiked with 0.75 g GHB obtained by UV-absorbance detection (A) and laser-induced fluorescence detection (B). Chromatographic conditions as described in Figure 5.3. Solutes: phosphoric acid (1), GHB (2).



**Figure 5.8.** Chromatogram of an 8-oz (240-mL) serving of coffee spiked with 0.75 g GHB obtained by UV-absorbance detection (A) and laser-induced fluorescence detection (B). Chromatographic conditions as described in Figure 5.3. Solutes: oxalic acid (1), formic acid (2), unknown (3), GHB (4).

observed previously for the alcoholic beverages, the chromatograms of the non-alcoholic beverages with fluorescence detection are greatly simplified compared to those with UV-absorbance detection. Simplification of the cola chromatogram is most impressive at retention times less than 3 min, where a number of non-acidic species are observed with UV-absorbance detection but not with fluorescence (Figure 5.7). These species may include artificial sweeteners, preservatives, and coloring agents. In the coffee chromatogram, the fluorescence method eliminates potential overlap between an unknown absorbing compound and GHB (Figure 5.8). Because this absorbing species is not acidic, no interference is observed with fluorescence detection. The cola and coffee samples, both dark brown in color, have the greatest potential for interferences when using UV-absorbance detection. The ability to determine GHB in these matrices by using the fluorescence method will be a great utility to forensic scientists. By comparison to the chromatogram of standard acids (Figure 5.3), phosphoric acid is identified in the cola sample (Figure 5.7) and oxalic and formic acids are identified in the coffee sample (Figure 5.8). Under these experimental conditions, the detection limit of GHB in non-alcoholic beverages is also determined to be 3 mM in the non-alcoholic beverages ( $S/N = 3$ ). As mentioned previously, this detection limit is sufficient for determination of GHB in adulterated beverages (Table 5.1).

#### **5.3.2.3 Effect of Ethanol on GHB Retention**

For qualitative identification of GHB, the retention factor is compared to a known value. The precision of the retention factor, therefore, will determine the

reliability of the method for identification of GHB in various unknown samples. The retention factor for GHB is constant at 2.1 in water, beer, wine, cola, and coffee, while the retention factor for GHB is 1.9 in rum. Because chromatographic retention is highly dependent on the relative polarity of the mobile and stationary phases, the decrease is most likely caused by the increased alcohol content of rum (35%) compared to the other beverages (<10%). In the rum sample, the decreased polarity causes GHB to spend less time in the stationary phase, relative to the other samples. Because less time is spent in the stationary phase, GHB elutes more rapidly. To confirm this theory, a 50 mM solution of GHB is prepared in 35:65 ethanol:water as a simulant of an alcoholic beverage. Upon injection of the simulant, a decreased retention factor (1.9) is observed for GHB. To avoid this effect, it is often recommended to dissolve samples in the mobile phase prior to injection in liquid chromatography. For the direct analysis of beverages, however, this approach is undesirable.

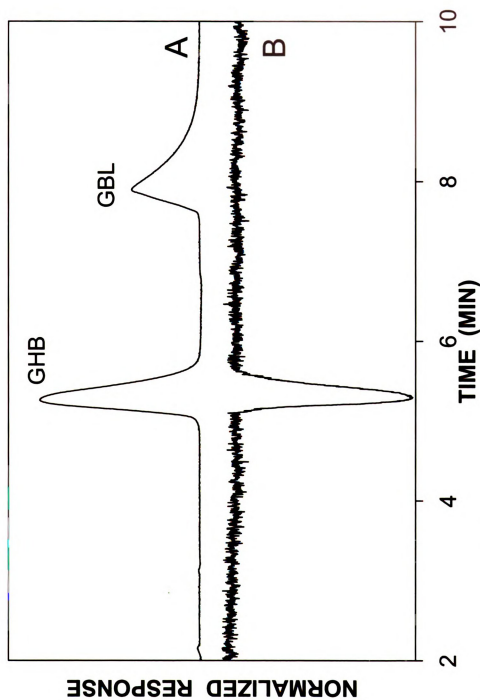
Another approach to confirm the presence of GHB is by coinjection of a standard. If an alcoholic beverage is suspected to contain GHB but the retention time is not statistically consistent, a small volume of a standard GHB solution may be added and the beverage reanalyzed. The presence of GHB is confirmed if a single peak is observed, where the retention factor remains constant and the peak height and area increase. For analysis of unknown beverages, the coinjection method is advantageous because *a priori* knowledge of the alcohol content is not necessary.

### **5.3.3 Interconversion of GHB to GBL**

Because GHB is more strongly regulated, the quantitation of GHB in a suspect beverage, without interconversion to GBL, is the most important determination to be made in a forensic case. As a result of these legal implications, it is necessary to validate the current method to ensure that selective interconversion of GHB and GBL is not promoted during sample analysis. A solution of 50 mM each GHB and GBL is analyzed using both UV-absorbance detection and the pH-dependent fluorescence detection method (Figure 5.9). Injections of individual standards are used to identify the first peak as GHB and the second peak as GBL. No GBL peak is observed for injection of a GHB solution, indicating that the method does not cause esterification of GHB to GBL. Also, no GHB peak is observed for injection of a GBL solution, indicating that the method does not cause hydrolysis of GBL to GHB. Because the indirect fluorescence method only detects acids, no peak is observed for GBL.

## **5.4 Conclusions**

The complex matrices of alcoholic and non-alcoholic beverages can obscure the forensic analysis of beverages adulterated with GHB. The proposed method eliminates interferences and allows quantitation of GHB in adulterated beverages with a detection limit of 3 mM and a linear range of 1 – 100 mM. This detection limit corresponds to a dose of 0.09 g of GHB in an 8-oz beverage, which is an order of magnitude below the therapeutic dose and 20 – 40 times below the typical recreational dose. A dose of GHB administered with malicious intent may further exceed these levels. The sensitivity of the method indicates



**Figure 5.9.** Chromatogram of 50 mM each GHB and GBL in water obtained by UV-absorbance detection (A) and laser-induced fluorescence detection (B). Chromatographic conditions as described in Figure 5.3.

that GHB may be detectable in trace amounts of a beverage left behind. Interconversion to GBL does not occur during sample analysis, and GBL is not detected using the proposed method. The ability to detect GHB in abandoned beverages may provide important forensic evidence in sexual assault cases in which biological evidence of GHB consumption is difficult to obtain.



## 5.5 References

1. Craig, K.; Gomez, H. F.; McManus, J. L.; Bania, T. C. *J. Emerg. Med.* **2000**, *18*, 65-70.
2. Galloway, G. P.; Frederick, S. L.; Staggers Jr, F. E.; Gonzales, M.; Stalcup, S. A.; Smith, D. E. *Addiction* **1997**, *92*, 89-96.
3. Tunnicliff, G. *Journal of Toxicology: Clinical Toxicology* **1997**, *35*, 581-590.
4. Ropero-Miller, J. D.; Goldberger, B. A. *Clin. Lab. Med.* **1998**, *18*, 727-746.
5. Gallimberti, L.; Cibi, M.; Pagnin, P.; Sabbion, R.; Pani, P. P.; Piratsu, R.; Ferrara, S. D.; Gessa, G. L. *Neuropsychopharmacol.* **1993**, *9*, 77-81.
6. Caputo, F.; Addolorato, G.; Trevisani, F.; Bernardi, M. *Lancet* **2005**, *366*, 981-982.
7. Couper, F. J.; Marinetti, L. J. *Forensic Sci. Rev.* **2002**, *14*, 101-121.
8. Centers for Disease Control *J. Am. Med. Assoc.* **1991**, *256*, 447-448.
9. Chin, M.-Y.; Kreutzer, R. A.; Dyer, J. E. *West. J. Med.* **1992**, *156*, 380-384.
10. Kam, P. C. A.; Yoong, F. F. Y. *Anaesthesia* **1998**, *53*, 1195-1198.
11. Drug Enforcement Administration **2000**, Addition of gamma-hydroxybutyrate (GHB) to Schedule I. 65 (49), 13235-13238.
12. Haller, C.; Thai, D.; Jacob, P.; Dyer, J. E. *J. Anal. Toxicol.* **2006**, *30*, 360-364.
13. Del Signore, A.; McGregor, M.; Cho, B. P. *J. Forensic Sci.* **2005**, *50*, 81-86.
14. Couper, F. J.; Logan, B. K. *J. Forensic Sci.* **2001**, *46*, 919-923.
15. ElSohly, M. A.; Salamone, S. J. *J. Anal. Toxicol.* **1999**, *23*, 141-146.
16. Wells, D. *Sci. Justice* **2001**, *41*, 197-199.
17. Bishop, S. C.; Lerch, M.; McCord, B. R. *Forensic Sci. Int.* **2004**, *141*, 7-15.
18. Zvosec, D. L.; Smith, S. W.; McCutcheon, J. R.; Spillane, J.; Hall, B. J.; Peacock, E. A. *New Engl. J. Med.* **2001**, *344*, 87-94.

19. Ciolino, L. A.; Mesmer, M. Z.; Satzger, R. D.; Machal, A. C.; McCauley, H. A.; Mohrhaus, A. S. *J. Forensic Sci.* **2001**, *46*, 1315-1323.
20. Brenneisen, R.; ElSohly, M. A.; Murphy, T. P.; Passarelli, J.; Russmann, S.; Salamone, S. J.; Watson, D. E. *J. Anal. Toxicol.* **2004**, *28*, 625-630.
21. Alston, W. C.; Ng, K. *Forensic Sci. Int.* **2002**, *126*, 114-117.
22. Badcock, N. R.; Zotti, R. *Ther. Drug Mon.* **1999**, *21*, 376.
23. Koppenhaver, D. J. *Microgram* **1997**, *30*, 130.
24. Andera, K. M.; Evans, H. K.; Wojcik, C. M. *J. Forensic Sci.* **1999**, *45*, 665-668.
25. Bell, S. C.; Oldfield, L. S.; Shakleya, D. M.; Petersen, J. L.; Mercer, J. W. *J. Forensic Sci.* **2006**, *51*, 808-811.
26. Bravo, D. T.; Harris, D. O.; Parsons, S. M. *J. Forensic Sci.* **2004**, *49*, 379-387.
27. Chappell, J. S.; Meyn, A. W.; Ngim, K. K. *J. Forensic Sci.* **2004**, *49*, 52-59.
28. Blair, S.; Song, M.; Hall, B.; Brodbelt, J. *J. Forensic Sci.* **2001**, *46*, 688-693.
29. DeFrancesco, J. V.; Witkowski, M. R.; Ciolino, L. A. *J. Forensic Sci.* **2006**, *51*, 321-329.
30. Couper, F. J.; Logan, B. K. *J. Anal. Toxicol.* **2000**, *24*, 1-7.
31. Ferrara, S. D.; Tedeschi, L.; Frison, G.; Rossi, A. *J. Forensic Sci.* **1995**, *40*, 501-504.
32. Elian, A. A. *Forensic Sci. Int.* **2000**, *109*, 183-187.
33. Elliott, S.; Burgess, V. *Forensic Sci. Int.* **2005**, *151*, 289-292.
34. Mesmer, M. Z.; Satzger, R. D. *J. Forensic Sci.* **1998**, *43*, 489-492.
35. Dahlen, J.; Vriesman, T. *Forensic Sci. Int.* **2002**, *125*, 113-119.
36. Patchett, M. L.; Minoshima, Y.; Harrington, P. B. *Spectroscopy* **2002**, *17*, 16-21.
37. Chew, S. L.; Meyers, J. A. *J. Forensic Sci.* **2003**, *48*, 292-298.
38. Lettieri, J. T.; Fung, H. L. *Biochem. Med.* **1978**, *20*, 70-80.

## **CHAPTER 6**

### **CONCLUSIONS AND FUTURE WORK**

Luminescence-based methods are of great importance in the search for a sensitive and selective detector for explosives and other forensically important compounds. By gaining a more detailed understanding of the mechanism of interaction between explosives and sensor materials, new fluorescent materials can be developed with an improved ability to detect explosives in complex field settings. This insight may also lead to identification of fluorescent materials that could be useful in determination of other forensically relevant compounds. The focus of this research has been the identification of new fluorescence quenching interactions that can be used to advance the field of forensic science.

The fluorescence quenching response of several solution-phase fluorophores in the presence of nitrated explosives has been investigated. Of the extended group of fluorophores investigated in this study, pyrene, purpurin, malachite green, and phenol red are most promising for explosives detection. These fluorophores demonstrate sensitive and selective quenching interactions with a target group of nitrated quenchers, with quenching constants greater than  $50 \text{ M}^{-1}$ . The remaining fluorophores under investigation demonstrate little or no response to nitrated compounds, with quenching constants less than  $50 \text{ M}^{-1}$ . Because each fluorophore may interact with the quenchers through a different mechanism, various degrees of sensitivity and selectivity are observed for pyrene, purpurin, malachite green, and phenol red. Of these, pyrene demonstrates the greatest sensitivity for nitrated molecules with quenching

constants on the order of  $10^2 \text{ M}^{-1}$ . The routine use of pyrene for explosives detection is undesirable, however, because of numerous health and waste disposal hazards. Purpurin, malachite green, and phenol red demonstrate less sensitivity than pyrene but comparable or greater selectivity for nitrated molecules. Both malachite green and phenol red exhibit pH-dependent fluorescence, but with buffering, the interference of acidic species on the quenching of malachite green fluorescence can be reduced. In general, pH-sensitive fluorophores are not ideal for application in the detection of explosives on-site, as various matrices may be encountered that could lead to erroneous results. Thus, among these potential fluorophores, purpurin shows the most promise for detection of nitrated explosives by fluorescence quenching.

Based on these solution-phase quenching results, the fluorescence of purpurin, malachite green, and phenol red is studied in more detail. Initial studies with a variety of solvents indicate that the fluorescence power of malachite green and phenol red is greatest in dioxane, while that of purpurin is greatest in more polar solvents such as methanol or water. The most promising substrate for incorporation of malachite green while maintaining fluorescence is poly(ethylene glycol). A mixture containing malachite green and poly(ethylene glycol) fluoresces in the solid state when coated on glass slides, filter paper, or silica particles. The use of a high-power source such as a laser causes degradation of malachite green fluorescence, however, indicating that a low-power source, such as a handheld UV lamp, is better for field applications. Upon further testing, the polymer containing malachite green can be coated on a paper-based substrate

for use as a wipe for detection of explosives on surfaces such as luggage or cargo. In addition, an air-sampling device could be developed based on coated silica particles enclosed in a quartz tube. For both of these applications, the use of available equipment such as handheld UV lamps and digital cameras is appropriate.

Future work in the development of sensors for explosives detection involves investigations of other solution-phase fluorophores to identify those that exhibit sensitive and selective quenching by nitrated compounds. In this work, only a limited number of potential fluorophores have been selected on the basis of their structural similarities to pyrene. From the results of this study, however, it is evident that mechanistic similarities do not follow directly from structural similarities. Consequently, a more broad and diverse selection of fluorophores may prove essential for the development of a fluorescence quenching method for the detection of nitrated explosives. For phenol red and purpurin, fluorophores identified in the original study, parallel studies to those conducted for malachite green are necessary to determine appropriate matrix polarity and verify fluorescence in the solid state. In addition, significant testing of any solid-state device with explosive particles and vapors is necessary to verify that the quenching behavior observed in the solution phase is also observed in the polymer or other matrices. Use of malachite green in the solution phase is still viable, and investigations into a post-column liquid chromatography system could lead to a selective explosives detection method. For all methods, the detection

limits of the explosives must be determined and optimized before the true utility can be known.

In a second application of luminescence-based methods for forensic sample determination, a novel method for detection of acidic species based on the pH-sensitive fluorescence of fluorescein has been developed. The native acid-base properties of fluorescein and the corresponding changes in fluorescence quantum yield are exploited for detection of acidic species in foods and beverages. Any compound that is more acidic than fluorescein allows sufficient proton transfer in aqueous and polar organic solvents and can thereby be detected. The fluorescence of fluorescein is sigmoidal with the logarithm of proton concentration. The linear range extends two orders of magnitude and is centered about the fluorescein concentration in solution. The linear range can be extended to four orders of magnitude using a sigmoidal transform function, and can be shifted to higher or lower concentrations by adjustment of the fluorescein concentration. This new method is verified by using a series of test acids, and applied to the analysis of grape juice and derivatives, including a variety of wine and vinegar samples following liquid chromatography. Improvements in detection sensitivity and selectivity compared to UV-absorbance detection are observed for acids found in these samples. This fluorescence method provides a new tool for analysis of acidic species with potential use in a variety of disciplines including forensic, environmental, and clinical analyses.

A forensic application of this acid detection method is in the determination of  $\gamma$ -hydroxybutyric acid (GHB), a drug commonly used in sexual

assaults. GHB is often administered in complex alcoholic and non-alcoholic beverages, complicating the forensic analysis of adulterated beverages. The proposed method eliminates interferences from other beverage components and allows quantitation of GHB with a detection limit of 3 mM and a linear range of 1 – 100 mM. This detection limit corresponds to a dose of 90 mg of GHB in an 8-oz beverage, which is an order of magnitude below the therapeutic dose and 20 – 40 times below the typical recreational dose. A dose of GHB administered with malicious intent may further exceed these levels. The sensitivity of the method indicates that GHB may be detectable in beverage residues remaining at the scene of a crime. In contrast to other GHB detection methods, interconversion to  $\gamma$ -butyrolactone (GBL) does not occur during sample analysis. In addition, GBL is not detected using the proposed method. The ability to detect GHB in abandoned beverages may provide important forensic evidence in sexual assault cases in which biological evidence of GHB consumption is difficult to obtain.

For applications of this method in other areas, the instrument parameters must be optimized for operation at lower fluorescein concentrations. This adjustment will allow detection of acids at lower concentrations, as present in environmental or clinical samples. The most important variables to control are the relative flow rates of fluorescein and sodium hydroxide. At low fluorescein concentrations, accurate flow control is critical to maintain a constant fluorescence background. Because this flow control can be difficult, adaptation of this method to capillary electrophoresis (CE) may be beneficial. In a CE method, the acidic species are separated as ions, and fluorescein could be

added into the non-buffered separation electrolyte, maintained at pH 8. As with the liquid chromatography method, acids present in the sample transfer a proton to fluorescein and the corresponding decrease in fluorescence is detected. Using the CE method, lower concentrations of fluorescein could be utilized, and lower acid concentrations could thereby be detected.

Overall, this work demonstrates a variety of analytical and forensic applications of fluorescence quenching. Each of these techniques demonstrates the use of luminescence methods in a way that has not been utilized in the forensic community. In addition, many of these applications can be easily implemented in a forensic laboratory by utilizing common equipment such as a handheld lamp, a digital camera, or a conventional fluorescence detector. In all, these methods provide a number of new tools for the forensic science and analytical chemistry communities.



## **APPENDIX**

### **INVESTIGATION OF QUENCHING MECHANISM**

#### **A.1. Determination of Fluorescence Lifetimes**

The fluorescence lifetime of each fluorophore is determined from single-photon counting data as described in Section 2.2.3. The fluorescence lifetime ( $\tau$ ) is exponentially related to the photons counted ( $F$ ) at time  $t$ .

$$F(t) = F_0 e^{-t/\tau} + C \quad (\text{A.1})$$

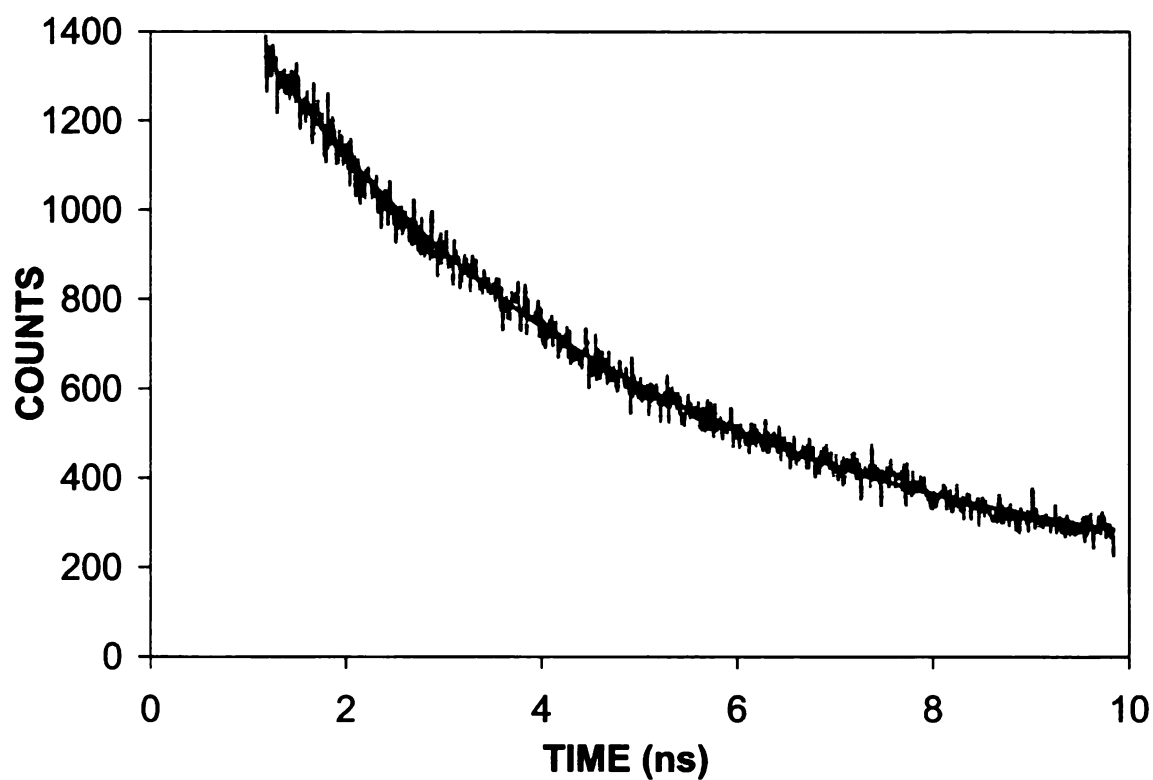
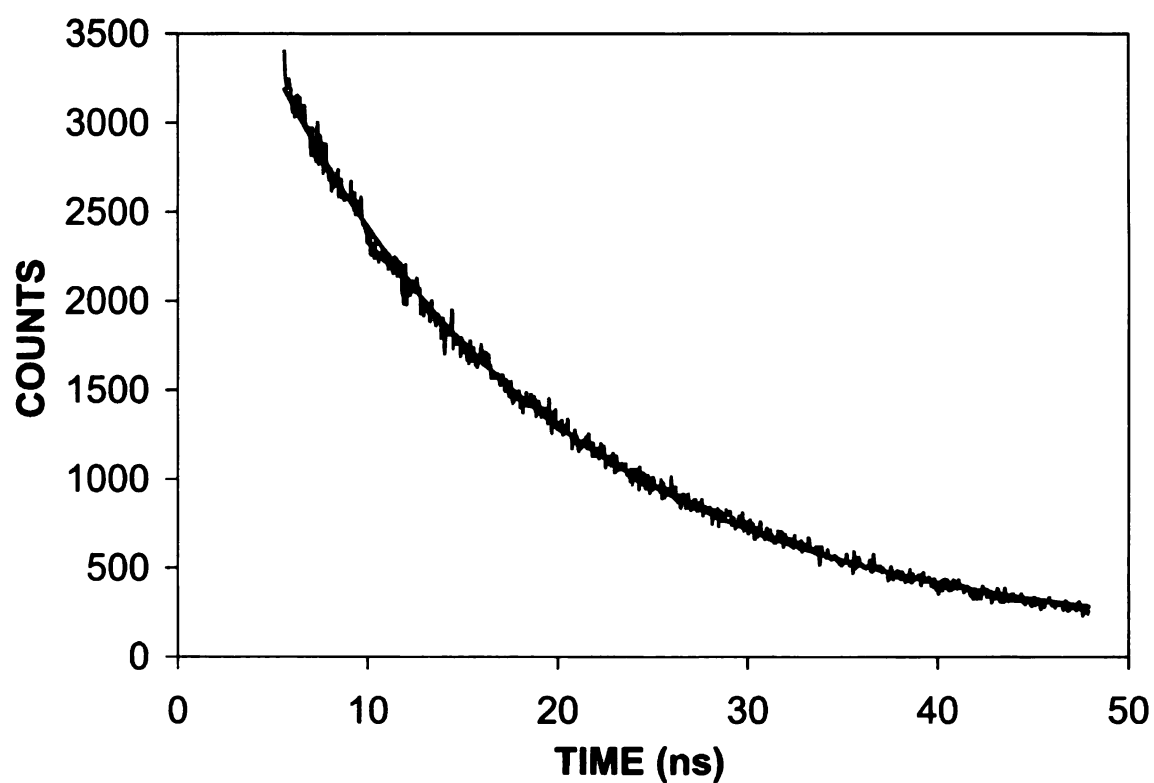
The initial number of photons counted ( $F_0$ ), the fluorescence lifetime, and the offset constant ( $C$ ) are determined from nonlinear regression of the data. Six replicate measurements are acquired for each fluorophore in methanol under the conditions given in Table A.1. The concentrations for each fluorophore are chosen to give a minimum integration time for single-photon counting. Wavelengths are determined from the emission spectra determined with excitation at 325 nm. Fluorescence decay curves for pyrene and purpurin are given in Figure A.1, and for malachite green and phenol red in Figure A.2.

#### **A.2. Determination of Redox Potentials**

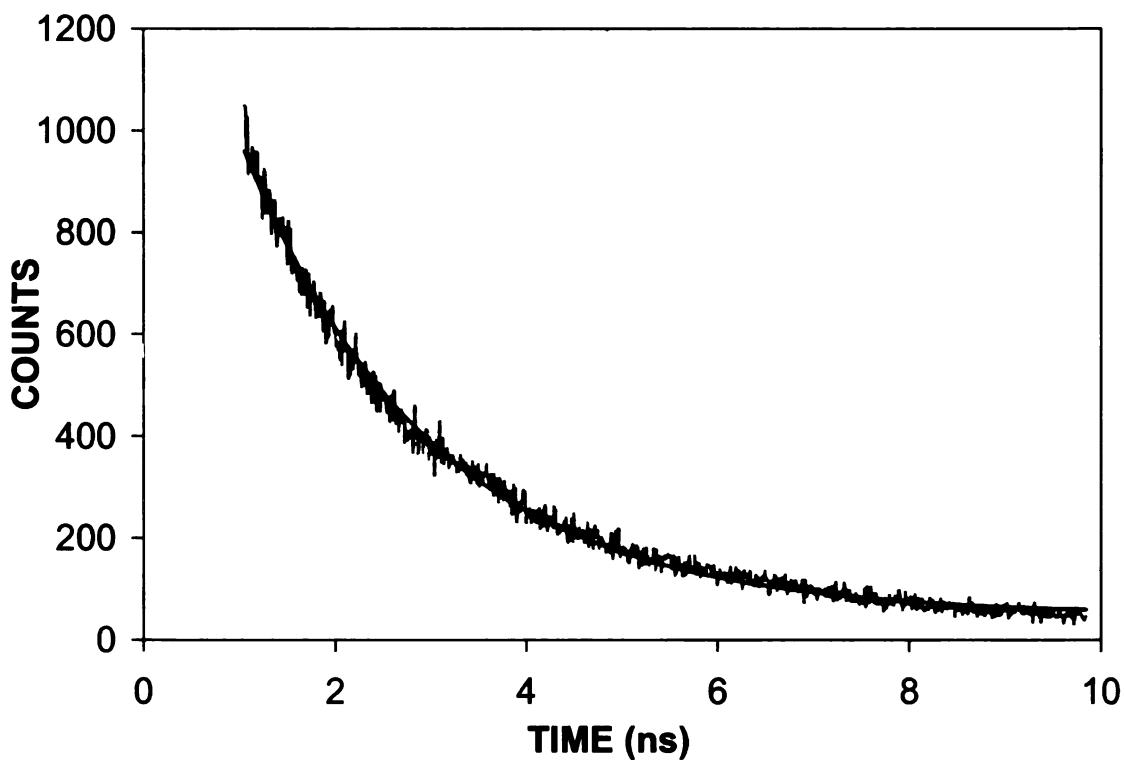
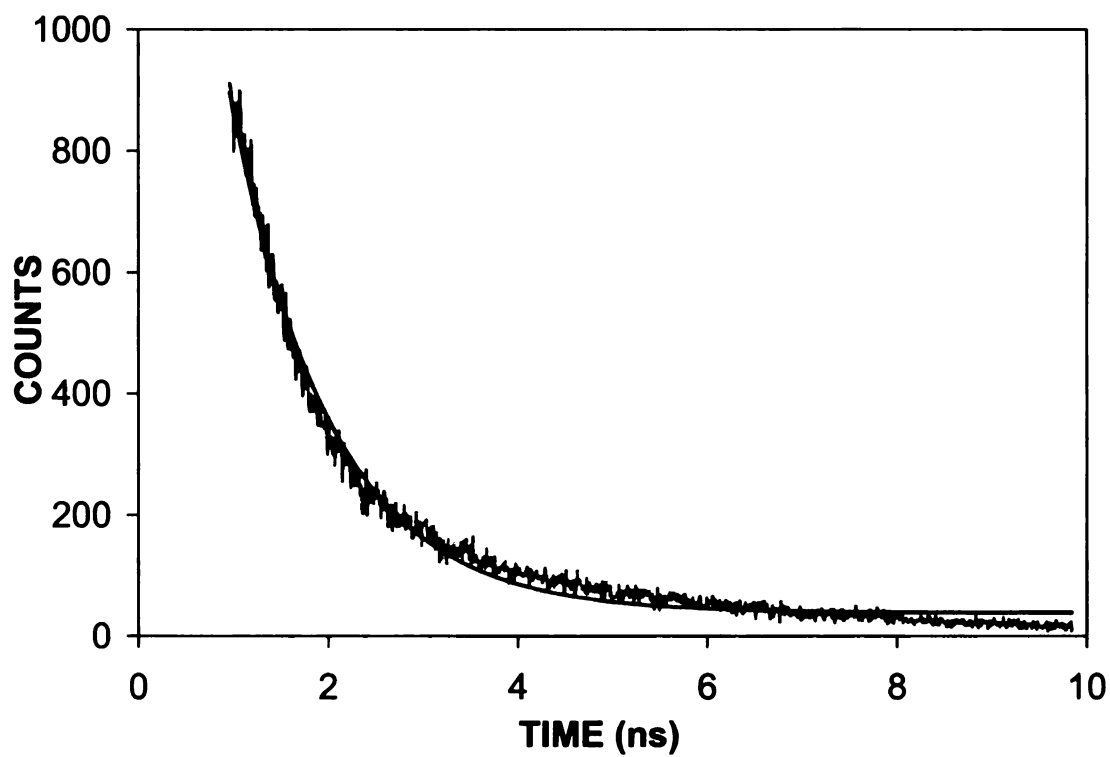
Redox potentials for each fluorophore and quencher are determined from cyclic voltammetry as described in Section 2.2.4. Potentials are scanned from 0.0 to +1.5 V at 0.5 V/s for determination of oxidation potentials and from 0.0 to -1.5 V at 0.5 V/s for determination of reduction potentials. For reversible systems,  $E_{\text{ox}}$  and  $E_{\text{red}}$  are calculated as the average of the anodic and cathodic

**Table A.1.** Parameters used for determination of fluorescence lifetimes.

<b>Fluorophore</b>	<b>Concentration</b>	<b>Emission Wavelength</b>
Pyrene	$10^{-4}$ M	390 nm
Purpurin	$10^{-3}$ M	413 nm
Malachite green	$10^{-4}$ M	379 nm
Phenol red	$10^{-3}$ M	369 nm



**Figure A.1.** Fluorescence decay curves for pyrene (top) and purpurin (bottom). For pyrene (top),  $F_0 = 4477$ ,  $C = 89.88$ ,  $\tau = 15.3$  ns,  $R^2 = 0.9975$ . For purpurin (bottom),  $F_0 = 1607$ ,  $C = 146.8$ ,  $\tau = 4.00$  ns,  $R^2 = 0.9933$ .

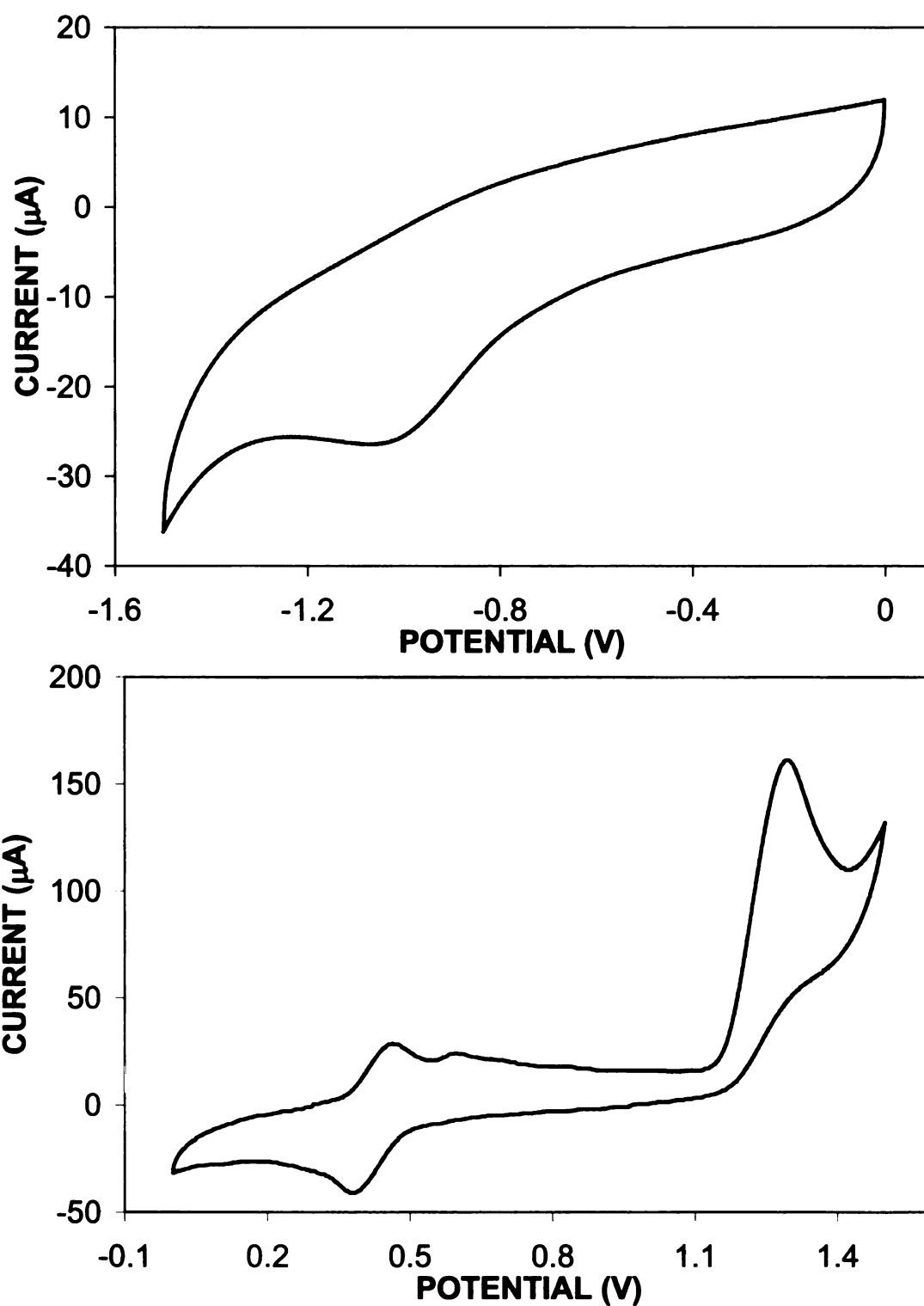


**Figure A.2.** Fluorescence decay curves for malachite green (top) and phenol red (bottom). For malachite green (top),  $F_0 = 2157$ ,  $C = 38.30$ ,  $\tau = 1.05$  ns,  $R^2 = 0.9887$ . For phenol red (bottom),  $F_0 = 1554$ ,  $C = 48.82$ ,  $\tau = 1.97$  ns,  $R^2 = 0.9936$ .

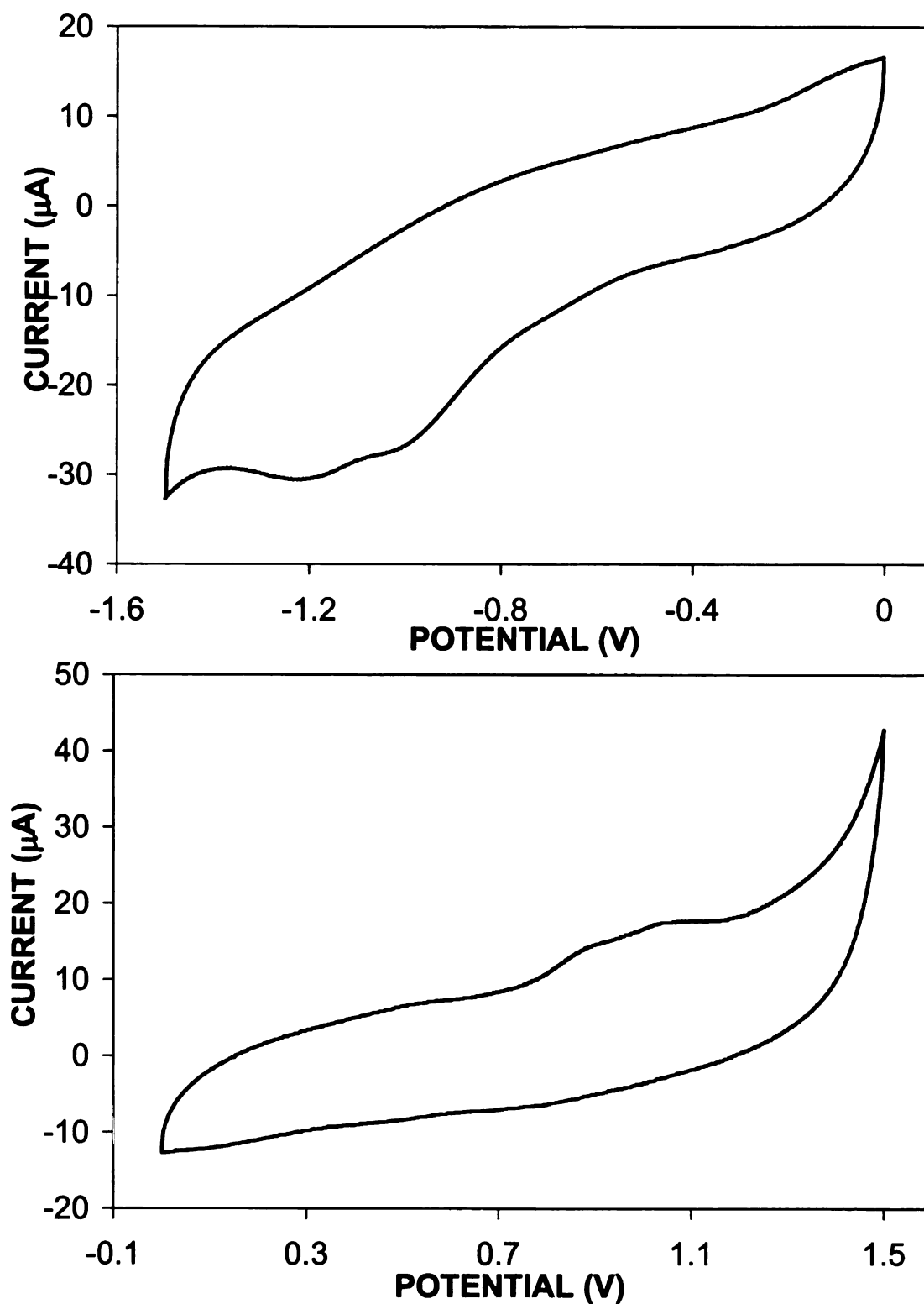
peak potentials. For irreversible systems,  $E_{ox}$  is reported as the anodic peak potential and  $E_{red}$  is reported as the cathodic peak potential. Cyclic voltammograms for pyrene, purpurin, malachite green, and phenol red are given in Figures A.3-A.6. Cyclic voltammograms for nitromethane, nitrobenzene, 4-nitrotoluene, 2,6-dinitrotoluene, aniline, benzoic acid, and phenol red are given in Figures A.7-A.13.

### **A.3. Determination of Singlet Excitation Energies**

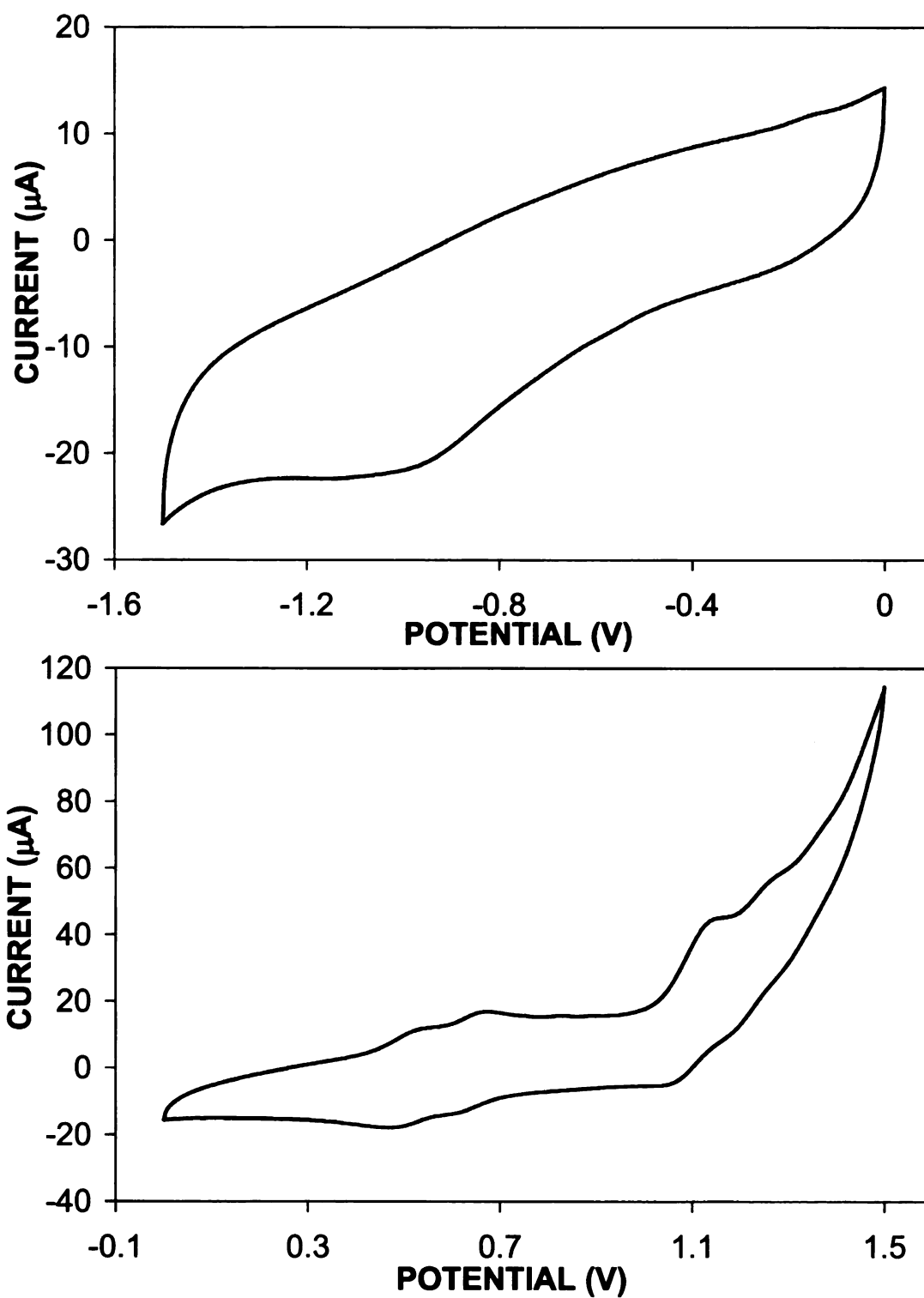
The singlet excitation energy for each fluorophore is determined from UV-visible absorbance and fluorescence emission spectra as described in Section 2.2.5. Spectra are acquired by using traditional spectrophotometers with 1-cm pathlength. The energy of the singlet excited state can be approximated as the wavelength at which the normalized absorption and emission spectra intersect. Spectra are normalized to the maximum absorbance or emission wavelength and overlaid to determine the intersection point. This wavelength is then converted to energy units of eV for calculation of the free energy of electron transfer (Equation 2.1). Normalized spectra for pyrene and purpurin are given in Figure A.14, and for malachite green and phenol red in Figure A.15.



**Figure A.3.** Cyclic voltammograms for pyrene in 0.1 M NaNO<sub>3</sub> in methanol, with potential scanned cathodically (top) and anodically (bottom).

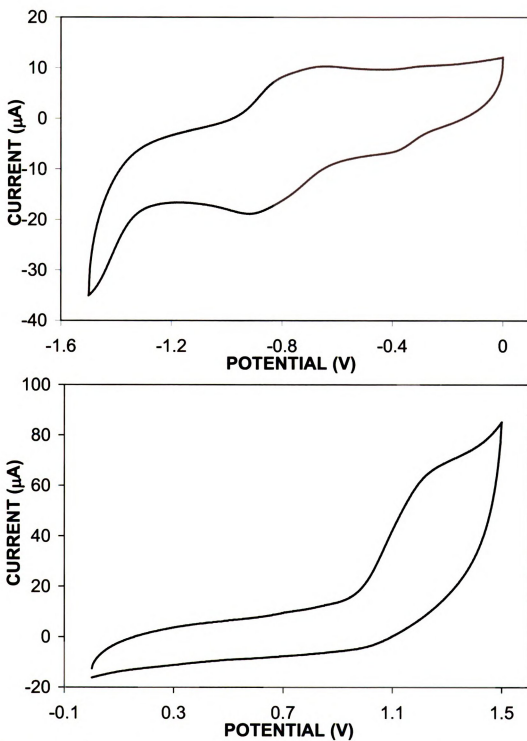


**Figure A.4.** Cyclic voltammograms for purpurin in 0.1 M  $\text{NaNO}_3$  in methanol, with potential scanned cathodically (top) and anodically (bottom).

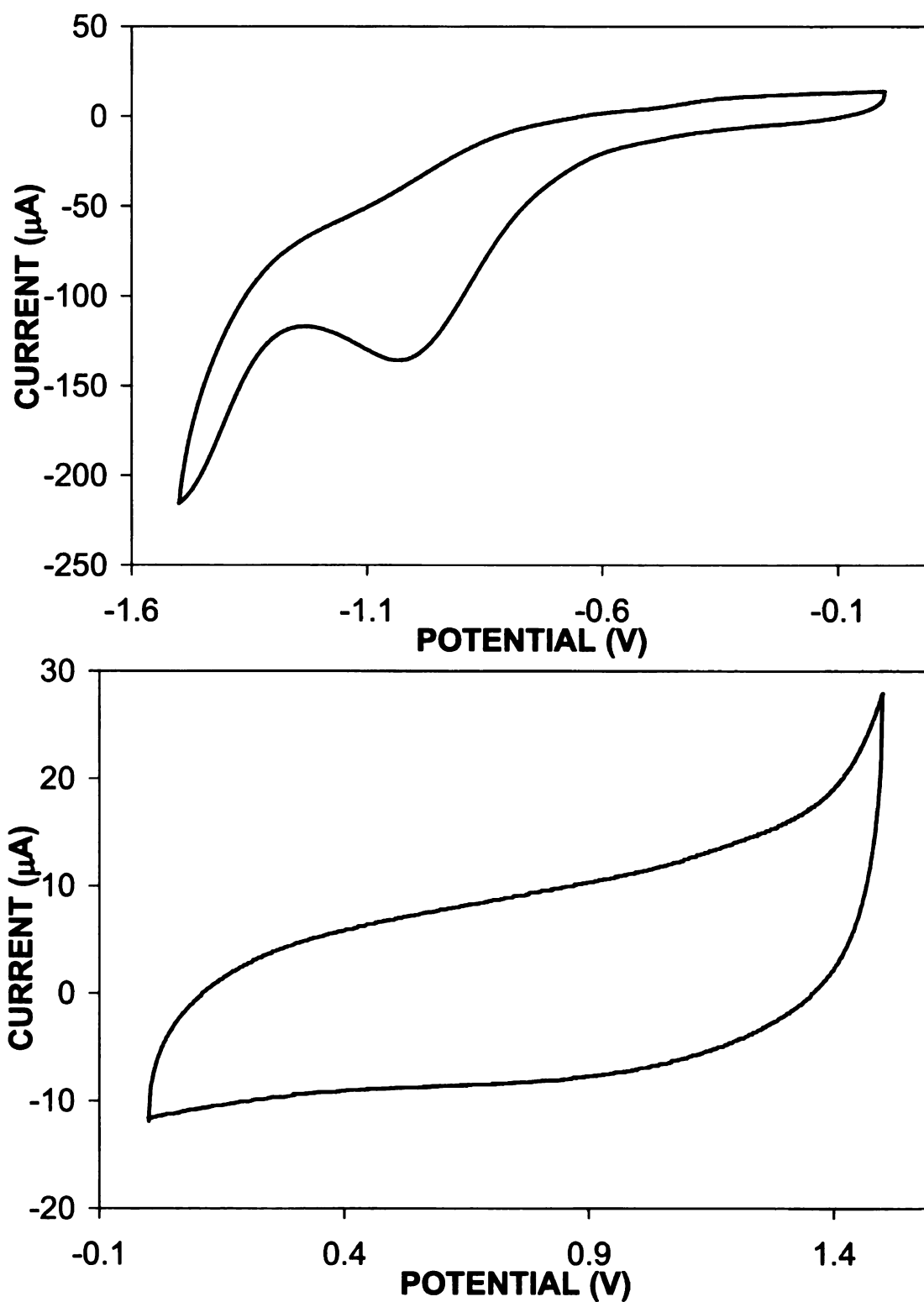


**Figure A.5.** Cyclic voltammograms for malachite green in 0.1 M NaNO<sub>3</sub> in methanol, with potential scanned cathodically (top) and anodically (bottom).

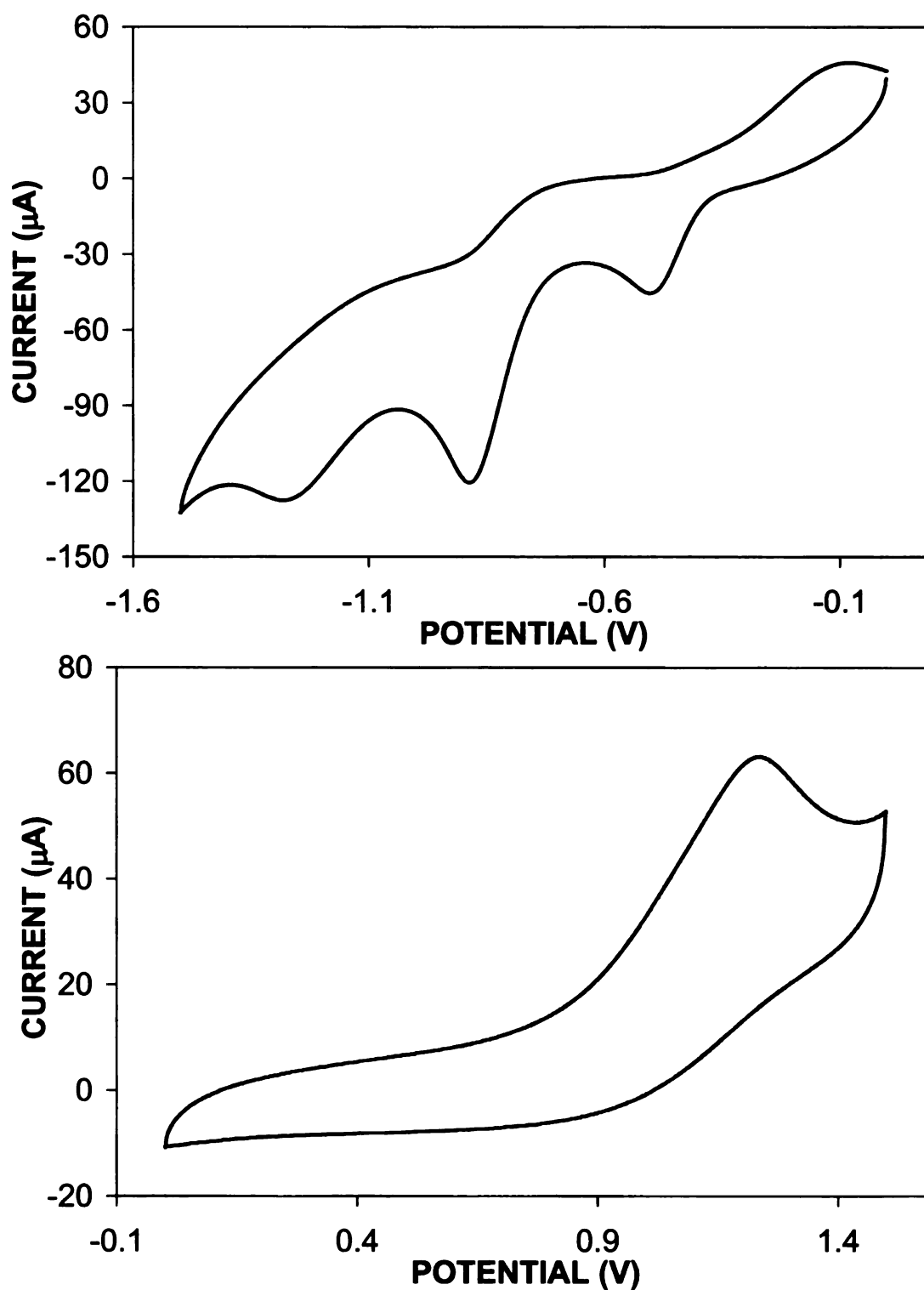




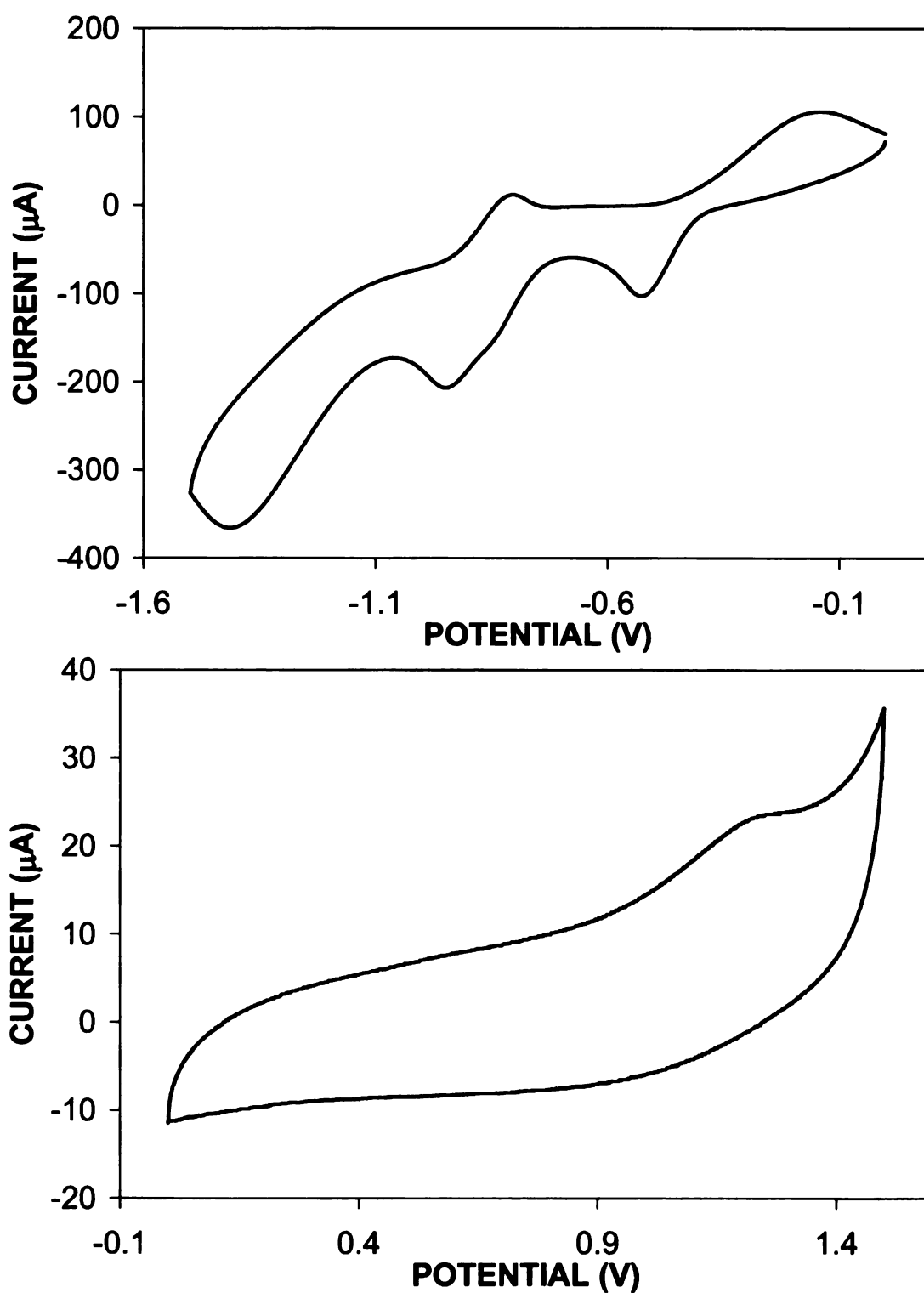
**Figure A.6.** Cyclic voltammograms for phenol red in 0.1 M NaNO<sub>3</sub> in methanol, with potential scanned cathodically (top) and anodically (bottom).



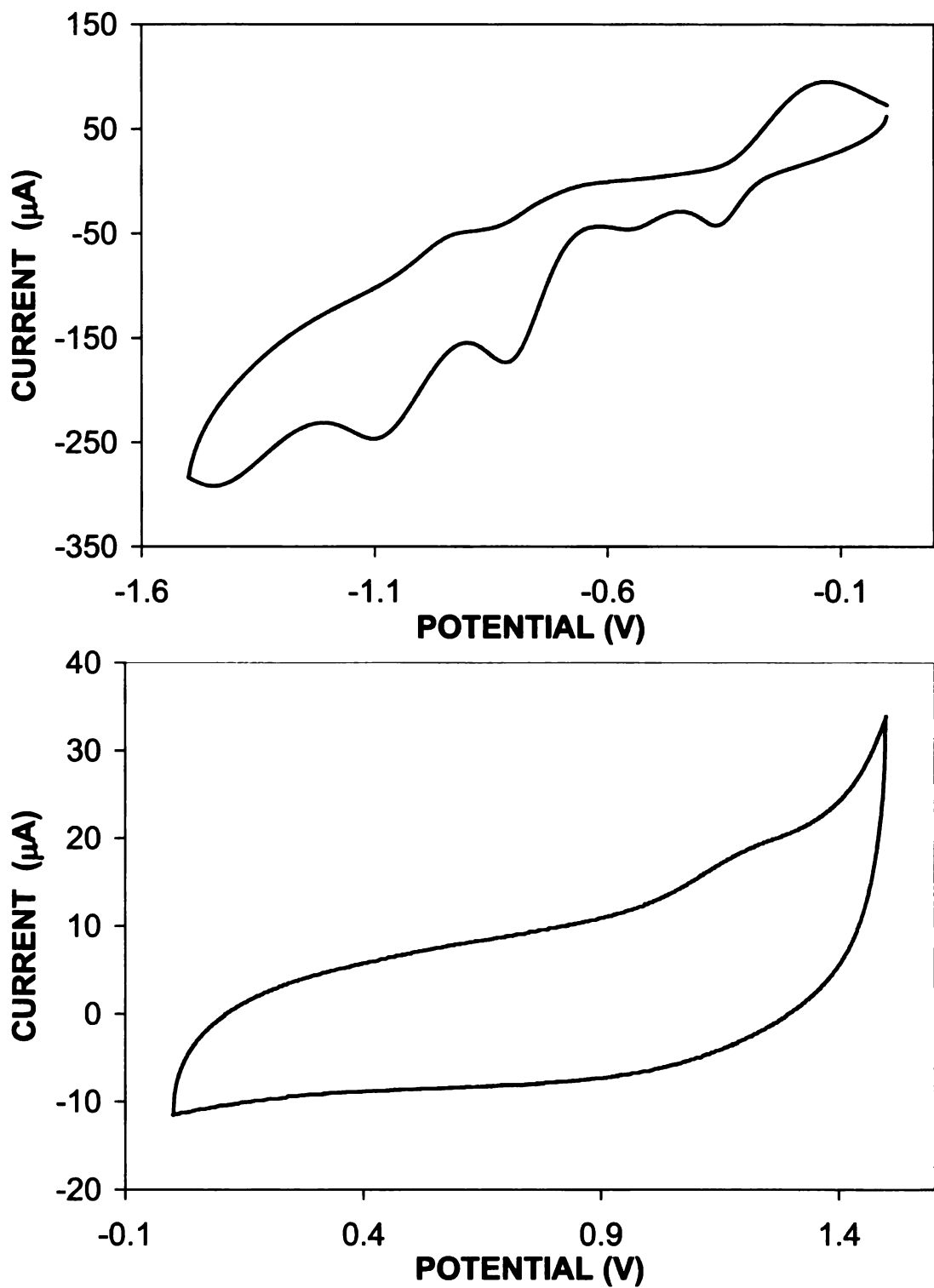
**Figure A.7.** Cyclic voltammograms for nitromethane in 0.1 M NaNO<sub>3</sub> in methanol, with potential scanned cathodically (top) and anodically (bottom).



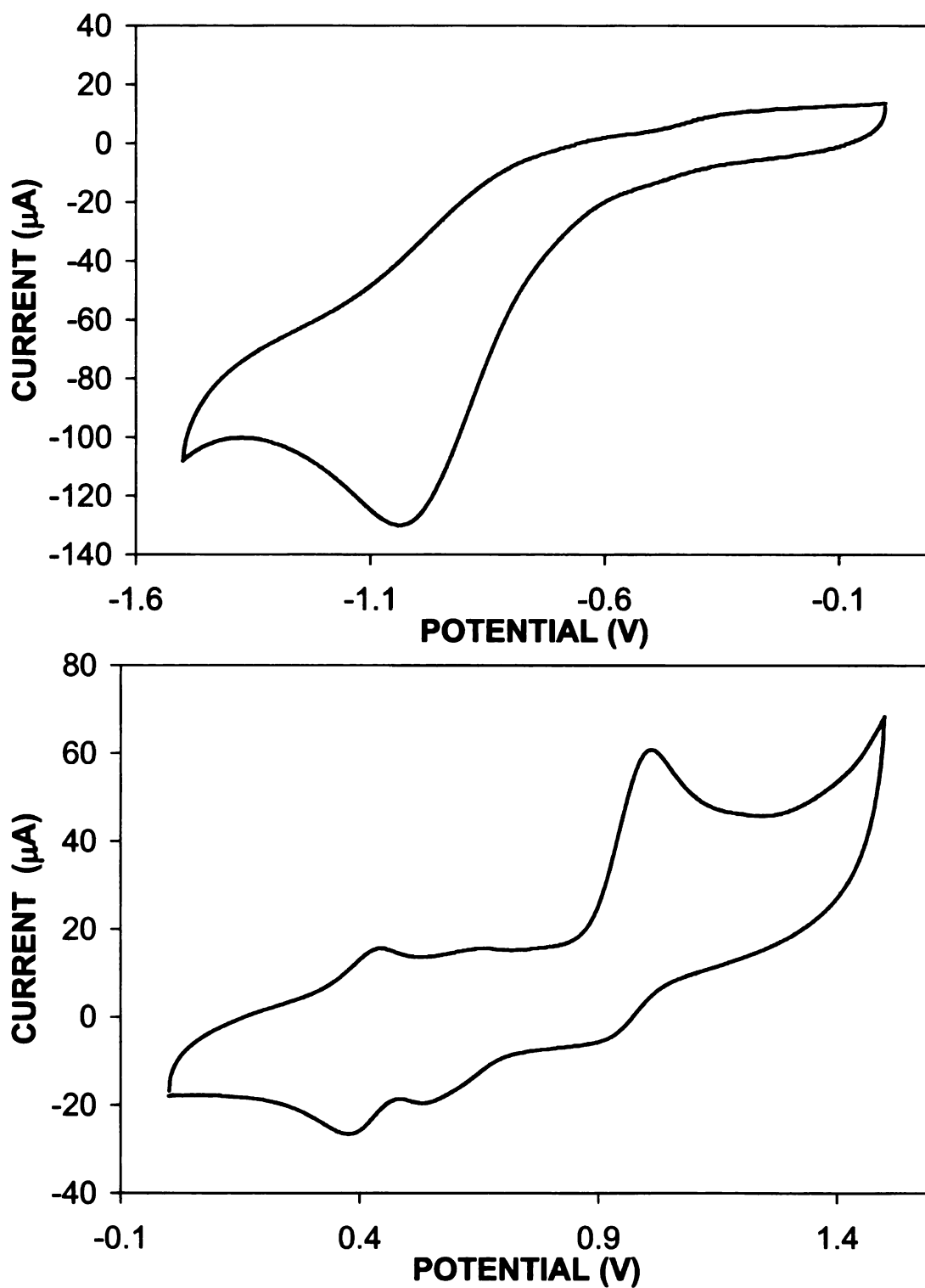
**Figure A.8.** Cyclic voltammograms for nitrobenzene in 0.1 M NaNO<sub>3</sub> in methanol, with potential scanned cathodically (top) and anodically (bottom).



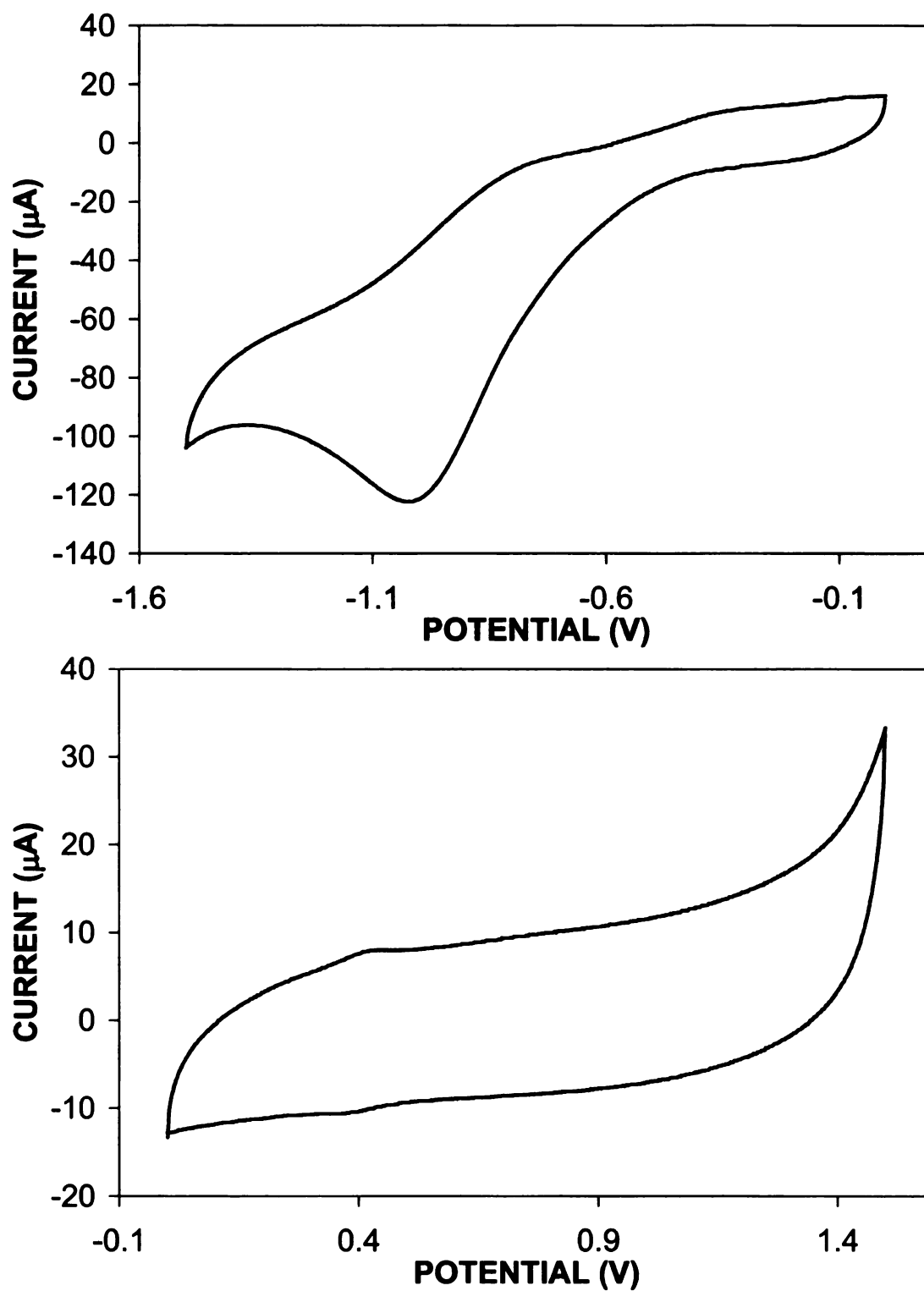
**Figure A.9.** Cyclic voltammograms for 2-nitrotoluene in 0.1 M NaNO<sub>3</sub> in methanol, with potential scanned cathodically (top) and anodically (bottom).



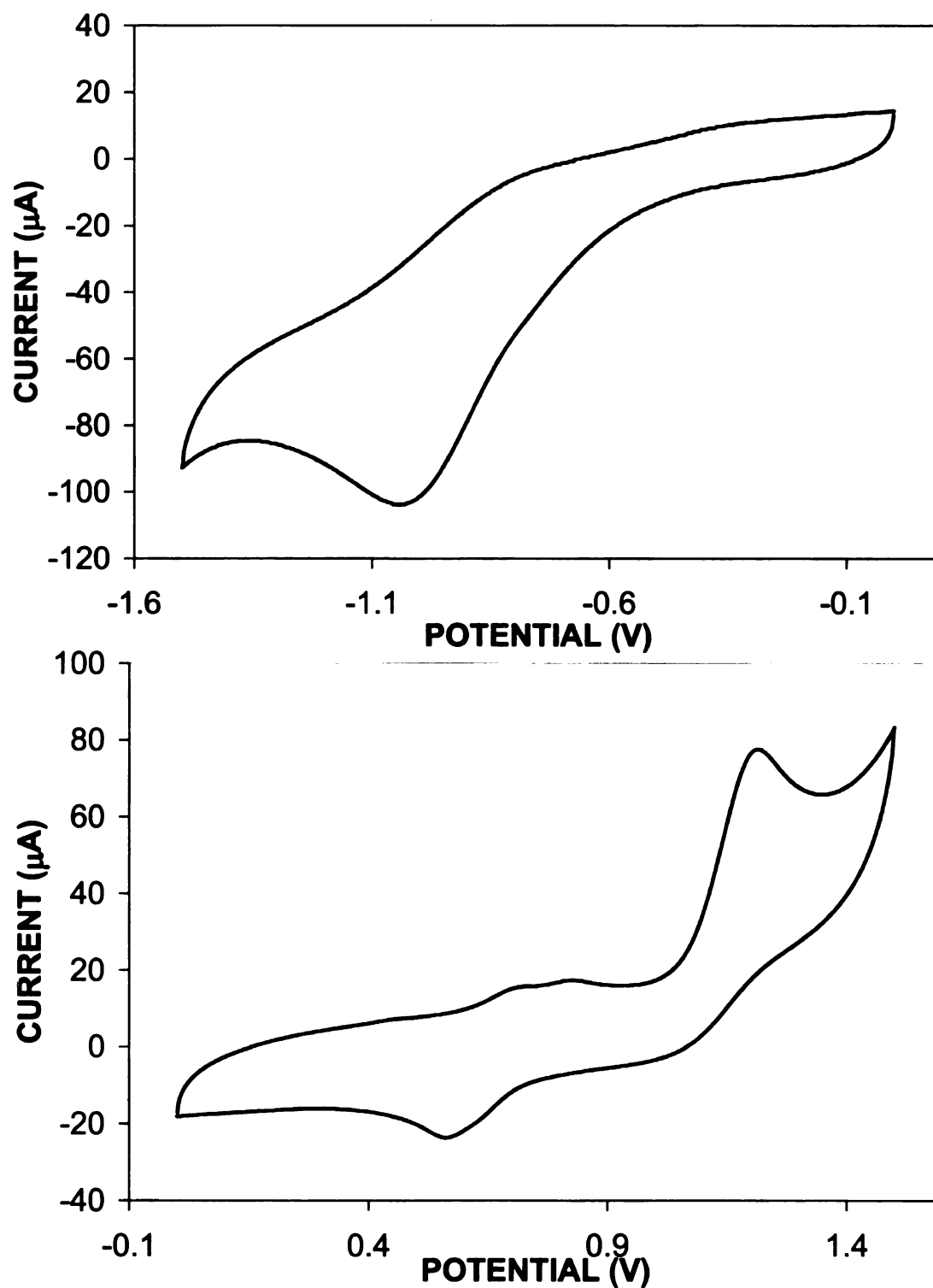
**Figure A.10.** Cyclic voltammograms for 2,6-dinitrotoluene in 0.1 M NaNO<sub>3</sub> in methanol, with potential scanned cathodically (top) and anodically (bottom).



**Figure A.11.** Cyclic voltammograms for aniline in 0.1 M NaNO<sub>3</sub> in methanol, with potential scanned cathodically (top) and anodically (bottom).

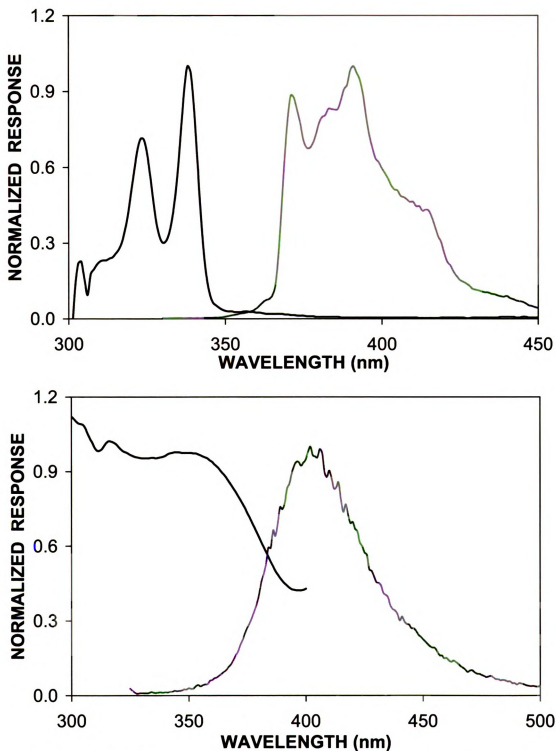


**Figure A.12.** Cyclic voltammograms for benzoic acid in 0.1 M  $\text{NaNO}_3$  in methanol, with potential scanned cathodically (top) and anodically (bottom).

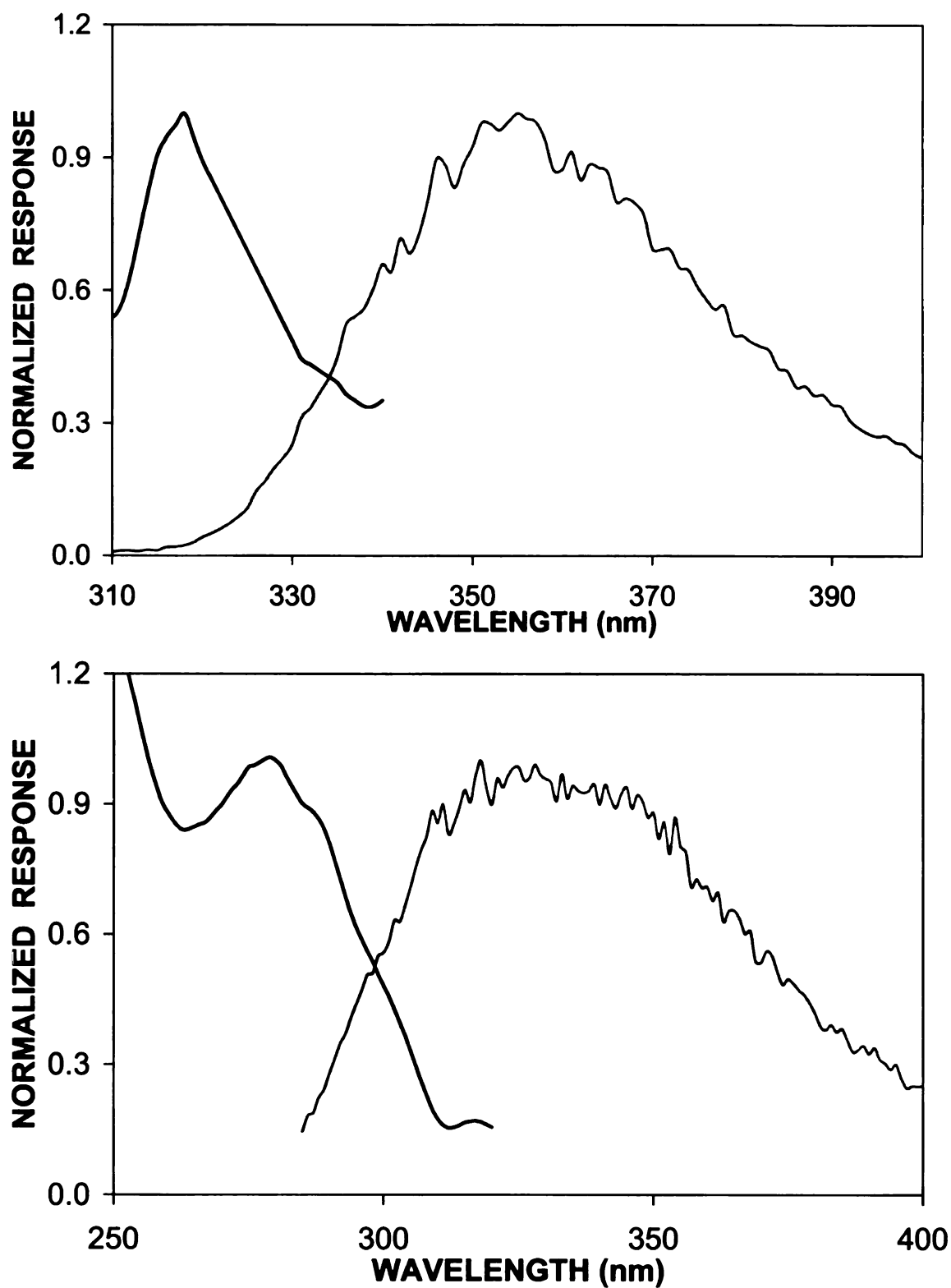


**Figure A.13.** Cyclic voltammograms for phenol in 0.1 M NaNO<sub>3</sub> in methanol, with potential scanned cathodically (top) and anodically (bottom).





**Figure A.14.** Normalized absorbance (—) and emission (—) spectra for pyrene (top) and purpurin (bottom). Emission spectra are collected by using the wavelength of maximum absorbance as the excitation wavelength. Singlet excitation energies are determined from the crossing point of the two spectra.



**Figure A.15.** Normalized absorbance (—) and emission (—) spectra for malachite green (top) and phenol red (bottom). Emission spectra are collected by using the wavelength of maximum absorbance as the excitation wavelength. Singlet excitation energies are determined from the crossing point of the two spectra.

MICHIGAN STATE UNIVERSITY LIBRARIES



3 1293 02956 5565